# The physical and structural changes throughout the drying of solvent based inks.

Chapman, Christopher

# The Physical and Structural Changes Throughout the Drying of Solvent Based Inks

**Prifysgol Abertawe**
**Swansea University**

Christopher Chapman

Swansea University

A thesis submitted for the degree of

*Doctor of Philosophy*

2011

DECLARATION

This work has not previously been accepted in substance for any degree and is not being concurrently submitted in candidature for any degree.

Signed ..... (candidate)

Date 3/1/12

STATEMENT 1

This thesis is the result of my own investigations, except where otherwise stated. Where correction services have been used, the extent and nature of the correction is clearly marked in a footnote(s).

Other sources are acknowledged by footnotes giving explicit references. A bibliography is appended.

Signed ... (candidate)

Date 3/1/12

STATEMENT 2

I hereby give consent for my thesis, if accepted, to be available for photocopying and for inter-library loan, and for the title and summary to be made available to outside organisations.

Signed ... (candidate)

Date 3/1/12

To Mum and Dad

# Acknowledgements

I would like to take this opportunity to thank all those who have contributed towards the research and thesis. In particular I would like to thank Professor Tim Claypole for instigating and supervising the project. I would also like to thank all those within the Welsh Centre for Printing and Coating I went to for advice and discussion.

I wish to offer my sincere gratitude to the Engineering and Physical Sciences Research Council (EPSRC) and the European Flexographic Industry Association (EFIA) for their financial assistance throughout the research.

Finally I wish to offer personal thanks to my friends and especially my family for their unwavering support throughout the research.

Drying is a critical step within the printing process of a solvent-based ink. This provides the means of generating a solid film from the fluid which has been printed. The drying process can determine the rate of evaporation and has a definitive effect upon the quality of the final film. Previous research has provided a qualitative understanding of polymer-solvent systems, but now that boundaries are being pushed, driven by practical and commercial applications, a quantitative understanding of the processes is required. The work reported here is designed to provide an understanding of the physical and structural processes involved within a drying solvent-polymer-pigment system. The research focuses upon the conventional solvent systems but the techniques and methodologies could be applied to water-based systems. The work has attempted to observe and analyse the structural changes, such as the gelation process, throughout the drying system by means of rheological tests, as well as the physical changes (eg. solvent loss) by use of Fourier Transform Infrared Spectroscopy (FTIR) and Multi Speckle Diffusing Wave Spectroscopy (MS-DWS). A number of parameters were varied to understand their influence on the processes, in particular the polymer resin (polyamide and nitrocellulose). The system was also tested with and without pigment and over a range of initial resin content. The polyamide system was a single solvent system, whereas the nitrocellulose system was a multiple solvent system.

Using the results from the experiments carried out, combined plots of diffusion coefficient, viscoelasticity and molecular movement for the polyamide and nitrocellulose systems are produced describing the complete process of drying in solvent-based ink systems. The two systems show fundamental differences in the way the structure changes throughout drying, with polyamide maintaining a fluidic structure throughout the drying process, gelating rapidly at higher polymer concentrations. The nitrocellulose system had a more gradual gelation process which in turn effects the diffusion process. Skinning is seen to occur rapidly, at a much earlier polymer concentration.

The plots show the decrease in diffusion coefficient with the increase in viscoelasticity. The rate at which this happens is greater for the surface than the bulk. The concentration at which this begins, decreases with increased capillary number, due to the film becoming dominated by viscous forces rather than surface tension. The polyamide system, with an extended period of low viscoelasticity (low Ca) allows a longer period for potential mass transfer of solute, whereas nitrocellulose does not. The increase in capillary number also reflects an increase in the rate of skinning at

the surface, increasing the gap in polymer concentration required for a viscoelastic change to occur in the surface and bulk.

It was found that the structural changes due to the gelation process of the polymer are critical to the physical changes, such as solvent loss, throughout the drying system. The polymer used within the system had a fundamental effect upon the process, with a different gelation process a critical factor. This gelation process occurs at different rates dependent on the initial resin concentration, especially at the surface. Increased resin concentration, increases the amount of skinning that occurs, hindering the solvent loss. The addition of a small percentage of pigment to the process does not have a substantial influence upon the gelation process within the bulk, but increases the effect of skinning further and hindering solvent loss. These results and values are able to provide data to be applied to a quantitative model to increase the knowledge and understanding of the processes involved throughout drying and the parameters that influence the process.

# Contents

# Chapter 1

# Introduction

Drying is a critical step within the printing process of a solvent-based ink. This provides the means of generating a solid film from the fluid which has been printed. The drying process can determine the rate of evaporation and has a definitive effect upon the quality of the final film. Within the industrial printing process, forced drying by heat and air is normally used, as this decreases the drying time.[1, 2, 3] For the printed electronics industry, high precision of the printed ink is critical.[4] For example, a small variation in the surface or dimensions of the printed area will cause large variation in the conductivity. A greater understanding of the effect of drying on the final properties of the printed ink is vital in creating working devices.

The objectives of the research were:

1. to establish the structural and physical processes occuring throughout the drying of polymer-solvent systems;
2. to understand the effects of the polymer (resin) used on the drying processes;
3. to understand the effects of the solvent mixtures on the drying processes;
4. to understand the effects of solid particle content had upon the drying processes;
5. to characterise the drying system, by observing and quantifying the influence and effects of the structural and physical processes involved.

## 1.1 The Printing Process

The printing industry has such large variation of printing substrate and printing ink able to be used within the printing processes, being adaptable to many applications. It has commonly been used for printing graphic-based products, such as on food

packaging or newspapers. It is however, also being used for the printed electronics industry.[5]

## 1.2 Ink Composition

The formulation of inks is a complex process, in which parameters such as rheology, adhesion and curing have to be taken into account and varied accordingly. [6, 7] There are various components that are changed to create the correct ink for the intended application. There are two basic ink types – liquid and paste. Both consist of four main components; pigment/dye, solvent, base and additives. Liquid inks are usually less viscous inks used within the gravure and flexography methods. There are three main types of liquid ink used: uv curable, water-based and solvent-based. Paste inks are typically oil based and usually used within lithography and screen printing due to being more viscous. Due to the variation of components to produce inks, the boundary between the two classes of inks is not distinct. This thesis will focus on liquid inks as they are the basis for solvent-based inks for flexography, used within graphics and electronics printing.

### 1.2.1 Liquid Inks

Water-based inks are becoming more favourable within the graphics industry due to a percieved reduction of environmental impact due to lower volatile organic compound (VOC) emissions. Water-based inks are used predominantly for printing on porous substrates such as paper or paperboard. There are major hurdles to be overcome for water-based inks to be used on non-porous films such as plastics, due to surface tension and lack of adhesion of the ink to the substrate. At this time, modifications to the ink as well as the substrate have to be carried out to minimise these effects. Furthermore, the drying of a water-based ink is very different than a solvent-based ink as usually water is not as volatile as solvents. For these reasons, the dryers used have increased air flow and the production speed is lowered to compensate. [1]

UV curable inks are used increasingly within the graphics industry due to their stability throughout the printing process and their ability to produce vivid colours. They do not dry in air, instead requiring direct concentrated uv radiation to cure. This is achieved by the cross-linking of the ink components by use of photo-initiators to form a solid. There is no removal of material, so the delivered volume is the applied volume to the substrate. The use of uv inks can reduce the time for cleaning and waste as the ink stays wet throughout the process until cured. There is also less

involvement from the operator as the consistency of the ink stays similar throughout the run. [2]

Solvent-based inks are predominantly used for non-absorbent substrates such as plastic and metal films. Even though there is increased regulation on solvent use, there are still a number of solvents that are available.[3] Due to some electronic materials only being able to successfully go into solution in solvents, along with their ability to print on non-porous substrates with a range of pigments and resins available, solvent-based inks are being used in the initial research on electronics printing. This is in addition to their use in the graphics industry.

### 1.2.2 Pigment

A pigment is used to provide colour or functionality to the ink. [6, 7] Pigments are used as there is a stronger colour imparted compared to that of dyes. The use of pigments within ink creates a solid particulate phase within a liquid phase dispersion. Pigment is needed to produce a colour density which is high and constant throughout the desired bandwidth. As well as the colorimetric criteria needed, the physical properties such as particle size, density and concentration have a large influence on the choice of pigment. Pigments can also be used to influence the overall physical properties of the ink dispersion. The practice, called pigment loading, is used to influence such properties as rheology, or in specialised groups of ink, the metallic content and conductivity. In metallic inks, micro platelets of metal are used to produce a visually metallic effect. In conductive inks, more expensive metals such as silver and palladium are used for the printing of electronics. The characteristics of the pigment geometry, loading and pigment surface properties affect the ink flow during drying so are critical in the formulation of an ink.

### 1.2.3 Solvent

The solvent provides a medium to which three roles can be satisfied.[6, 7] It provides a means to disperse other constituents in a liquid, and provides a means by which the viscosity can be altered. The third role is to provide a medium that is volatile and is released throughout the drying process. The solvent volatility is affected by the evaporation rate which is governed by the solvent boiling point, heat of vaporisation and vapour pressure. As well as the volatility, there are other factors that influence the choice of solvent. The chemical properties are important for the other two roles that a solvent satisfies. The solvent needs to be chemically stable when

part of a dispersion, where chemical solubility and compatibility are required. This chemical compatibility has to satisfy not only the dispersion, but the printing press and substrate. The bonding between substrate and ink relies on chemical interactions between the components which in some cases is initiated by the solvent. Printing on polymer substrates, however, may lead to the softening of the substrate due to the solvent.[7]

The solvent must be able to dissolve the resin precursor but not the pigment while not adversely affecting the final application method. Industrial pigments are normally developed to be inert to solvents, however leaching of solvents into pigments can occur causing a reduction in the colour strength. The final application can also be affected by retained solvent present after the drying process, for example food packaging, where migration of the solvent to the product is possible. In this instance, the choice of solvent is restricted. The physical characteristics of the solvent have a large effect on the suitability. Surface tension, viscosity and volume ratio of solvent are all important to optimise the print.

### 1.2.4 Base

The base consists of a polymer or copolymers chosen to form a binding film when polymerisation has taken place. The polymer required is usually supplied as an incompletely reacted prepolymer which is dissolved in the appropriate solvent. The viscosity can be determined by the prepolymer molecular mass and can be tailored by the chemistry of the prepolymer.

The base provides a medium, with the appropriate viscosity and rheological properties, for storage and transport of the particles/pigments within the ink.[6, 7] The base also provides a binding agent between the pigment particles and between the pigment and the substrate.

There are two types of polymer used in the printing industry: natural and synthetic. Natural polymers are rosins found from pine tree amber secretions. The rosins normally undergo modification and purification before use. Another natural polymer is cellulose, although it is normally considered synthetic due to the number of modification and purification processes it undergoes. There are a number of synthetic polymers used in inks. Common synthetic polymer groups employed are acrylics, alkyds, epoxies, amides and nitrocellulose. Acrylics are used due to their flexibility and solubility in most solvents. Alkyds are used predominantly in paste inks to provide flexibility and adhesion to the hard polymers. Epoxies are used for

their adhesion quality, amides for their flexibility and adhesion on a variety of films, and nitrocellulose is used for its rub resistance and solubility. [6, 7]

### 1.2.5 Additives

An additive provides a particular physical or chemical property required by the ink for a specific printing process or final application.[6, 7] Many additives are used to overcome problems within the printing process. Another important group of additives are surfactants, which alter the surface chemistry, to improve interaction between the base, pigment and substrate, allowing normally immiscible liquids /solids to mix. To alter the mechanical properties of the ink, plasticisers are used, which provides the ink film with an acceptable degree of flexibility to allow for deformation within the printing method and final application. [6, 7]

### 1.2.6 Substrate

The substrate influences the ink flow process. It is the foundation on which the process takes place. Therefore, the composition of the substrate and factors such as porosity and roughness are important. It is due to these factors, phenomena such as capillary action can take place. External pressures and effects can also be accentuated by the substrate.

Barros et al [8] found that the ink transfer is directly influenced by the substrate and the print forme properties. The surface roughness and the hardness of the forme were found to be more important than that of the substrate surface energy. Absorbancy, pre-wetting and drop instability due to the substrate roughness are all sources of variability for the contact angle which can lead to deterioration within the wetting, spreading, levelling and drying processes.

### 1.2.7 Viscosity

Viscosity is the measure of the resistance of a fluid to being deformed by shear stress or extentional stress and clearly showing the relationship held between them. A shear stress can be applied to a fluid, resulting in a decrease or increase in viscosity due to shear thinning or thickening respectively. The viscosity of the fluid on a substrate will also affect the shear stress it exerts upon the substrate when the fluid is flowing. This relationship is complicated by the classification of Newtonian and non-Newtonian fluids, where non-Newtonian fluids do not conform to the basic linearity model of Newtonian fluids. [9]

The viscosity of certain fluids within the viscoelastic range are dependent on the degree of shear load. When the viscosity decreases with an increase in shear, this is classed as shear thinning. When the viscosity increases with increasing load, this is classed as shear thickening. Both shear thinning and shear thickening can be ascribed to the behaviour of polymers within the fluid.

For a shear thinning fluid, during the shear process, the polymer will align with the shear direction. In doing this, they will be able to disentangle, lowering the flow resistance. This corresponds to a decrease in viscosity.

Shear thickening can occur in concentrated unlinked polymers due to entanglements between the molecule chains. An increase in shear load increases the degree to which the molecules prevent the relative motion between the molecules.

Viscoelastic fluids can undergo time dependent shear behaviour. Thixotropic behaviour involves the fluid decreasing in structural strength when undergoing a shear load. When the shear load is removed, the structure returns. This is a cyclical process performed with a constant shear load. If the process is not cyclical, it is referred to as structural decomposition, not thixotropic.

Rheopectic behaviour involves the fluid increasing in structural strength when undergoing a high shear load. When the shear load is removed, the structure is lost. This, again, is a cyclical process performed with a constant shear load. [10]

## 1.3 Closure

The work reported here is designed to provide an understanding of the physical and structural processes involved within a drying solvent-polymer-pigment system. The research focuses upon the conventional solvent systems but the techniques and methodologies could be applied to water-based systems. The work has attempted to observe and analyse the structural changes, such as the gelation process, throughout the drying system by means of rheological tests, as well as the physical changes (eg. solvent loss) by use of Fourier Transform Infrared Spectroscopy (FTIR) and Multi Speckle Diffusing Wave Spectroscopy (MS-DWS).

The thesis is set out in the following format:

- Chapter 2 - A Literature review of the processes that effect the drying of solvent-polymer-pigment systems.
- Chapter 3 - A description of the techniques and apparatus used throughout the experimental research to test the drying processes.

- Chapter 4 - This chapter describes an investigation into the bulk rheology of a drying system to assess the structural changes within the system, by monitoring the viscoelasticity.
- Chapter 5 - Following on from chapter 4, this chapter investigates the surface rheology of a drying system to assess the structural changes at the surface, by means of viscoelasticity. A novel geometry (Dunouy Ring) was also used and compared to the standard Bicone geometry.
- Chapter 6 - This chapter describes an investigation into the structural changes as well as the solvent loss of a drying system by means of MS-DWS.
- Chapter 7 - This chapter describes an investigation into the solvent loss of a drying system by monitoring the chemical absorption using FTIR.
- Chapter 9 - This chapter uses the results from the previous investigations and discusses the overall drying process.
- Chapter 10 - This chapter draws conclusions from the results and discussion and suggests further work.

# Chapter 2

# Literature Review

## 2.1 Introduction

The key processes within drying have received some attention in the literature and are often considered as a series of isolated phenomena, although they may in fact take place concurrently. The thesis is focused on the drying process once the ink is transfered as a film to a substrate. This chapter will review the research carried out on these key processes and phenomena of a drying system. These are as follows:

1. The transfer processes involved in the printing process prior to a film being formed on the substrate.
2. The stages of drying of a water-based and solvent-based polymer system and the factors that effect the evaporation rate.
3. The physical processes involved in the mass transfer of solvent through a drying system.
4. The theory of diffusion of solvent through a polymer system.
5. The structural changes of a polymer system through gelation and polymer interaction.

An understanding of the processes and phenomena are developed throughout the review of literature and provides a basis for which to develop the research carried out in this thesis.

## 2.2 Ink Flow During Transfer Processes

The transfer processes, and their potential influence upon the ink flow in printing are briefly discussed. The drying process will be affected by the outcome of the transfer processes and their influence upon the ink flow and fundamentally on the topography of the film.

### 2.2.1 Surface Tension

Surface tension is a significant factor within the transfer and drying processes and acts to minimise the total energy of the interface interaction. It is a property of the surface of the liquid that causes it to behave as an elastic sheet. The phenomenon is the result of intermolecular attraction and capillary action. Within the bulk of the fluid, the molecules are attracted equally in all directions by neighbouring molecules. This creates a net force of zero. The molecules at the surface are attracted inwardly, balanced only by the resistance of the liquid to compression. This leads to no net inward force, but instead a driving force to decrease the surface area. Surface tension is equivalent to line tension acting in all directions parallel to the interface. When no force is acting upon a tensioned surface, the surface remains flat. When a pressure is applied to the surface, the pressure difference over the surface area produces forces as shown in Figure 2.1, where $F_F$ ,$F_B$, $F_L$ and $F_R$ are the force over the surface to the forward, back, left and right directions and $R_y$ and $R_x$ are the principal radii of curvature in the y and x directions:

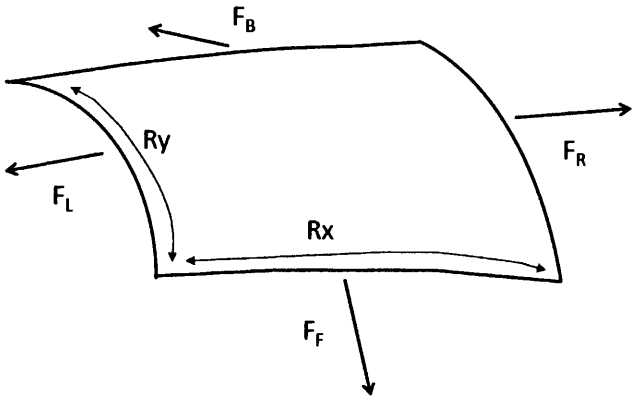


Figure 2.1: Schematic Diagram of Surface Tension and the Related Forces

For surface tension to cancel the force due to pressure, the surface has to be curved. The balanced forces of the surface area results in the Young-Laplace equation [11]:

$$\triangle p = \gamma \nabla . \bar{n} \tag{2.1}$$

$$= 2\gamma H \tag{2.2}$$

$$= \gamma \left( \frac{1}{R_x} + \frac{1}{R_y} \right) \tag{2.3}$$

where $\Delta p$ is the pressure difference across the fluid interface, $\gamma$ is surface tension, $\bar{n}$ is the unit normal to the surface, $H$ is the mean curvature and $R_x$ and $R_y$ are the principal radii of curvature. [11]

### 2.2.2 Wetting

Dynamic wetting involves the displacement of two immiscible fluids (air by liquid in this case) on a solid surface. The phenomenon is a result of intermolecular interactions when the two interfaces are brought together.

The contact angle ($\theta$) between the interfaces is the angle at which a liquid interface meets a solid surface and is a key indicator in the wetting process. The wettability of the surface is defined by the contact angle; $90^0$ or greater is not wettable and below $90^0$ is wettable.

The wetting process can be greatly influenced by the contact angle.[12] The magnitude of the dynamic contact angle is a function of the velocity of a fluid-fluid interface (air to liquid in this case) relative to a solid wall. The dynamic contact angle varies with the capillary number (Ca) as the dynamic wetting process is affected by solid surface properties such as material nature, roughness, porosity and electrical charges.

Dewetting is the rupture of thin liquid films on a substrate. The determining factor of the process may be expressed by the spreading coefficient [13] and is dependent upon the surface tension of each interface.The result of the phenomenon is the formation of droplets upon the substrate due to the spreading of the thin film.

A study [14] showed that the spreading of liquid drops, formed by liquid injection through an orifice, was the result of capillarity and gravity forces - capillarity force for small drops when gravity is negligible and gravity for large drops.

### 2.2.3 Levelling

Levelling is what naturally occurs when a liquid film spreads out on a substrate. This process leads to a smoothing of the initial irregular film deposited. Surface tension

is a significant factor influencing the levelling, although its effect is opposite to that of spreading. ie. an increase in surface tension leads to accelerated levelling. Other external forces are influential in the levelling process as well as the deposited film itself.

Modelling of the levelling process has been undertaken. Orchard [15] produced a linear theory based on a two-dimensional, sinusoidal Newtonian coating layer. This described the rate of levelling as a function of average film thickness, surface tension, viscosity and ripple wavelength. This is illustrated in Figure 2.2, where $h(\tilde{x}, \tilde{y}, \tilde{t})$, is the coating height, $h^{(0)}$ is the average initial coating height, $g$ is the acceleration due to gravity, and $\lambda\tilde{x}$ is the wavelength of the initial disturbance in the $\tilde{x}$ direction.

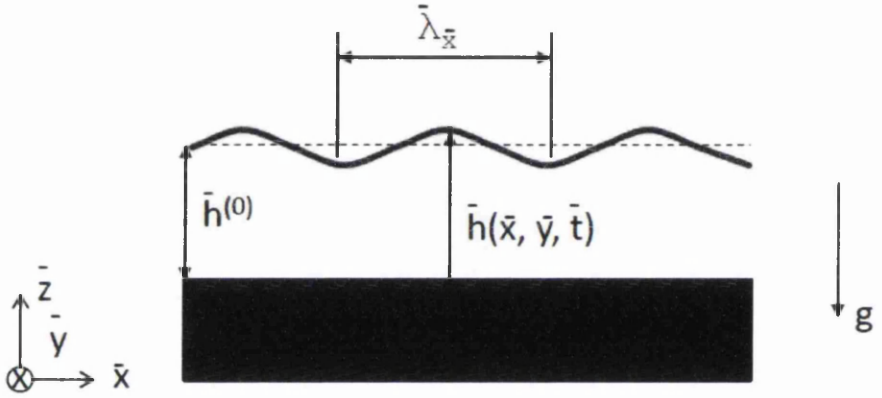


Figure 2.2: Schematic Diagram of a Thin Liquid Film Coating on an Impermeable Horizontal Substrate.

A study by Tekin et al [16] of thin polymer films produced by droplet array was undertaken to show the significance of the solvent on the levelling of the film within the drying process. Use of a single solvent solution led to ring formations. These could be reduced by use of low vapour pressure solvents. This however, did not completely prevent ring formation. The use of mixed solvents was studied using a low and a high boiling point solvent. A large difference between the boiling points was seen as advantageous and prevented ring formation. If the contact line is fixed and the evaporation losses are replenished, the liquid is transported from the centre of the film to the edges. One solvent will evaporate slower than the other. This will lead to an increase in concentration of that solvent at the edges. The increase in concentration will produce a decrease in local vapour pressure and in the rate of evaporation at the edges, as well as a decrease in the volume of liquid transported from the centre to the

edge. Overall, a combination of mixed solvents with low contact angles was found to be advantageous in terms of film uniformity.

## 2.3 Drying

### 2.3.1 Stages of Drying

Drying is the process of mass transfer, resulting in the removal of fluid by evaporation, and leading to a solid state. Within the ink printing process a solvent is the fluid to be evaporated to leave the pigment and base upon the substrate. This varies depending upon the ink composition.

Mujumdar [17] describes three stages in the thermal drying of a wet solid in a water-based system and analyses the factors controlling the rate of drying at each stage. Figure 2.3 represents the three stages of drying:

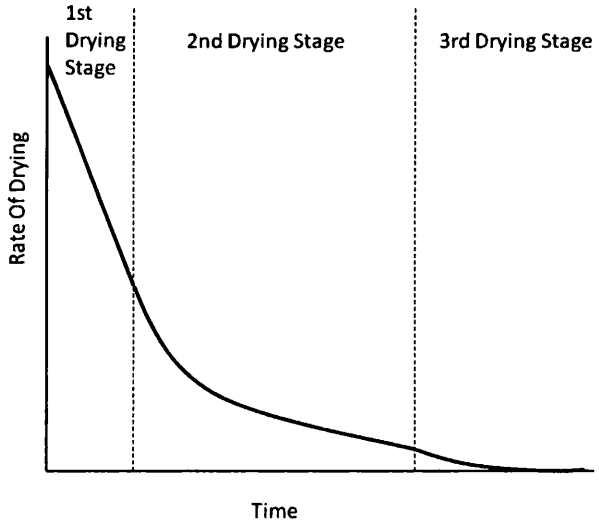


Figure 2.3: Representation of Three Drying Stages Theorised by Mujumdar

According to Mujumdar [17] there are two distinct processes that occur simultaneously during drying. The first process is a transfer of energy, mostly as heat, from the surrounding environment to evaporate the surface moisture. This involves the removal of water as vapour from the material surface. This process is reliant upon external conditions such as temperature, air humidity and air flow, pressure and the area of surface exposed. The second process is a transfer of internal moisture to the surface of the solid and its evaporation due to the primary process. This process is a function of the physical nature of the solid, temperature and moisture content.

These two processes occur throughout the three stages of drying where the unbound moisture is removed from the wet solid by either evaporation or vaporisation. Evaporation occurs when the vapour pressure of the moisture on the solid surface is equal to the atmospheric pressure.

The first stage described by Mujumdar [17] has a constant drying rate where vaporisation removes the free moisture from the surface. When the entire solid surface ceases to be wetted, the first stage of drying ends and the second stage begins. The drying rate decreases at this point while the rate per unit wet solid surface area remains constant. The vapour movement by diffusion and capillarity from within the solid to the solid surface control the rate at this point. The third stage consists of heat transfer to the surface and heat conduction within the product. The rate at which moisture travels through the solid is controlled by concentration gradients from within the solid to the solid surface. Throughout this stage the rate of drying decreases rapidly. Throughout the drying process, the transition between the stages is not abrupt. Throughout the drying process, moisture content within the wet solid or liquid is a key factor.

Another contribution to the process of drying was made by Hansen [18] where he considers two distinct phases in the drying of a polymer film on an impermeable substrate. The objective of the research was to understand the evaporation of solvent through a polymer film formation which applies directly to the systems researched in this thesis. These phases are dependent upon the resistance to solvent loss at the air-liquid interface and the resistance to diffusion of the solvent within the film to air interface. The first resistance ($R_s$) is affected by the vapour pressure of the solvent (the latent heat of vaporisation) and the solvent transport through a thin air layer which is constant during drying. The second resistance ($R_d$) is the diffusion coefficient during drying which decreases exponentially as the solvent concentration decreases. The two phases are dependant on the dominance of $R_s$ and $R_d$ in retarding solvent loss.

Solvent loss in the first phase is controlled by phenomena at the air-liquid interface. Within the first phase, when $R_s$ is greater than $R_d$, there is a major resistance to solvent loss at the air surface. $R_d$ then increases as the solvent evaporates. When $R_s$ is less than $R_d$, the solvent concentration at the surface falls rapidly to zero. The solvent has either a linear or compact molecular structure resulting in a higher diffusion coefficient. With ten to twenty percent of solvent is remaining within the film, the solvent acts as a plasticizer. However, some solvent escapes from the film by an $R_d$ controlled process before sufficient rigidity is achieved. Five to ten percent

of the solvent remains in the polymer film near the air surface, due to exceptionally high diffusion rates at zero solvent concentration. This process of solvent diffusion is hastened by heat and air circulation. During the first phase the drying rate is proportional to the film thickness, with the time doubling when thickness doubles. This is due to double the solvent needing to pass through the air-liquid interface.

The transition period between the phases occurs when both $R_d$ and $R_s$ are of the same order of magnitude. Throughout the transition period, $R_s$ remains constant while $R_d$ increases at a rapid rate. The surface concentration falls to zero and the internal diffusion resistance slows the transport of solvent to the surface. The degree of solvent evaporation within the second phase is effected by changes within this period.

The concentration of volatile solvent in the film at a point in the drying process ($C_a$) is related to the amount of solvent required to reduce the glass transition temperature ($T_g$) to the film temperature. If the polymer's $T_g$ is less than the film temperature then there will be no clear, prolonged second phase. The solvent that remains within the polymer film with high $T_g$ after the drying will become a permanent part of the film.

Temperature is not the only external influence upon the polymer film. High air velocities across the surface results in cooling of the film producing slower through dry leading to case hardening. Therefore a lower film temperature leads to a higher concentration of volatile solvent in the film ($C_a$). $C_a$ is important for the start of the second phase. The second phase is controlled by the internal diffusion and reducing $C_a$ can result in the acceleration of subsequent solvent loss.

The second phase is the slow diffusion of solvent through the dense polymer matrix. The concentration of solvent is uniform throughout with a drop at the air interface. Due to this change in concentration, retarded diffusion occurs, leading to diffusion several orders of magnitude slower near the air surface than close to the substrate. Surfactants within the film, such as pigment particles etc, produce obstructions to free solvent diffusion also resulting in retarded diffusion. When there is an increase in the polymer chain segment mobility, there is an increase in solvent diffusion coefficient. A temperature increase or addition of plasticizer leads to increased softening of the film. Figure 2.4 shows the change in diffusion coefficient as a function of the volume fraction of solvent in the polymer film as reported by Hansen[18].

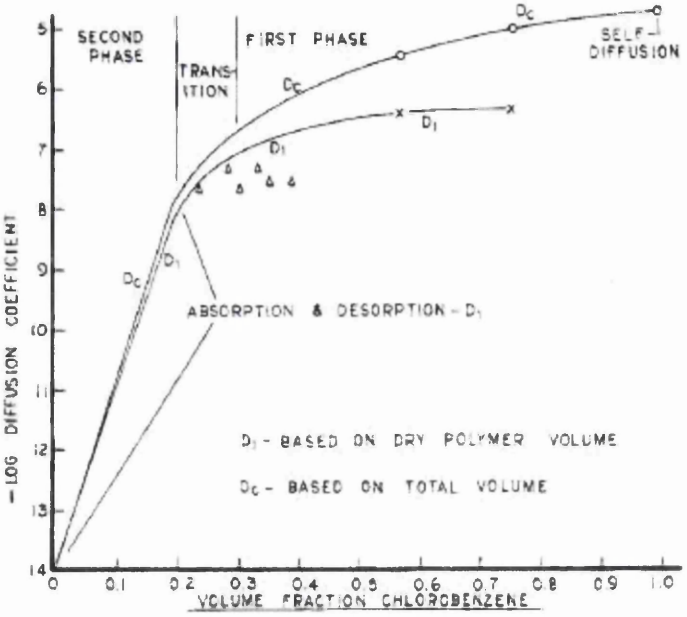


Figure 2.4: Diffusion Coefficients of Chlorobenzene in Poly(vinylacetate)

Solvent-based polymer films were modelled by Croll [19]. The magnitude of the residual drying stress within the film was found to be a function of Young's modulus as well as the volume fraction of solvent at the point of solidification in a dry film. The volume fraction at the point of solidification identifies the solvent concentration at which the transition temperature of a polymer-solvent system is equal to the ambient temperature. The glass transition temperature ($T_g$) can be illustrated by the Gordon-Taylor model [20] or alternatively, the Fox [21] or Couchman-Karasz model [22]. This transition temperature ($T_g$) has a decisive influence upon the stress development during drying, controlling the shrinkage of polymer film beyond the solidification point. In agreement with the Hansen study [18], a high $T_g$ will lead to more solvent being left in the polymer after solidification. This will increase shrinkage. The addition of plasticizers will reduce the film drying stress, altering the polymer properties and the transition temperature ($T_g$). The magnitude of the drying stress is governed by the stiffness of the polymer which is related to the Young's modulus.

#### 2.3.1.1 Evaporation

The evaporation rate is affected by many external factors as well as the physical properties of the system. The first stage is governed by the rate of evaporation of a solvent and is affected by four variables. These are temperature, vapour pressure,

surface/volume ratio and rate of air flow. Relative humidity also has an effect on certain solvents. The second stage is governed by the diffusion rate, and is controlled primarily by free volume availability. [23]

The surface air interface is the surface at which solvent evaporation occurs. Therefore, the properties of the interface are paramount in the process. The surface area the ink covers affects the rate of evaporation. The larger the area, the more solvent is able to evaporate from the system at one time. The rate therefore increases with increase in surface area.

The temperature that effects the evaporation of the solvent is the temperature of the liquid at the surface at the air. This is initially the temperature of the surrounding air. While the solvent evaporates, this temperature decreases. This cooling of the surface leads to the decrease in vapour pressure that in turn slows down evaporation. A solvent that evaporates rapidly, has a high cooling effect on the surface and leads to a sharp drop in temperature. This leads to a decrease in vapour pressure that slows the evaporation. If the evaporation occurs more slowly, the temperature drop is not as sharp, leading to the vapour pressure and consequently the evaporation rate decreasing less.

Once the solvent escapes from the surface, the molecules disperse into the air. The rate of this dispersion affects the rate of evaporation of the remaining solvent within the system. If the dispersion is slow, the evaporation is suppressed due to the partial pressure of solvent increasing at the surface. The air flow over the surface, disperses the solvent molecules away from the surface, allowing the evaporation of solvent to occur more freely from the fluid. The air flow is rarely uniform, leading to evaporation rates becoming non-uniform over the area. [23, 24]

The evaporation rate of neat solvent has been shown to be affected by a small amount by atmospheric humidity. The evaporation rate of an oxygenated solvent, such as isopropanol and ethyl acetate is found to be affected by an increase in relative humidity. Humidity also affects the evaporation of water miscible solvents, but has no affect on water immiscible solvents. Molecular interaction affects the evaporation of components from a mixture. This is especially the case if one component is hydrogen bonded and another is not. [25]

Once the evaporation of the solvent is no longer able to continue, diffusion takes over. The diffusion is not directly dependent on the volatility of the solvent. Other factors are present such as the molecular shape and size. As the diffusion of the solvent is dependent on the space between the polymer matrix to escape, the molecular size and shape of the molecule are important. Generally, the smaller the solvent molecule

is the easier it will diffuse. However, branching and functional groups increase the cross-sectional area of a molecule, leading to the increase in diffusion time. A small, linear molecule will have a high volatility and therefore diffuse easily through the polymer matrix. The larger and more complicated the molecule the longer periods of diffusion. [23, 24]

Isopropanol and ethyl acetate were used in this research. The evaporation rate of these solvents are different. Under constant evaporation conditions, ethyl acetate will evaporate approximately four times quicker than isopropanol. [26] This is significantly faster and will lead to ethyl acetate being evaporated off in the first stage of the drying process. The second stage for both the nitrocellulose and polyamide resins consist of only isopropanol diffusing through the polymer matrix formed. [24, 27]

### 2.3.2 Mass Transfer

Mass transfer describes the physical processes included in the transport of atoms and molecules within physical systems. The driving force for this is the difference in concentration and the transfer of mass between areas of high and low concentration.

This movement of molecules from areas of high and low concentration by molecular motion is known as diffusion. The result of diffusion is a gradual equating of material towards equilibrium maintaining uniform temperature and without external forces acting upon the particles. The term mass transfer also covers convective transport processes as well as diffusion. Van Dam[28] discusses the competition between these processes and his model is illustrated in Figure 2.5, where r is the radial coordinate and h is the wet layer thickness of the drop.

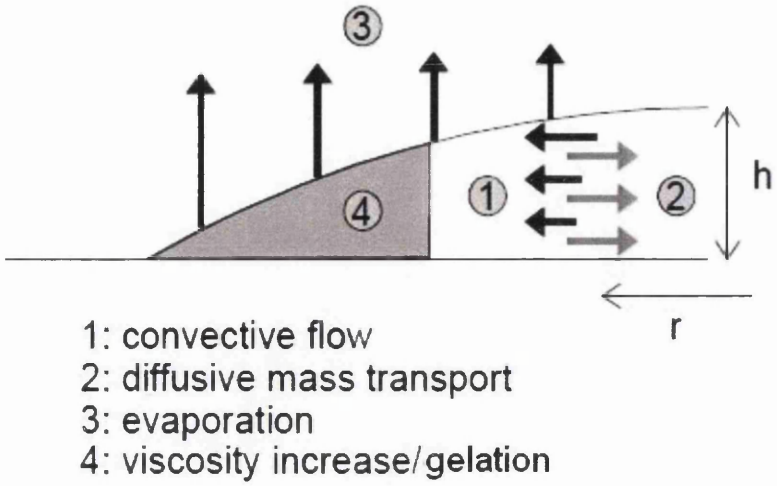


Figure 2.5: Schematic Representation of the Mass Transfer Model Situation

The difference in concentration throughout the fluid occurs through many phenomena [29]. One of these is caused by uneven evaporation of solvent resulting in local changes in concentration and temperature gradients. The primary reason for uneven evaporation is surface roughness. The fluid will dry faster on a convex surface rather than a concave surface. On a convex point, there is an increase in surface tension compared to that of the concave area which has a reduced surface tension. The surface tension is also dependent upon temperature, decreasing with an increase in temperature. The surface roughness produces areas at which the fluid or solvent can evaporate at different rates, which varies the surface tension within these localised areas, in turn changing the temperature of the fluid, producing temperature gradients. An increase in viscosity will decrease the effect of Marangoni flows. [29]

The drying of a film containing plasticizer, solvent and polymer can be affected by diffusion [30]. For example, if the diffusion rate is fast relative to the rate of interaction, then the ratio of the plasticizer to polymer remains the same throughout the interaction. There is said to be no diffusion limitation on the film. When the diffusion rate is the same order of magnitude or slower than the rate of interaction, the ratio of plasticizer to polymer will increase within the film, but decrease at the free surface. This counter diffusion of solvent and plasticizer is said to have a diffusion limitation. Significant concentration gradients can lead to potential phase separation of the fluid. [31]

Diffusion limited drying leads to an inhomogeneous distribution of solvent which leads to non-uniform stress build-up [30]. This is true for drying of suspensions of

solid particles. Due to the non-uniform mechanical properties within the suspension, the limited diffusion can lead to non-uniform diffusivity. The residual internal stress is independent of coating thickness and the initial concentration of solvent, but the mechanical properties and diffusivity vary greatly with fluid depth, even within the finished product. The internal stresses control the dispersion of solid particles within a suspension. The internal stresses in the upper layer of the fluid push the solid particles into the lower layers. This leads to holes and thin spots being created upon the surface, with the stresses being concentrated at the imperfections or boundaries. This relieves the stress at these localised areas.

The rate of drying can be limited by the mass transfer of the liquid into the overlying gas and diffusion through the liquid as well as the volatility of the solvent and contaminants. The solvent molecules leaving the interface collide with others. This reduces evaporation rate. At atmospheric pressure the rate can become proportional to the ambient partial pressure due to the condensation of solvent vapour in the overlying gas. This modifies the mass flux. Due to this, the diffusion through the overlying gas layer needs to be accounted for. This can be done through the accommodation coefficient or by the use of the mass transfer coefficient. [31]

The drying process is not isothermal. This is in part due to the equilibrium solvent vapour pressure, $p_e$, being sensitive to temperature. This temperature sensitivity of the fluid film can change the rate of evaporation. The evaporation of the fluid film during drying produces evaporative cooling, which slows the process and needs to be accounted for when it is a significant effect. [30]

If the removal of solvent at either the liquid/gas or liquid/substrate interface exceeds the rate of diffusion of solvent through the liquid to the interface, then depletion of solvent will occur. This will allow concentration gradients within the film to develop. If this continues during the transition of the film in to a solid state, it can lead to even smaller coefficients of diffusion of the solvent through the solid. This may trap solvent or impurities in the film body.

The surface tension gradients along a free surface of a fluid are balanced by viscous stresses. The surface tension net force upon the body is opposed by a retarding shear force due to the fluid viscosity. The shear force is only generated when there is a gradient in fluid viscosity which produces fluid flow. The flow is determined by the viscosity and viscous stress variations, as well as variations in pressure and surface tension. These normal and tangential components of the fluid dynamic boundary condition operate together and all affect the fluid flow. [31]

Once solidified, a liquid film can develop significant stress build up. This stress, once beyond a critical value can produce defects within the film. Shrinking from loss of solvent is a factor due to increased stress. Other factors that cause stress throughout the film are phase transitions and separations, reactions and temperature changes. [30]

Stress within an ordinary Newtonian liquid is nonzero only during deformation with a nonzero rate of strain. For liquids other than Newtonian liquids where stress can exist without concurrent stress, ie. viscoelastic, or suspensions of solids, stress can be determined by past deformation. The point of transition between liquid and solid is not well defined. Bierwagen [32] modelled the transition to occur when there had been enough solvent removed from the liquid so that the particles were closely packed. The diffusion rate decreases, which hinders the film drying. Whitham and Perera [33] measured the rheological behaviour and drying rates, finding that rheology and diffusional resistance were related, but did not correlate well with idealized predictions. Beyond the transition period, further drying causes film shrinkage and stress buildup. If diffusional resistance is minimal within the film, the volume fraction of solvent is independent of positon. This produces a transition solvent volume fraction. When solvent decreases below the volume fraction, there is an increase in stress within the film. Where the film adheres to the substrate, the $x - y$ plane can be said to be fixed. [29] Therefore the liquid film can only shrink in the $z$ direction, normal to the film. This stretches the $x - y$ plane and compresses the $z$ direction

When mass transfer ceases, there is a viscosity change during evaporation. There comes a point at which there is a critical solute concentraton and viscosity increase due to evaporation resulting in no solute transport being possible. This provides a sudden change in rheology and a subsequent increase in capillary number $C_a$. The capillary number is a dimensionless number that relates surface tension and viscosity by the ratio [11]:

$$Ca = \frac{\eta v}{\sigma} \tag{2.4}$$

where $\eta$ is viscosity, $v$ is the characteristic velocity and $\sigma$ is the surface/interfacial tension between two fluid phases.

In each case the main parameters are the same, but the exact equation does vary slightly dependent on the system. Van Dam [28] relates this to the drying inkjet situation with spherical cap geometry, e.g. a dome with a flat top. This is as close to the model ink system used in the thesis that is currently available. The equation is shown in equation 2.5. [28]

$$Ca = \frac{\eta \times V_e, a_v}{\sigma} \left(\frac{r_0}{h_0}\right)^4 \tag{2.5}$$

where $\eta$ is the viscosity and $\sigma$ is the surface tension of the solution. $v_e, a_v$ is the average evaporation rate of a droplet of solution defined as the evaporating volume per unit of time divided by $\pi r_0^2$, and $r_0$ and $h_0$ are the radius and central layer thickness of the droplet during drying.

The capillary number quantifies the relative importance of viscous forces to surface tension forces in distorting the interface away from a static-looking shape.[34]With small, non-zero capillary numbers, there is a distinction between static and dynamic problems. The shape of the interface may remain static-looking but due to the dynamic contact angle, the interface is flowing. For Newtonian fluids, the capillary number governs the instabilities such as pressure gradients generated by viscous flow and which are stabilized by surface tension. For non-Newtonian fluids the critical capillary number can be reduced by small amounts of elasticity. This enables control over the fluid by the varying of capillary number. [35]

Another dimensionless number relating viscosity and surface tension is the Marangoni number ($Mg$). This differs from the capillary number as it relates viscosity with surface tension gradients. When viscosity is low, this decreases the film thickness which in turn reduces the Marangoni number. Rehg and Higgins [36] state that spin coated films from low viscosity solutions are stabilized by the dynamic thinning process. If a fluid is initially susceptible to Marangoni convection, the instabilities do not increase to an appreciable magnitude. Instead, the flow is restabilised by viscous forces which become more important as the film thins. [37]

## 2.4 Diffusion

Fick's law [38] and the subsequent theoretical models describe the process of absorbtion of a solvent into a polymeric material. This is the reverse process carried out during the drying process, however the mass transport and the mechanisms involved are similar.

### 2.4.1 Fick's Law

A polymeric material has many physical properties. Associated with these are transport mechanisms. The mass transport process of a solvent through a polymeric material involves three steps; the solvent molecules are absorbed onto the surface of

the polymeric material; the molecules then diffuse through the polymer; and finally desorb on the downstream surface of the polymer [39, 40]. Polymer chains rearrange within the material to accommodate small molecules causing the polymer to swell. The duration and intensity of the steps are influenced by factors such as the structure of the substrate, fillers and temperature [41, 42]. On diffusion through a material in a rubbery state, large segments of the polymer participate due to chain rotation, translations and vibrations. This is due to an accessible large internal void space. When the material is in a glassy state, the polymer is hard and brittle with limited chain motion. There is therefore less free volume than in the rubbery state. In a polymeric material with a temperature below that of the glass transition temperature ($T_g$), a state of non-equilibrium exists, and properties are time dependent.

#### 2.4.1.1 Fick's Law Case I

The mass transport process is governed by Fick's law, or Fickian diffusion, which relates the flux linearly with concentration gradient. This is shown in equations 2.6 and 2.7 [38] :

$$J = -D\frac{\partial c}{\partial x} \tag{2.6}$$

$$\frac{\partial c}{\partial t} = -\frac{\partial J}{\partial x} \tag{2.7}$$

where $J$ is the diffusion flux, $D$ is the diffusion coefficient, $c$ is the concentration gradient, x is the position and t is time.

The first law assumes the flux ($J$) through a unit area of material is proportional to the concentration gradient ($c$), measured normal to the material. The constant of proportionality is called the Diffusion Coefficient ($D$) [43]. The second law states that the concentration change (as a function of time), is related to the change in flux (with respect to position).

Fick's Law requires that the surface concentration attains it's equilibrium value immediately upon a change in conditions and remains constant through the sorption process. Solvent-polymer systems, however, do not behave as such. This is represented by Case II Diffusion.[44, 45]

#### 2.4.1.2 Non-Fickian Case II Diffusion

Non-Fickian diffusion or Case II diffusion dictates that a sharp front, which separates the dry polymer from the swollen polymer moves linearly with time.[46] The mass uptake ($M$) of solvent can initially be represented by [46] :

$$M = kt^n \tag{2.8}$$

where $t$ is the time, and $k$ and $n$ are constants. In this case Fickian sorption corresponds to $n = 1/2$. Case II diffusion is associated with $n = 1$ and anomalous diffusion is associated with $1/2 < n < 1$.

Case II diffusion features a sharp boundary front that separates the swollen region from the dry/glassy region, established after an initial induction time. This front moves into the polymer with a constant velocity, causing the amount of fluid being absorbed to increase linearly with time. Ahead of the front is a small Fickian precursor within the dry region. [47]

The transport of a penetrant into a polymeric material can also be explained in terms of the thermodynamics and kinetics. [48] Thermodynamics is considered as the solubility and swelling while the kinetics is regarded as the diffusion. Solubility can be formulated in terms of a solubility parameter originally proposed by Hildebrand. [49] Swelling is closely related to the solubility although similar Hildebrand parameters do not always result in swelling. This was expanded by Hansen [23] into three components; the dispersion force, hydrogen bonding and polar components. The molecular dimensions of the permeant molecules have to be small enough to enter the lattice network of the polymer. Due to the swelling of the network caused by permeant molecules, the network chains assume elongated configurations and elastic restrictive forces develop in opposition to this swelling. Equilibrium is reached when the elastic restoring force of the network chains balance the osmotic pressure driving the penetrant into the polymer. [50] Deviations from the Fickian diffusion occur as a consequence of finite rates of diffusion. This results in changes in polymer structure in response to stresses imposed upon the material before and after the sorption/desorption process. If a polymer is partially crystalline or contains fillers, the transport process is dependent upon the degree of crystallinity and the properties of the fillers. [50, 51] The polymer may exhibit penetrant induced crystallization, which results in orthotropic swelling, increasing the complexity of the process. [52, 53]

### 2.4.2 Diffusion Coefficient

The diffusion coefficient is a proportionality constant. The diffusion coefficient is used throughout fluid mechanics and physical chemistry as a comparitive measure of diffusion rate between substances and systems. The constant is used within Fick's law to relate flux with concentration. The higher the diffusion coefficient of a substance,

the quicker the substance will diffuse into the other. The diffusion coefficient of a rigid spherical particle through a continuum of solvent can be estimated using the Einstein-Stokes equation. This states that for a sphere of radius r, dispersed within a fluid, the diffusion coefficient is related to temperature and the inverse of viscosity by:

$$D = \frac{k_B T}{6\pi\eta r} \tag{2.9}$$

where $D$ is the diffusion coefficient, $k_B$ is the Boltzman constant, $T$ is temperature, $\eta$ is viscosity and $r$ is the radius of the spherical particle. This equation was derived for larger spherical particles within a small solvent and is said to be only twenty percent accurate. [31] However, this is the relationship upon which other correlations are judged.

Adaptations of the Einstein-Stokes equation have been undertaken for various situations. For use with small solutes, the factor of $6\pi$ is replaced by $4\pi$ or $2\pi$. The $4\pi$ factor is to signify the slipping of the solvent over the surface of the solute molecule. $2\pi$ is due to the theory of absolute reaction rates. However, these substitutions do not always work. The diffusion coefficient of solvent through dilute polymeric solutions is more complex to estimate. A correction to the equation is made to allow for the non-rigid non-spherical particles. The equivalent radius of the polymer is estimated instead by:

$$R_e = 0.676(R^2)^{1/2} \tag{2.10}$$

where $(R^2)^{1/2}$ is the root mean square radius of gyration; a measure of polymer radius. This correction is used for polymer systems in which an ideal solvent is used. When a 'good' or 'poor' solvent is used, the polymer radius ratio is less well known and can vary significantly with increased viscosity.

The Einstein-Stokes equation is used to estimate the diffusion coefficient of a wide variety of systems, however there is not an adaptation that provides an accurate estimate. This becomes less so when trying to estimate the diffusion coefficient of polymer-based systems. [31]

## 2.4.3 Theoretical Models

### 2.4.3.1 Assumed Boundary Conditions

Theoretical studies to model the diffusion process are based on Fick's Law. Explicitly, the rate of transport through a unit area is proportional to the concentration gradient

measured normal to the area. Assumptions are made, the easiest being the diffusion coefficient, $D$, is constant and the surface concentration of solvent immediately attains equilibrium and remains constant throughout the sorption process. As well as assumptions for boundary conditions, the models do not include the interaction of the penetrant and polymer, or the physical properties of the polymer.

#### 2.4.3.2 Polymer Involvement

Thomas and Windle [54, 55, 56] made a major advance by suggesting that the diffusion process is strongly coupled to the mechanical response of the polymer. The model represents a coupling between the osmotic pressure driven viscous response and the Fickian diffusion. It does not account for the effect of external stress or strain upon the polymer but it can qualitatively predict most characteristics of Case II diffusion.

Wu and Peppas [57, 58] researched two kinetic processes governing Case II diffusion; the kinetics of solvent penetration and a process that involves highly non-linear material deformation. The process was characterized by the use of a diffusion Deborah number [59],which is the ratio of mechanical to diffusion relaxation time. A large Deborah number is associated with the sorption process which is controlled by mechanical relaxation.

It is widely accepted that possible polymer swelling plays an important role due to osmotic stress. The transport of penetrants are driven by molecular diffusion and by the stress associated with swelling [60, 61, 62, 63, 64]. The previous models are a modification of the classical Fickian diffusion equation in order to account for the effect of stress. The introduction of a constitutive equation to account for the time evolution of stress is added.

Depending upon the polymer used within the drying process, the final product can finish in the rubberised state, or continue to the glassy state. The mass transfer through a glassy polymer involves non-equilibrium states, therefore the thermodynamics has to be extended to account for the irreversible processes. [65] A mesoscopic method to describe the non-Fickian diffusion processes has been used [66, 67, 68, 69, 70]. The method is able to account for the reversible and irreversible processes involved, as well as the structural changes of the polymer due to swelling or other external stress effects. The model still maintains the effects of the concentration of the penetrant and the flux state variables within the polymer. The mesoscopic theory is advantageous as it automatically satisfies the laws of thermodynamics. The model shows the flux is driven by the concentration gradient and also a conformation

tensor gradient. This accounts for the internal structural change of the polymer. This also includes the effects of a moving boundary.

The rate of diffusion has been shown to have a clear dependence on solvent structure and polarity. (Guo et al [71]) A more streamlined shaped solvent permeates more rapidly than that of a bulky one. Also, non-polar solvents permeate more rapidly than polar ones in non-polar polymeric structures. The reverse is true for polar solvents. Theoretical attempts to correlate these properties with gas or liquid permeations have not been successful.

Elafif [69]couples the Fickean equations of diffusion with rheology for a simple-complex fluid system within a framework of equations. This framework unifies previous formulations and extends them to a more complete analysis. Using this framework of equations it was able to be observed that in the absense of external forces the mixture reaches an equilibrium state described by equilibrium thermodynamics. It is also observed that when close to equilibrium, the diffusion within the mixture is described by classical fickean diffusion. The diffusion-rheology coupling for a simple-complex fluid system, involves the application of Fickean law with the addition of stresses and a new rheological equation of state in which the diffusion flux is involved. Using the equations gained by Elafif for simple-simple fluid systems, it is shown that when the system is inhomogeneous, the diffusion is non-fickean and the rheology viscoelastic. This shows that the homogenity of the fluid system has a significant effect upon the diffusion and rheology. This also shows that the diffusion has an influence upon the rheological measurements observed.

### 2.4.4 Free Volume Theory

Mass transport through a complex polymeric material is not accurately described by Fick's law. The diffusion process can be considered by free volume theory [72]. This considers the creation and size distribution of space required for the motion of diffusing molecules. The creation of the space depends on the segment chain mobility and on the cohesive energy of the polymer. The diffusion process relies upon the ease and degree of chain packing, related to the free volume and the density. [73] This will be affected by the degree of crystallinity and of crosslinking of the polymer structure. Additives will also affect the diffusion process. [74]

When a solvent penetrates into a polymer, the polymer network assumes an elongated configuration. The elastic forces oppose and restrict the swelling process. An

equilibrium state is reached when the elastic forces of the network balance the osmotic pressure driving the solvent into the polymer. The viscoelastic properties consequently play an important role in the process, controlling the polymer's response to the change in configuration. If the characteristic time of diffusion is much larger than that of the polymer relaxation time, the diffusion process is referred to as case I Fickian diffusion. If the characteristic time is much smaller it is referred to as Case II diffusion. [46, 75]

Using free volume theory [72], diffusion in polymers occur as small molecules travelling through available spaces between the polymer chains. The total free volume of the polymer and the permeating small molecules is larger than that of the polymer alone. This allows easier segmental motion of the polymer chains. Therefore, the diffusion of the molecules is increased as the local concentration increases. This is called plasticization, ie. when the solvent concentration exceeds a threshold value, a glassy state polymer structure will change to a rubbery state. [76] The diffusion coefficient in the rubbery state is significantly higher than in the glassy state. [77]

Crystallinity also has an effect on diffusion according to the free volume theory [78]. This occurs due to the presence of solvent in a polymer structure. The crystalline structure then rejects the solvent that was absorbed prior to formation. These crystalline regions are considered impermeable to penetrant solvent molecules, usually resulting in a decrease in mass transport within polymer structures with increased crystallinity. [79, 80, 81]

Additives affect the diffusion process by providing a more tortuous path for the penetrant molecules through the polymer structure. According to a study carried out by Unnikrishnan and Thomas [82], a decrease in additive particle size results in a decreased polymer chain mobility and flexibility. Therefore the permeation decreases with smaller particles size additives.

Joubert et al [83] discusses the diffusion of a solvent through a polymer by means of rheology, combining the free volume theory with the theories proposed by Elafif. From the rheological measurements the self-diffusion coefficient of the penetrant solvent is able to be determined. This self-diffusion coefficient was found to be exponentially dependent on the inverse of temperature and exponentially dependent on the weight fraction of the solvent. Experimental data of Diethyl 2-hexyl phtalate and copolymer ethylene and vinyl acetate were used to verify the model.

## 2.5 Gelation

Gelation is the conversion of a liquid to a disordered solid by formation of a network of chemical or physical bonds between the molecules or particles composing the liquid. The liquid is called the 'sol', and the solid formed is the 'gel'.[10] This gelation can be formed from a polymeric liquid. There are two types of gelation generally thought to occur from a polymeric liquid; physical gelation and chemical gelation. These differ by the means in which the polymer bonds. Chemical gelation arises from covalent attachments between two atoms, which are close to permanent bonds, whereas physical gelation is a weak, reversible bonding or clustering due to Van de Waals forces, electrostatic attractions or hydrogen bonding.

The formation of a gel due to chemical gelation is reliant upon the branching and multifunctionality of the liquid where different types of chemical reactions can be generated. To create branching within the polymeric liquid, there are three generic types of chemical reaction that can take place. Condensation reaction is where a molecule of two or more reactive groups react with loss of water. Addition polymerisation is the linking of monomers by the opening of double bonds by free-radical reaction. The third way to create branching is the cross-linking or vulcanizing of linear polymers by the introduction of chemical links that bond them together.

The formation of a gel due to physical gelation occurs as a result of intermolecular association, which leads to a network formation. This network is held by interactions between the molecules: local helical structures, where one polymer winds around another; microcrystallites; and nodular domains, where a polymer chain is heterogeneous and associations only occur at preferred sites. i.e. where specific groups along the polymer chain physically bond to similar groups, producing physical networks. This is found in polymers containing hydrophobic groups. The hydrophobic groups shield themselves from the aqueous environment by huddling together. This huddling forms a gel-like network between the polymers. The converse is found, when hydrophilic groups are added to hydrophobic polymers. The hydrophilic groups are found to associate, again forming a gel-like structure. Another type of attraction is that of ionic attraction, where there is aggregation due to dipole-dipole interactions. Aggregation can also occur due to hydrogen bonding between polymer groups. These bonds are not permanent, with an enthalpy at room temperature of around 5-10 kbT, but with many of them occurring, movement and diffusion of a polymer chain will be slowed.

The attractive physical interactions between polymers, which contribute to physical gelation, can also lead to degrees of phase separation. The preparation of a physical gel within the presence of a solvent is common. The solvent is then removed due to evaporation . This process causes shrinkage due to capillary forces acting upon the liquid-air surface, producing a dense material with moderate or low porosity. This is called a xerogel. The model inks using both nitrocellulose and polyamide resin can be called a xerogel. The properties of each are very different, however, as seen in the bulk rheology results discussed.

A gel can be prepared in different ways, leading to different results. A gel in a dry state can be prepared, then swollen with the introduction of solvent, or the gel can be that of the gel cross-linked with the solvent already present. This sensitivity to preparation conditions also effects the reproducibility within experimentation. [10, 84, 85]

Ricardo et al [86] and Chaibundit et al [87] observed the gelation of copolymers Pluronic p123 and f127 within a dilute aqueous solution respectively. Ricardo et al observed the effect of n-, s- and t-Butanol on the gelation and micellization. Samples of various polymer concentrations were made. Oscillatory rheometry was used to confirm gel formation at each concentration and at various temperatures. The results suggest that gel formation occurs at the lowest temperature with the highest elastic modulus within n-butanol/water solution. The concentration as well as temperature have a significant effect upon the gel formed. Chaibundit et al conducted similar experiments using oscillatory rheometry with three polymer concentrations (10%, 20% and 30% ethanol weight). The results suggest the temperature at the sol-gel boundary is lowered slightly for 10% and 20%, but is increased greatly for 30%, showing a dependence upon solvent concentration in the formation of a gel. Both papers use similar techniques to that carried out within this thesis using aqueous systems. The observation of the gelation process is by use of various preformulated concentrations of the system.

### 2.5.1 Polymer Crystallinity

The structure of a polymer as well as the physical properties determines the degree of crystallinity of the material. The arrangement of chains within the polymer molecule allow the chains to align, usually where the minimum energy is required. This arrangement to minimise energy requires a close packed arrangement of linear or close to linear chains. An ordered microstructure, or a regular arrangement of units within the polymer makes it capable of crystallising. The chains, however, only have local

knowledge of the surrounding polymer chains close to them. This may lead to the ability for close packing for one section of the polymer with other segments within an amorphous state. Small defects are able to be included within a crystalline structure, only leading to slight distortions of the lattice. Branching within the polymer inhibits crystallinity and instead is part of the amorphous region. The higher the degree of branching, the less chance there is of crystallinity. [10, 84, 85]

### 2.5.2 Polymer Interactions

The interaction of polymers is not able to be treated as a whole. Instead, the interactions between segments of the polymer must be considered. These segments can be chemical units or chemical functional units. Polymers have a certain distribution of electrons in certain bonds, such that there can be a permanent dipole moment. There is a certain weak force of attraction between such dipoles, which depends on their distance apart and relative orientation. The dipoles are able to interact directly with one another, or a dipole is able to induce a dipole and subsequently interact with it. There is also a dispersing interaction. These interactions are grouped together as Van der Waals forces.

A stronger interaction is that of hydrogen bonding and ionic interaction. The interaction of dipoles amongst polymers relies upon the shape and the rotational entropy. For polymers which contain strong dipoles this relies on the flexibility of the polymer. Hydrogen bonding occurs for those polymers in which rotation is strongly hindered. A hydrogen bond is seen as the interaction of a hydrogen atom to two atoms instead of one, creating a bond between the two. These normally form between functional groups; usually the most electronegative, such as oxygen and nitrogen. The hydrogen bond leads to a contraction of the two atoms, where the distance between the two bonded atoms is less than the Van der Waals radius. The strength of the hydrogen bond is dependent upon the atoms involved, but are not considered as cross linking.

Ionic bonding is stronger than that of hydrogen bonds and is classed as cross linking. They are usually copolymers where the minor component has a functional group with the ability to form ionic bonds. This is achieved by the attracting of spare protons or electrons within the functional groups. The ionic domain phase separates into some form of cluster. [10, 84, 85]

### 2.5.3 Gelation of Nitrocellulose

Several studies into the gelation of nitrocellulose have been carried out primarily using 'good' solvents such as ester solvents. [88, 25] These report the formation of gel particles due to unreacted cellulose, where hydrogen bonding of hydroxyl groups serve as cross-links of micro-gels. However macroscopic gelation due to this theory has not been reported. Other reports have attributed the mechanical behaviour of nitrocellulose gelation to the presence of crystallites.[25] There is evidence to support the presence of crystallites but not that they contribute to gelation. Research carried out by Chen and Mao [25] indicate that entanglements of the nitrocellulose polymers are essential in the formation of gels. The gel stability was found to increase with increased nitrocellulose concentration. At a critical concentration the gel stability was dependent on the molecular weight. This relationship between resin concentration and molecular weight upon the gelation is evidence of gelation due to physical entanglement. Using the Ferry and Eldridge [89] relationship they found that there were more than two polymers involved in each junction, which would be the case for physical entanglements. They summised that physical entanglements of polymers cannot be the only intermolecular process to contribute to the gelation of nitrocellulose. Instead of just entanglements, aggregation of nitrocellulose to form micro-gels due to the unreacted cellulose portion was suggested. This does not lead to large scale gelation but instead modifies the network junctions and inserts extra polymer chains in a junction point. As well as aggregation due to unreacted cellulose, aggregation can result from energetically favourable contacts between polymer segments. This is affected by the use of solvent being either a 'good' or 'poor'. A 'poor' solvent is seen to enhance gel stability whereas a 'good' solvent reduces it. This can be due to the intersegmental contacts within the polymer being strengthened with a 'poor' solvent, leading to a more stable gel structure. [24, 27]

### 2.5.4 Solvent Interactions

The purpose of a solvent is to dissolve the polymer resin and to reduce the viscosity to the desired state. The solubility of the polymer resin in the solvent is paramount, although the solvent also effects many other factors. Isopropanol and Ethyl Acetate are classed as hydrogen-bond donor-acceptor solvents and hydrogen-bond acceptor solvents respectively.

The alcohol Isopropanol is classed as a true solvent to polyamide and a latent solvent for nitrocellulose. A true solvent means it is able to dissolve the resin completely

at room temperature. A latent solvent cannot dissolve the resin alone, needing to be combined with a true solvent to become a true co-solvent. Esters, which ethyl acetate is an example of, is known as a true solvent for nitrocellulose and is therefore used with isopropanol to dissolve nitrocellulose. Solvents are also called 'good' or 'poor' solvents as to whether the solvent is energetically favourable for polymer-solvent interaction. A 'good' solvent is energetically favourable for polymer-solvent interaction to form. A 'poor' solvent is one in which it is not energetically favourable to do so, instead polymer-polymer interactions are preferred. This is dependent on the polymer and solvent used.

Isopropanol is a high hydrogen bonding solvent, with high dispersion and medium polar properties. Polyamide is also highly hydrogen bonded due to the functional groups. The solvent is able to dissolve the solid resin by being small enough to get between the polymer molecules at the surface. This swells the polymer matrix, allowing more and more molecules to go between until the solvent has swollen the complete polymer matrix. The polymer is finally dispersed within the solvent to be classed as a solution. To be able to achieve the breakdown of the polymer matrix, the polyamide molecules need to be able to hydrogen bond to other sites when broken. Isopropanol is able to provide the hydrogen bonding sites for this to happen.

Nitrocellulose is a very different resin with a highly nitrated segment. The nitration rate has a great influence upon the solubility of the resin. Ethyl acetate is combined with Isopropanol to provide this nitration solubility within the system. Nitrocellulose is particulary sensitive to the solvents in which it is dissolved. It is necessary to use a solvent mixture that maintains the resin in solution throughout the evaporation process. The use of a non solvent such as a hydrocarbon, could end up with the precipitation of the resin before the solvent has evaporated. Within industry, a blend of over ten solvents can be used to maintain a good evaporation, as well as minimising costs. [24, 27]

## 2.6 Addition of Solid Content

There is very little experimental data available for research carried out on solid spheres suspended within a polymer gelation. Instead there are theoretical models[90, 91] which look at the problem. The drying of such systems has not been extensively researched. The theoretical models use depletion interactions as a basis. This theoretical work was pioneered by Asakura and Oosawa [92] and by Vrij [93]. This was verified by experimental studies carried out by Vincent and co-workers [94] and

Sperry et al. [95] Most of the theoretical approaches replace the polymer chains by penetrable hard spheres in order to simplfy the polymer chains.

When the system is analysed, the solid spheres will restrict the movement of the polymer molecules within the fluid taking up free space between the polymer molecules. This will also restrict the diffusion of the solvent due to less free space for the solvent molecules to diffuse through. [90, 91]

## 2.7 Closure

There are many theoretical models that independently research areas of the drying process. The means in which a solvent-polymer based system dries has been observed, with the solvent known to escape from the system in two stages; the solvent loss slowing in the second stage due to the change from evaporation to diffusion. Models based on Fick's law discuss the process of diffusion of a solvent through a polymer. The combination of this with free volume theory can include the means of measuring the diffusion with rheology. Separate to this, gelation of a polymer-solvent system has been researched. The specific gelation process can be determined through the chemical makeup of the polymer, and the interaction it has with itself and the solvent. These processes of a drying polymer-solvent system have not been combined to produce an overall picture of the drying process. The effect of solvent evaporation on the gelation of the polymer, the effect of polymer type and concentration on gelation, the effect of gelation on diffusion. The models have provided a qualitative understanding of polymer-solvent systems, but now that boundaries are being pushed, driven by practical and commercial applications, a quantitative understanding of the processes is required.

The gelation of polymer systems have been studied by producing a series of preformulated samples with different polymer concentrations and measuring the rheology of each. [87, 86] Each concentration represents the system in a different 'dried' state. However this method does not account for the other processes that are happening to induce gelation, such as the mass transport of the solvent and solute, the evaporation of the solvent at the surface, the movement and entanglement of the polymer. The consideration of the dynamic nature of the gelling system has not been researched. The resins and solvents used within the model systems have not been studied in previous research. The initial attempts at observing the gelling system due to solvent loss are shown in this thesis, where the rheology of the bulk and surface are measured

throughout the drying process. The research examined the effect of this dynamic drying process upon the gelation process.

The effect of solid particles within these processes has not been extensively researched. The inclusion of such particles will develop the understanding further into their influence. The experimental research carried out within this thesis hopes to develop the understanding of the processes that influence the drying of polymer-solvent and polymer-solvent-particle systems and whether the processes have a fundamental influence upon each other.

A computational model that describes the drying process, including the gelation of the polymer and the diffusion of the solvent is required within the printing industry, to understand what parameters and properties influence and effect the drying process. The drying process will effect the levelling of the printed layer, as well as the homogeneity of the system, which will have a fundamental effect within both the electronics and graphics industry. With developments in the printing industry a need to develop a quantitative model to further the understanding of the drying process is necessary. From the literature reviewed, the mass transfer of solvent through a polymer can be thought of as a wave going through the polymer layer by layer as shown in Figure 2.6.

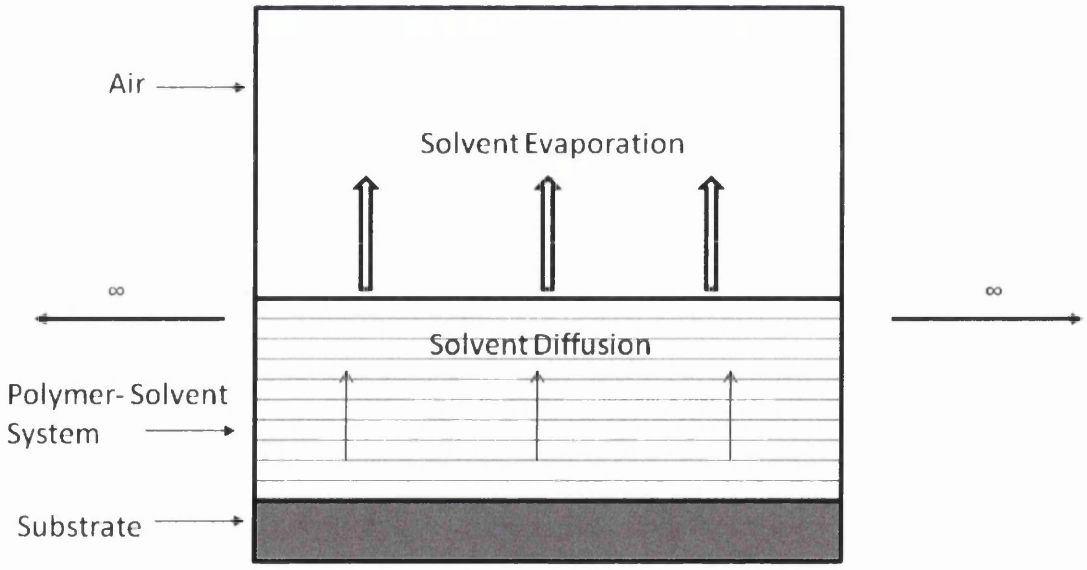


Figure 2.6: The mass transfer of solvent through a polymer-solvent system

The solvent evaporates from the surface and this extends through the polymer

until no solvent is present. This is carried out by the solvent diffusing through the polymer and then evaporating at the surface. The experiments carried out throughout the thesis are able to add to the data needed to produce a comprehensive model. The gelation is monitored by using rheology techniques, showing the point at which gelation occurs and what the effects are upon the process. The surface and bulk gelation are measured to observe any differences between them. The solvent loss by means of diffusion as well as solvent retention is monitored by multi-speckle diffusing wave spectroscopy (MS-DWS), which observes the brownian motion of the molecules. The solvent loss at the bottom layers of the system as well as the order of solvent diffusion was monitored by Fourier Transform Infrared Spectroscopy (FTIR) which observes the chemical makeup of the compound. These techniques will provide valuable data for both single-solvent and multi-solvent polymer systems. They will show the differences between the different systems as well as the influence the polymer, initial polymer concentration and addition of solid content have upon the drying process.

# Chapter 3

# Methodology

## 3.1 Introduction

There has been limited experimental research carried out to understand the processes that influence the drying of polymer-solvent systems and their influence upon each other. A series of experiments were carried out to establish the influence of physical processes, such as solvent loss, and structural process, such as gelation, on the drying process. Two different model polymer-solvent systems were developed using polymers and solvents commonly used within the printing industry, as well as a commercially available system to understand the influence the polymer, solvent, solid particle and concentration have upon the drying process. The model polymer-solvent systems were used because commercial ink formulations are highly complex and contain many additives. To understand how the parameters and components influence the processes, model systems were used. A commercial ink was used to verify the research and methodology for use with commercial formulations. The resins and solvents used within the model systems have not been studied in previous research. Rheometry was used to observe the physical process of gelation by monitoring the viscoelasticity of the bulk and surface. Multi Speckle Diffusing Wave Spectroscopy (MS-DWS) was used to observe the solvent loss, as well as gain an insight into the structural processes by monitoring the molecular movement within the system. Fourier Transform Infrared Spectroscopy (FTIR) was used to observe the physical process of solvent loss by monitoring the transmittance peaks of the solvent.

This chapter describes the materials and apparatus used in the experimental research.

## 3.2 Ink Formulation

Four ink compositions were formulated using two types of resin and two solvents and solid metal particles. The resins used were polyamide provided by Thomas Swan and nitrocellulose provided by DOW. The polyamide resin was a Casamid 874 resin. The Nitrocellulose resin was a Walsroder$^{tm}$ Nitrocellulose A 500 Ethanol 35% resin. There was greater than 60% cellulose nitrate and less than 35% Ethanol within the resin. The solvents were analytical grade Propan-2-ol (IPA) and Ethyl Acetate (EA) from Fischer. The metal particles were 4 micron spherical aluminium particles provided by Gwent Electronic Materials. The first ink formulation contained polyamide with IPA; the second contained nitrocellulose with IPA and EA at a ratio of 5:1; the following two ink formulations are the same as inks one and two, with the addition of 10% of aluminium particles by weight of the total ink . These compositions were chosen as the resins and solvents are commonly used within the graphic printing industry and increasingly used within electronics printing. The aluminium particles were chosen as they were able to represent the particles used within the printing of electronics as well as graphic printing. Spherical particles were used with future modelling of the process in mind. The particle would be simpler to define. The model inks are closer to inks used within graphics printing.

The four inks were formulated by creating an initial mix of 50% resin to 50% solvent and 45% resin to 45% solvent with 10% solid. The initial mix was diluted down into five resin content percentages; 10%, 20%, 25%, 30% and 40%; using the relevant solvent. Additional solid was added to maintain a 10% solid content throughout all inks. This provided five different initial viscosities for two different ink systems with and without solid content. The procedure provided a means of creating formulations with known resin, solvent and solid content which were consistent throughout each formulation.

The actual percentages of the inks are shown in Figure 3.1. The initial mixed formulations were produced within metal tins. The tin was then placed in a paint mixer for 90 seconds to provide an initial period of high energy mixing. It was then left on a rock-and-roller for 24 hours to provide constant agitation. The final inks were subjected to the same mixing procedure as the initial mix. The inks were then separated into three smaller sub-samples per resin content percentage and stored in sealed tins. One tin was opened at a time throughout experimentation, to preserve the initial integrity. The tins were stored at room temperature until use.

| Formulation | | Composition | | |
|---|---|---|---|---|
| Resin | % Resin Ink | Resin % | Solvent % | Solid % |
| Polyamide | 10 | 10.1 | 89.9 | |
| | 20 | 20 | 80 | |
| | 25 | 25 | 75 | |
| | 30 | 30 | 70 | |
| | 40 | 40 | 60 | |
| Polyamide with solid | 10 | 10 | 80.7 | 9.3 |
| | 20 | 20 | 70.5 | 9.5 |
| | 25 | 25 | 65.5 | 9.5 |
| | 30 | 30 | 60.3 | 9.7 |
| | 40 | 40 | 50.1 | 9.9 |
| Nitrocellulose | 10 | 10 | 90 | |
| | 20 | 20 | 80 | |
| | 25 | 25 | 75 | |
| | 30 | 30 | 70 | |
| | 40 | 40 | 60 | |
| Nitrocellulose | 10 | 10.1 | 80.6 | 9.3 |
| with solid | 20 | 19.8 | 70.8 | 9.4 |
| | 25 | 24.8 | 65.6 | 9.6 |
| | 30 | 29.9 | 60.5 | 9.6 |
| | 40 | 39.9 | 50.3 | 9.8 |

Figure 3.1: Ink Formulations

As well as conducting experiments on a series of model inks, the same experiments were carried out on a commercially formulated flexographic ink. This was a FlexiPrint MF - WC5A packaging ink provided by Flint Group Inc. This is a pigmented Nitrocellulose based ink.

## 3.3 Rheology

Rheology is the study of deformation and flow of a material.[96] It reveals information on the flow behaviour of liquids and the deformation behaviour of solids. This leads to the shear behaviour of materials and fluids throughout the spectrum from ideal viscous liquids to ideal elastic solids. This behaviour is based on a combination of both the viscous and elastic components of materials, called viscoelasticity.[96] Two geometries are commonly used in two-plate rheometry: parallel plate and cone and plate. A parallel plate is commonly used for higher viscoelastic material whereas a cone and plate geometry is commonly used for low viscoelasticity materials to minimise the difference in shear between the outside of the plate and the inside. Due to a large range in viscoelasticity, a parallel plate was used to maintain experimental consistency throughout the range of systems.

### 3.3.1 Shear Rheology

The fundamentals of rheometry (the measure of rheology) is simply defined by consideration of a two-plate model. This is described by Mezger as follows and shown in Figure 3.2.[96] The top plate with shear area, $A$, moves with a shear force, $F$. The resulting velocity ($v$) is measured. The bottom plate is stationary and a distance, $h$, away from the top plate. The sample is sheared in the gap. It is assumed that the sample adheres to both plates and therefore does not slip, and that there is laminar flow. The sample is seen to move in the form of layers along each other.

### 3.3.2 Oscillatory Shearing

To examine viscoelastic fluids, small-amplitude oscillatory shearing or Dynamic Mechanical Analysis (DMA)[96] is used. The model is described by Mezger as follows and shown in Figure 3.2. The two plate model is used to explain the test. The bottom plate is stationary, whereas the top plate with shear area, $A$, rotates back and forth with shear force, $\pm F$. The gap between the two plates is the shear gap dimension. The rotation of the top plate causes shearing of the sample placed between the two

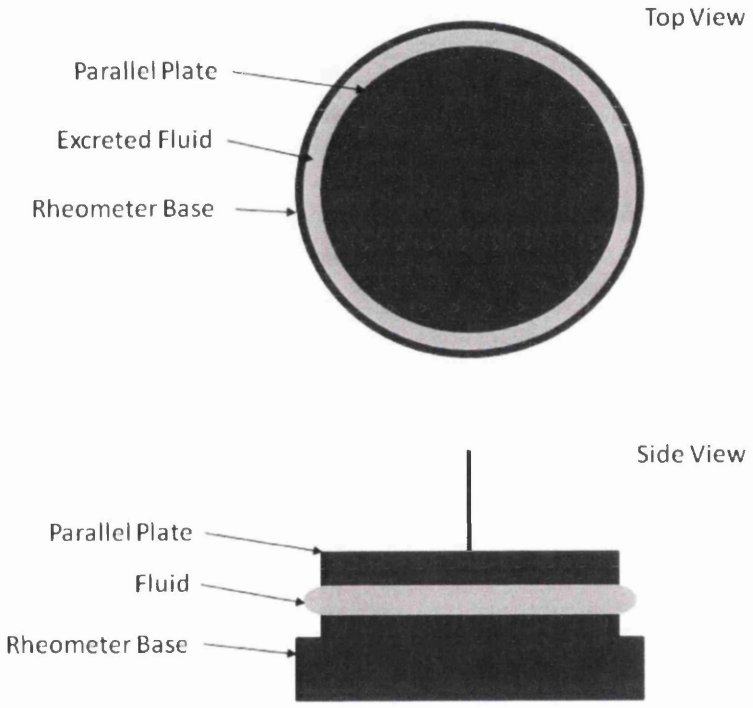


Figure 3.2: Schematic Diagram of Parallel Plate

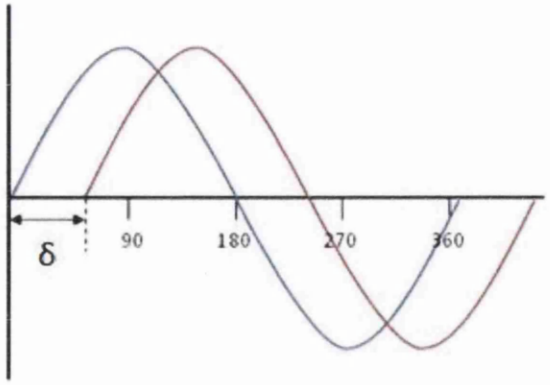


Figure 3.3: The Phase Difference Between Storage and Loss Moduli

plates. This results in a deflection path $\pm s$ and deflection angle $\pm\delta$. It is assumed that throughout the test there is no slipping of the fluid from the plates and that the sample is deformed homogeneously throughout the entire shear gap.

The storage modulus, $G'$, is a measure of the deformation energy stored by the sample during the shear process. This represents the elastic behaviour of the material as it shows the energy stored by the material after shear. The storage modulus is notated as a cosine function:

$$G' = \left(\frac{\tau_A}{\gamma_A}\right) \cdot cos\delta \tag{3.1}$$

where $\tau_A$ is stress and $\gamma_A$ is strain.

The loss modulus, $G''$, is a measure of the deformation energy used by the sample during the shear process. This represents the viscous behaviour of the material as it shows the energy lost by the sample during the shear process. The loss modulus is notated as a sine function:

$$G'' = \left(\frac{\tau_A}{\gamma_A}\right) \cdot sin\delta \tag{3.2}$$

The phase angle is the difference in phase between the storage and loss moduli functions. This is shown in Figure 3.3. A phase angle of $90^0$ shows a purely viscous material and $0^0$ shows a purely elastic material. A material with a phase angle between these two angles shows the degree of viscoelasticity. Appendix C shows the derivation of oscillatory shear rheometry as applied to simple-shear deformation according to the theory of linear viscoelasticity.


Figure 3.4: Picture of the Bohlin Gemini HRNano Rheometer

### 3.3.3 Transient Effects

The study of rheology assumes laminar flow of the sample between the plates as discussed. Using the two-plate model, at the initial time when the top plate begins to move, not all flowing layers are shifted in relation to its neighbour. The shear rate at this time is therefore not constant throughout the entire area. It takes a certain period of time, an "induction period", for the motion of the top plate to reach all the layers throughout the entire area.

### 3.3.4 Equipment

The Bohlin Gemini HRNano Rheometer is a high performance, modular rheometer system which enables the measurement and control of nano-torque levels (Figure 3.4.

The rheometer is able to perform strain and stress controlled tests over a large range and with high sensitivity. The Gemini Nano rheometer is capable of characterization of low viscosity, low volume and weakly structured systems. There are many properties and structures that can be characterized by the rheometer due to the modular set-up. Viscometry tests as well as oscillation tests can be undertaken. [97]

## 3.4 Bulk Rheology Experimental Methodology

The geometry used for the bulk rheology tests was a 60mm parallel plate. This is the top plate which is able to osciallate while in contact with the fluid. A photograph and schematic are shown in Figures 3.4 and 3.2 respectively.

### 3.4.1 Frequency and Amplitude Sweeps of Model Inks

Prior to tests on the rheological change of an ink during the drying process, the parameters for the rheology tests had to be determined. The polymeric state of the ink had to be tested in order to determine the linear viscoelastic range. This allows the rheology test to be carried out without changing the polymer structure and viscoelasticity. A frequency sweep was carried out from 0.01 Hz to 100Hz at a constant shear stress of 0.1Pa. This sweep produced a plot over the frequency range, showing a change in G' and G". It was performed for the highest, middle and lowest concentrations for all four model ink types. A frequency of 1 Hz was within the linear viscoelastic range throughout testing.

A number of observations of the polymer can be made from the frequency sweep. At low frequencies, there is a dominance of the viscous component, shown by G" greater than G'. This exhibits the behaviour of a viscoelastic liquid. With an increase in frequency, the longer polymer molecules are unable to avoid each other, causing entanglements to begin forming temporary networks. This is shown by an increase in elasticity (G'), exhibiting viscoelastic behaviour with gel-like characteristics. This dominance of elasticity increases with increasing frequency, until a plateau is reached. This is caused by the immobilization of the polymer network due to entanglement. At this frequency the polymer structure acts as a rigid solid. This curve will differ for different polymer structures. Longer more branched polymer molecules will take a shorter time to entangle than smaller linear molecules. This will be witnessed by an increase in G' at lower frequencies. An example of this is shown in Figure 3.5.

Once a frequency has been established within the linear region, an amplitude within the linear region is determined. An amplitude sweep at 1Hz is carried out from

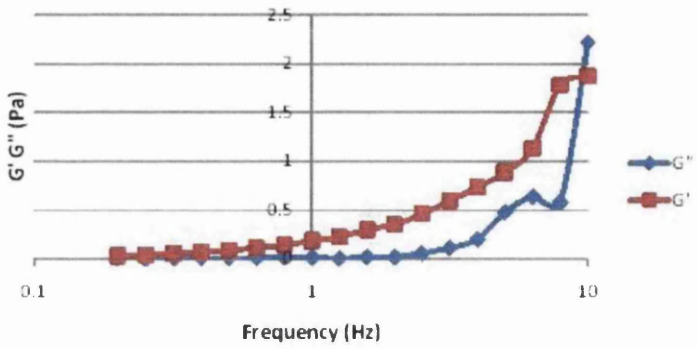


Figure 3.5: An Example Frequency Sweep

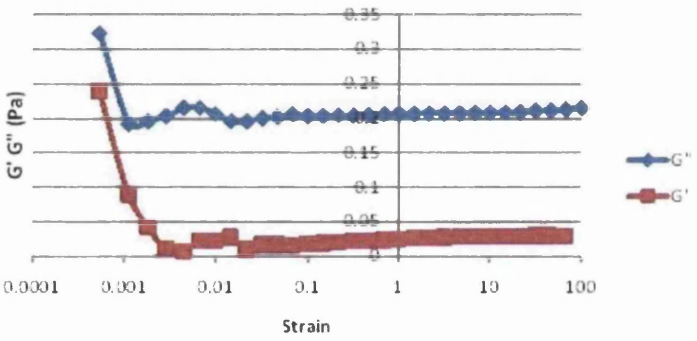


Figure 3.6: An Example Amplitude Sweep

a strain of 0.0005 to 100. An amplitude of 0.03 was chosen as this was within the linear region, but importantly would not interact with the tested fluid in a detremental fashion. The amplitude was enough to produce an accurate reading, but not enough to change the structure or properties of the system. As with the frequency sweep, a linear region was observed with a rapid increase in G' outside this. An example of the amplitude sweep is shown in Figure 3.6

### 3.4.2 Bulk Rheology Drying Tests of Model Inks Using Bohlin Rheometer

A number of methods were carried out to determine a reliable and repeatable process to observe the viscoelasticity changes of the ink during the drying process. The methodologies are detailed below.

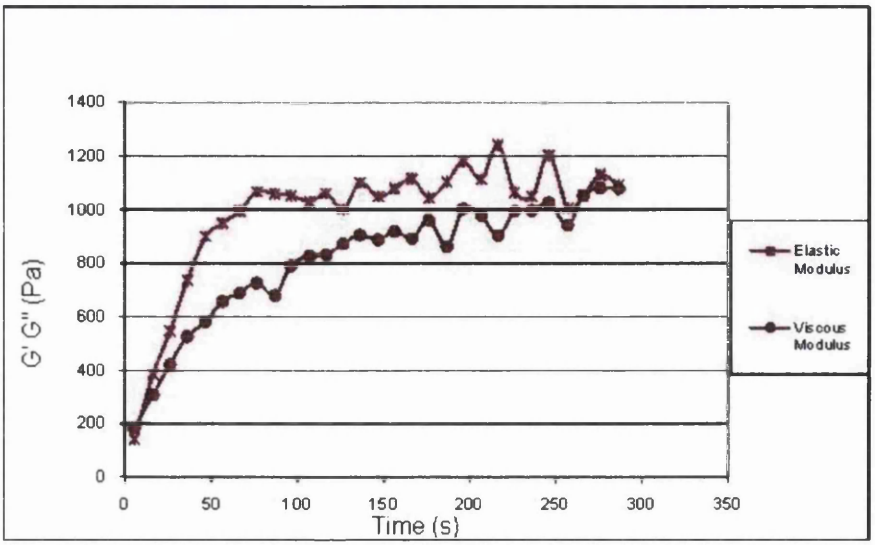


Figure 3.7: Common Test Result from Inital Testing Procedure

#### 3.4.2.1 Initial Drying Tests Using Bohlin Rheometer

A number of tests were performed using a simplified technique where the ink was allowed to dry on the Bohlin rheometer plate. A sample of ink large enough to cover the base plate was placed on the rheometer using a spatula. The top plate was brought down to the test level and a solvent trap was placed around the rheometer. The test was then ran. The delay time for the plate to engage the ink surface and the test to start was recorded using a stopwatch. This process was repeated for various delay times; the stopwatch started when the sample was placed on the rheometer base and stopped when the test was started. These tests were combined to show the rheology change throughout the drying process. This process while relatively simple to use, was not considered adequate to produce an accurate representation of the bulk rheology. This was due to skinning effects hardening the outer surface of the ink. The rheometer, while testing, would break up this skinning and change the rheology within the time of the test. An increase in the elastic and viscous moduli would occur at the start of each test, as well as variability throughout the test. This is shown in Figure 3.7. Figure 3.7 shows the effect of skinning as a change in rheology initially before a steady state was achieved. This induction period is thought to be the result of the breakdown of skinned ink into the bulk.

#### 3.4.2.2 Drying Tests Using Bohlin Rheometer

The bulk rheology of ink was determined by a remote technique where drying and sampling was performed in separate apparatus (Figure 3.8). Samples of each model ink were placed in a metal container on a mass balance. The height of the container was initially 75mm. This setup was found to trap solvent within the container and inhibited the evaporation of the solvent during the drying run. The height of the container was then lowered to 40mm. This allowed the evaporation to occur and did not artificially trap solvent. The ink was continually stirred using a drill stirrer throughout the run. This consisted of 4 paddles at $90^0$ to each other. The stirrer was lowered into the container with the mass balance switched on and set to zero. The stirrer was lowered until a reading was observed on the mass balance. At this point, the stirrer was increased in height until the reading on the mass scale was zero. This allowed the stirrer to be as close to the bottom of the container, without touching to minimise stagnant ink within the container. The stirrer was turned on at a speed of 100rpm. This was found to maintain an adequate stirring of the ink throughout the drying process. Once the stirrer height was set, and the stirrer was revolving, the ink was added to the container. The ink was poured into the container over the stirrer paddles. This allowed an even distribution of the ink in the container and between the paddles. The stopwatch was started at this point. Once the ink had been added, the stirrer was stopped. The weight was taken when the stirrer had stopped and the mass scale became settled. This initial mass reading was taken as the mass at zero time. Approximately 45 grams of ink was added for each run. This allowed a number of samples to be taken from the bulk of the ink throughout the run. A smaller amount of ink did not leave enough ink, near the end of the run, for a suitable sample to be taken from the bulk. A larger amount of ink, took a longer time to dry with no benefit. A small sample from the container was removed each time using a spatula. This was taken from the area between the paddles. A sufficiently large sample was taken and placed on the rheometer base plate. The sample was large enough to provide even coverage over the whole base area, so when the top plate came to the test position, a small quantity of the sample was excreted from the gap formed between the base and plate. Once the plate came to the test position, a solvent trap was placed around the rheometer, to minimise solvent loss throughout the rheometry test. The rheometry test was started. The mass left in the container was noted after the sample was removed from the container. The stirrer was turned on again and the test repeated.

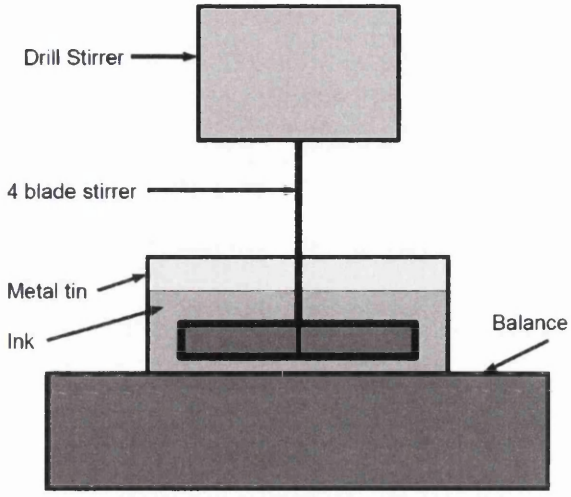


(a)

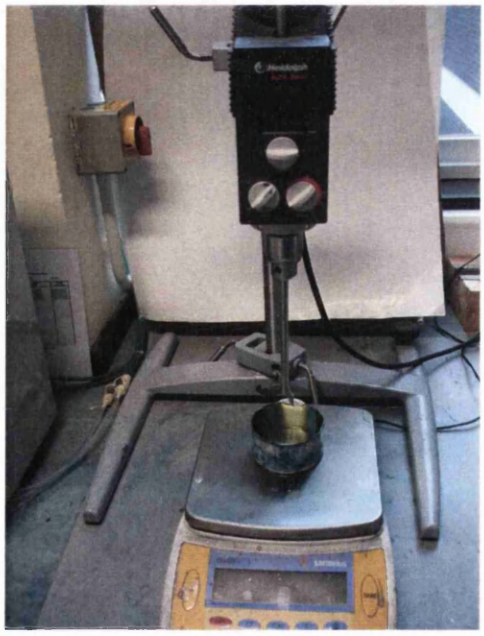

(b)

Figure 3.8: Diagram (a) and Picture (b) of Apparatus used for Bulk Rheology Experiments

After the initial test, a sample was taken between every 10 minutes and 2 hours dependent on the run time. A run was anywhere between 30 minutes and 10 hours. Each time, the stirrer was stopped and the time was noted. This procedure continued throughout the run until a sample was no longer able to be taken due to its solid like nature. The run was repeated a number of times for each formulation to allow repeatability to be assessed.

Each test throughout a run was plotted with phase angle on the y-axis and test time on the x-axis. The time at which each test was carried out was recorded. The mean phase angle was taken for each test carried out. The standard deviation over the test period was calculated. This allowed the variation of the test from the steady state rheology to be determined. Test results with too high standard deviation were removed from the analysis. The reasons for their variation are discussed later. The tests that remained for each run were combined. The time at which the test was taken, the mass before and after the test was taken and the mean phase angle for the test were all collated. From the data, the percentage mass loss over the time period of the test was calculated. The mass was adjusted to allow for the decrease in mass due to a sample being taken from the container each time. The percentage mass loss for each test was then noted, with the corresponding mean phase angle for the test. All tests over the run period were plotted, with the percentage mass loss on the x-axis and the mean phase angle of each test on the y-axis. This allowed the change in phase angle over the drying period to be correlated with the amount of solvent lost from the ink.

## 3.5 Surface Rheology Experimental Methodology

The frequency and amplitude tests were carried out using the bicone and Dunouy ring prior to the oscillatory experiments.

### 3.5.1 Interfacial Rheology

Investigation into the interfacial rheology is undertaken by use of a biconial disc geometry and a Dunouy ring. $G_s^{'}$ and $G_s^{"}$ are the 2D storage modulus and loss modulus, respectively. These depend, in general, on the oscillation frequency $\omega$, and the surface dynamic viscosity $\eta_s$.

$$G_s^{'} = |G_s^*| \, cos\delta \tag{3.3}$$

$$G_s^{"} = |G_s^*| \, sin\delta \tag{3.4}$$

A general expression for $G_s^*$ is expressed as

$$G_s^*(\omega) = G_{surf,0} + G_s^{'}(\omega) + iG_s^{"}(\omega) \tag{3.5}$$

The inclusion of the constant $G_{surf,0}$ indicates there is the presence in the surface layer of solid-like properties, in particular the appearance of a structured, ordered state. The phase angle is found in the same manner to that of the bulk rheology.

$G_i^{'}$ and $G_i^{"}$ can also be defined for the interfacial elastic and viscosity moduli respectively. The use of an interfacial rheometer with a disk, ring or bicone geometry can be assumed to have the interface decoupled from the bulk phase flow. This is due to the dissipation of the interfacial stresses into the bulk phases being negligible. In this case, the rheometer may be treated as a two-dimensional couette device, i.e. for laminar flow between parallel plates; allowing the interfacial shear viscosity to be calculated from the torque. Interfacial rheology techniques and theory have been reviewed by G. Fuller [98].

### 3.5.2 Bicone

A 50mm diameter bicone attachment allowed drying tests to take place directly on the Bohlin rheometer plate and to monitor the rheology change at the surface in real time. The bicone geometry is different to that of bulk rheology geometry plates. It is shaped as if there are two shallow angled cones placed base to base. The bottom cone is placed within the fluid, with the point at which the bases meet at the fluid surface. The top cone is outwith the fluid. The bicone oscillates in the same manner as the parallel plate. This is illustrated in Figure 3.9.

A 88mm diameter petri dish was attached to the rheometer base. The bicone was brought to a position a short distance above where the fluid surface would be, and the test was started. A sample of model ink was pipetted from the storage tin into the Perti dish. The more concentrated samples were transferred by use of a spatula. The bicone was brought down to the surface until there was a meniscus formed at the edge of the bicone. At that point the bicone was lowered until the meniscus was no longer extruding from the main surface. This allowed the test to continue throughout the loss of height due to evaporation of solvent. The bicone covered a substantial area of the drying ink, leaving only the ink between the edge of the bicone and the petri dish sides to freely evaporate. The test was then left to continue until the bicone

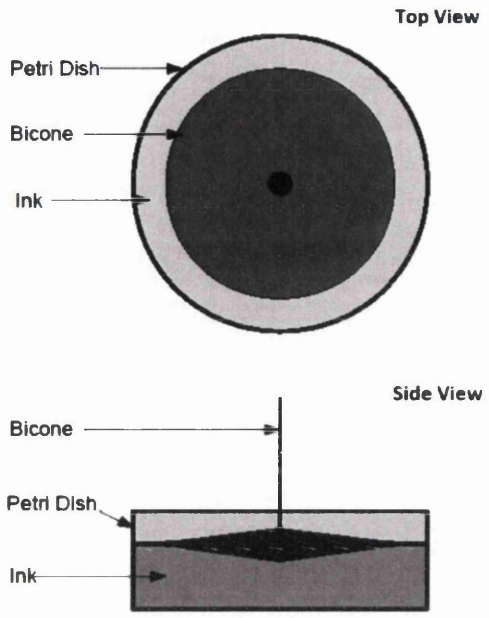


Figure 3.9: A Schematic Diagram of the Setup of a Bicone for Surface Rheometry

was unable to oscillate without causing large erratic oscillatory motions due to the sticking of the bicone to the ink system.

Repeat drying runs for each ink, especially those based on the polyamide resin, produced greater variation with time at which the abrupt change in phase angle occurred. It meant that the runs were not able to be averaged simply by averaging the individual points throughout the runs, this would not gain an accurate representation of the averaged time. Instead, the time at which the minimum phase angle occurred for each run was found and the average time at which the minimum occurred calculated. The plots for each run were then reviewed, and a representative plot was used to show the phase angle change.

In further tests, an identical sample volume of ink was placed onto a similar Petri dish which was placed on a mass balance. The mass loss was then measured over time. This was repeated three times for each ink. The mean data for each ink was plotted with an exponential trendline fitted. The equation parameters for this trendline was obtained. The time for each test run was then inputted into the equation, and a percentage mass loss throughout the drying period computed. The percentage mass loss thus replaces the time on the x-axis. In order to carry out accurate conversion tests, a similar volume of ink was placed in the Petri dish, as had been placed for the bicone tests. This provided the same unit volume of ink per unit surface area as for

the critical zone in the bicone tests. Evaporation through the smaller surface area for the bicone rheology tests and the larger surface for the mass conversion will occur at proportionally the same rate under identical ambient conditions. This allowed a conversion to mass loss to be undertaken and the results to be compared on a mass loss basis directly with data obtained in the other experiments.

The phase angle data was found to be more erratic throughout the initial rheological period than for comparable bulk rheology. This can be explained by the low viscosity of the ink. The bicone oscillating on the surface with the bulk of the fluid below is thought to produce slippage, the bicone having little surface resistance. Toward the end of the initial period, a slight increase in phase angle as well as a decrease in erratic behaviour was observed. The rheometer was unable to measure the surface rheology accurately until the viscosity had increased suffciently so that a measurement could be made without slippage.

### 3.5.3 Dunouy ring

A Dunouy ring was used to assess changes in the surface rheology. A similar set-up and procedure was used for the bicone tests with a 50mm petri dish attached to the rheometer base. A diagram of the set up and geometry are shown in Figure 3.10. The main theoretical advantage of using the Dunouy ring compared to the bicone is there is less obstruction of the surface. Therefore evaporation is not hindered, leading to a more realistic situation. The main disadvantage is that the Dunouy ring is made of thin wire, which means it is more susceptible to bending and becoming misshapen due to the forces upon it during measurement.

## 3.6 Multi Speckle Diffusing Wave Spectroscopy

### 3.6.1 Light Scattering

To study complex fluids, scattering methods are widely used and are discussed by Larson [10]. This ranges from light to x-ray to neutron scattering, probing a length scale of anywhere from 10Å using neutrons to $100\mu m$ using light. Scattering methods rely on a change in direction of propagation of the radiation, due to interaction with inhomogenities within the material. A beam of radiation will be scattered at an angle of $\theta$ by the inhomogenities within the medium. If the scattering is elastic (kinetic energy is conserved), the radiation wavelength ($\lambda$) of the incoming and outgoing beams will be the same. If the scattering is inelastic, the beams will be different.

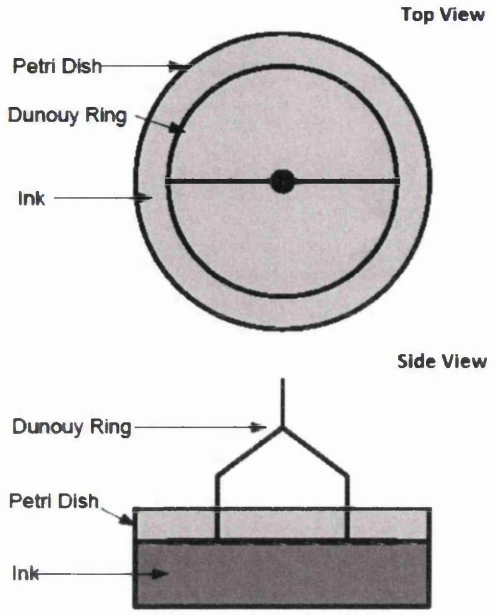


Figure 3.10: A Schematic Diagram of the Setup of a Dunouy Ring for Surface Rheometry

Traditional light scattering analysis assumes that no photon is scattered from more than one scattering point. This is not valid for more opaque fluids. A photon within such a fluid is scattered many times before exiting the fluid leading to each photon executing a many-step random walk through the sample. The propagation of light in this limit is described by a diffusion equation with a diffusivity given by $c\ell^*/3$, where $c$ is the speed of light in the medium and $\ell^*$ is the distance the light travels before it's direction is randomised. A CCD or CMOS camera is used as a sensor to detect the light emitted from the sample, called the speckle grain. This is shown in Figure 3.11. This is the basis for Diffusing Wave Spectroscopy (DWS).[99]

### 3.6.2 Equipment

The instrument used for this work was the Horus developed by Formulaction. A photograph of the instrument is shown in Figure 3.12 and a schematic diagram in Figure 3.13. The Formulaction Horus uses a backscattering configuration, with the sensor and laser source located at a single optical head. The camera sits within a half-angle cone of approximately $10^0$. To remove any unwanted light, an interference filter of bandwidth 10nm is placed over the hole in the cone. The laser is a 0.9mW laser diode with wavelength of 850nm. The camera is a 320x240 pixel sensor with

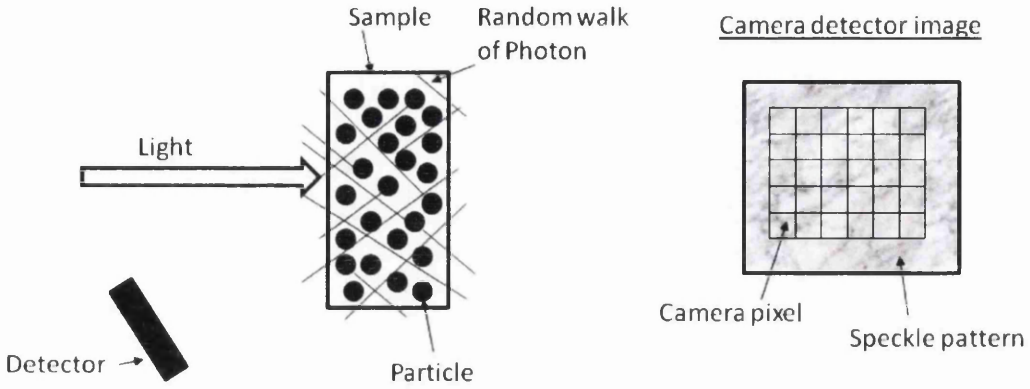


Figure 3.11: Detection of Speckle Grain using Camera

frame rate of 30 images/s. The head is able to be moved closer and further away from the sample in order to optimise the area the laser is monitoring. Backscattering is used, where the wavelengths reflected from the material are collected, as this allows for a less sensitive sensor and a less powerful laser to be used. A thin layer of the sample is placed on a substrate beneath the laser source. The plate on which the substrate is placed, is fixed and rigid, and levelled, using a spirit level, to avoid fluid flow. The whole system is designed to minimise external vibration, as this could be considered as movement within the fluid sample. [99]

The base level of vibrational movement was initially measured. This was achieved by carrying out a test without a fluid sample under the laser. This was left to stabilise. The value was recorded, and was used to show the minimum fluidity factor the experiments could reach. This value was 0.003Hz. For each experiment, the instrument was set to take two simultaneous tests of two independent samples. The parameters were not adjustable. The fluidity factor, in Hz, is the value used for molecular movement by the Horus.

### 3.6.3 Experimental Methodology

A K-bar coater was used to create a film of model ink on a glass substrate. In a k-bar tester a steel bar is used to draw the ink over the glass substrate at a constant speed and pressure. The steel bar consists of a series of uniform grooves which control the wet ink film thickness. There are a range of bars available to apply various film thicknesses. The bar used for the experiments was a number 7 bar which produces a wet film of $80\mu m$ on the substrate. The glass substrate with ink coating was

Figure 3.12: Picture of Formulaction Horus MS-DWS Equipment

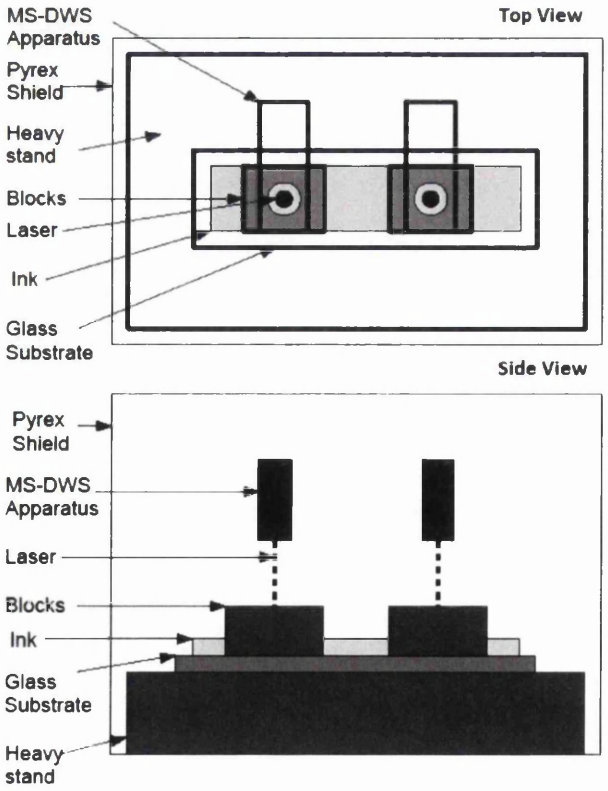


Figure 3.13: A diagram of the setup for MS-DWS

transferred to the MS-DWS where it was placed on the plate and aligned under the laser and camera. Two heavy blocks with spherical holes in the middle were placed on the sample so that the laser was shining on the film through the hole. This provided a consistent area over which to measure the range of inks. There were two lasers that measured simultaneously two separate areas of the substrate. This provided two independent test results. The MS-DWS equipment was contained within a Perspex guard with a door.

In addition, a seperate wet film was coated upon the glass substrate and placed upon mass scales. The mass loss was measured over time. This was used to convert the test results from time to percentage mass loss.

## 3.7 Fourier Transform Infrared Spectroscopy

### 3.7.1 Infrared Spectroscopy

Fourier Transform Infrared Spectroscopy (FTIR) is a spectroscopic technique in which the infrared wavelength irradiates a sample for a short period of time, with the absorption spectrum generated by mathematical manipulation of the wavelengths transmitted through the sample, using Fourier transform analysis [100]. The technique is used to identify compounds and investigate the composition of a sample. [101]

Infrared spectroscopy relies on the molecule vibration due to the absorption of radiation. Depending on the atomic structure and the bonding between the atoms, the molecule has various degrees of freedom. Vibrations can involve a change in bond length (stretching) or bond angle (bending). Some can bend in phase (symmetrical) or out of phase (asymmetric). For the vibrations to occur there must be a change in the dipole moment of the molecule. The larger this change the more intense the absorption band will be. Each vibration within the molecule occurs at a specific frequency, which allows many functional groups to be characterised through their distinctive infrared frequency. [101]

In order to study the infrared spectrum of a molecule or structure, a beam of infrared light is passed through the sample. Observing the transmitted light reveals the energy absorbed at a given wavelength. One method is to pass a single wavelength of infrared light through at a time, which is called a monochromatic beam. This can be repeated for all different wavelengths. Another method is to pass many wavelengths through the structure at once and measure the amount of the beam absorbed by the sample. The process is repeated many more times with different combinations of wavelengths, giving many variations of wavelengths absorbed. The data can be

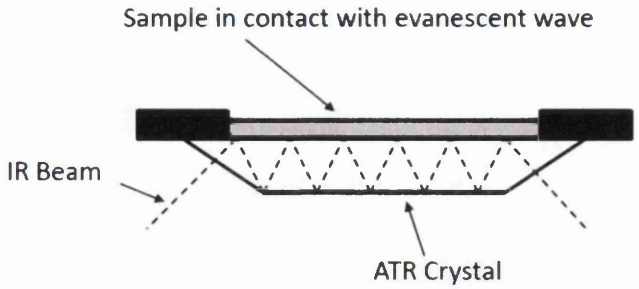


Figure 3.14: Schematic Diagram of an FTIR-ATR Attachment

combined then be used to infer the absorption at each wavelength by use of Fourier transform. [101]

### 3.7.2 Attenuated Total Reflectance

FTIR can be used in conjunction with Attenuated Total Reflectance (ATR) to enable samples to be examined in their natural state with little preparation. ATR operates by measuring the changes within a totally internally reflected infrared beam when the beam comes in contact with the sample (Figure 3.14). The distance at which the evanescent wave penetrates is approximately $0.5\mu m$ to $5\mu m$. [102, 103]

### 3.7.3 Absorption Spectra

The common functional groups and their corresponding absorption wavelength are presented in Figure 3.15. [101]

| Functional Group | Characteristic Absorption(s)($cm^{-1}$) |
|---|---|
| Alkyl C-H Stretch | 2950 - 2850 (m or s) |
| Alkenyl C-H Stretch | 3100 - 3010 (m) |
| Alkenyl C=C Stretch | 1680 - 1620 (v) |
| Alkynyl C-H Stretch | ~3300 (s) |
| Alkynyl C≡C Stretch | 2260 - 2100 (v) |
| Aromatic C-H Stretch | ~3030 (v) |
| Aromatic C-H Bending | 860 - 680 (s) |
| Aromatic C=C Bending | 1700 - 1500 (m,m) |
| Alcohol/Phenol O-H Stretch | 3550 - 3200 (broad, s) |
| Carboxylic Acid O-H Stretch | 3000 - 2500 (broad, v) |
| Amine N-H Stretch | 3500 - 3300 (m) |
| Nitrile C≡N Stretch | 2260 - 2220 (m) |
| Aldehyde C=O Stretch | 1740 - 1690 (s) |
| Ketone C=O Stretch | 1750 - 1680 (s) |
| Ester C=O Stretch | 1750 - 1735 (s) |
| Carboxylic Acid C=O Stretch | 1780 - 1710 (s) |
| Amide C=O Stretch | 1690 - 1630 (s) |
| Amide N-H Stretch | 3700 - 3500 (m) |

Figure 3.15: A Table of Functional Groups and Corresponding Characteristic Infrared Absorptions

### 3.7.4 Equipment

The equipment was a spectrum 100 Perkin Elmer FTIR Spectrometer with ATR attachment. The wavelength was from $4000cm^{-1}$ to $650cm^{-1}$ with a resolution of $4cm^{-1}$. Percentage transmittance was used with four scans taken per measurement. The ATR crystal used was a diamond/ZnSe. An additional piece of software called autohotkey [104] was used to create a macro. This was to allow the FTIR spectrometer to automatically take measurements every 90 seconds for an hour. [105]

### 3.7.5 Experimental Methodology

A droplet of model ink was placed on the prism of the FTIR-ATR of sufficient volume that it covered the prism throughout the drying period. A spatula was used. A

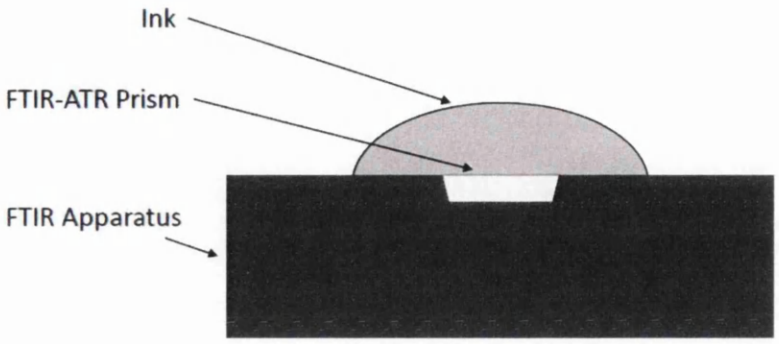


(a) A diagram of the setup for FTIR-ATR without brass ring

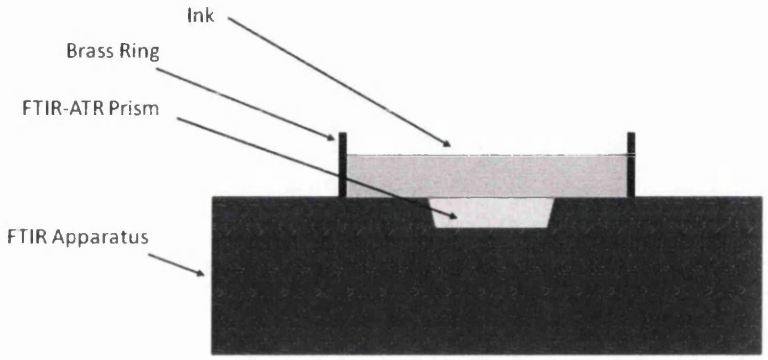


(b) A diagram of the setup for FTIR-ATR with brass ring

Figure 3.16: Setup of FTIR-ATR Equipment

brass ring was used to capture the ink if the ink was too wetting and was unable to sufficiently cover the prism. Both setups are shown in Figure 3.16. The FTIR-ATR test was started. A macro program was used to repeat the test every 90 seconds for an hour. The prism is at the bottom of the ink droplet, and therefore measures the bottom of the droplet up to $5\mu m$. Separate tests were run, where the brass ring was filled and the test carried out to assess if the difference in surface area would have an effect upon the results. It was found there was no significant effect, therefore the tests were carried out using a droplet, and with the brass ring for those inks too wetting.

To analyse the results, the peaks that changed were identified. Examples are shown in Figure 3.17. The infrared transmission spectrum for each ink system was analysed and the spectral peaks were correlated to functional groups present. The identification of functional groups was achieved by a combination of correlation charts [101] and comparison with the known spectra of the resins and solvents used. Polyamide resin ink had only isopropanol solvent present, which displayed peaks indicative of alcohol; broad OH peak between roughly 3200 and $3500 cm^{-1}$, CH peak

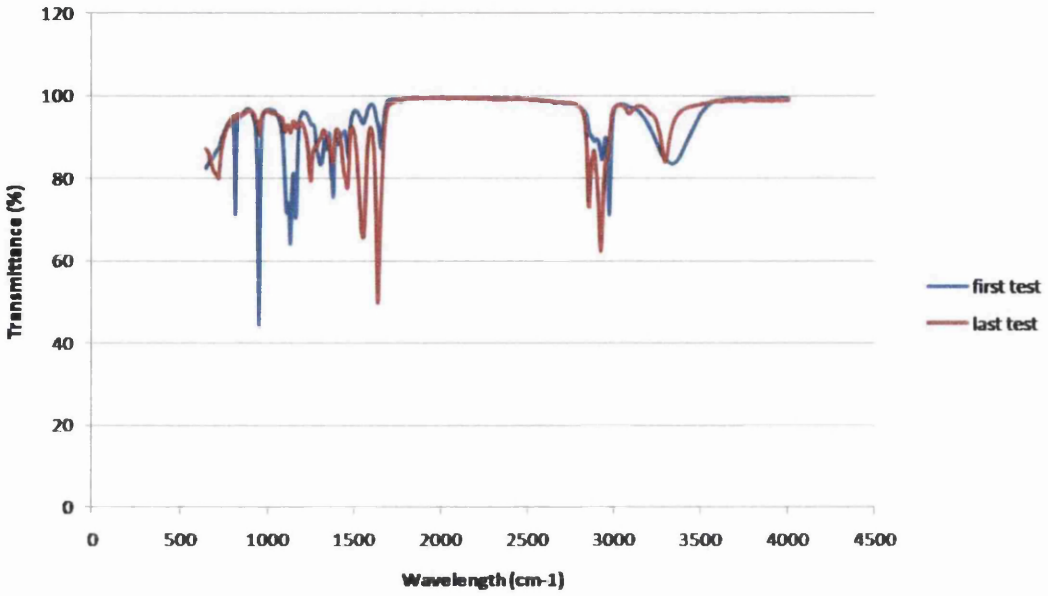


(a)

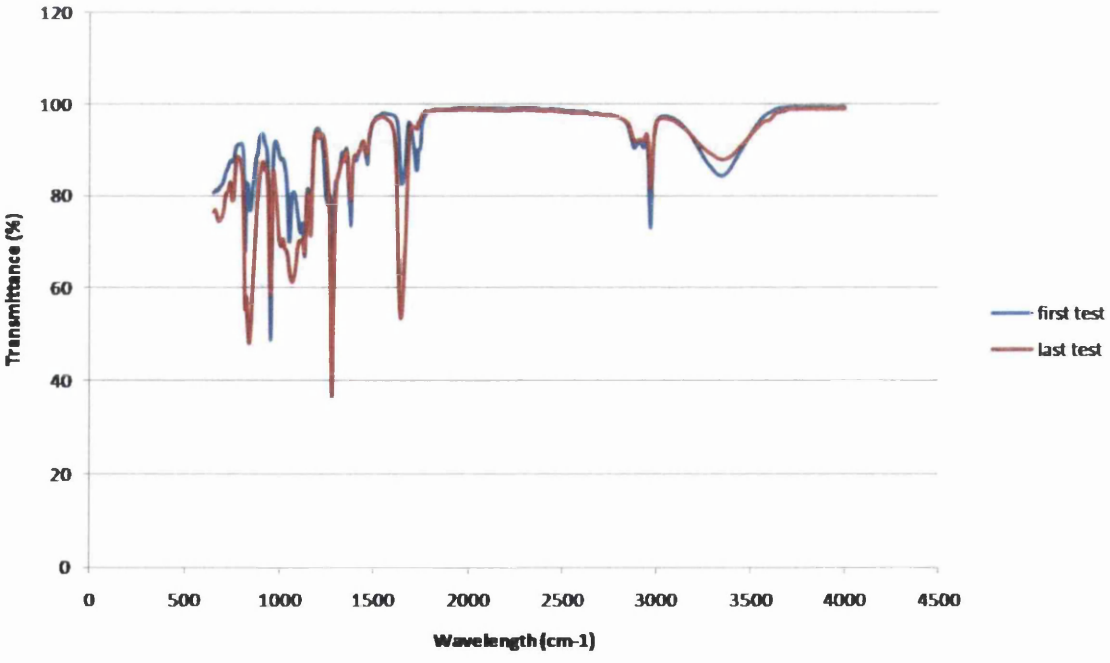


(b)

Figure 3.17: Examples of Changing Peaks for Polyamide (a) and Nitrocellulose (b) Based Inks

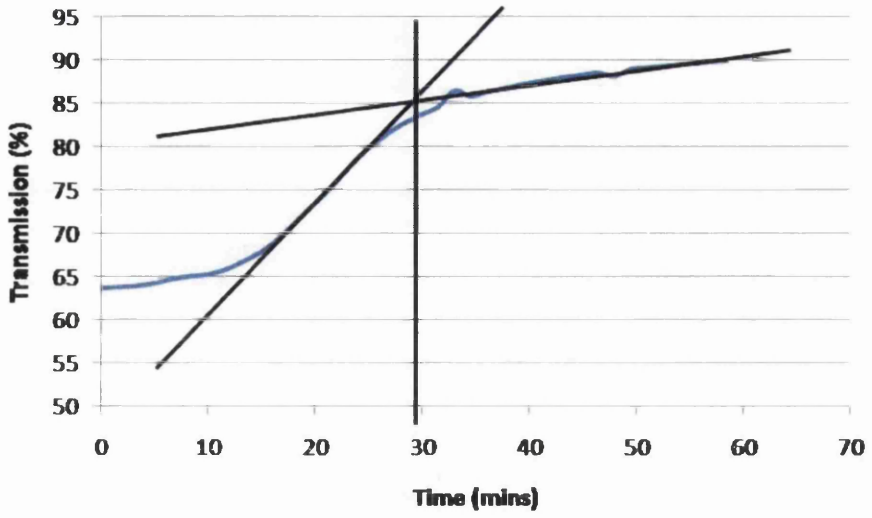


Figure 3.18: Example of Process to find the "Characteristic Time"

between 3000 and $2800cm^{-1}$ and a CO stretch at approximately 800 to $900cm^{-1}$. Polyamide itself has a prominent OH peak and CH peak. For this reason, the CO stretch was used in the polyamide inks to monitor the decrease in solvent concentration in the film.

Nitrocellulose resin inks had isopropanol and ethyl acetate solvents present. Therefore the isopropanol peaks were present, plus the saturated ester carbonyl stretch at $1752cm^{-1}$ and additional CH peaks and CO stretch peaks similar to those for the isopropanol. To observe the ethyl acetate reduction, the saturated ester peak at $1752cm^{-1}$ was used. The CO stretch was unable to be used to monitor the isopropanol due to ethyl acetate and the nitrocellulose resin itself having peaks in that range. Instead, the broad OH peak was used to observe the decrease in isopropanol.

The "characteristic time" was used to compare the inks. This was found by the intersection of the tangent situated at both extremities of the curve. The time at which the intersecion point occurs is used as the "characteristic time". These were plotted to show the relationship between the initial resin content and the time for the solvent to evaporate from the ink. An example plot is shown in Figure 3.18.

# Chapter 4

# Bulk Rheology

## 4.1 Introduction

The aim of the work described in this chapter was to gain an understanding of the structural changes that occur within the bulk of an ink during the drying process. This was achieved by monitoring the viscoelasticity using rheometry. The tests were conducted at room temperature and humidity which varied between $18^0$ to $23^0$ and 58 to 70%, respectively which was measured at the start of each test. The temperature was required to be as close to constant as possible, therefore room temperature was used. A series of rheological tests were carried out on model inks with two different resins, various initial resin concentrations and with and without solid particles. The range of inks allowed the effects and influence of resin type, initial resin concentration and the addition of solid particles upon the structure of the ink during the drying process, to be determined.

## 4.2 Results

The plate used for bulk rheology testing was a 60mm flat plate. A solvent cap was used over the plate to minimise solvent evaporation throughout the test period. Single frequency oscillatory testing was used, with no pre shear before the test was undertaken. The tests were at a frequency of 1Hz and a strain of 0.03. The gap used was $150\mu m$.

### 4.2.1 Polyamide

A series of drying tests were performed on inks of polyamide resin and isopropanol solvent.

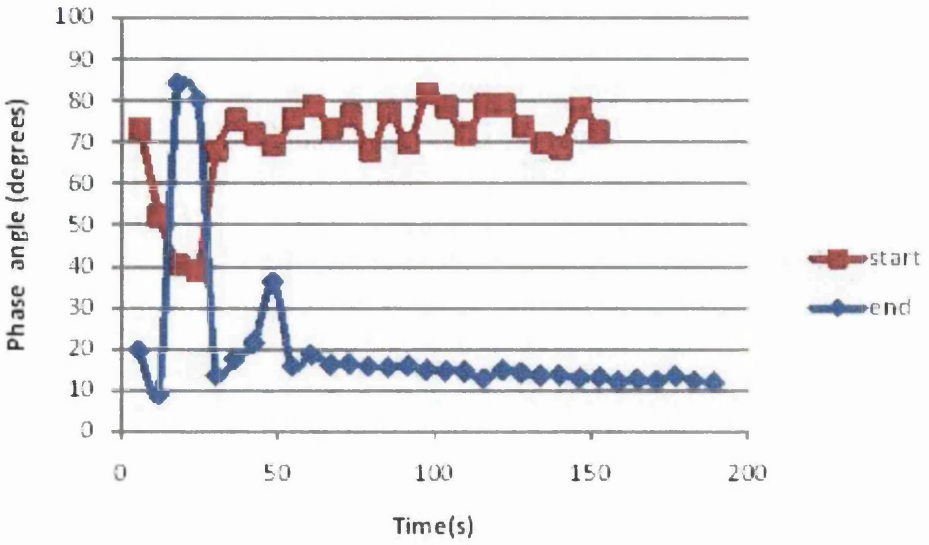


Figure 4.1: Initial Phase Angle of 25% Polyamide Resin Inks at Start and end of Drying

The oscillatory results at the beginning of the drying runs for each initial resin concentration showed a steady rheological profile throughout the period of the test. After an initial induction period from 0s to 60s the phase angle remained level throughout the remainder of the test, indicating the rheology was low and had little viscoelasticity. The induction period is a measuring artefact produced by the changes in shear at the initial stages of the experiment and was not included in analysis. There is slight variation throughout the level period due to the viscoelastic component being so small. The phase angle did not generally fall below $70^0$. This is illustrated by the plot named 'start' in Figure 4.1, which shows a typical test profile from one run with 25% initial resin content of polyamide.

The results at the end of the drying runs did not consistently produce such a steady rheological profile. They showed an increase in viscoelasticity over time. The plot named 'end' in Figure 4.1 shows the profile from one test from one run with the 25% resin content ink. After an initial induction period of large change from 0s to 60s, a measurement artefact caused by changes in shear, it shows a slight decrease in phase angle over the test period from $20^0$ to $10^0$. This indicates the viscoelasticity is high and increases throughout the test.

Figure 4.1 shows the change in viscoelasticity between the start and end of the drying of a 25% polyamide resin content ink. The phase angle dropped from approximately $70^0$ to below $20^0$ throughout the drying time. This shows a significant increase

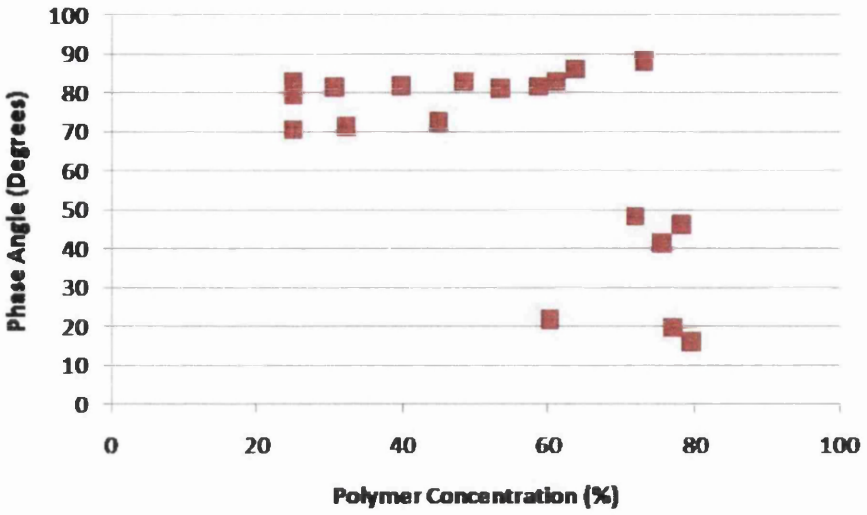


Figure 4.2: Phase Angle of 25% Polyamide Resin Ink over Drying Period.

in the viscoelasticity.

For each drying run the phase angle after the induction period was plotted against the calculated percentage resin content within the system. Figure 4.2 shows the phase angle change with percentage resin content for an ink with a resin content of 25% (A more comprehensive set of results for all experiments are shown in Appendix A). Each point on the graph shows the phase angle for each individual test. For this content there were five repeat test runs. The plot shows a level trend up to a critical point of approximately 75% resin content. At this critical concentration the phase angle drops abruptly, signifying a change in rheology towards more elastic-dominant. The phase angle at the critical concentration fell from $85^0$ to approximately $20^0$ over a percentage resin mass increase of only 5%. There is also an individual test that has a phase angle of $20^0$ at 60%. This can be regarded as an erronious result.

The plots of phase angle over the drying period for each initial resin content may be compared. The percentage resin gain required for a significant viscoelastic change to occur was determined for all the different resin content inks. These were plotted to show the relationship between the specified initial resin content and the actual resin mass gain for the significant change in viscoelasticity. The plot is shown in Figure 4.3. When plotted together, it is shown that there is a critical resin percentage at which viscoelastic change takes place, independent of initial resin content. The resin percentage is approximately 85%. There are some individual test results that sit outwith the general trends which can be regarded as erronious (the points below $50^0$

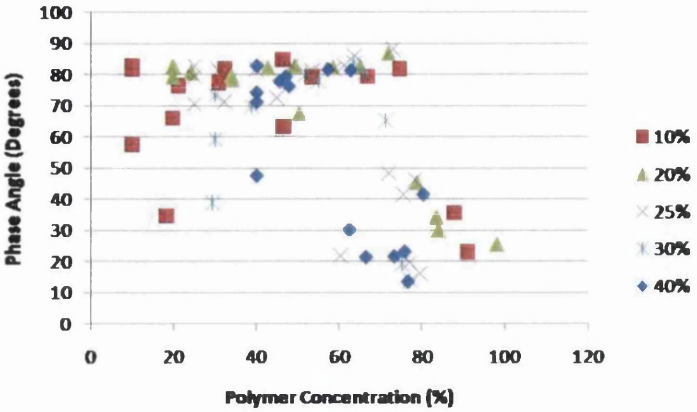


Figure 4.3: Resin Content Drying Profile for Polyamide Ink

at polymer concentrations below 60%).

### 4.2.2 Nitrocellulose

A series of drying tests was performed on inks containing nitrocellulose resin with isopropanol and ethyl acetate solvents.

The original oscillatory tests at the beginning of each drying run gave greater variability in the phase angle. Some showed a steady viscoelastic profile similar to that seen with the polyamide but others showed slight decreasing profiles. This generally amounted to about $10^0$ change throughout a test period. Typical test profiles for resin contents of 10, 25 and 40% are shown in Figure 4.4.

A 10% resin content started with a $70^0$ phase angle and remained steady throughout the test period. There is slight variation throughout the test due to the low viscoelasticity of the ink. At 25% the phase angle begins at $60^0$ and falls to $50^0$ throughout the test period. At 40% resin content the phase angle is between $20^0$ and $10^0$. Figure 4.4 shows the effect initial resin content has upon the viscoelasticity. The results for the nitrocellulose inks generally showed slightly lower phase angles at the end of their test periods.

Figure 4.5 shows one test from one run at 25% initial resin content at the end of a drying run. It again shows a very slight decrease in the phase angle from $10^0$ to $5^0$ over the time period indicating a slight increase in viscoelasticity during a test.

In contrast to the polyamide resin the nitrocellulose resins inks followed a progressive decrease in phase angle with percentage resin mass increase. A typical example is shown in Figure 4.6. The initial resin content is 25%. Each point on the graph represents the phase angle from an individual test after the induction period. There were

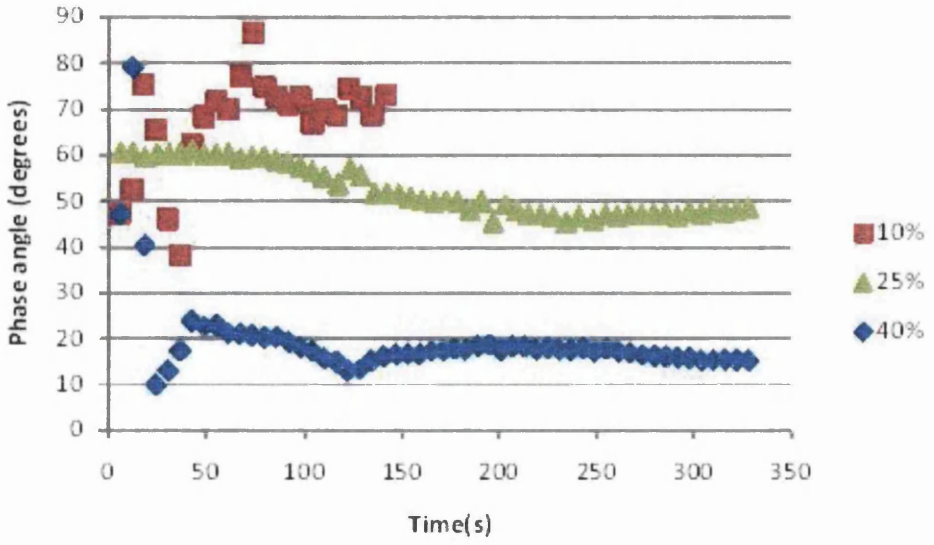


Figure 4.4: Phase Angle of 10%, 25% and 40% Nitrocellulose Resin Ink at Start of Drying Period.

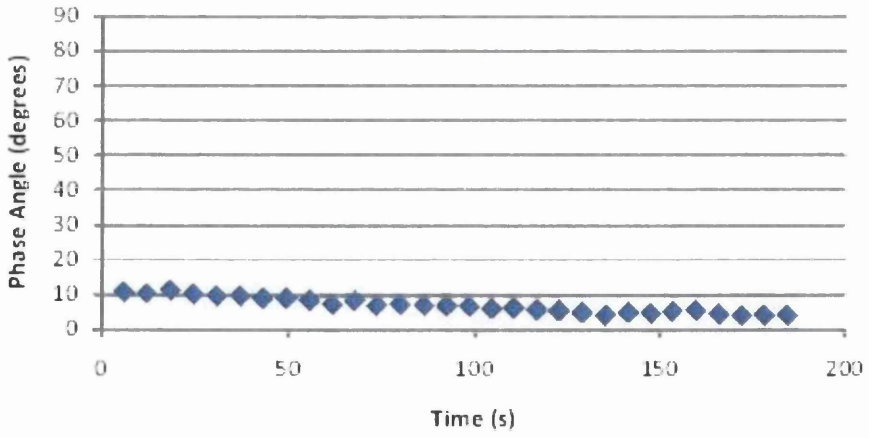


Figure 4.5: Phase Angle of 25% Nitrocellulose Resin Ink at end of Drying Period.

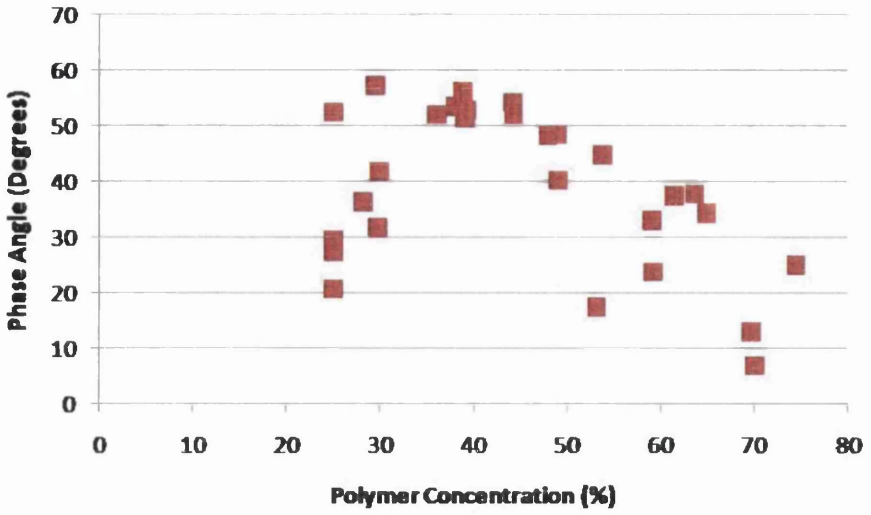


Figure 4.6: Phase Angle of 25% Nitrocellulose Resin Ink over Drying Period.

five individual test runs. A sudden drop-off in phase angle was not evident. Instead a trend line was plotted and the concentration at which the phase angle dropped to a minimum was taken as the critical point. In this case the change occurred with approximately 75% resin content in the system.

The plots of the phase angle over the drying period for each initial resin content can be compared as before. The percentage resin increase required for a significant rheological change to occur was determined for all the different resin contents. These were plotted to show the relationship with known initial resin content. The significant change, in this case, was taken as when the phase angle had dropped to a minimum at the end of the test. The plot is shown in Figure 4.7. It shows that the viscoelastic increase occurs at a similar rate, and at a similar point, independent of initial resin content. The point at which a minimum occurs is approximately 75%.

### 4.2.3 Polyamide with Solid

A series of drying tests was performed on polyamide resin inks with the addition of 10% $4\mu m$ spherical aluminium.

The oscillatory results at the beginning of the drying runs for each initial resin concentration showed a steady rheological profile throughout the period of test. After an initial induction period the phase angle remained level throughout the remainder of the test, the rheology was low and had little viscoelastic component. The phase angle did not generally fall below $70^0$. This is illustrated in the plot named 'start'

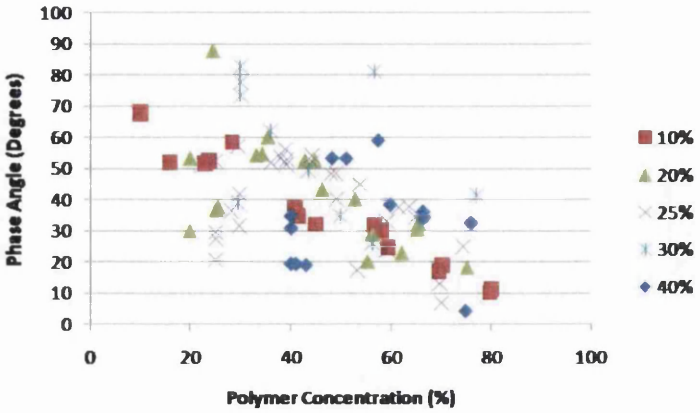


Figure 4.7: Resin Content Drying Profile for Nitrocellulose Resin Ink.

in Figure 4.8, which shows a typical test profile from one run with 25% initial resin content of polyamide.

The results at the end of the drying runs did not consistently produce such a steady rheological profile. They showed an increase in viscoelasticity over time. The plot named 'end' in Figure 4.8 shows the profile from one test from one run with the 25% resin content. It shows a slight decrease in phase angle over the test period from $20^0$ to $10^0$. There was an overall change in phase angle of $> 70^0$ to about $15^0$ during the entire drying period, indicating a substantial increase in viscoelasticity.

For each drying run the phase angle was plotted against the calculated percentage resin content. Figure 4.9 shows the phase angle change with percentage resin content for an ink with a resin content of 25%. Each point on the graph shows the phase angle for each individual test. For this content there were five repeat test runs. The plot shows a level trend up to a critical point of approximately 70% resin content. At this concentration the phase angle was found to drop abruptly signifying a change in rheology towards more elastic-dominant. The phase angle at this concentration fell from $85^0$ to approximately $20^0$ over a mass loss of only 5%, one thirteenth of the potential total mass loss.

The plots of phase angle over the drying period for each initial resin content may be compared. The percentage resin content required for a significant viscoelastic change to occur was determined for all the different resin content inks. These were plotted to show the relationship between the specified initial resin content and the the actual percentage resin content for the significant change in viscoelasticity. The plot is shown in Figure 4.10. It shows that there is a critical resin content percentage at which a viscoelastic change takes place. The resin percentage is 80%. Initial resin

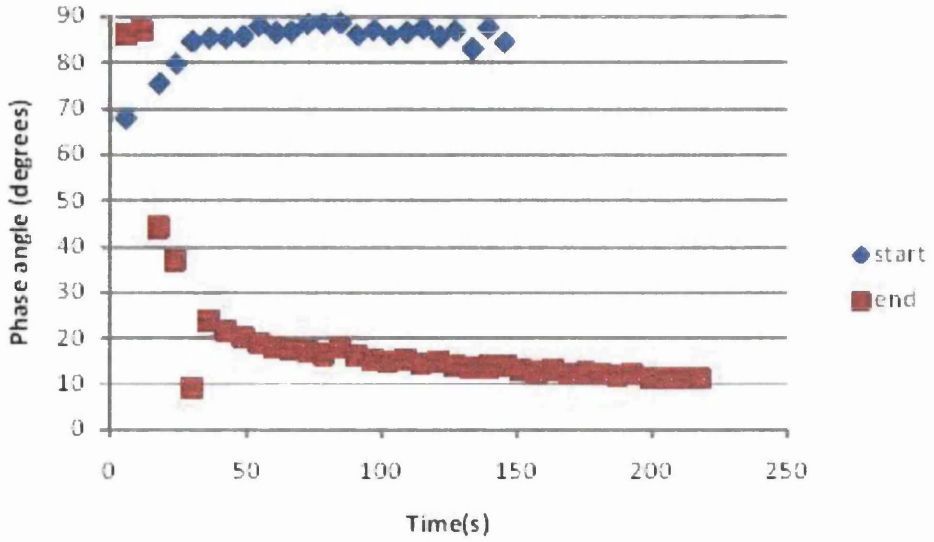


Figure 4.8: Phase Angle of 25% Polyamide Resin Ink with Solid Content at Start of Drying.

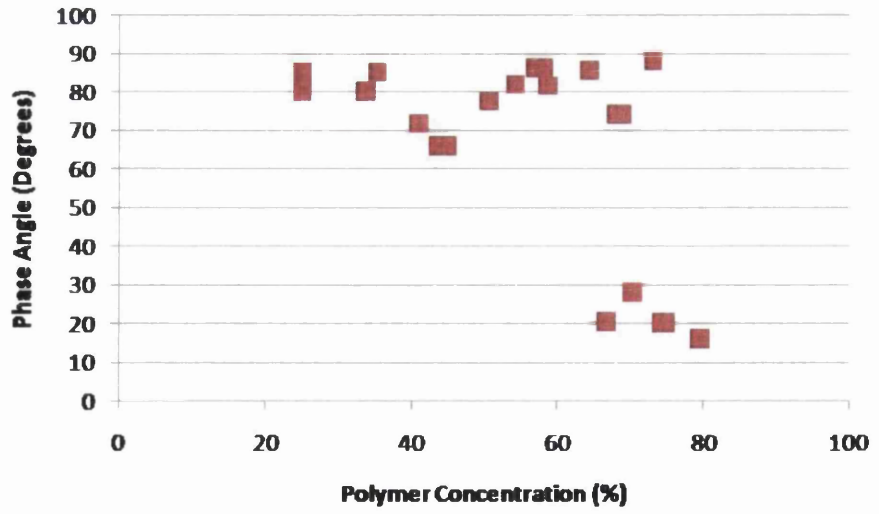


Figure 4.9: Phase Angle of 25% Polyamide Resin Ink with Solid Content over Drying Period.

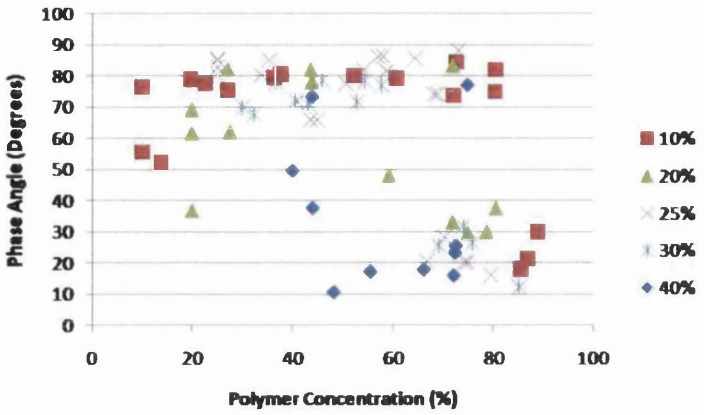


Figure 4.10: Resin Content Drying Profile for Polyamide Resin Ink with Solid Content.

content of 40% is an exception, where the viscoelastic change occurs at approximately 50% resin content.

### 4.2.4 Nitrocellulose with Solid

A series of drying tests was performed on a nitrocellulose resin with the addition of 10% 4$\mu m$ spherical aluminium.

The original oscillatory tests at the beginning of each drying run gave greater variability in the phase angle. Some showed a typical steady viscoelastic profile to that seen with the polyamide but others showed slight decreasing profiles. This generally amounted to about $15^0$ change throughout a test period. Typical test profiles for resin contents of 10, 25 and 40% are shown in Figure 4.11.

An initial period between 0s and 70s where large changes occur was observed for all three resin content inks. After this initial period the 10% resin content started with a $70^0$ phase angle and falls to $50^0$ throughout the test period. At 25% the phase angle remained steady throughout the test period at $45^0$. At 40% resin content the phase angle remained steady throughout the test period at $15^0$. The results for the nitrocellulose inks generally showed slightly lower phase angles at the end of their test periods.

Figure 4.12 shows one test from one run at 25% initial resin content at the end of a drying run. It again shows a very slight decrease in the phase angle from $30^0$ to $10^0$ over the time period indicating a slight increase in viscoelasticity during a test.

In contrast to the polyamide resin, the nitrocellulose resin inks followed a progressive decrease in phase angle with percentage resin content. A typical example

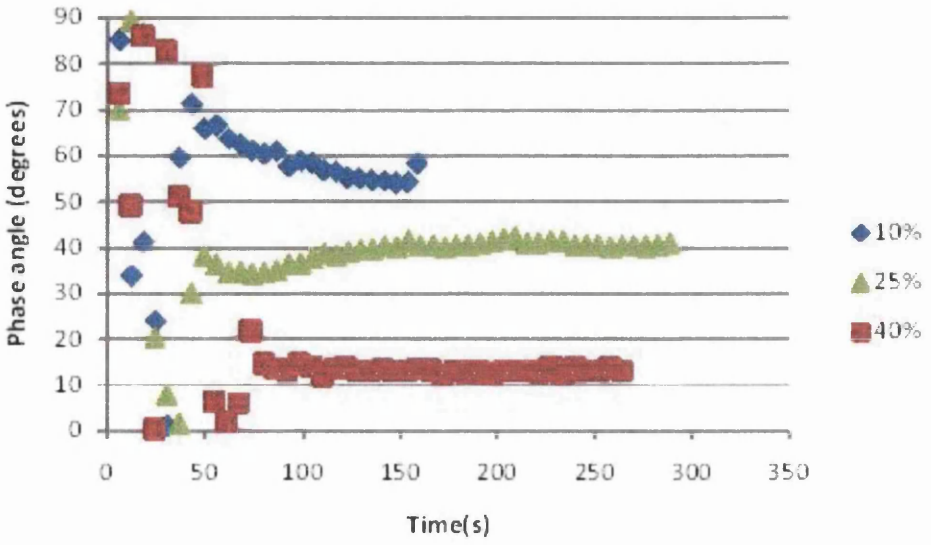


Figure 4.11: Phase Angle of 10%, 25% and 40% Nitrocellulose Resin Ink with Solid at Start of Drying Period.

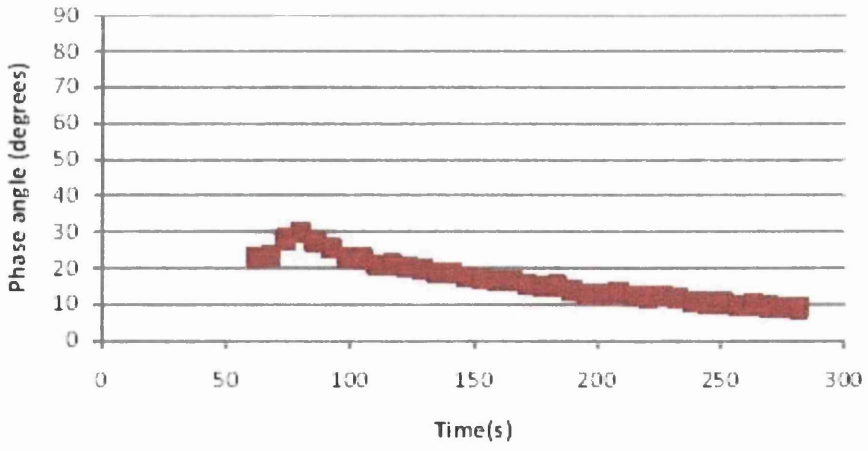


Figure 4.12: Phase Angle of 25% Nitrocellulose Resin Ink at End of Drying Period.

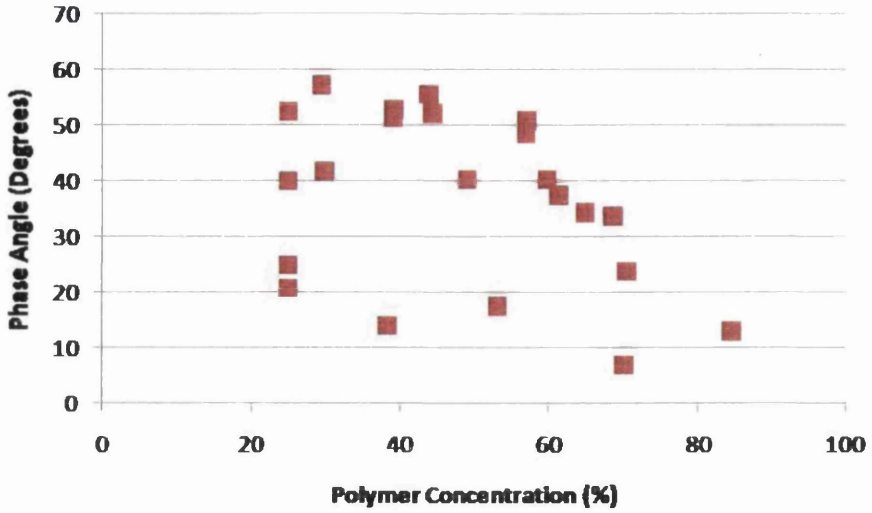


Figure 4.13: Phase Angle of 25% Nitrocellulose Resin Ink over Drying Period.

is shown in Figure 4.13. The initial resin content is 25%. Each point on the graph represents the phase angle from an individual test. There were five individual test runs. A sudden drop-off in phase angle was not evident. Instead a trend line was plotted and the concentration at which the phase angle dropped to a minimum was taken as the critical point. In this case the change occurred with approximately 80% resin content.

The plots of the phase angle over the drying period for each initial resin content can be compared as before. The percentage resin content required for a significant rheological change to occur was determined for all the different resin contents. These were plotted to show the relationship with known initial resin content. The significant change, in this case, was taken as when the phase angle had dropped to a minimum at the end of the test. The plot is shown in Figure 4.14. It shows that the viscoelastic increase occurs at a similar rate and at a similar point independent of initial resin content. The point at which the minimum occurs is approximately 75%. Initial resin content of 40% is an exception, where the minimum occurs at approximately 60% resin content.

### 4.2.5 Commercial Ink Bulk Rheology

The bulk rheology was taken over the drying period using the same methodology as the model inks. The results are shown in Figure 4.15. This shows that there is a gradual rheological change over the drying period. The phase angle is within the

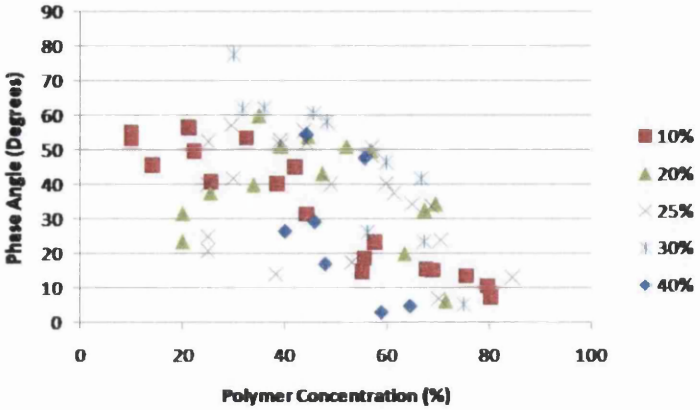


Figure 4.14: Resin Content Drying Profile of Nitrocellulose Resin Ink with Solid.

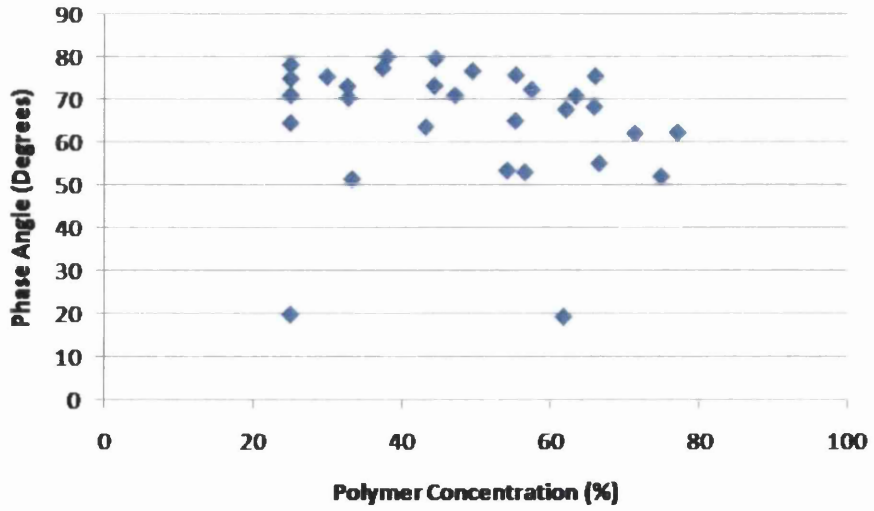


Figure 4.15: Bulk Rheology over Drying Period for Commercial Ink

range of $50^0$ to $80^0$. The mean trendline shows a slight decrease from approximately $70^0$ to $60^0$.

A gradual rheological decrease during the drying process is attributed to the amount of solid content in the ink. The ink is of a high viscosity and with more solid content than the model inks tested. The solid therefore has a more significant effect on the rheology than the resin or solvent. A decrease of phase angle is observed, showing an increase in rheology throughout the period is consistent with the model ink experiments of nitrocellulose.

### 4.2.6 General Observations within Drying Tests

The viscoelasticity change for all four inks occur at very similar percentage resin content. The point at which the viscoelasticity changes, occurs with approximately 10% less resin content for nitrocellulose than polyamide. The addition of 10% solid does not make a significant difference to either polyamide or nitrocellulose systems. The only exceptions were the 40% initial resin content polyamide and nitrocellulose model inks with solid. The viscoelastic change occuring at lower resin content; approximately 35% less for polyamide and 15% less for nitrocellulose.

There are two rheological measurement artefacts present within the tests. Firstly the initial induction period within the tests and secondly the rheology test results that are produced at the latter stages of the run when the fluid is becoming more elastic and are no longer steady state. Instead, a decrease in phase angle over the time of the test was observed. There is an increase in the elastic and viscous moduli over the test time, with the elastic modulus increasing rapidly compared to the viscous modulus. This is illustrated in Figure 4.16. This phenomenon would be regarded as rheopexy and is highly unusual in fluids. However, it is more likely to be explained as a measurement artefact. Both artefacts can be explained by the rheological settling of an elastic fluid. The material undergoes a number of procedures before it is tested that produce a shear. Firstly there is a constant shear upon the fluid by the drill stirrer where it is mixed. A smaller sample of the fluid is then removed from the container using a spatula, creating shear. This sample is then spread on the rheometer base where the test is run. The series of shears decreases the elasticity of the ink. When on the rheometer plate, and throughout the rheology test it is allowed to regain its natural viscoelasticity. This is due to the strain in the rheology tests being very small and having very minimal effect upon the bulk rheology. The tests are carried out with no rest time given for the fluid to relax and so the induction period observes the relaxing behaviour. Throughout the test, the increase in viscoelasticity is observed.

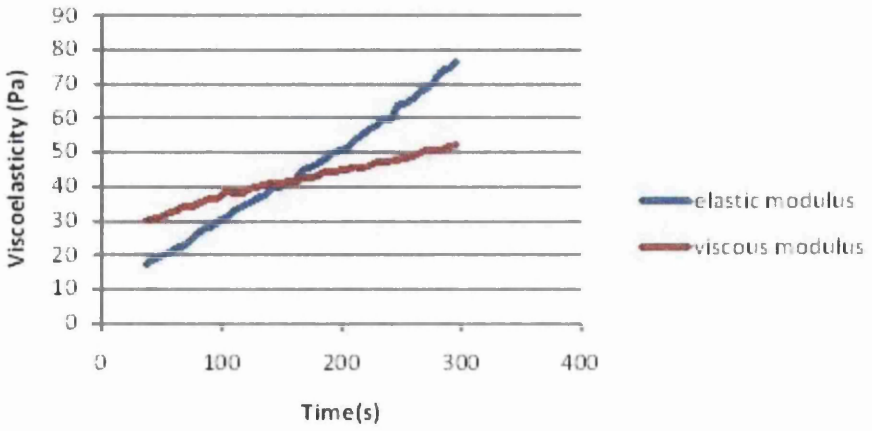


Figure 4.16: Elastic and Viscous Moduli of Initial Tests over Time

This can be an explanation for the rheopectic behaviour found in the latter stages of the runs. This would not be apparent in a low viscous fluid as there is very little elasticity and therefore is not affected by shear to such an extent.

## 4.3 Discussion

### 4.3.1 Model Ink Drying

Polyamide resin consists of frequent inner molecular ring structures and a repeating amino amide structure. This produces strong polar and especially hydrogen bonding forces. They are therefore soluble in solvents with similar properties. Isopropanol is a strongly hydrogen bonding solvent and polyamide is therefore able to be dissolved in isopropanol. According to Hinden[106], polyamide resin with Isopropanol as a solvent has a maximum solute concentration of 58%. This was achieved by heating the solution while mixing. This was comparable with the formulations used in the tests, where 50% resin was the maximum concentration achieved using the method described in Section 3.2.

The polyamide ink was prepared by dissolving the polyamide resin in Isopropanol solvent. Evaporation of the solvent molecules from the ink throughout the drying period, leads to the polymer matrix density of the polyamide molecules increasing. This increase in matrix density decreases the ease at which the solvent can evaporate through the polymeric matrix. There comes a point at which the overlapping of the

polymers becomes sufficient for the polyamide molecules to form hydrogen bonds. At this point the solvent is unable to evaporate freely from the matrix and instead diffusion occurs. Physical gelation occurs as the matrix is continually increasing in density forming more and more hydrogen bonds and consequently trapping solvent molecules. This is seen in the bulk rheology results, where there is close to steady state Newtonian rheology for a long period of solvent loss. This is where there is freely evaporating solvent from the ink and no real gel formed. There is then a sudden increase in viscoelasticity shown by the sudden decrease in phase angle. This represents the critical concentration at which the polymer matrix has become sufficiently dense to create a gel and stops the solvent from freely evaporating. Diffusion occurs with the gel becoming increasingly rigid.

Nitrocellulose resin is manufactured by the nitrating of cellulose by use of nitric acid. [107] Cellulose in its untreated state, is insoluble in water and most organic solvents, and so to be used within these environments, a more reactive, less insoluble group is added. Doing this creates a polymer with two distinct segments. An unreacted insoluble side and a reactive functional side. [108] This is found to be true for nitrocellulose resin within the solvent mix of isopropanol and ethyl acetate. 50% was again the maximum solute concentration that could be achieved.

The bulk rheology for nitrocellulose observed in the tests outlined here is indicative of a dominant entanglement process. With the evaporation of solvent from the ink, the resin polymers get closer together. The closer they are, the greater the overlapping and entanglement. The nitrocellulose polymer is classed as a rigid polymer and therefore entanglement may be expected to take place over a longer period before it becomes critical. This period of entanglement, along with aggregation due to the complexity of nitrocellulose, is speculated to lead to the relative gradual increase in elasticity with this system. [10, 84, 85, 24, 27]

This gelation process of entanglement and aggregation can result in phase separation. This phase separation is found within the results of this research for all nitrocellulose resin content inks. Phase seperation occurs as aggregation and is seen as the energetically favourable contact between the polymer. The white colour appears throughout the range of nitrocellulose inks due to the light wavelength being altered by the crystal structures formed. [85, 84] In systems with higher solvent content, there is a tendency for phase separation to result in 'powdering', shown in Figure 4.17. This is a white crystalline powder that is formed throughout the system and is unable to adhere to the substrate. The polymer in a high solvent percentage, has more time and space to find the energetically low state. Isopropanol and ethyl

Figure 4.17: Picture of Powdering Effect that Occurs from Drying of Nitrocellulose Resin Ink

acetate are both 'good' solvents, as they readily allow contacts to be made between the solvent and polymer. The use of a 'poor' solvent may enhance the gel stability by reducing the ability of these contacts to occur. However at such low resin content, it will always be hard to maintain homogenous gel stability for such a complex polymer.

### 4.3.2 Addition of solid

The rheological properties of polymeric systems filled with solid are governed by the properties of the polymer and also the suspended solid. The adhesive properties between the polymer and solid also affect the rheology. This provides for a large range of rheological phenomena. The properties will depend on the amount of solid suspended within the polymer. With a low percentage loading of solid, the properties of the polymer dominate, whereas when the solid is heavily loaded the properties of the solid are dominant. When the loading is low there is very slow agglomeration of the solid due to the polymer inhibiting the particle movement and this can lead to settlement. This was observed throughout the inks used.

A drying ink involves evaporation of solvent with the gelation of polymer. This gelation and evaporation of solvent, results in the contraction of the polymer structure. With a suspended solid within the polymer structure, the volume fraction of the solid increases over the drying period. This will influence the affect of the solid over the drying period. This will be reflected in the rheology throughout the drying period.

The addition of solid content into the inks tested showed very little effect upon the rheology of the bulk of the system. This is probably due to the small percentage

of solid introduced to the system. 10% solid within the bulk of the system will have little effect on the bulk rheology as there are not sufficient solid spheres to restrict the movement of the polymer or solvent.

## 4.4 Closure

The physical process of gelation was observed within the bulk of the film with respect to the polymer concentration. It was found that the polymer used has a large effect upon the gelation process due to the bonding processes involved. The point at which the gelation creates a significant change within the structure is independent of polymer and of the initial polymer concentration. This occurs at approximately 80% resin content. The addition of solid content changes this relationship to initial polymer concentration, where at high initial polymer content (40%) viscoelastic change occurs significantly sooner than the stated value. The significant points are:

- Polyamide: steady drying profiles with critical concentration point at which viscoelasticity increases dramatically. Due to simplistic hydrogen bonding gelation process where matrix becomes significantly dense to form a structured gel at the critical concentration point.
- Nitrocellulose: progressive increase in viscoelasticity throughout the drying process due to complex entanglement and aggregation processes.
- Percentage resin content within system required to produce a viscoelastic change is independent of initial resin content for both polyamide and nitrocellulose.
- Solid content has little effect upon both Polyamide and Nitrocellulose inks due to insufficient solid to restrict movement of polymer and/or solvent.

As well as observing the physical processes of the bulk, the same processes at the surface of the film should be considered. The physical processes of gelation at the surface will be able to be compared to those in the bulk and contribute additional information to how the drying process occurs and the factors that influence it. This will be carried out in Chapter 5.

# Chapter 5

# Surface Rheology

## 5.1 Introduction

The aim of the work described in this chapter was to gain an understanding of the structural changes of an ink's surface during the drying process. The changes in the viscoelasticity were monitored by means of rheometry. These results were able to be compared to that of the bulk. The tests were conducted at room temperature and humidity which varied between $18^0$ to $23^0$ and 58 to 70% respectively for the same reasons as stated in Chapter 4. A series of rheological tests using the same range of inks as Chapter 4 were made.

## 5.2 Results

Single frequency oscillatory testing was used. The parameters used were the same as chapter 4, with a frequency of 1Hz and a strain of 0.03. The gap was varied throughout the test runs from 150 to $3500\mu m$. This was to bring the geometry into the correct contact with the surface.

The results for the surface rheology are presented as plots of phase angle on the y-axis and percentage solvent mass loss on the x-axis unless stated otherwise.

### 5.2.1 Surface Rheology During the Drying of model inks using a Bicone

#### 5.2.1.1 Polyamide

The polyamide resin inks follow a flat rheological profile with time until an abrupt change in phase angle occurred at a singular percentage resin content. This point occurred at a different percentage resin content depending on the initial resin content.

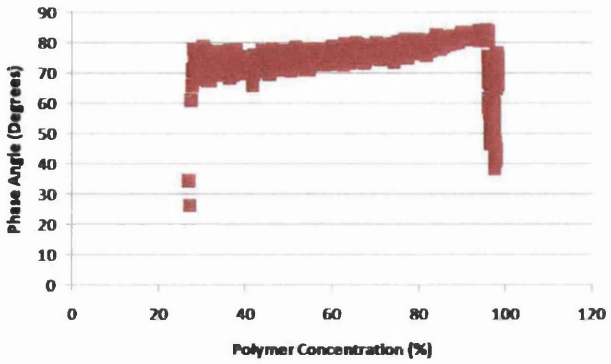


Figure 5.1: A Plot of Phase Angle of 25% Polyamide Ink over Drying Period.

The initial stages of the drying tests indicate an unchanging rheology of low viscosity and little viscoelasticity after the initial induction period. This is represented by a high phase angle of approximately $70^0$ throughout this period for all the polyamide inks except that with 40% resin content. This test showed a decrease of the phase angle over this period from $80^0$ to $60^0$, suggesting a slow increase in viscoelasticity throughout the period. At a certain percentage resin content, the rheology changed dramatically and decreased sharply towards zero.

The phase angle fell to under $20^0$ for all the inks tested, showing a dramatic increase in viscoelasticity over a small increase in resin content. This trend is shown in Figure 5.1. This plot shows the phase angle change with percentage resin content for an initial resin content of 25% polyamide. There were five repeat runs for this resin content. Each run produced a similar plot profile. The plot shows a roughly flat profile at approximately $75^0$ phase angle. This continues in the initial period up to approximately 60% resin content. After this there is a slight increase in phase angle until a critical point is reached. At this critical point, the phase angle drops abruptly, signifying a change in rheology towards more elastic dominant. In Figure 5.1 the critical point occurs at approximately 95% to 100% resin content. At this point, it abruptly falls from approximately $85^0$ phase angle to $40^0$ phase angle over an resin content increase of only 1%.

The plots of the phase angle over the drying period for each initial resin content were compared. The percentage resin content required for a significant rheological change to occur was determined for all the different resin contents. It is shown that the viscoelasticity change occurs at a similar percentage resin content for the initial resin contents between 20% and 30%. This occurs at just under 100%. However 10% and 40% are exceptions, occuring at 60% and 80% respectively. The relationship

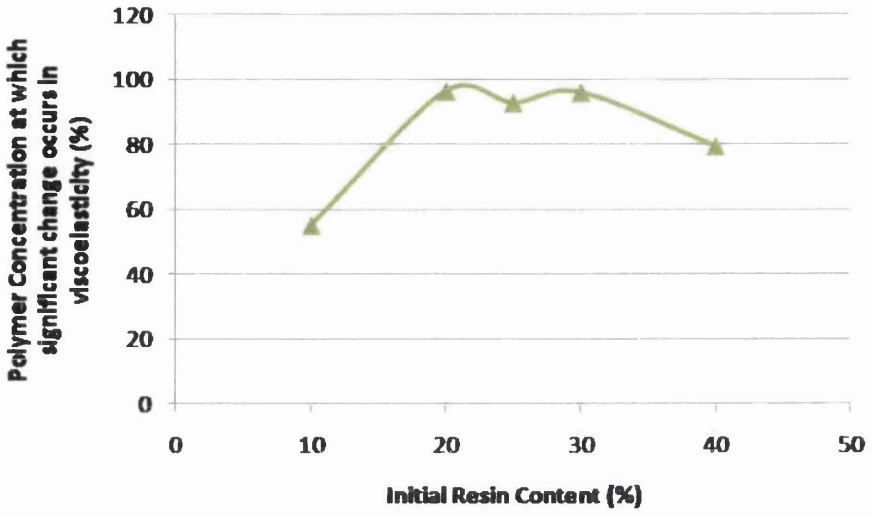


Figure 5.2: The Polymer Concentration Required for a Rheological Change Against Polyamide Resin Content Using Bicone

between the initial resin content and the mass loss required for a significant change in rheology to occur is shown in Figure 5.2. There is a decrease in solvent mass loss with an increase in initial resin content but this trend does not extend through to the 10% initial resin content where there is a decrease from the 20% resin content ink. Comparing the profile with the corresponding profile for the bulk rheology (Figure 4.2) there is little variation in the solvent loss needed to cause a rheological change throughout the range. The profile is also flatter.

#### 5.2.1.2 Nitrocellulose

The nitrocellulose resin was found to give very different results to the polyamide. The nitrocellulose resin inks followed a steady decrease in phase angle indicating an increase in rheology throughout the drying period.

The test results at the beginning of the drying run do not indicate a steady rheological state over the range of initial resin contents. Each test, however, started at approximately $75^0$ phase angle throughout the range of inks. This suggests a rheology of low viscosity and with little elasticity. In most tests a decrease of the phase angle over the drying period was observed from approximately $75^0$ to $30^0$, with the exception of 40% initial resin content, which had a minimum of $35^0$. This suggests a slow increase in viscoelasticity throughout the drying period. This trend is shown in Figure 5.3, for an initial resin content of 25% nitrocellulose resin. There were five

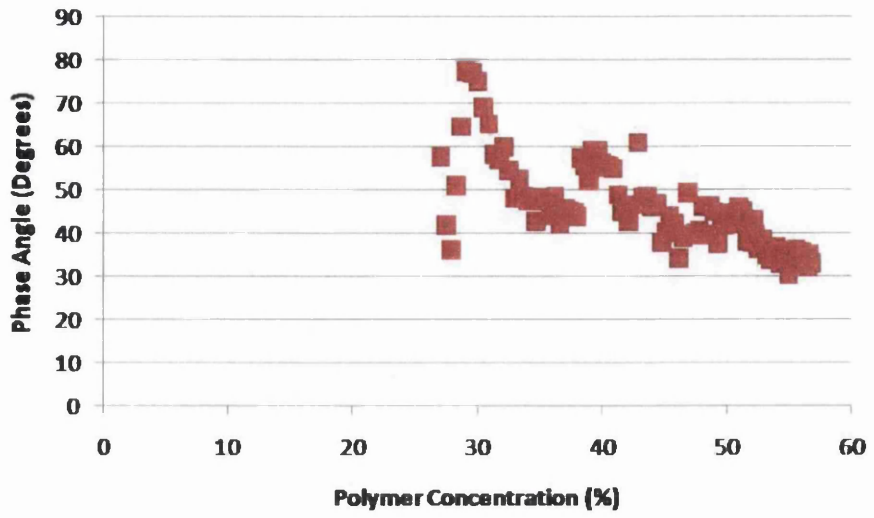


Figure 5.3: A Plot of Phase Angle of 25% Nitrocellulose Ink over Drying Period.

individual runs. Each run produced a plot similar in profile. After an induction period similar to that observed in the bulk rheology tests, the plot starts at approximately $85^0$ phase angle followed by a decrease of the phase angle throughout the increase in resin content. The phase angle after the decrease is approximately $30^0$. The change occurs up to a resin content of 58%.

The plots of the phase angle over the drying period for each initial resin content may be compared. The percentage resin content required for a significant rheological change to occur was determined for all the different initial resin contents. These were plotted as before to show the relationship between the initial resin content and the resin content required for a significant change in rheology to occur. The significant change taken as the minimum phase angle observed during the final period of the test. The plot is shown in Figure 5.4. Throughout the range of initial resin content inks, the viscoelastic change to occur is independent of initial resin content. 20% intial resin content is an exception, where the viscoelastic change at a much higher polymer concentration.

#### 5.2.1.3 Polyamide with solid content

Tests were performed with the bicone on the samples of ink with 10% 4 $\mu m$ spherical aluminium solid pigment added to the polyamide resin.

The polyamide resin inks followed a steady rheological profile until an abrupt change in phase angle occured at a percentage resin content. A similar trend to the

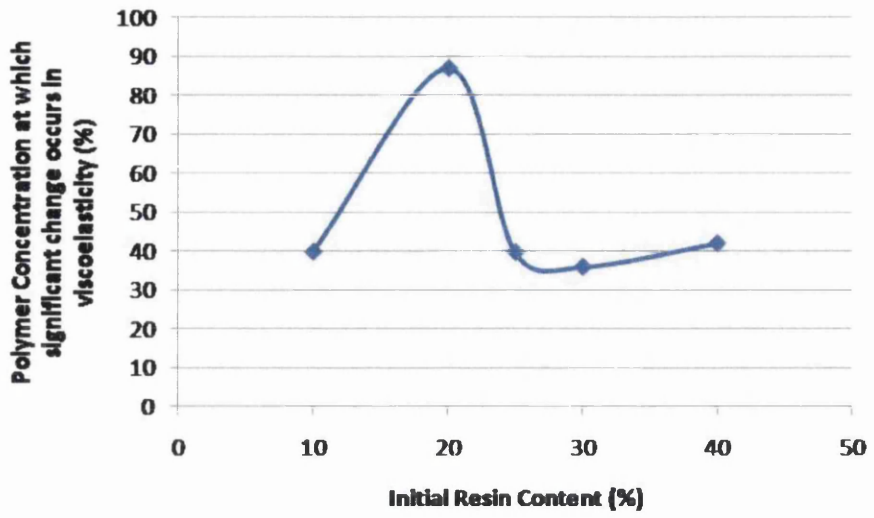


Figure 5.4: The Polymer Concentration Required for a Rheological Change Against Nitrocellulose Resin Content Using a Bicone.

non-pigmented polyamide inks tested previously.

The test results show a steady state profile of low viscosity with little elasticity over the majority of the drying period, represented by a high phase angle of approximately $70^0$ throughout for 20%, 25% and 30% resin content. The 10% resin content ink maintained a steady profile at approximately $50^0$. The 40% test showed a decrease of the phase angle over this period from $75^0$ to $55^0$ indicating a slow increase in viscoelasticity throughout the period. After the initial period, a rapid decrease of phase angle followed. The phase angle fell to under $20^0$ for all inks indicating a dramatic increase in viscoelasticity over a small increase in resin content.

This trend is shown in Figure 5.5. The initial resin content was 25% polyamide resin with 10% solid content. Each run produced a plot similar in trend. A flat profile continues up to approximately 50% resin content where a slight increase in phase angle to approximately $85^0$ followed. At a percentage resin content, the phase angle dropped abruptly to approximately $5^0$. The critical point occured at approximately 90% resin content.

As previously, a graph was plotted to show the relationship between the initial resin content and the percentage resin content required for a significant change in rheology to occur. The plot is shown in Figure 5.6. The polymer concentration required for a viscoelastic change occurs close to 100% for inks up to 25% initial resin content. For 25% to 40% initial resin content inks, the concentration decreased with an increase in initial resin content. These results show that the addition of solid to

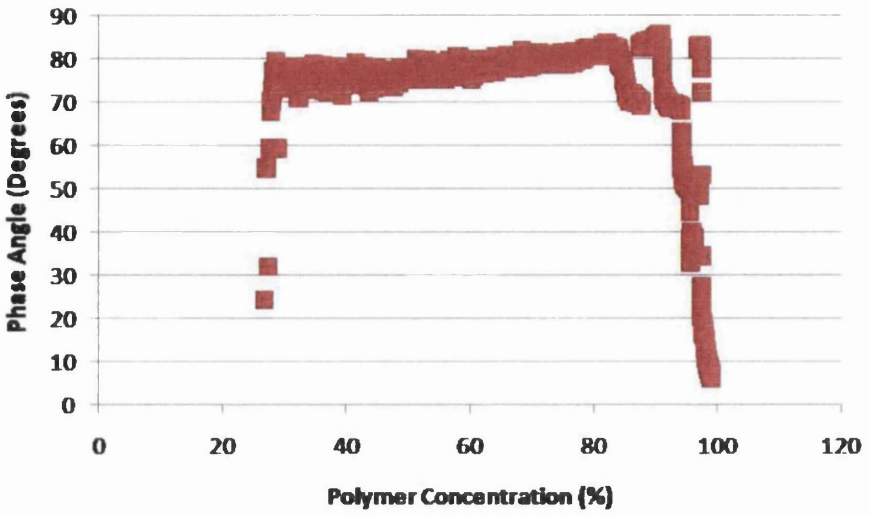


Figure 5.5: A Plot of Phase Angle of 25% Polyamide Ink with Solid Content over Drying Period.

the ink, produces a decrease to the percentage resin content required to produce a change in viscoelasticity.

#### 5.2.1.4 Nitrocellulose with solid content

A series of bicone drying tests were performed on the nitrocellulose resin inks with the addition of 10% pigment.

The nitrocellulose resin ink with 10% solid content followed a steady decrease in phase angle throughout the drying period similar to un-pigmented inks, with the exception of 10% and 20% inks. For 10% and 20% resin content, at the beginning of the run the phase angle remains steady at $75^0$ and $85^0$ respectively, indicating a low viscosity with little elasticity. After the initial steady period, the phase angle decreases to approximately $20^0$. The 25%, 30% and 40% tests begin, however, at approximately $85^0$ phase angle. The test shows a gradual decrease of the phase angle over the drying period from approximately $85^0$ to $20^0$ with the exception of 30% initial resin content which has a minimum of $35^0$.

The typical profile of the higher initial resin content inks is shown in Figure 5.7. The plot starts at approximately $85^0$ phase angle followed by a decrease of the phase angle throughout an increase in percentage resin content. The phase angle after the decrease is approximately $20^0$. The change occurs over a mass loss of 25%.

As previous, a graph was plotted to show the relationship between the initial resin content and the percentage resin content required for a significant change in rheology

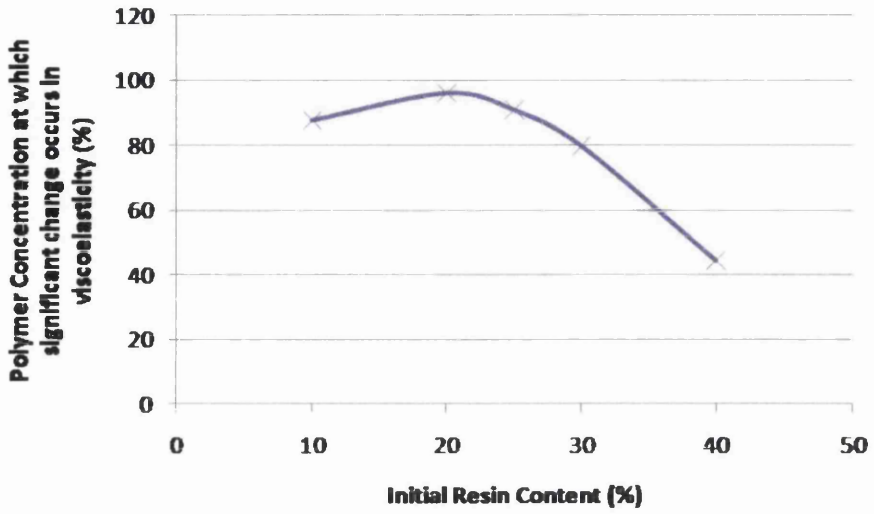


Figure 5.6: The Polymer Concentration Required for a Rheological Change Against Polyamide Resin Content.

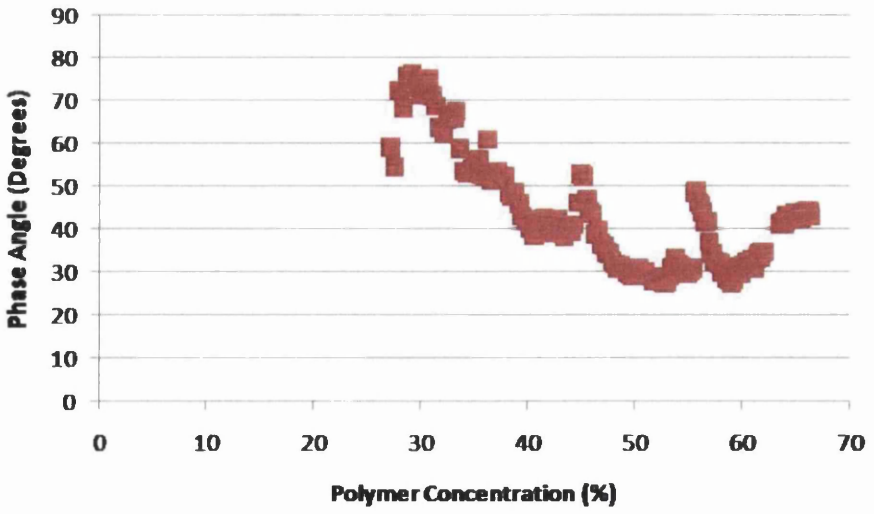


Figure 5.7: A Plot of Phase Angle of 25% Nitrocellulose Ink with Solid Content over Drying Period.

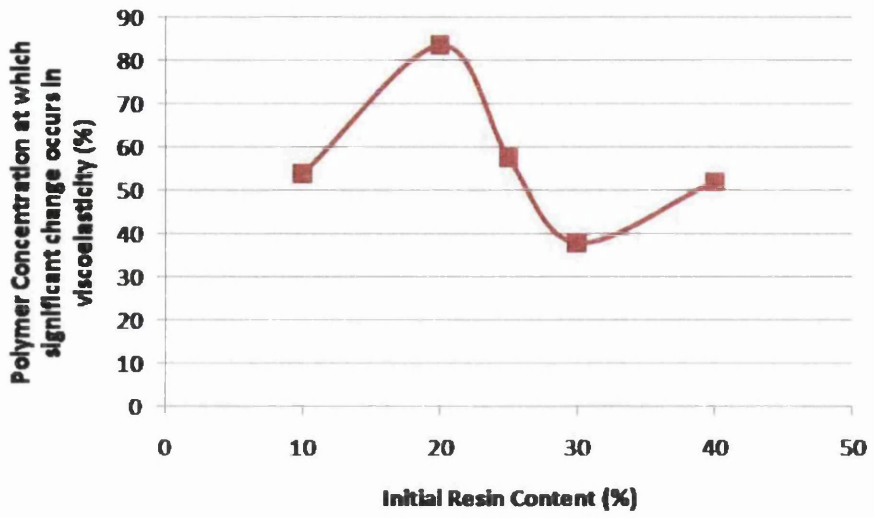


Figure 5.8: The Polymer Concentration Required for a Rheological Change Against Nitrocellulose Resin Content.

to occur. The plot is shown in Figure 5.8. There is no definitive trend present with 10%, 25% and 40% similar in concentration, whereas 20% and 30% require a higher and lower concentration respectively to produce a viscoelastic change. The results suggest an increased sensitivity to the gelation process.

## 5.2.2 Drying Tests for Surface Rheology of Model Inks using Dunouy Ring

A series of tests using a Dunouy Ring attachment were performed with both polyamide and nitrocellulose inks, using the same procedure as for the bicone.

### 5.2.2.1 Polyamide

The polyamide resin inks followed the flat rheological profile until an abrupt change in phase angle occurs at a certain percentage resin content. This point occurs at different percentage resin contents depending on the initial resin content. This trend is similar to that of the bicone, however the phase angle in the initial period was only $10^0$, much lower than found on the bicone. The phase angle rises abruptly towards the end of the initial period. This increase is from approximately $10^0$ to a phase angle of between $35^0$ and $60^0$. The 40% resin content increases gradually throughout. After the increase in phase angle, the familiar rapid decrease followed. The phase angle fell

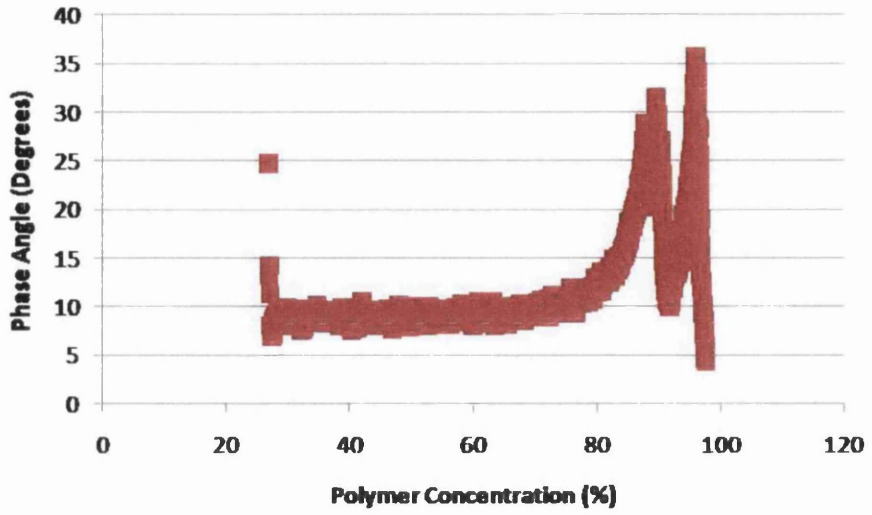


Figure 5.9: A Plot of Phase Angle of 25% Polyamide Ink over Drying Period.

to approximately $10^0$ for all inks. This increase and decrease occured over a small change in resin content.

This trend is shown in Figure 5.9 for an initial resin content of 25% polyamide resin. The plot shows an initial steady period of viscoelasticity at a phase angle of approximately $10^0$. At roughly 70% resin content, the phase angle increases to $35^0$ at 90%. At this point there is a sudden drop in phase angle to under $50^0$. It is thought that the apparent initially 'high' level of viscoelasticity observed in the ink is the result of the Dunouy attachment inability to respond to low viscosity fluids accurately.

A percentage resin content correlation graph is plotted the same as for the bicone. The plot is shown in Figure 5.10. There is a decrease in percentage resin content with an increase in initial resin content from 20% onwards. The plot shows the same flat profile to that found using the bicone. This trend does not extend through to the 10% initial resin content, there being a decrease from the 20% resin content. It can be seen that at 10% initial resin content, there needs to be 60% resin content required to produce a significant rheological change, whereas at 20%, close to 100% resin content is required.

#### 5.2.2.2 Nitrocellulose

There is considerable variation throughout the nitrocellulose tests, leading to no clear profile in many cases. This is thought to be due to the delicate nature of the Dunouy

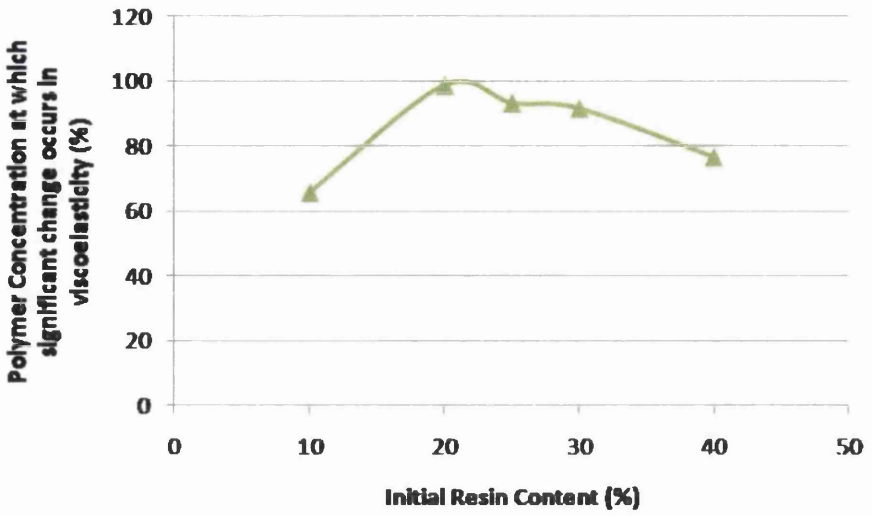


Figure 5.10: The Polymer Concentration Required for a Rheological Change Against Polyamide Resin Content.

ring which may be sensitive to the gel structures developed by this ink. All ink resin contents generally had a low phase angle of between $10^0$ and $20^0$ rising to a phase angle of over $50^0$. There then followed a decrease to under $40^0$. A typical plot is shown in Figure 5.11. The plot shows a steady increase in phase angle from approximately $5^0$ to $70^0$. There is a steady period from 30% onwards when the phase angle varies between $70^0$ and $80^0$. From 25% initial resin content onwards the plots do not have a clear trend.

The plot comparing the percentage resin content with initial resin content is shown in Figure 5.12. There is a decrease in percentage resin content with an increase in initial resin content up to 25% initial resin content. 30% and 40% initial resin content inks show an increase in concentration. However, the accuracy of the plots must be questioned due to the poor definition of the rheology profiles obtained.

#### 5.2.2.3 Polyamide with solid content

Tests were performed on the inks containing the addition of 10% solid to the polyamide resin. The viscoelastic drying profiles followed a similar trend to that of the polyamide ink without solid.

The test results show a steady state rheology of approximately $10^0$ throughout this period for 10%, 20% and 25% resin content. The 30% and 40% tests show a gradual increase of the phase angle over this period. At a certain percentage resin content, the

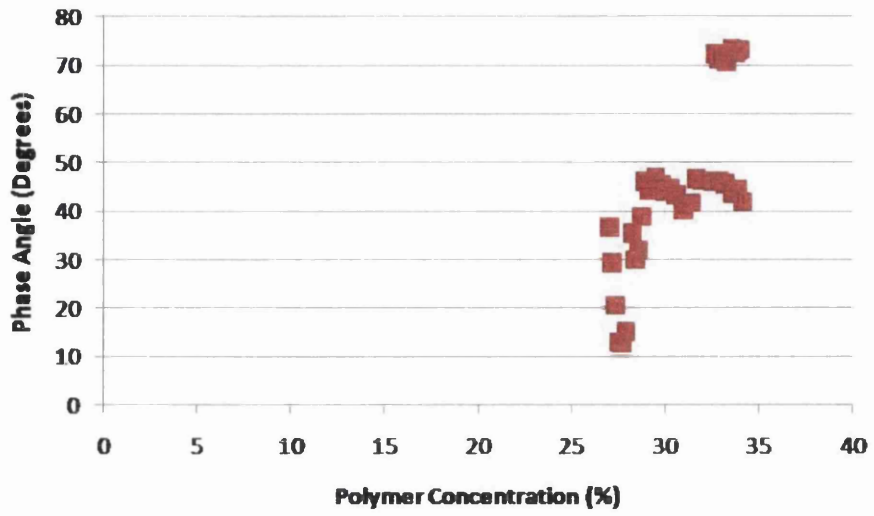


Figure 5.11: A Plot of Phase Angle of 25% Nitrocellulose Ink over Drying Period.

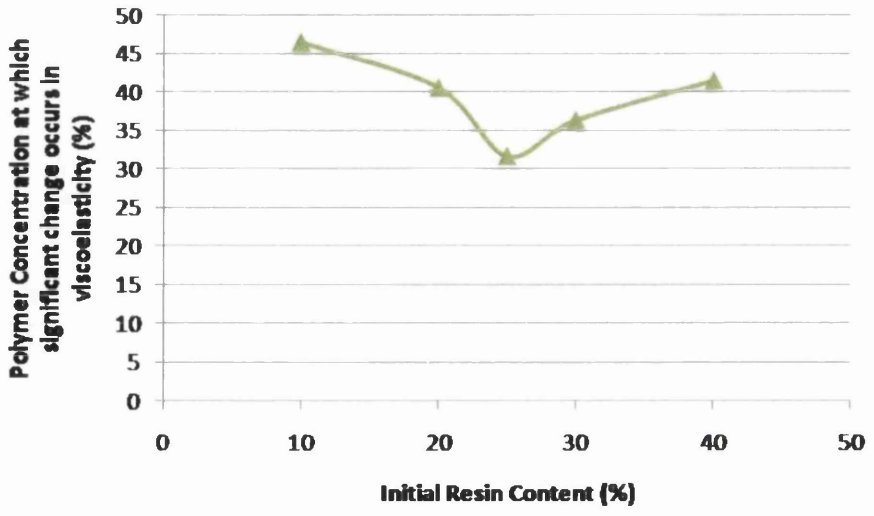


Figure 5.12: The Polymer Concentration Required for a Rheological Change Against Nitrocellulose Resin Content.

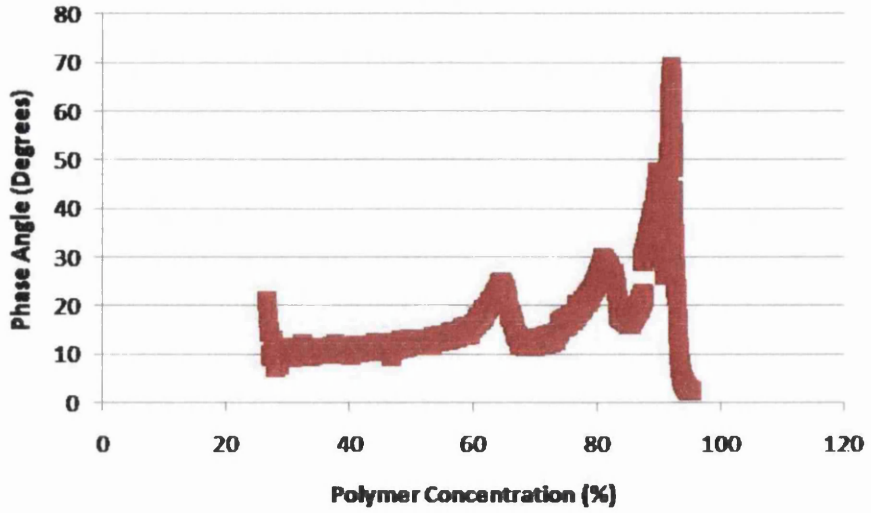


Figure 5.13: A Plot of Phase Angle of 25% Polyamide Ink with Solid Content over Drying Period.

rheology changed dramatically for all the inks. The phase angle increased abruptly towards the end of the steady state period for 10%, 20% and 25% resin content inks to a phase angle of $60^0$, $70^0$ and $55^0$ respectively. The phase angle then fell to approximately $10^0$ or under for all inks over a small increase in percentage resin content.

This trend is shown in Figure 5.13. The initial resin content was 25% polyamide resin with 10% solid content.

The plot shows a linear trend at approximately $10^0$ phase angle. This continues in the initial period up to approximately 60% resin content. There are two small peaks followed by a significant increase in phase angle to $70^0$, dropping abruptly to under $5^0$. This occurs at approximately 90% resin content. The two peaks are an artefact of the averaging of the multiple tests carried out.

The plot comparing the percentage resin content with initial resin content is shown in Figure 5.14. There is a general decrease in percentage resin content required for viscoelastic change with an increase in initial resin content. These results show that with the addition of solid to the ink, less resin content is required for a viscoelastic change to occur.

#### 5.2.2.4 Nitrocellulose with solid content

A series of drying tests were performed on the nitrocellulose based ink with the addition of 10% pigment.

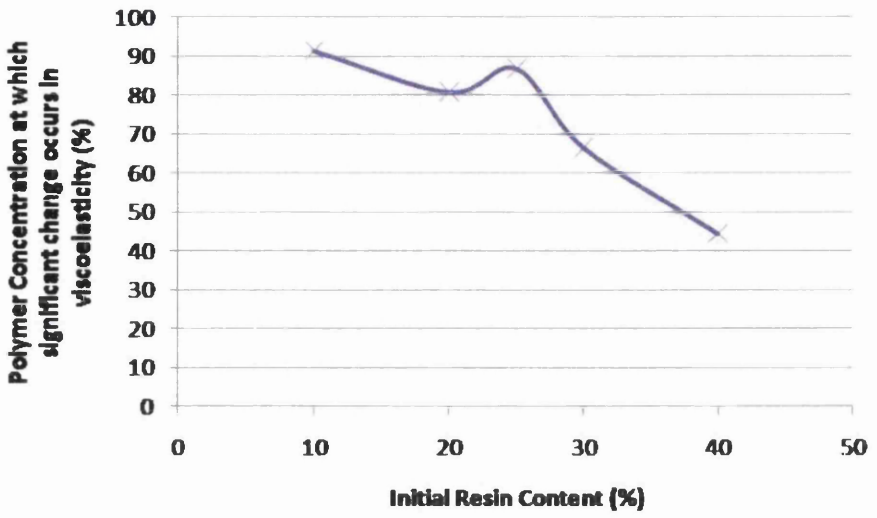


Figure 5.14: The Polymer Concentration Required for a Rheological Change Against Polyamide Resin Content.

In general, all the inks begin with a phase angle of $10^0$ or under, with the exception of 30%, which had a phase angle of $40^0$. There is not a general trend present throughout the range of inks. 10% to 25% increase from $10^0$ to between $60^0$ and $70^0$. 20% and 25% then decrease to $10^0$ and $30^0$ respectively. 30% and 40% begin at $45^0$ and $15^0$ respectively and decrease linearly to $30^0$ and $5^0$ respectively.

This trend of the lower initial resin content inks is shown in Figure 5.15 which is a plot of 10% initial resin content ink. There is an initial low phase angle of approximately $10^0$ until 20% resin content, after which it rises to approximately $60^0$ at 35%.

The plot comparing the percentage resin content with initial resin content is shown in Figure 5.16. There is a general increase in percentage resin content with an increase in initial resin content. The accuracy of the results again have to be questioned due to the definition of the rheology profiles obtained.

### 5.2.3 Commercial Ink Surface Rheology

The Surface Rheology was conducted using both the bicone and Dunouy ring. The results are shown in Figure 5.17.

The bicone shows a decrease in phase angle from $85^0$ to approximately $40^0$. This occurs up to 50% resin content. From this point onward, the results have a high degree of variability up to 75%. The Dunouy ring results show a rise in phase angle

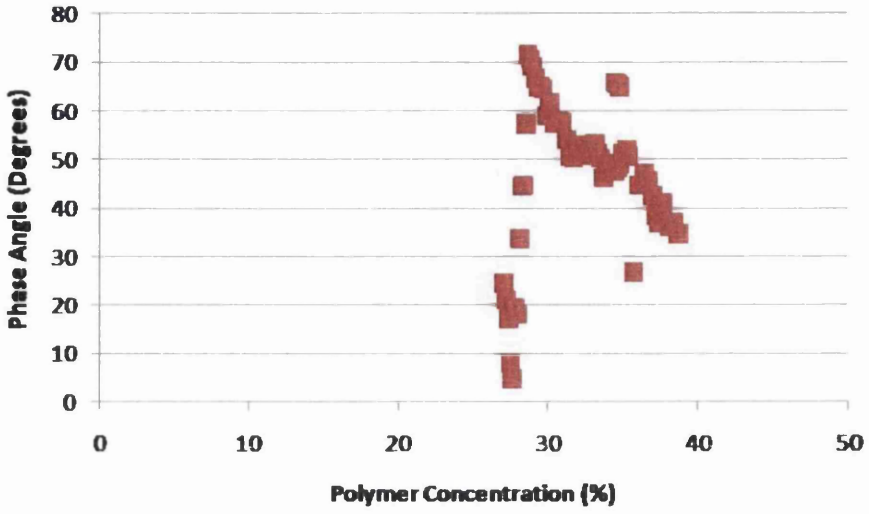


Figure 5.15: A Plot of Phase Angle of 25% Nitrocellulose Ink with Solid Content over Drying Period.

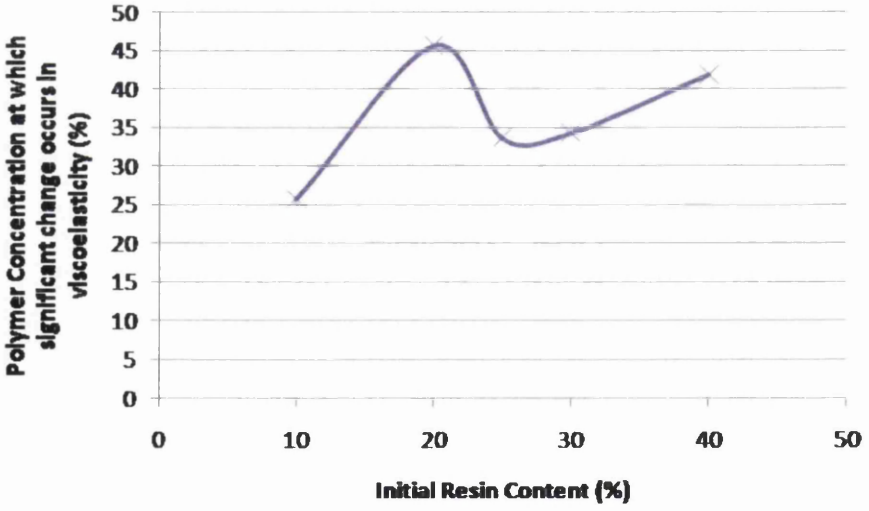


Figure 5.16: The Polymer Concentration Required for a Rheological Change Against Nitrocellulose Resin Content.

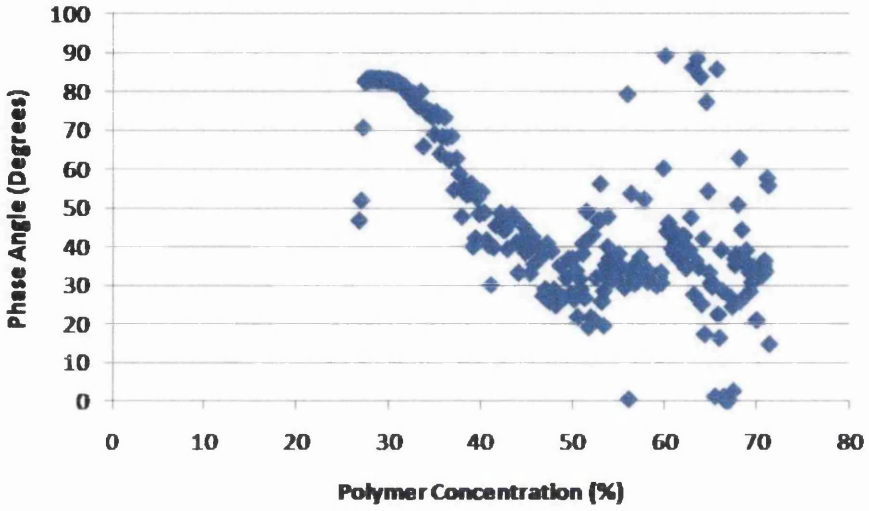


(a) Surface Rheology of Commercial Ink using Bicone

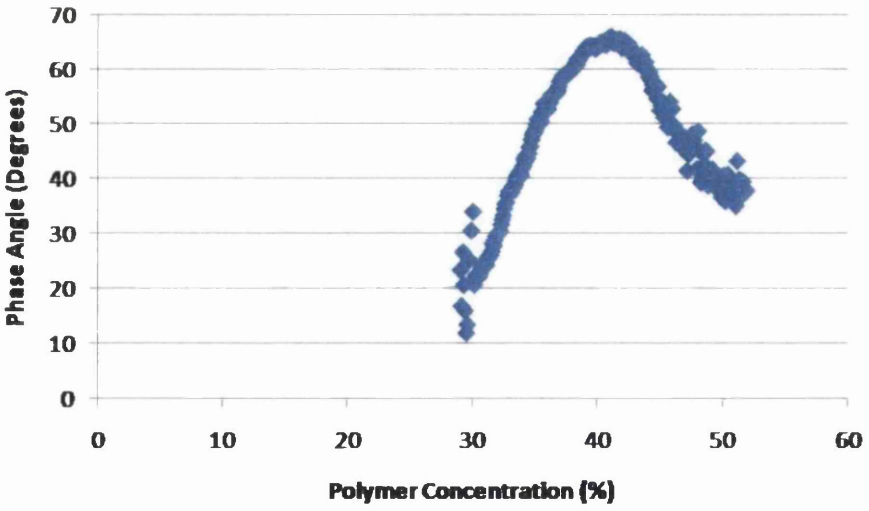


(b) Surface Rheology of Commercial Ink using Dunouy Ring

Figure 5.17: Surface Rheology over Drying Period for Commercial Ink

from approximately $20^0$ to $65^0$. The phase angle then decreases to approximately $40^0$ at approximately 50% mass loss. There is a distinct change in the rheology of the surface.

The bicone shows the rheology increases similar to that of the nitrocellulose inks, as expected due to the nitrocellulose formulation of the commercial ink. This shows skinning occurs quite rapidly with drying. There is a more dramatic decrease with the surface rheology than that of the bulk rheology results, where there is only a slight decrease in rheology observed over this period of time. The Dunouy ring does not produce a clear result. This is similar to the results of the model inks, where the delicate nature of the Dunouy ring obscures the results. The minimum phase angle at the end of the test occurs at approximately 50% resin content which is similar to when large variability within the bicone results are observed.

These results are consistent with the model ink results. Skinning is observed to occur before a change in bulk rheology. The addition of solid content and higher viscosity increase the skinning effect of the system. The bicone proved an effective method for analysis of drying time for this ink.

### 5.2.4 Repeatability factors of Dunouy Ring

There are thought to be particular factors related to the use of the Dunouy ring in drying tests. The polyamide test results show the phase angle to be at $10^0$ during initial drying period. This indicates that the viscoelasticity is initially high and close to solid like, despite using the same test procedure as carried out with the bicone. The Dunouy ring has very little surface area, and therefore when a fluid is very low in viscosity and close to no elasticity it encounters very little resistance to the oscillatory motion which it is undergoing. Instead of measuring the viscoelasticity of the fluid it measures the mass of the Dunouy ring through the air. As soon as there is resistance to the oscillatory movement of the Dunouy ring, the viscoelasticity of the fluid is able to be measured and the phase angle registers accurately. The time period under which the drying takes place can be taken as relatively accurate, although the viscoelasticity cannot.

The opposite problem can be seen for the nitrocellulose resin. The nitrocellulose inks increase in viscoelasticity quite quickly and an accurate phase angle is registered relatively early on in the drying test and continues to decrease. The oscillatory motion of the Dunouy ring is resisted quickly after the start of the test, especially at the higher resin content inks. The Dunouy ring is a very delicate piece of thin wire therefore the high resis

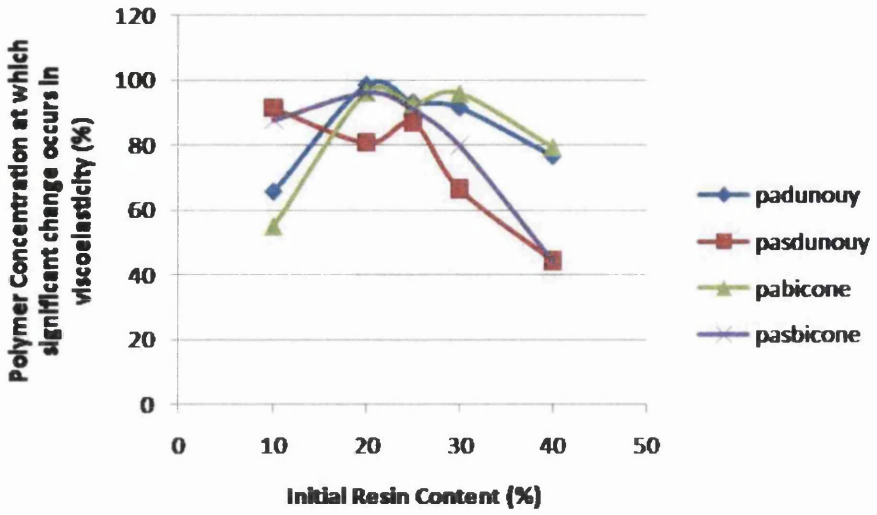


Figure 5.18: The Polymer Concentration Required for a Rheological Change Against Polyamide Resin Content.

tance to movement can lead to bending of the Dunouy ring instead of the surface of the ink moving.

## 5.3 Discussion

### 5.3.1 Correlation between Bicone and Dunouy Ring Measurement of Surface Rheology

The polyamide inks show a close correlation between the different sets of data for bicone and Dunouy ring used to construct the drying profiles. They are shown in Figure 5.18. The trend of decreasing percentage resin content with increasing initial resin content is evident, with the phase angle changes being quite similar. This is true both with and without solid content. However, already discussed, the Dunouy ring test results are unable to be used to show explicit phase angle changes throughout the drying period. The main variation is visible at the very lowest resin contents ($<$ 20%).

The correlation for the nitrocellulose inks including solids content is lost. This is shown in Figure 5.19. Both experimental techniques show that there is very little effect of solid content on the percentage resin content required to provide a rheological change. The percentage resin content required is significantly different throughout the lower resin content inks up to 25%. The difference at these lower resin contents

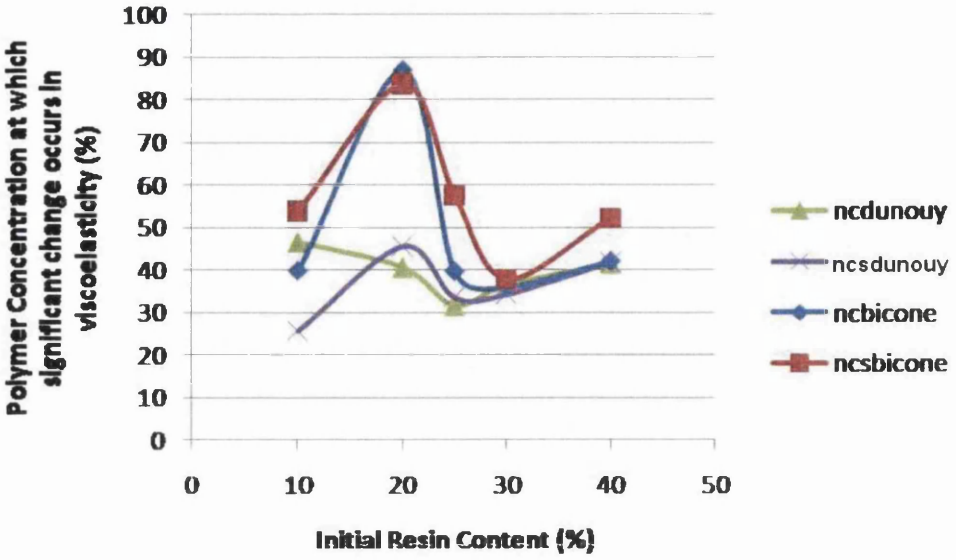


Figure 5.19: The Polymer Concentration Required for a Rheological Change Against Nitrocellulose Resin Content.

with and without solid is up to 50% resin content. The percentage resin content is similar at the higher resin contents, more likely due to the initial viscoelasticity of the inks being so high.

The nitrocellulose data (Figure 5.19) is too variable for any trend to be apparent with the addition of solid content. This is probably the result of phase separation. The phase separation of an ink with such a low resin content, causes powdering of the system which the highly sensitive surface attachments are detecting. However, the addition of solid to polyamide resin inks does show significant difference in the percentage resin content required for viscoelasticity to develop (Figure 5.18). There is a noticeable difference to the resin content required at the higher resin content inks which is revealed by use of both bicone and Dunouy ring techniques. At the lower resin content, settling out of the solid content is possible due to the initially low viscoelasticity of the polyamide inks. The higher resin content inks are more likely to support the solid content and therefore increasing the viscoelasticity.

### 5.3.2 Physical Differences between Bulk and Surface

During the drying process, there is a change in state from a rubbery state when the polymer is nearly saturated, to a glassy state when the polymer is nearly dry. When a polymer film is desorbed, a glassy region develops at the exposed surface. The

polymer is now in two distinct states of a glassy skin and a rubbery bulk. This is called literal skinning.[109, 110] The glassy region of the surface has a much lower diffusion coefficient than the rubbery bulk. The lower the diffusion coefficient, the longer the solvent will take to diffuse through the film. The results suggest that with the high resin content for both polyamide and nitrocellulose inks, skinning readily takes place. This is reflected in the differences between the viscoelastic profiles of the ink measured using bulk and surface techniques. This skinning will slow the diffusion process down and if prominent enough will inhibit the diffusion process completely.

The surface rheology for nitrocellulose inks is seen to increase before that of the bulk. Less solvent is required to leave the system for skinning to occur than that required for the bulk to change rheology. There is an initial resin content at which point the skinning of the system plateaus and occurs rapidly and with less solvent loss. This occurs at 25% resin content for inks both with and without solid content. Before this point, phase separation is dominant, with powder being formed instead of a gelated skin. Once the resin content is sufficient, gelation is more dominant than phase separation and skinning is formed readily.

Polyamide shows the surface rheology changes at similar mass loss to that of the bulk rheology up to approximately 25% initial resin content. This can be explained by settling of the resin within the system. As the system is low in viscosity throughout the majority of the ink range, the resin and solid settle due to gravity. With this, it is predominately solvent at the surface of the ink. Only when the concentration in the system is sufficient due to drying is the resin able to bind together and the resin forms a tightly bound matrix at the surface. Without solid content, the initial viscoelastic concentration has not reached a high enough concentration to cause a critical skinning point where there is a plateau reached similar to that of nitrocellulose. With the addition of a solid, the sensitivity to increasing solid content is significantly greater and skinning occurs more rapidly.

Polyamide resin without solid present is dependent upon the initial resin content for the rate at which skinning occurs compared to that of the bulk. There is no plateau at which point skinning occurs with very little solvent loss. This is the case for nitrocellulose, where a plataeu is reached at which point skinning occurs rapidly.

## 5.4 Closure

The physical process of gelation was observed upon the surface of the film with respect to the polymer concentration. The polymer used has a large effect upon the gelation

process due to the bonding processes involved, similar to that found in the bulk. The point at which the gelation creates a significant change within the structure, is dependent on polymer and on the initial polymer concentration. An increase in initial resin content, decreases the resin content required for a viscoelastic change to occur. Nitrocellulose plateaus after a certain initial resin content (25%), whereas polyamide continues to decrease. The addition of solid content does not effect this relationship to initial polymer concentration for nitrocellulose, however for polyamide it decreases the resin content required further. The significant points are:

- Similar drying profiles to those observed in bulk rheology occur at the surface for polyamide and nitrocellulose systems.
- Polyamide: Difficulty in forming skin readily due to low viscosity of polymer. Gravity causes settling of polymer. Once able to form skin, the skin is formed dependent on the initial resin concentration.
- Polyamide: Addition of solid increases the sensitivity to initial resin concentration and increases the rate of skin forming due to an increased ability to form a bound matrix at the surface.
- Nitrocellulose: Once "powdering" ceases, the system readily forms a skin independent of the initial resin concentration, due to the high viscosity of the polymer.
- Nitrocellulose: Addition of solid has little effect on the results due to the high viscosity of the system. The solid is unable to increase the bound matrix further.
- Bicone gave predictable and reproducible surface rheology data on drying inks.
- Dunouy ring found to give unpredictable surface rheology data in drying inks due to the fragile nature of the attachment.

The physical process of gelation have been observed for both the bulk and surface with differences having been observed between the two. One of the main observations is the effect of the polymer system upon the gelation. The effect of the polymer and gelation can be further analysed by use of MS-DWS to monitor the molecular movement. The technique is able to establish the solvent retention within the system, and how the polymer type and initial polymer concentration effect this.

# Chapter 6

# Multi Speckle Diffusing Wave Spectroscopy (MS-DWS)

## 6.1 Introduction

The aim of the work described in this chapter was to gain an understanding of the physical processes of solvent loss as well as the structural changes during the drying process, by monitoring the change in Brownian motion using Multi Speckle Diffusing Wave Spectroscopy (MS-DWS). The tests were conducted under the same ambient conditions as previous testing. The objectives were achieved through a series of tests using the range of model inks. The work concentrates on the effect of resin type and resin content upon the solvent loss as well as to investigate the possible retention of solvent within a resin matrix.

## 6.2 Results

Each test was repeated four times, with the 25% resin content inks being repeated six times, and the results averaged. The results for the MS-DWS are presented as plots of fluidity factor on the y-axis and time on the x-axis with percentage mass loss on a secondary axis.

### 6.2.1 Polyamide

A series of drying tests were performed on samples of the polyamide resin inks.

The polyamide resin inks were found to have an initial period in which there was a rapid decrease in fluidity factor. Once this has occurred, a degree of irregularity was observed, until there was a steady and slow decrease of the fluidity factor until a minimum value was reached and maintained.

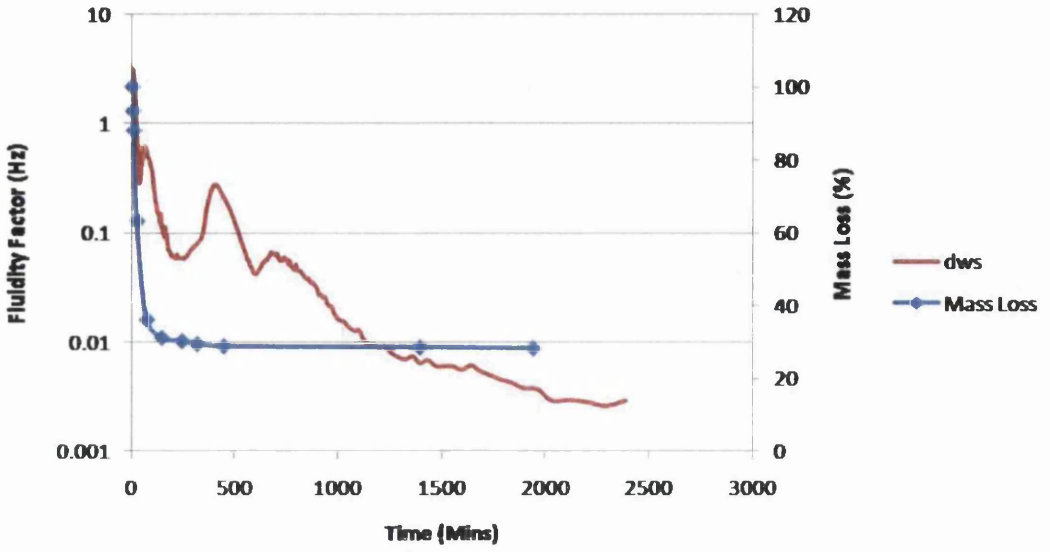


Figure 6.1: A Plot of Fluidity Factor (Hz) and Mass Loss (%) with Time (s) for 25% Polyamide Resin Ink

An initial fluidity factor between the range of 5Hz and 1.6Hz is observed. This decreased to a value of between the range of 1.5Hz and 0.8Hz. After this rapid drop in fluidity factor, there was a continuing decrease over the drying period. There were certain irregularities throughout the initial portion of decrease after which there was a steady decrease towards a fluidity factor of 0.003Hz. The decreasing profile represents the slowing of the molecules within the film throughout the drying process.

A typical plot of this trend is shown in Figure 6.1 which shows the rapid decrease in fluidity factor from 3Hz to 0.3Hz within 40s. After this rapid decrease, a period of slower decrease with irregularity occured up to approximately 600s where the fluidity factor was close to 0.1Hz. From this time onward there is a slow decrease toward the minimum value of 0.003Hz. Once this has been reached the value is maintained until the end of the test at 2300s. This shows the continuation of movement past the point the mass loss graph levels, indicating there was residual solvent left within the system.

The plots of the fluidity factor over the drying period for each initial resin content may be compared. The time required for the fluidity factor to reach a minimum was found for all the different resin contents. These were plotted to show the relationship between the initial resin content and the time required for molecular movement to end. The plot is shown in Figure 6.2. There is a decrease in time with an increase in initial resin content from 25% resin content onwards, and an increase in time from

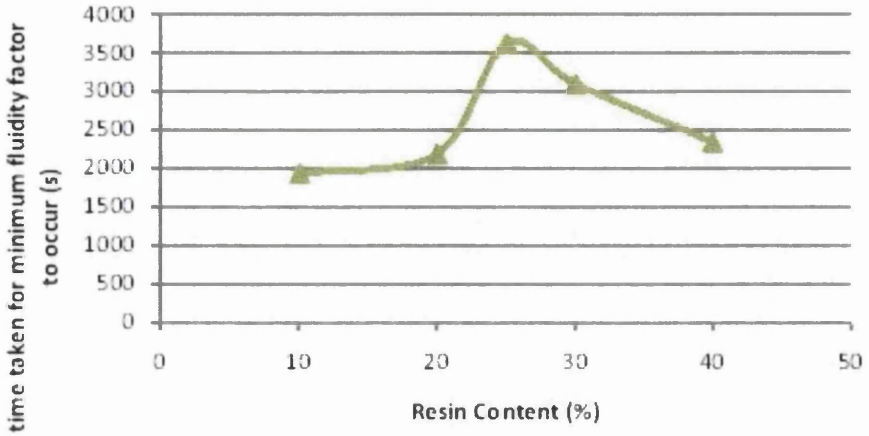


Figure 6.2: A Plot of Time (s) for Fluidity Factor to Reach Minimum for Different Polyamide Resin Content Inks

10% resin content to 25%. It can be seen that at 10% initial resin content, the time taken for molecular movement to end is approximately 1932s, whereas at 40%, it is 2348s The results suggest that there is a distinctive peak at approximately 25% resin content, in which the time period for movement to end is at its longest. The second stage drying step for 30% resin content began after the shortest time.

### 6.2.2 Nitrocellulose

A series of drying tests were performed on a nitrocellulose resin.

The nitrocellulose resin inks were found to have an initial period of highly irregular changes within the fluidity factor. Once this had finished, there was a steady decrease of the fluidity factor towards a minimum value of 0.003Hz where it was maintained.

The test results show a large degree of molecular movement throughout the initial period of drying. This was represented by the fluidity factor varying between the range of 0.5Hz and 3Hz. After the irregularity stopped, there was a steady decrease towards a fluidity factor of 0.003Hz representing the slowing of the molecules within the ink.

This trend is shown in Figure 6.3, which shows the large variation of fluidity factor within the initial period of 570s. After this initial period of irregularity there is a slow decrease towards the minimum from an initial value of 1Hz over the time period of 570s to 900s. Once this has been reached, it is maintained until the end of the test at 2300s. Residual solvent was indicated by the movement continuing past that of the mass loss graph.

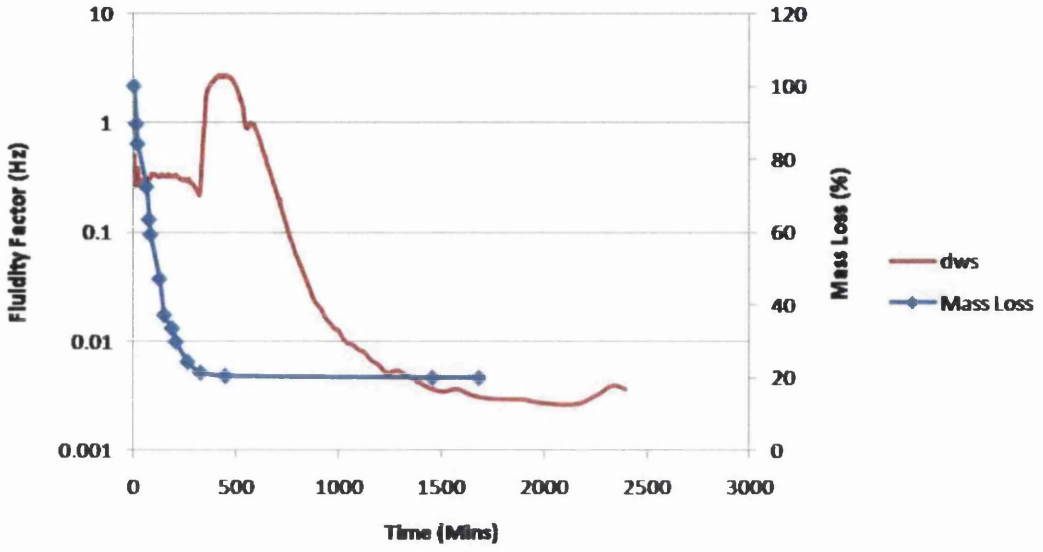


Figure 6.3: A Plot of Fluidity Factor (Hz) and Mass Loss (%) with Time (s) for 25% Nitrocellulose Resin Ink

The plots of the fluidity factor over the drying period for each initial resin content may be compared. The time required for the fluidity factor to reach a minimum value was determined for all the different resin contents. These were plotted to show the relationship between the initial resin content and the time required for molecular movement to end. The plot is shown in Figure 6.4. The shape of this curve is similar to that observed with the polyamide resin ink. Over 25% resin content the time period is high, under 25% resin content the time period is low. It can be seen that at 10% initial resin content, the time taken for molecular movement to end was approximately 2345s, whereas at 40% it was 2989s. This indicates that there is a crossover resin content at approximately 25% resin content.

### 6.2.3 Polyamide with Solid Content

Tests were performed on samples of ink with the addition of 10% $4\mu m$ spherical aluminium solid pigment to the polyamide resin. The inks had an initial period in which there was a rapid decrease in fluidity factor and a degree of irregularity followed by a steady and slow decrease of the fluidity factor until a minimum value of 0.003Hz was reached and maintained. The profiles were similar to those observed for this ink without pigment.

The test results showed a decrease in molecular movement initially, represented by a change in initial fluidity factor from 12Hz to 6Hz, decreasing to about 0.5Hz.

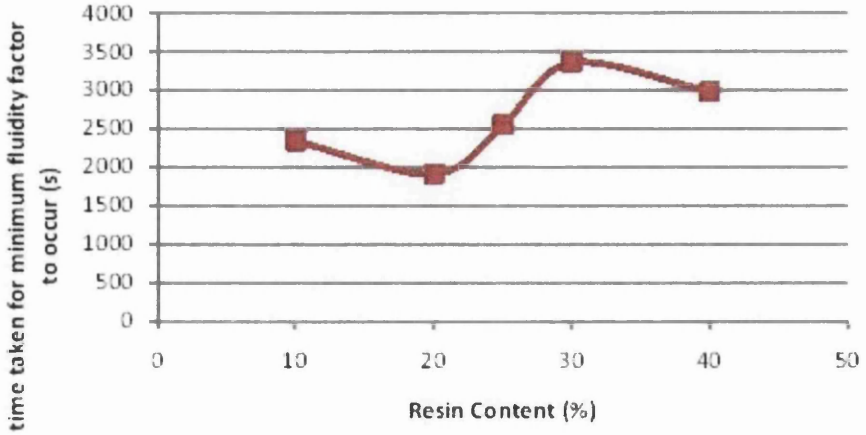


Figure 6.4: A Plot of Time (s) for Fluidity Factor to Reach Minimum for Different Nitrocellulose Resin Content Inks

After this drop in fluidity factor, there was a continuing decrease over the drying period with certain irregularity throughout. After the irregularity stopped, there was a steady decrease towards a fluidity factor of 0.003Hz.

This typical trend is shown in Figure 6.5. This plot shows the decrease in fluidity factor from 9Hz to 4.5Hz within 300s. After this decrease, a period of slower decrease with irregularity occurs up to approximately 700s where the fluidity factor ends at close to 0.1Hz. From this time onward there is a slow decrease toward the minimum of 0.003Hz. Once this has been reached, it is maintained until the end of the test at 2800s. Residual solvent was found to be evident within the system, with the movement continuing past the levelling of the mass loss plot.

A plot to show the relationship between the initial resin content and the time required for molecular movement to end is shown in Figure 6.6. It can be seen that at 10% initial resin content, the time taken for molecular movement to end was approximately 3532s, whereas at 40% it was 2856s. An initial resin content of 20% gave the longest time at over 4000s whereas 25% took approximately 3766s. These results show that with the addition of solid content, there was a similar trend to that observed with increasing resin content in solid-free inks, with a maximum time being observed at approximately 20% content.

### 6.2.4 Nitrocellulose with Solid Content

A series of drying tests were performed on a sample of the nitrocellulose based inks with the addition of 10% pigment. The nitrocellulose resin inks had an initial period

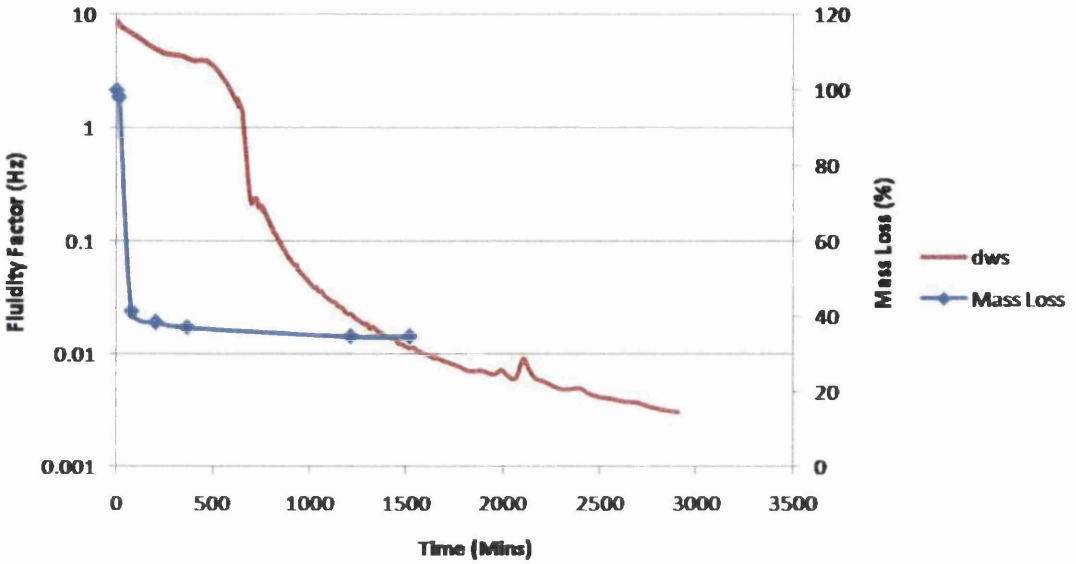


Figure 6.5: A Plot of Fluidity Factor (Hz) and Mass Loss (%) with Time (s) for 25% Polyamide Resin Ink with Solid Content

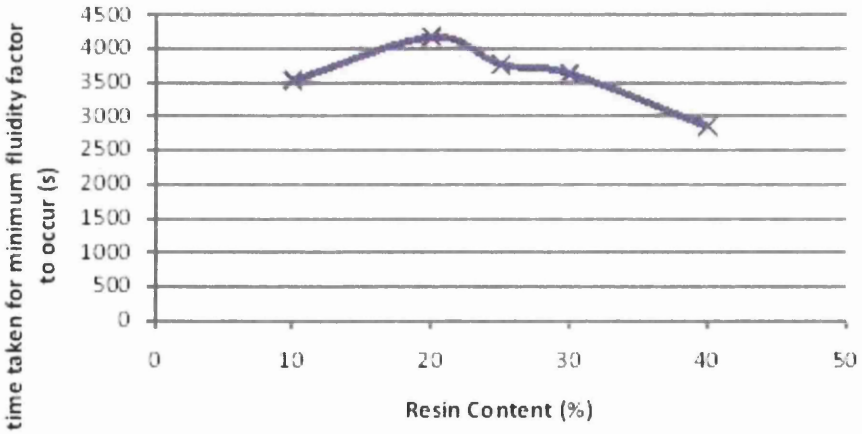


Figure 6.6: A Plot of Time (s) for Fluidity Factor to Reach Minimum for Different Polyamide Resin Content Inks with Solid Content

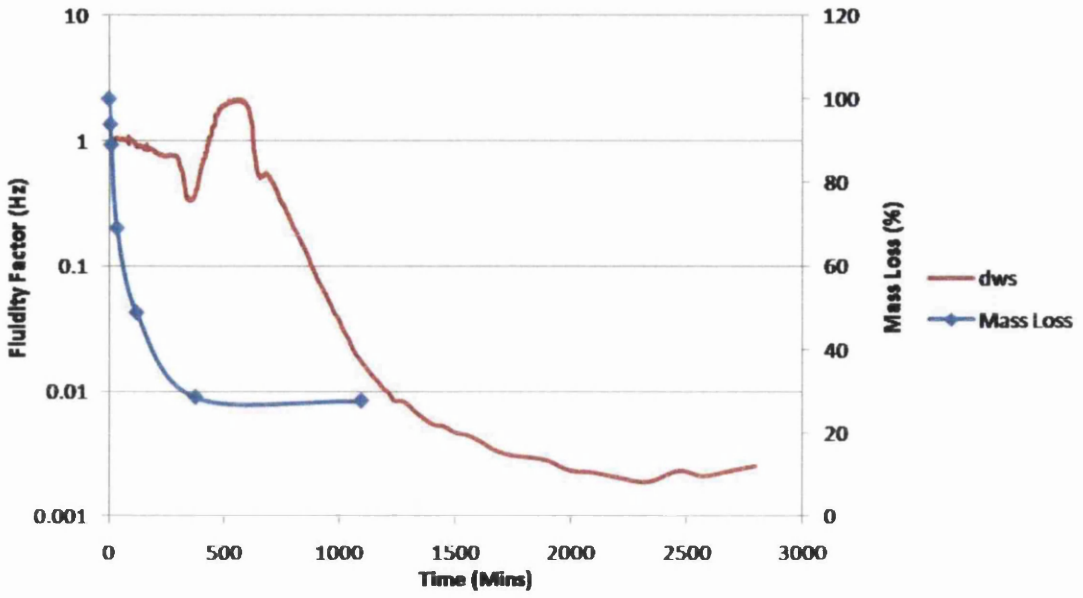


Figure 6.7: A Plot of Fluidity Factor (Hz) and Mass Loss (%) with Time (s) for 25% Nitrocellulose Resin Ink with Solid Content

of highly irregular changes within the fluidity factor. Once this had occurred, there was a steady decrease of the fluidity factor towards a minimum of 0.003Hz where it was maintained.

The test results showed a large degree of molecular movement throughout the initial period of drying. This is represented by the fluidity factor varying between the range of 0.3Hz and 2.3Hz. After the irregularity stopped, there was a steady decrease towards 0.003Hz.

This typical trend is shown in Figure 6.7.After this initial period of irregularity there was a slow decrease toward the minimum from an initial value of 0.5Hz over the time period of 680s to 1100s. Once 0.003Hz has been reached, it is maintained until the end of the test at 2800s. This figure shows the continuation of movement past the point at which the mass loss graph levels, indicating there was residual solvent left within the system.

The plots of the fluidity factor over the drying period for each initial resin content may be compared. As before the plot is shown in Figure 6.8.There was a general decreasing trend with increasing initial resin content with a similar peak at about 25% resin content seen in previous tests with inks without pigment.

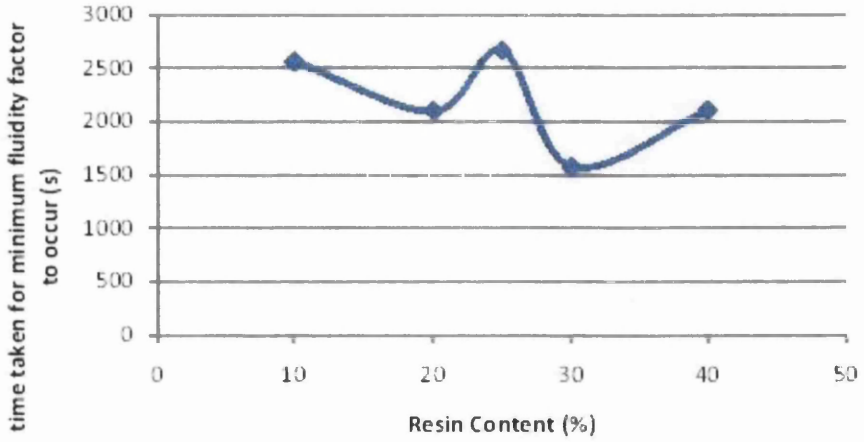


Figure 6.8: A Plot of Time (s) for Fluidity Factor to Reach Minimum for Different Nitrocellulose Resin Content Inks with Solid Content

### 6.2.5 Commercial Ink

The MS-DWS experiments were carried out in the same manner as the model inks. The results are shown in Figure 6.9. The results show a flat line region for approximately 700s. The fluidity factor decreases at this point with some variability until roughly 1200s. From this point onward, there is an exponential decrease to a minimum at 3200s where the test ends. This shows the continuation of movement past the point at which the mass loss levels off, indicating there was residual solvent left within the system.

This reflects the two stages of solvent loss described by Hansen [18] and observed in the model ink results. The molecular rearrangement during and after the free evaporation of the solvent and before the diffusion commences is also shown.

## 6.3 Discussion

Comparison of the MS-DWS plots with the mass loss plots show the continuation of molecular movement past the levelling of mass loss. This suggests there is a small percentage of residual solvent within the system which continues to move throughout the system while the polymer structure is adjusting.

The MS-DWS results were plotted with respect to mass loss. This showed the change in molecular movement up to 100% mass loss. The plots show a decrease in molecular movement throughout the mass loss. Polyamide systems showed an

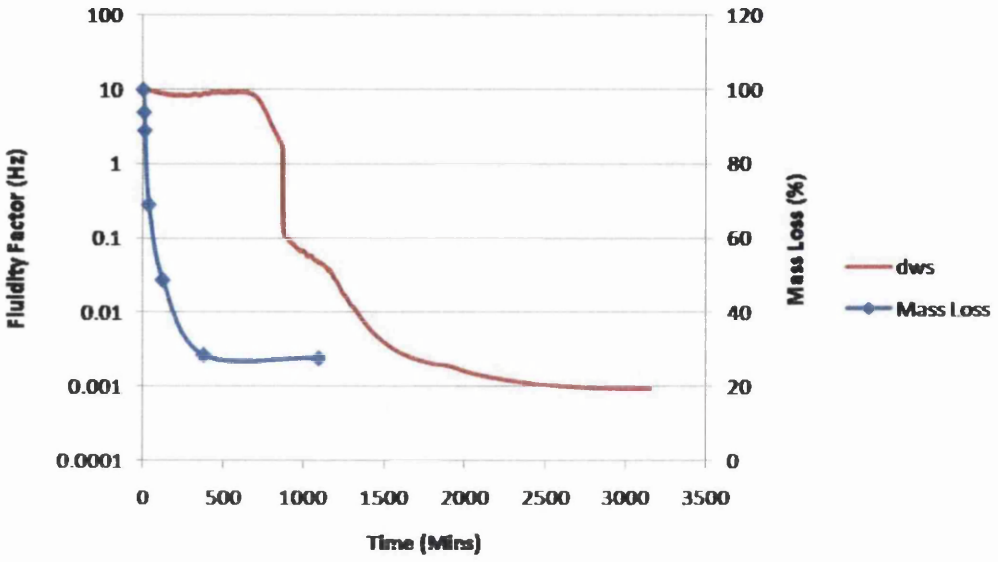


Figure 6.9: A Plot of Fluidity Factor (Hz) and Mass Loss (%) with Time (s) for Commercial Ink

increasing rate of decrease in molecular movement with mass loss, compared to nitrocellulose systems. For all systems, a high initial viscoelasticity reduced the overall decrease in molecular movement as did the introduction of solid.

The profiles obtained with the MS-DWS can be interpreted in terms of the two stage drying model proposed by Hansen [18]. Stage one corresponds to the evaporation of solvent, increasing the concentration of the polymer within the system. The variations within this initial part of the curve corresponds to the rearrangement of the polymer molecules with increasing concentration. Stage two starts once there is sufficient entanglement present, and diffusion is dominant. The molecular movement slows due to the polymer molecules becoming increasingly closely packed.

With the exception of resin content under 20%, polyamide inks take a shorter time for movement to stop compared to nitrocellulose. The MS-DWS is conducted on thinner films and the surface area to volume is much higher compared to those used for rheology results. Once the resin content is sufficiently high with an ordered polymer matrix, the solvent has a similar probability to reach the surface. Higher resin content inks generally led to a longer time for molecular movement to stop. This implies there was trapped solvent at the end of the tests influenced by high viscoelasticity and large amounts of skinning. "Powdering" of lower viscoelasticity nitrocellulose inks occured which would influence the means at which solvent was lost and consequently molecular movement within the film.

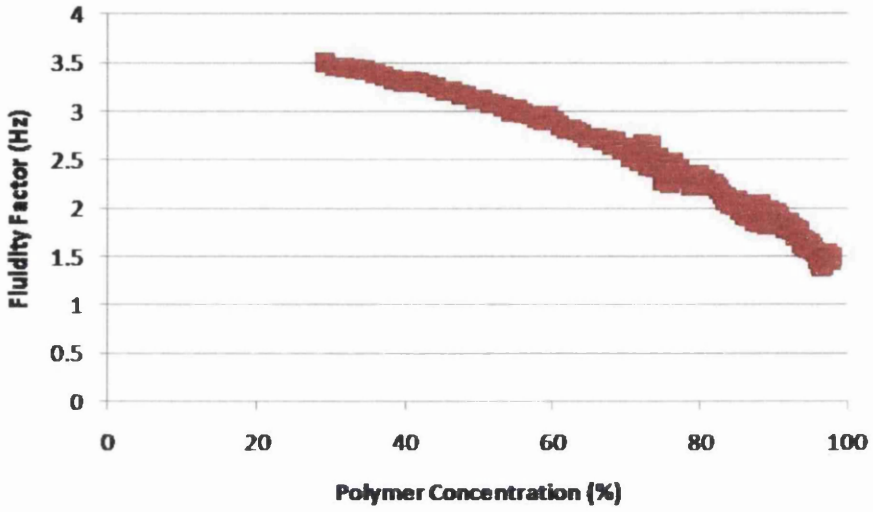


(a) 25% Polyamide Ink

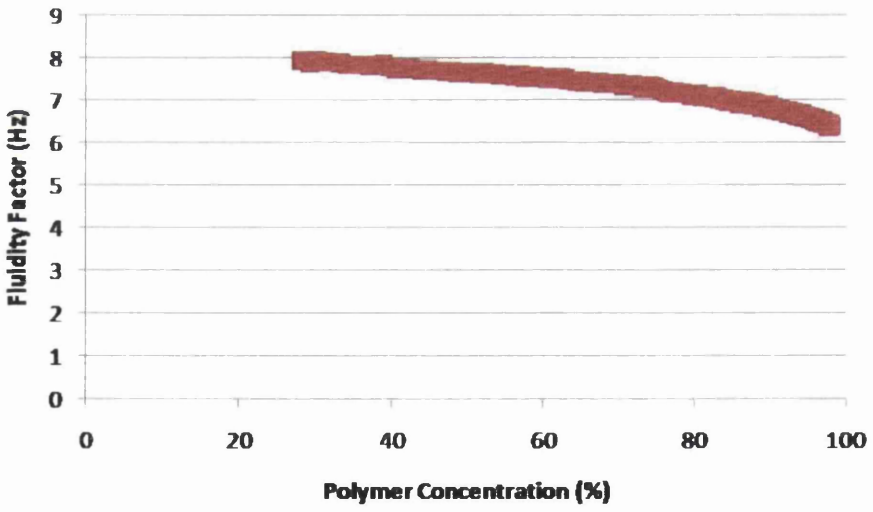


(b) 25% Polyamide Ink with Solid Content

Figure 6.10: Plot of Fluidity Factor (Hz) with Polymer Concentration (%) for Polyamide-based Systems

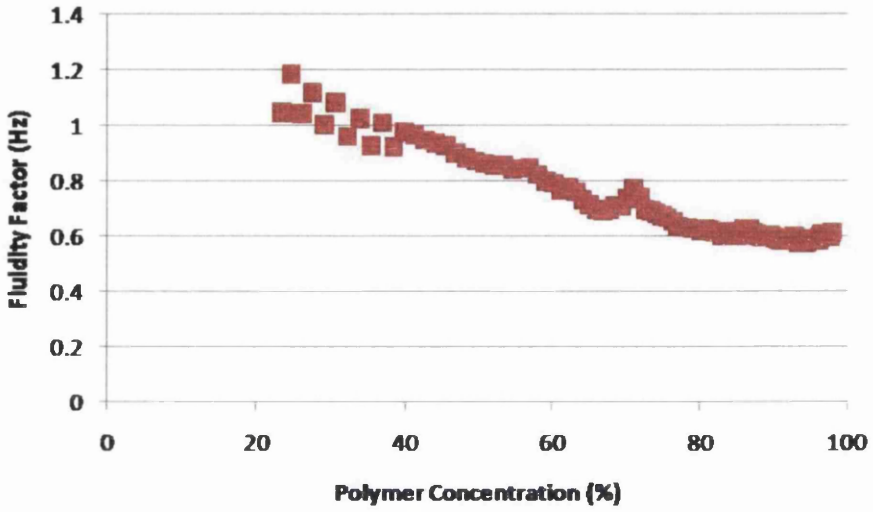


(a) 20% Nitrocellulose Ink

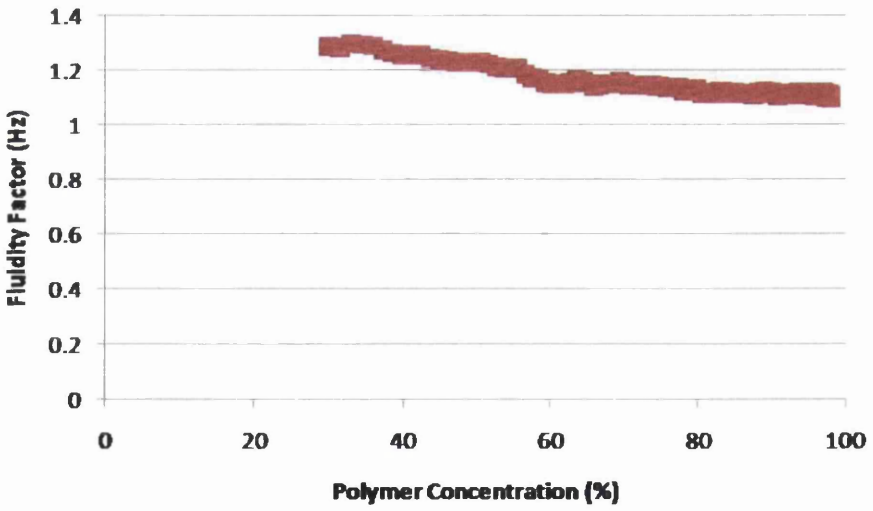


(b) 25% Nitrocellulose Ink with Solid Content

Figure 6.11: Plots of Fluidity Factor (Hz) with Polymer Concentration (%) for Nitrocellulose-based Systems

The MS-DWS experiments were conducted using thin films of the model inks in comparison to the rheology. There are comparative results between the tests, with differences between the two resins being able to be observed as well as with the addition of solids. Similar trends to those in rheology tests were observed, where increased resin content produces a decrease in time for drying to occur. The advantage of this system is the ability to see past the point at which solvent has evaporated. It is possible to monitor the diffusion rate of the solvent and consequently the point at which the system becomes completely dry. This is unable to be achieved using FTIR or rheology. Another advantage and benefit is the simplicity of the equipment. It is able to observe the change in molecular movement of the drying system with minute detail in a completely non-invasive manner.

## 6.4 Closure

The diffusion process of a film was observed using MS-DWS. Solvent was retained within the system more so for nitrocellulose than polyamide. The higher initial resin content inks take longer for movement to cease independent of polymer, indicating that the gelation processes at the surface (eg. skinning) inhibit solvent diffusion. The significant points are:

- MS-DWS was able to observe the two stages of solvent loss through the systems.
- Technique indicates residual solvent within the system for both polyamide and nitrocellulose.
- Higher resin content inks take longer for movement to stop, indicating the solvent is more easily trapped by the structure of the system and skinning is more prevalent.
- Polyamide takes a shorter time for movement to cease than nitrocellulose systems, indicating there is less residual solvent trapped within the polyamide system.
- MS-DWS is a straightforward, reproducible and controllable technique for investigating drying of inks.

The physical processes of gelation have been observed for both the bulk and surface as well as the drying process due to solvent loss. As well as different polymers, there is also a single solvent within the polyamide system and two solvents in the

nitrocellulose system. This could influence the drying process as well as emphasise the gelation processes observed. A clear understanding of the evaporation process is necessary to establish the differences, if any, between a single solvent and a multiple solvent system. The following chapter uses FTIR to observe the diffusion of the solvents through a droplet of ink, to understand how the diffusion process is effected by the resin type and the initial resin content, as well as the differences in single and multiple solvent systems.

# Chapter 7

# Fourier Transform Infrared Spectroscopy (FTIR)

## 7.1 Introduction

The aim of the work described in this chapter was to gain an understanding of the evaporation and diffusion of solvent from an ink during the drying process by monitoring the change in certain chemical peaks using FTIR-ATR. An understanding of the effects of multiple solvents in a system compared to a single solvent were important as well as the order in which the solvents evaporate so it was clear what was happening in the evaporation process and not presumed from the literature. The tests were conducted in conditions close to those employed for the rheological tests in Chapter 4. The objectives were achieved through a series of tests using the range of model inks. The work concentrates on the effect of resin type and resin content upon the solvent loss as well as the order in which the solvents are lost from the bottom layers of a droplet of ink.

## 7.2 Results

The test results are plotted with percentage peak transmittance on the y-axis and time in minutes on the x-axis.

### 7.2.1 Polyamide

The polyamide resin inks showed an increase of transmittance peak throughout the time period. The rate varied throughout the time period. After an initial slow rate of change, there was a fast rate of increase, which then decreased toward the end of the period. This represents the evaporation rate of the solvent from the ink. The

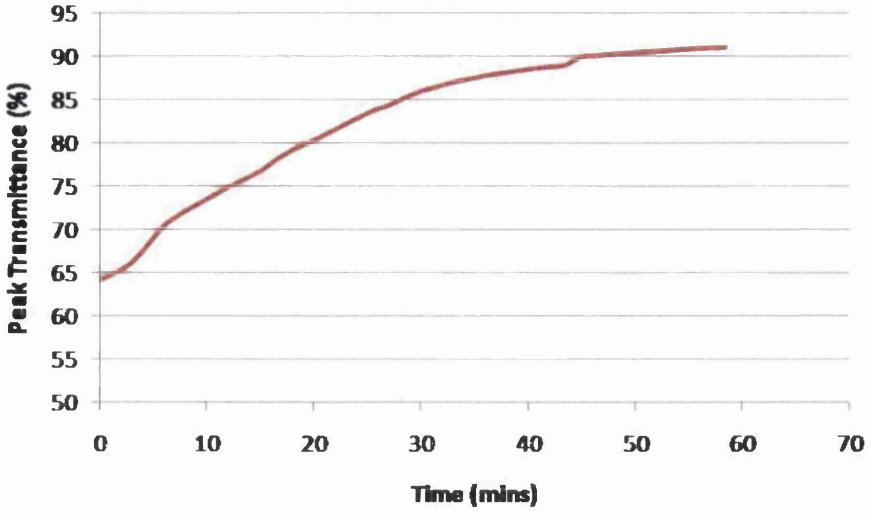


Figure 7.1: Plot of Transmission Peak (%) over Time (mins) for 25% Polyamide Resin Ink

initial slow rate is potentially due to the crystal measuring the solvent being at the bottom of the sample. There will therefore be a delay in solvent evaporation whilst the solvent above evaporates from the surface, producing a flatter profile initially, until the change in solvent becomes significant. The initial percentage transmittance for all inks was approximately 65%. This increased to approximately 90% for all inks except for 30% and 40% resin content which ended at roughly 80% and 72% respectively, which indicates solvent retention at higher resin content.

This trend is shown in Figure 7.1 and shows the average of five tests. It shows the increased transmittance at the spectrum peak over the time period, with the rate decreasing toward the end. The initial percentage is 65% increasing to 90% in a time of 58 minutes.

The plots of the percentage transmittance peak over the drying period for each initial resin content may be compared. The "characteristic time" for the curves were determined for all the different resin contents. The plot is shown in Figure 7.2. The plots of characteristic time for each initial resin content may be compared. These were plotted to show the relationship between the initial resin content and the time for each solvent to evaporate from the ink. A general increase in characteristic time with increasing resin content is observed. This is with the exception of 30% resin content which is opposite to the trend. This increase starts at 22 minutes for 10% and ends at 38 minutes for 40%. 30% has a time of 15 minutes.

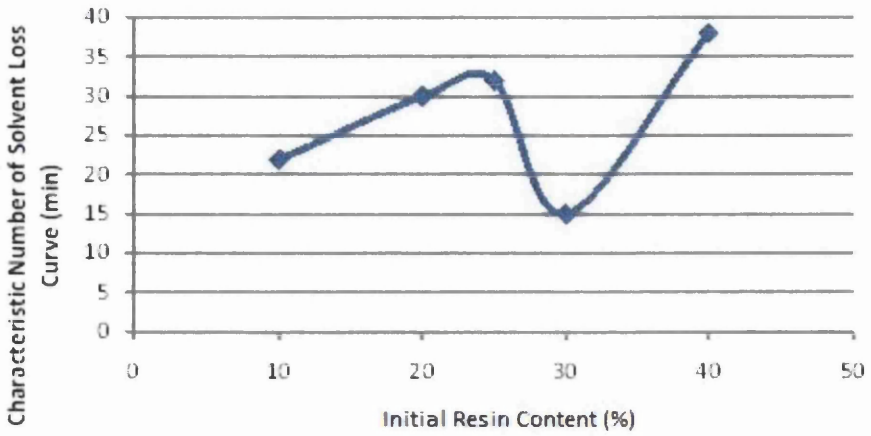


Figure 7.2: Plot of characteristic number (mins) for Different Polyamide Resin Content Inks

### 7.2.2 Nitrocellulose

There are plots of the two different solvents (isopropanol and ethyl acetate) present within the system.

The isopropanol plots for nitrocellulose resin inks have an initial period of very little change followed by an increase in percentage peak transmittance. The rate decreased toward the end of the period. The initial percentage transmittance for all inks was approximately 84%. The percentage remaining was approximately 92% for all inks, except 25% and 40% resin content which had 88% and 84% transmission remaining at the end of the test respectively.

This trend is shown in Figure 7.3. This shows the average of five tests. It shows an initial period of little change followed by a sudden increase which eventually becomes steady throughout the time period. The initial percentage is 84% increasing to 88% percent in a time of 58 minutes.

The ethyl acetate plots for nitrocellulose resin inks had an initial period of no change, followed by a period of increasing rate of change in percentage peak transmittance. The rate decreased toward the end of the period. The initial percentage of all the inks were between 85 and 88%, increasing to between 93 and 96%.

This trend is shown in Figure 7.4. This shows the initial period of no change followed by an increase in the transmittance throughout the time period. The initial percentage was 85.5% increasing to 94.5% in a time of 58 minutes.

A plot of characteristic number against initial resin content is shown in Figure 7.5. Generally there is a slight decrease in characteristic time with resin content. The

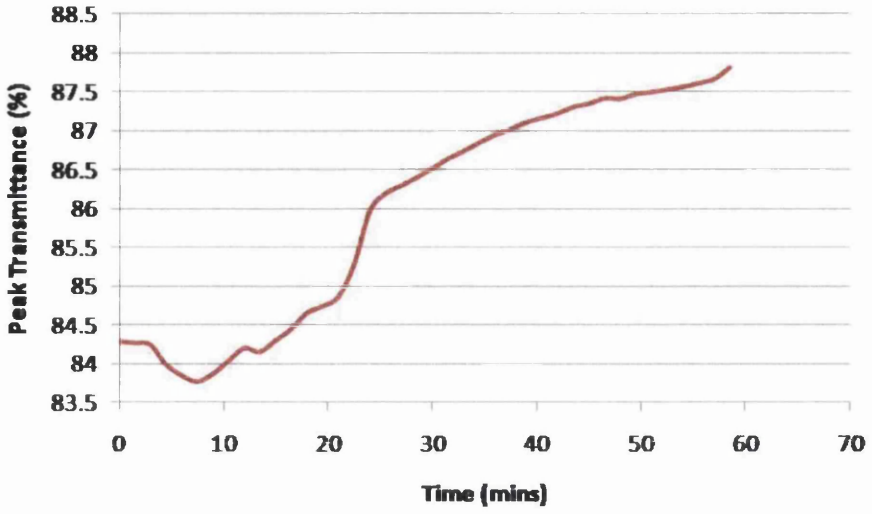


Figure 7.3: Plot of Transmission Peak (%) for IPA over Time (mins) for 25% Nitrocellulose Resin Ink

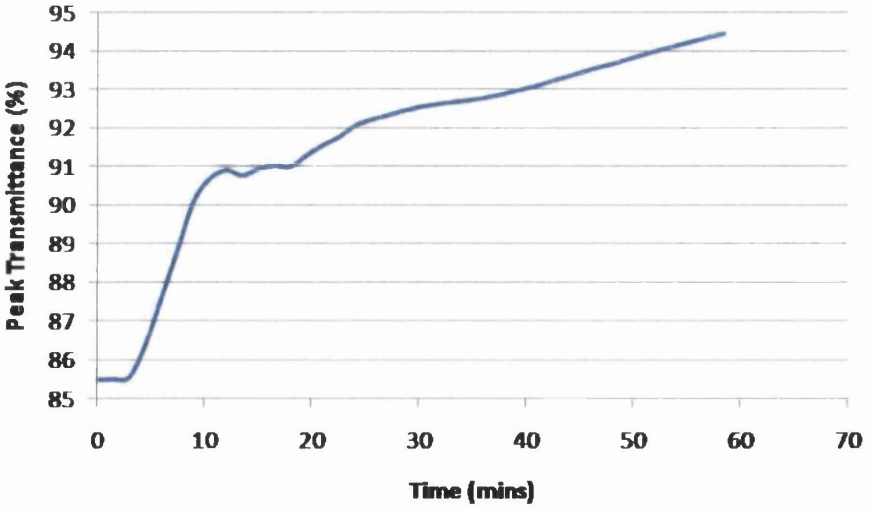


Figure 7.4: Plot of Transmission Peak (%) for EA over Time (mins) for 25% Nitrocellulose Resin Ink

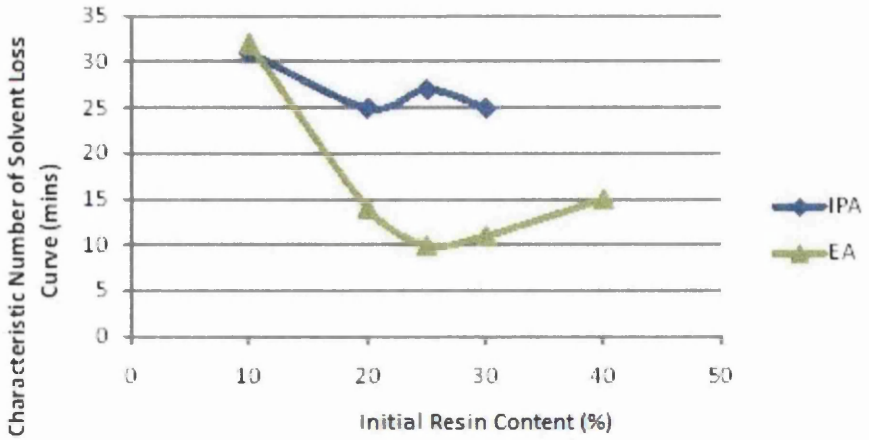


Figure 7.5: Plot of Transmission Peaks (%) over Time (mins) for Different Nitrocellulose Resin Content Inks

characteristic time for IPA is quite consistent throughout increasing resin content. After an initial time of 31 minutes for 10% resin content, there was a constant time of approximately 26 minutes. The plot for the 40% resin content is close to flat, therefore a characteristic time was unable to be calculated. The characteristic time for EA has a similar trend. At 10% resin content, the time is 32 minutes. Thereafter, the time is approximately 12 minutes for increasing resin content.

### 7.2.3 Drying Tests of Model Inks with Solid Content

FTIR was carried out in the same way for samples of the polyamide and nitrocellulose resin inks with the addition of solid content. The results, however were not well defined and the transmittance output was erratic. This was due to the scattering of the infrared light by the aluminium solid used within the inks. FTIR–ATR uses a prism which transmits and receives infrared light through the substance placed upon it. If a large degree of scattering occurs, there is little light received back, therefore not producing a clear result. Example test results are shown in Figure 7.6 for the isopropanol in polyamide inks and in Figure 7.7 for both isopropanol and ethyl acetate within nitrocellulose inks.

### 7.2.4 Commercial Ink

The FTIR-ATR experiments were conducted over the drying period using the same methodology as the model inks. The wavelength used to monitor the solvent loss

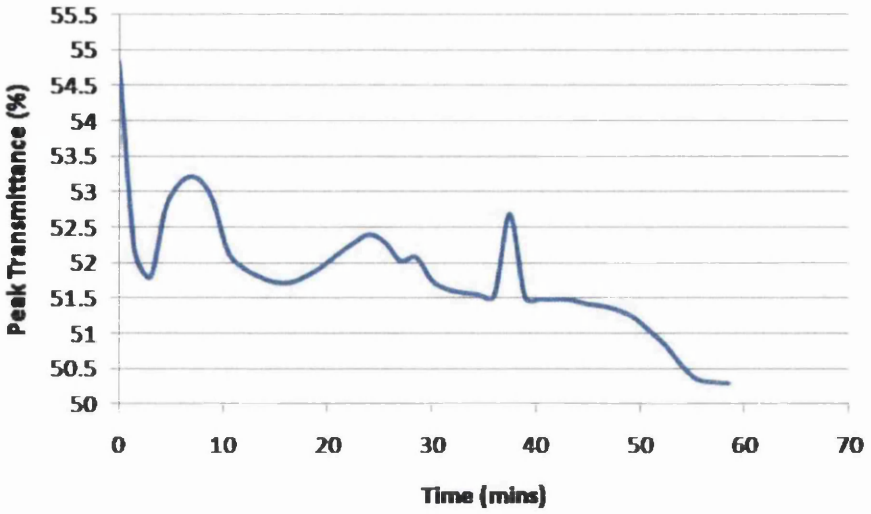


Figure 7.6: Plot of Transmission Peak (%) over Time (mins) for 25% Polyamide Resin Ink with Solid Content

was between 1705 and $1767cm^{-1}$. The peak was the saturated ester carbonyl stretch at $1752cm^{-1}$ which was one used for monitoring the nitrocellulose model ink. The results are shown in Figure 7.8. This shows an increase in peak from approximately 80% to approximately 86% over a time period of 42 minutes. There is a constant increase over the period with no plateau reached.

There is no plateau reached toward the end of the experiment. This suggests that there was still solvent within the system. It correlates with the rheology results, which show significant skinning occurring quickly. This will inhibit solvent loss and with the higher solid content increase the time for the solvent to be lost from the system. This trend was also observed in the model ink results.

## 7.3 Discussion

FTIR measurements provide a method of directly following the loss of solvent from a drying film. The aim would be to attempt a correlation of drying rate as measured by solvent loss with the viscoelastic changes taking place at the time.

The change in concentration is able to be determined by using the FTIR data. From this the results show the solvent is lost over two stages, with the loss being slower in the second stage. This is evident for both the IPA and EA within nitrocellulose as well as IPA in polyamide resin. The addition of a solid within the polymer system

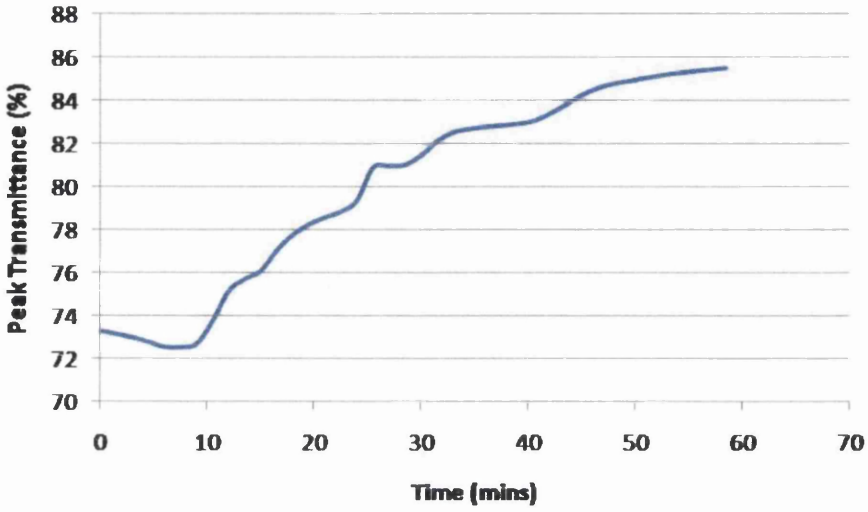


(a)

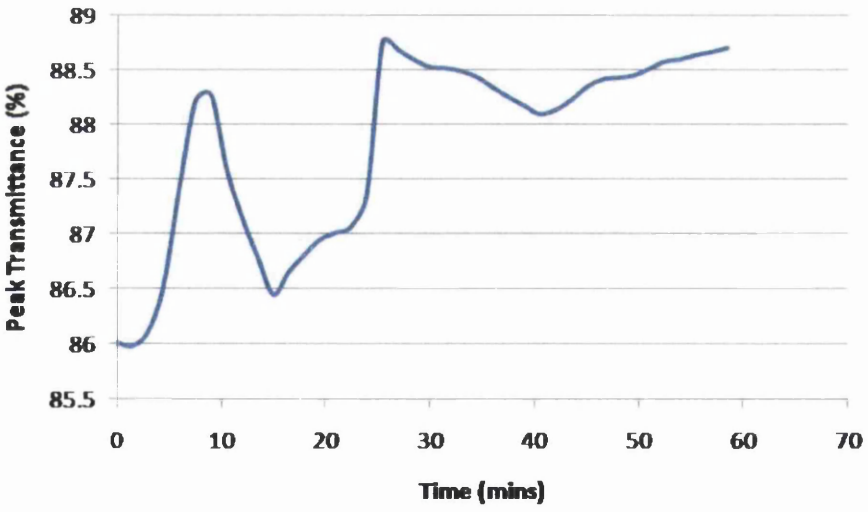


(b)

Figure 7.7: Plots of Transmission Peaks (%) over Time (mins) for 25% Nitrocelluose Resin Ink with Solid Content. (a) shows IPA, and (b) shows EA

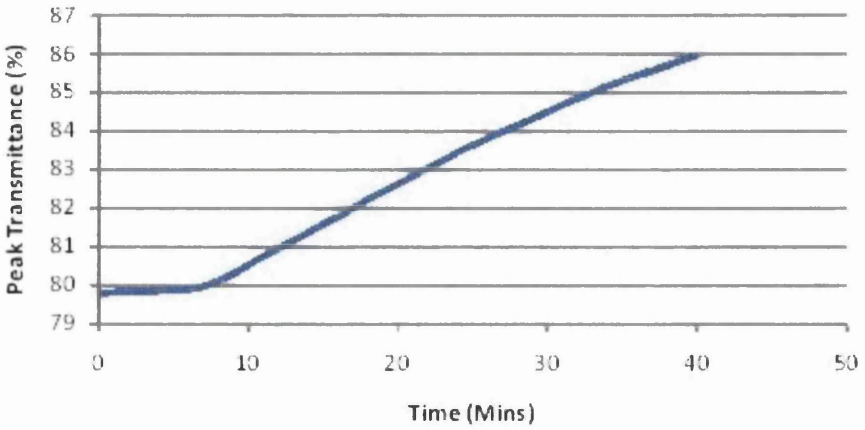


Figure 7.8: FTIR of Commercial Ink

was not able to be compared using FTIR, so the effect of solid upon the drying rate cannot be commented on.

The characteristic time for solvent evaporation in polyamide is dependent upon the resin content. The higher the resin content, the longer the solvent is retained within the system. The gelation process is ordered and forms a structured matrix dependent on hydrogen bonding. The solvent plays a large part in this, donating hydrogen bonding sites throughout the gelation process. The time increases with increasing resin content, implying that the solvent is unable to evaporate and disperse from the surface as readily. The polymer matrix will start to be formed quicker as the concentration is higher, therefore there is a higher probability of hydrogen bonds being formed. This will decrease the time for the solvent to evaporate through free space.

The characteristic time for IPA evaporation in nitrocellulose becomes independent of resin content from 20% resin content upward. The characteristic time is within the same time frame of the IPA in polyamide. The time is higher for 10% resin content compared to the other concentrations. This is thought to be due to phase separation occurring at the low concentrations. This high characteristic time compared to the other resin concentrations is also seen with EA evaporation, both being at approximately 32 minutes. However, overall, the characteristic time for EA at higher resin contents is significantly lower than that of IPA; on average EA is half that of IPA. The viscosity of nitrocellulose is significantly higher than that of polyamide. The gelation process is complex compared to the polyamide and starts earlier in the drying process. In this multiple solvent system, where a high concentration of the more

volatile and higher solvency solvent is at the start of the process, the solubility will decrease more rapidly once the EA has evaporated and IPA is left compared with a single solvent system. This may acccount for the more complex gelation process.

The FTIR results show a fundamental difference between the gelation of the two different resin inks and their effect on the solvent evaporation and diffusion through the system. However, the technique is not adequate to determine final residual concentrations of solvent in the film. The assigning of strong peaks for measurement which are clear of interfering peaks is difficult. For example the OH peak is weak and the CH peak is in the crowded fingerprint region. A better peak definition is required for the seperate solvents within a mixed solvent system. Other equipment is considered more accurate in determining the make-up of a system, such as UV spectrophotometry. The tests, however, are normally carried out in an enclosed container, therefore this technique was unable to be used to measure the evaporation throughout the drying period.

## 7.4 Closure

The diffusion process from the bottom layers of a droplet was observed using FTIR spectroscopy. It was found that the polymer used had a large effect upon the diffusion process due to the bonding processes involved, similar to that found in the rheology results. However, an increase in initial resin content decreases the rate of diffusion, independent of polymer. The two solvents within the nitrocellulose system diffuse at different rates dependent on their volatility (Ethyl acetate diffuses before isopropanol), leaving mostly isopropanol within the system towards the end of the drying process. The inclusion of solid in the system was unable to be observed using this technique. The significant points are:

- Solvent loss is greatly effected by the resin type of the system, as the gelation of the polymer effects the evaporation and diffusion processes.
- In multiple solvent systems, differing solvent volatility can effect the time dependence of the gelation due to a change in solubility parameter throughout the drying process.
- Solvent loss is effected greatly by the initial content of both polyamide and nitrocellulose resin due to increased rate of gelation with increased concentration. Skinning is also increased at higher concentrations inhibiting solvent loss further.

- A two stage rate profile for solvent loss was observed for both polyamide and nitrocellulose ink.
- FTIR not sufficiently accurate to determine residual solvent concentrations in ink films and is unable to be used with reflective solid particles.

The diffusion process of solvent through a polymer has been observed using FTIR. The influence of the polymer and gelation process have been observed, as well as the effect of single solvent and multiple solvents on the drying process. The following chapter brings the results of the previous chapters together and discusses the significance of the findings and their relationship with one another.

# Chapter 8

# Overall Discussion

## 8.1 Solvent Evaporation

The process of solvent evaporation from a polymer film is described by Hansen [18] and shown in Figure 8.1. The loss of solvent occurs in two distinct stages. The first stage is controlled by the surface resistance to solvent evaporation and the second is controlled by diffusion. The first stage is accompanied by a gradual decrease of diffusion coefficient, whereas the second stage has an increasing rate of diffusion coefficient decrease throughout the period; with the solvent being able to evaporate with relative ease throughout the first stage, while the evaporation rate decreases throughout stage two.

The loss of solvent, as determined directly by FTIR, was found to show a similar two stage trend throughout the drying period. The time over which this occurred was different for the different resins. The characteristic time for the change from first to second stage for solvent evaporation within the polyamide resin was highly dependent upon the initial resin concentration; the change in the first stage unable to occur as rapidly with higher initial resin concentrations, leading to more solvent being retained in the second stage. Nitrocellulose based inks showed the characteristic time for both solvents remains independent of the initial resin concentration. Ethyl acetate is lost at a faster rate than that of isopropanol, indicating that the more volatile solvent molecules are able to diffuse more easily through a polymer matrix but which may in turn effect the time scale of the gelation process and subsequently the overall drying rate. Retention of solvent, generally, within nitrocellulose was generally greater than that for the polyamide resin.

The loss of solvent in the stirred bulk tests showed a similar change over the first stage but due to the constant agitation in the bulk system a clear transition to a second stage for each resin was not evident and solvent retention was observed. As

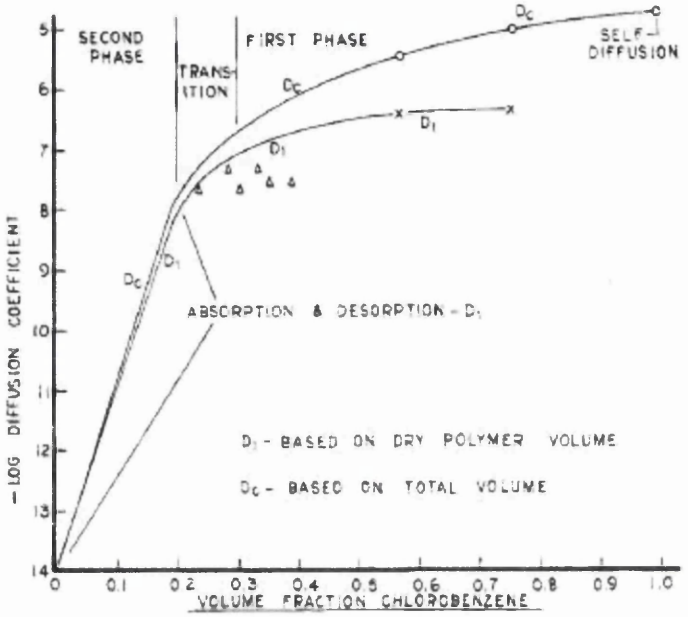


Figure 8.1: Diffusion Coefficients of chlorobenzene in poly(vinylacetate)

in the FTIR tests, this occurred more readily for nitrocellulose based inks than for polyamide.

The drying process, monitored with increased detail by the change in molecular movement using MS-DWS, showed the two stage process as well as the beginnings of gelation by entanglement within the film. Throughout the first stage of drying, there was a progressive decrease in the molecular movement characteristic of the the free evaporation of solvent. The polymer concentration within the system increased followed by rearrangement of the polymer leading to entanglement and then gelation. The second stage is characterised by decreasing molecular movement towards a minimum level. This shows the structure becoming more rigid, with diffusion of solvent becoming increasingly difficult. This correlated well with the FTIR results, where the rate of solvent loss decreased from the first to second stage.

The gelation process was significantly different for each resin. The polyamide resin had a flat plateau stage in viscoelasticity independent of mass loss, and then an abrupt increase in viscoelasticity at a critical point. This suggests the polyamide system reaches a critical concentration where it is possible for the polymer molecules to be entangled and for hydrogen bonding to occur. Once this point has been reached, the change is abrupt and diffusion becomes controlling. Within the bulk, the concentration at which viscoelasticity changes is independent of initial resin content. At the

surface, the viscoelastic change occurs more quickly with increased initial resin content. The surface gelation is greatly influenced by atmospheric and physico-chemical conditions. The quicker the viscoelastic change happens, both in the bulk of the system and at the surface, the increased amount of solvent is retained within the system. The addition of solid content within the system makes the gelation of the bulk no longer independent of initial resin content. Instead, the viscoelasticity change occurs more quickly for increasing initial resin content systems.

Nitrocellulose gained viscoelasticity over time with decreasing rate of solvent loss. This shows that the gelation process is not bond dependent to as large a degree as polyamide. Instead, the polymer molecules come together over the drying period, decreasing the free space for the solvent to move into. Agglomeration of the polymer is also possible, causing aggregation within the system. The viscoelasticity increases during this process, with the ratio of polymer to solvent increasing. The gelation also involves entanglement of the polymer once the polymer concentration is high enough. The rate at which this happens is independent of initial resin content. Due to the high viscosity of the polymer, the entanglement processes occur quickly and leads to solvent being readily retained. At the surface, the same process of gelation happens at an increased rate due to atmospheric and physico-chemical conditions. The addition of solid content within the system makes the bulk no longer independent of initial resin content.

The results of this work allow the solvent loss and gelation processes involved in the drying film to be shown in parallel. These show that the solvent loss follows a two stage process with the second being highly dependent on the polymer concentration and gelation involved. This dependency is shown clearly within the polyamide resin where gelation occurs at a critical point independent of initial resin content. At this point, it is significantly more difficult for solvent loss to occur. The nitrocellulose results show that the high viscosity of the resin with decrease in the solvent loss. The gelation process does not occur at a critical concentration, but there is viscoelasticity increase throughout the range of initial resin content inks, which leads to a decrease in solvent loss and potentially retention of the solvent within the system. A minor addition of solid content is found to inhibit the solvent loss of both systems further, without apparently changing the gelation processes.

The general drying model is illustrated in Figure 8.2. The two stage solvent loss is observed, with the gelation process alongside the solvent loss. This shows the influence of each process on the other as well as the order in which they occur.

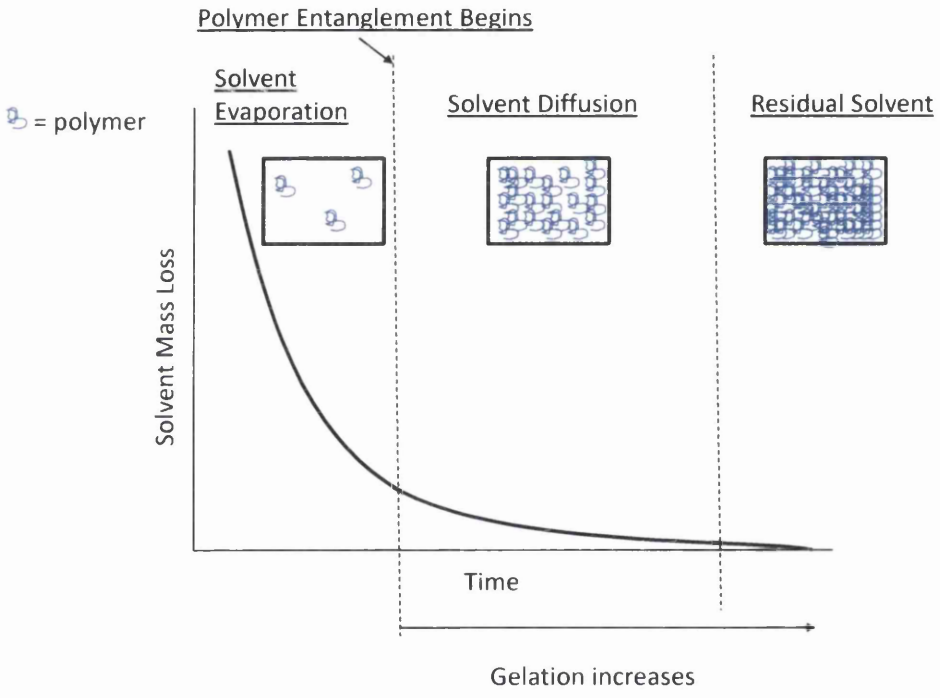


Figure 8.2: Schematic of Model Drying Process

## 8.2 Solvent Retention

Solvent may be retained within the drying film due to both environmental or physico-chemical factors. The environmental factors are temperature and air velocity over the surface. The temperature will increase the mobility, increasing the rate of solvent loss. The volatility of the solvent(s) are also important. The physico-chemical differences include the mobility of the polymer chain segments as defined by the glass transition temperature, Tg. If Tg is room temperature or higher, then significant solvent retention can occur. The addition of solid content can also inhibit the loss of solvent by filling more of the free space between the polymer molecules. Nitrocellulose develops a higher intrinsic viscosity per weight compared to polyamide; the polymer molecules therefore present a denser network and this decreases the free space within the matrix for the solvent to move to and escape.

## 8.3 Solute Transport

Mass transfer in the ink system as it dries consists of the transport of solvent through the film and solvent evaporation. There is also the potential for transport of solute by diffusion-convection mechanisms. At the start of the drying process all the transport options are available to some extent, as the ink is of sufficiently low viscosity to allow these transports to take place. The capillary number (Ca) is used to give a relative magnitude of viscous forces and surface tension controlling transport forces within a system.

The capillary number is a ratio of surface tension and viscosity. The surface tension, if greater than the gravitational force, tends to maintain a drop in a spherical structure. Gravity tends to flatten the shape. In the surface tension driven state, diffusive and convective transport of the solute exists because of the differences in the shape of the interface. This affects the rate of local evaporation and the distribution of solute, leading to concentration gradients being developed. An even dispersion of solute is vital to ensure an even rate of evaporation. If the dispersion is not even, unusual ring formations and morphological irregularities can be observed. In a surface tension driven system, the capillary number, Ca, is under one. At some point during the evaporation process, the viscous forces within the system start to become dominant. The capillary number increases along with the viscosity. At a point, it is argued that no solute transport can occur. At this point, the mass transport consists mainly of solvent diffusion through the stationary solute film and loss due to

evaporation. At this stage, the mobility of the solvent as well as the interaction of the solvent with the solute become important. The capillary number is greater than one at this stage.

Van Dam [28] quotes figures for capillary number of 0.03 and 0.05 for his colloidal particle ink-jet inks. The work does not take into account the possible difference in gelation or solidification due to differences between various polymer matrices. Only the simple Newtonian viscosity at a single shear rate was measured. However, equation 8.1 was used to calculate the capillary number:

$$Ca = \frac{\eta \times V_e, a_v}{\sigma} \left(\frac{r_0}{h_0}\right)^4 \tag{8.1}$$

where $\eta$ is the viscosity and $\sigma$ is the surface tension of the solution. $V_e, a_v$ is the average evaporation rate of a droplet of solution defined as the evaporating volume per unit of time divided by $\pi r_0^2$, and $r_0$ and $h_0$ are the radius and central layer thickness of the droplet during drying.

Estimates of the capillary number have been made based on equation 8.1 for the two model inks. While the equation is considered valid for ink-jet drops the geometry of films for flexographic printing is diffferent. However, relative difference between systems are throught to be significant and valid. The results are also consistent with other experimental results reported in this thesis. Estimates were based on the nitrocellulose and polyamide resin model inks without solid content. A single droplet placed on a metal surface, was used to estimate the radius and height. The surface tension was estimated using the pendant drop method [111] (Fiberdat Dat 1100) and the viscosity used was the complex viscosity from the bulk rheology tests. The time was the time taken for the significant rheological change to occur. The capillary number for polyamide resin ink at the start of drying was $6.9 \times 10^{-3}$, whilst at the end of drying tests the capillary number had increased to 3.7. Nitrocellulose resin ink had an initial capillary number of 7.9, increasing to 13.02. This shows a significant difference between the two resins.

These results show the polyamide resin was well within the surface tension driven regime at the beginning of the drying process. This implies that there is potential for free solute transport throughout the system as well as freely evaporating solvent. At the end of the drying process, the viscosity had increased, increasing the capillary number. The capillary number at the end of the drying process is greater than one which implies that there is no longer free transport of solute and instead diffusion of solvent is the dominant source of mass transport.

The nitrocellulose resin ink begins with a figure greater than one. This increases further throughout the drying period. This implies that the viscous forces are dominant throughout the drying process, even before significant solvent loss. As a consequence, there is no mass transport of solute possible, with only diffusion of the solvent occurring at a decreasing rate throughout the drying process.

The capillary number approach of Van Dam provides a clear way of distinguishing between surface tension and viscosity dominated systems. This in turn provides an insight into the mass transport occurring within the system. It is seen that with a more viscosity dominant system, skinning occurs more readily, which will have a significant effect upon the solvent loss of the system. Nitrocellulose inks are viscosity dominated throughout the drying process. Skinning occurs readily throughout the range and is significantly more than that of the polyamide system where the capillary number shows a much more surface tension dominated system. This fundamental difference in viscoelasticity has a significant effect upon the solvent loss and retention of solvent.

## 8.4 Diffusion

The diffusion coefficient is a common comparative measure of the ability for diffusion to take place. A low diffusion coefficient results in the solvent taking longer to diffuse and potentially being retained. Within a high polymer system containing organic solvents the diffusion coefficient varies with concentration of solute in the solvent in the low solvent concentration range. This leads to an added degree of complexity within the second stage of solvent loss. Furthermore, this only accounts for the concentration dependence and does not account for any structural changes within the matrix resulting from gelation for example. This increases the complexity further and estimation of the diffusion coefficient to any accuracy.

The Einstein-Stokes equation (equation 8.2) has been used to estimate the diffusion coefficient for spherical particles within solvents of certain limited viscosity. The diffusion coefficient of solvents and polymers is more commonly measured directly. This is possible by means of measurements being taken within an experimental setup to replicate Fick's law. More recently, diffusion NMR spectroscopy has been used. [112, 113] This utilises magnetic field gradients to monitor the movement of particles by means of their spin. Hansen [18] shows a decrease of diffusion coefficient throughout the volume fraction of solvent of chlorobenzene in poly(vinyl acetate) from 1 x$10^{-5} m^2 s^{-1}$ to 1 x$10^{-14} m^2 s^{-1}$. Van Dam [114] utilises diffusion NMR Spectroscopy

| Initial Resin | Polyamide | | Nitrocellulose | |
|---|---|---|---|---|
| Content (%) | start | end | start | end |
| 10 | 1.21E-04 | 1.82E-09 | 1.43E-05 | 2.06E-11 |
| 25 | 4.14E-05 | 6.09E-09 | 1.43E-07 | 6.72E-12 |
| 40 | 2.00E-05 | 1.70E-11 | 1.54E-07 | 5.64E-12 |

Table 8.1: Solvent Diffusion Coefficient for both Polyamide and Nitrocellulose Resin Systems

to calculate the diffusion coefficient of a range of polymers in ink-jet inks before evaporation. The diffusion coefficients were found to be between 0.4 x$10^{-11}m^2s^{-1}$and 1.3 x$10^{-11}m^2s^{-1}$. The diffusion coefficient for m-xylene in one ink was measured to be (1.1 $\pm$ 0.1) x$10^{-9}m^2s^{-1}$. Comparison between these two systems shows possible large variation between diffusion coefficients.

Using the Einstein-Stokes equation the diffusion coefficient can be estimated for both polyamide and nitrocellulose systems. The equation considers sphercial particles within a fluid by means of viscosity. Assumptions do need to be made, however. For this case the solvent was treated as a spherical particle within the polymer resin. The equation is shown in equation 8.2.

$$D = \frac{k_B T}{6\pi\eta r} \tag{8.2}$$

where $D$ is the diffusion coefficient of the solvent through the polymer, $k_B$ is the Boltzman constant, $T$ is temperature, $\eta$ is the complex viscosity taken from the rheology results and $r$ is the calculated radius of the solvent molecule if assumed spherical. Using the Einstein-Stokes equation with the assumptions made, the diffusion coefficient for both resin systems are shown in Figure 8.1.

The estimates show that the nitrocellulose resin system has a lower diffusion coefficient throughout the range of initial resin contents than polyamide. For all the systems, there is a large decrease in diffusion coefficient over the drying period estimated at approximately $10^5$ fold. The results compare favourably with Van Dam's value in the case of the polyamide resin. The values for the nitrocellulose are some $10^3$ fold smaller, however.

The values estimated using the Einstein-Stokes equation show a similar trend and magnitude to those measured by Hansen. This shows that the Einstein-Stokes equation, with the assumptions made, forms a reasonable basis for estimates of the diffusion coefficient in polymer systems. There are further parameters that may need to be considered, such as gelation. In order to refine the estimates further,

an additional term may need to be added to decrease the diffusion coefficient with increasing gelation throughout the drying period. The contribution of terms such as capillary number may also be considered in order to define the effects of skinning on the inhibition of diffusion.

Using the results from the experiments carried out, combined plots of diffusion coefficient, viscoelasticity and molecular movement for the polyamide and nitrocellulose systems are shown in Figures 8.3 and 8.4 respectively. These plots show the best attempt from the results of describing the complete process of drying in solvent-based ink systems. The polyamide system results show the surface viscoelasticity and diffusion coefficient after changes in the bulk of the system. The two systems show fundamental differences in the way the structure changes throughout drying, with polyamide maintaining a fluidic structure throughout the drying process, gelating rapidly at higher polymer concentrations. The nitrocellulose system had a more gradual gelation process which in turn effects the diffusion process. Skinning is seen to occur rapidly, at a much earlier polymer concentration.

The plots show the decrease in diffusion coefficient with the increase in viscoelasticity. The rate at which this happens is greater for the surface than the bulk. The concentration at which this begins, decreases with increased capillary number, due to the film becoming dominated by viscous forces rather than surface tension. The polyamide system, with an extended period of low viscoelasticity (low Ca) allows a longer period for potential mass transfer of solute, whereas nitrocellulose does not. The increase in capillary number also reflects an increase in the rate of skinning at the surface, increasing the difference in polymer concentration required for a viscoelastic change to occur in the surface and bulk.

## 8.5 Summary

The physical process involved throughout the entire drying process were observed using the series of experiments described throughout the thesis. The structural changes of the bulk and surface were observed by the development of rheological tests. The following points can be made:

- The polymer concentration required for a rheological change to occur is independent of initial resin content for the bulk of the system.
- Surface rheology was more dependent upon initial resin content than bulk rheology.

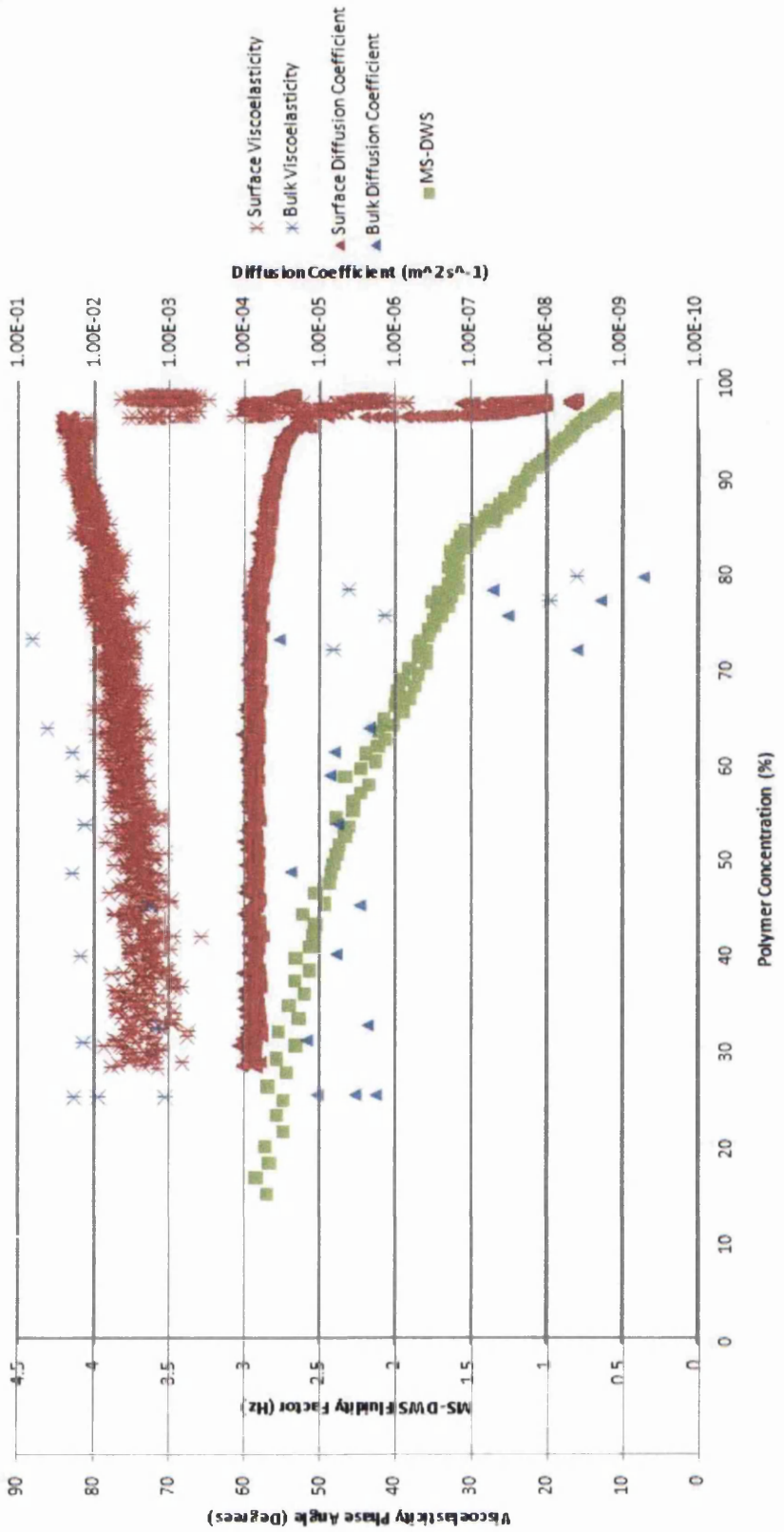


Figure 8.3: Plot of Mass Transfer over the Drying Period for Polyamide-based Systems

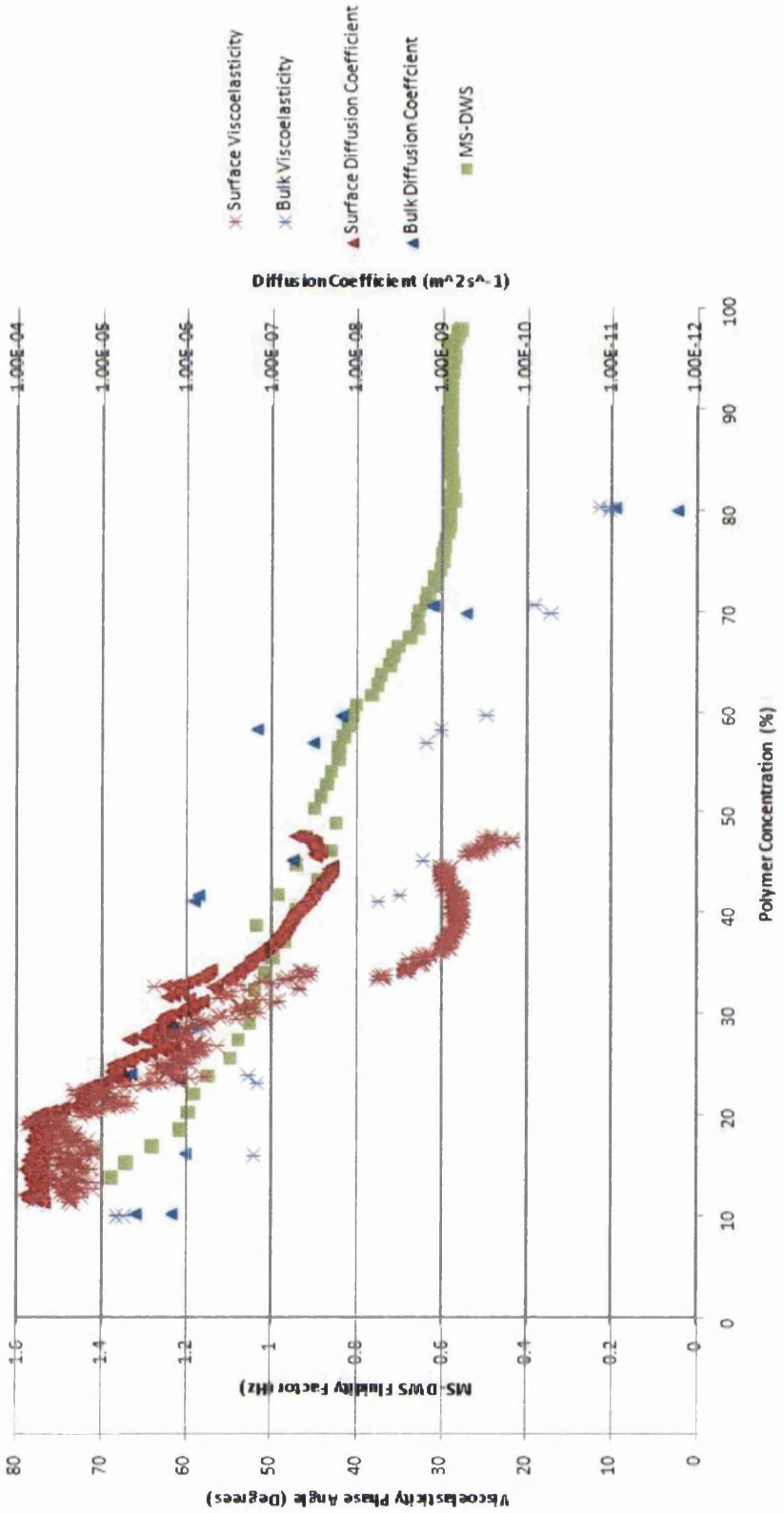


Figure 8.4: Plot of Mass Transfer over the Drying Period for Nitrocellulose-based Systems

- The addition of solid content increased the dependence of rheology upon initial resin content.

The physical changes of solvent loss were observed using FTIR and MS-DWS, showing a two-stage loss of solvent in the system with a decrease in rate between the two.

- The rate of solvent loss was dependent upon both the resin type and the initial resin content;
- The rate decreased with increasing initial resin content.
- Nitrocellulose gave a lower overall rate compared to polyamide.

The diffusion coefficient for the systems as well as the capillary number were both estimated to give further understanding towards the drying process. The capillary number reflects fundamental differences in the dominant forces acting upon the systems.

- Polyamide began dominated by surface tension allowing mass transfer of solute, eventually becoming more viscous dominated throughout the drying process.
- Nitrocellulose was viscous dominated throughout the drying process, allowing only diffusion to occur and increased skinning.

The estimated diffusion coefficients calculated from the viscosity results using the Einstein-Stokes equation showed values within the range of those measured directly.

- The estimates showed a decrease in diffusion coefficient throughout the drying process.
- Nitrocellulose had lower diffusion coefficient than polyamide, indicating the solvent is less able to diffuse through the system.

These results and values are able to provide quantitative data to be applied to a model similar to that proposed in Chapter 2. This will be able to increase the knowledge and understanding of the processes involved throughout drying and the parameters that influence the process.

# Chapter 9

# Conclusion

The experiments undertaken throughout this research have been used to develop a further understanding of the physical and structural processes of a drying polymer-solvent-pigment system. A number of experimental methods were used to gain an understanding of both the physical changes that occur during the drying process, such as solvent loss, and the structural changes, such as gelation. A number of parameters were varied to understand their influence on the processes, in particular the polymer resin (polyamide and nitrocellulose). The system was also tested with and without pigment and over a range of initial resin content. The polyamide system was a single solvent system, whereas the nitrocellulose system was a multiple solvent system.

The use of rheometry was able to show the change in structure throughout the drying process by monitoring the viscoelasticity. The choice of resin was critical in influencing the gelation process and the structure which it created. From the rheometry results, it was found polyamide viscosified in an orderly manner before sudden structural development through entanglement and hydrogen bonding, whereas nitrocellulose gelated in a complex progressive manner with a dominant entanglement process along with aggregation. The addition of a small amount of solid to either system, however, did not make a substantial impact. This gelation process was found to occur at a specific concentration, independent of initial resin concentration for both resins.

The surface change was also measured using rheometry so that a direct comparison between the surface and the bulk structure was able to be observed. Strong skinning effects were found to occur more quickly with increased initial resin content, independent of resin type. However, the viscoelasticity of the skin was higher for nitrocellulose than the polyamide resin at a comparative concentration. The pigment increased the effect of skinning; suggesting the influence of the pigment is greater on the surface than in the bulk. The capillary number was used to show the effects of

initial viscoelasticity upon the skinning of the system. The more viscosity dominant a system is, the more significant the skinning throughout the drying process.

Another method used to understand the structural changes, as well as the physical changes, was MS-DWS. This was able to monitor the molecular movement, and doing so, the early stages of gelation throughout drying. Both resins underwent an entanglement process observable in the rheology results. As well as showing the gelation of the polymer it was also able to monitor the solvent loss throughout the process. Solvent loss could be described by changes in diffusivity of the film. The method allowed the point at which the solvent loss was complete, where no residual solvent was left after diffusion, to be pin-pointed. Movement was found to continue after the system had reached 100% polymer concentration, indicating residual solvent and movement within the film for both polyamide and nitrocellulose systems. The nitrocellulose based system produced a stronger skin, which hindered the rate of solvent loss and increasing the likelihood of solvent retention.

FTIR was used to measure the solvent loss directly by monitoring the chemical absorption peaks of the solvents used. Using the method, it was confirmed that an increase in initial resin content hindered the rate of solvent evaporation for both resin types. However it illustrated the added complexity in terms of drying rate, due to the presence of multiple solvents. It was observed that the more volatile solvent was lost first from the system, resulting in a greater change in solubility throughout evaporation, in turn effecting the gelation of the system. The solvent loss within polyamide was found to be dependent on initial resin content, with the solvent retained longer at higher resin contents. 'Powdering' was found to occur for nitrocellulose systems under the same conditions, probably as a result of sudden changes in solubility parameter. This affected the lower resin concentration systems more significantly than the higher. It shows the influence solvent evaporation has upon the gelation process in multicomponent systems.

The diffusion coefficients for the different systems were able to be estimated from the rheology results. It allowed the effect of viscoelasticity upon the diffusion of the solvent through the system to be quantified. The diffusion coefficient was estimated to be significantly lower for nitrocellulose than polyamide.

The capillary number, which gives the ratio of surface tension and viscosity effects, was estimated for each system. It was found that the polyamide system had the potential to be initially surface tension driven, but became viscosity driven over the drying period; indicating that mass transfer of solute was possible throughout the initial stage of drying. Nitrocellulose systems, however, were viscosity driven

throughout the period allowing no mass transport throughout drying, only diffusion. This would also increase skinning of nitrocellulose inks.

Overall, it was found that the structural changes due to the gelation process of the polymer are critical to the physical changes, such as solvent loss, throughout the drying system. The polymer used within the system had a fundamental effect upon the process, with a different gelation process a critical factor. This gelation process occurs at different rates dependent on the initial resin concentration, especially at the surface. Increased resin concentration, increases the amount of skinning that occurs, hindering the solvent loss. The addition of a small percentage of pigment to the process does not have a substantial influence upon the gelation process within the bulk, but increases the effect of skinning further and hindering solvent loss.

## 9.1 Applications

The analytical methods and techniques developed during the course of this work were used to test a commercial ink. The results for this one commercial ink show very similar trends to that of the model inks tested. It gives validity to the methodology used and its application in testing more complex polymer-solvent-pigment systems and fully formulated inks. The results were able to provide information on the physical and structural processes taking place in the drying ink. The use of the techniques may be applied to the formulation of inks. To formulate an ink with certain properties, a knowledge of the drying process as well as the initial composition is necessary. The testing methodology developed here may be applied to drying processes involved in the manufacture of commercial ink. Modifications of the ink would be able to be made based on the test results to achieve the desired outcome in terms of drying time and quality of the final film. This can provide an economical means of achieving the correct formulation and monitoring production. Only small quantities of ink are required for each test and they are suitable for multiple screening of formulations. Once achieved, this is able to be scaled up to manufacturing quantities. The testing methodologies could also be used to refine existing formulations to become more economical and effective, creating a superior print quality or an ink with less expensive materials. It may be found that a less expensive or more enviromentally friendly solvent or resin may be used to achieve the same results, or the concentrations lowered to produce the same effect, in terms of drying pattern.

## 9.2 Further Work

Due to the large number of variables present in the ink drying process, only a select few of the basic and vital parameters were varied during the course of this work. Future work could be used to expand the matrix of parameters tested and to understand further the effect these have upon the physical and structural processes of drying polymer-solvent-pigment systems. These would include:

1. Temperature and air flow. These are significant parameters to be researched in the future. These parameters may expand upon the understanding of skinning and solvent retention that has already been gained.

2. Develop the methodology. These methods can be developed further toward more valuable industrial tools. DWS, in particular, is a relatively new technique with obvious advantages in terms of final stage drying monitoring.

3. Expanding the matrix of resins and solvents. This will lead to comparisons between the various resins and solvents, particulary in the developing area of printed electronic applications using solvent-based flexographic ink.

4. Expanding the types of systems tested to include water-based systems. Ink systems more suitable for printing using ink-jet, gravure and lithography may also be considered.

5. The development of a full theoretical model for the drying film in solvent flexo inks. This should incorporate:

- All possible mass transport options throughout the drying process
- All possible viscoelasticity development regimes i.e. resin types
- Incorporate Capillary number and Diffusion coefficient variations with time.
- Confirm estimates of Diffusion coefficient by experimental measurements.
- Lead to theoretical estimates of drying times and final retained solvent under all possible environmental conditions.

# References


[1] Printer's National Enviromental Assistance Center. Water based inks for flexographic printing, June 2011.

[2] D. Lanska and S. Cellramic. Stork sheds light on uv inks. *Converting Magazine*, 1997.

[3] European Flexographic Industry Association. Solvent based flexographic inks. Technical report, 1996.

[4] D. Deganello, J. A. Cherry, D. T. Gethin, and T. C. Claypole. Patterning of micro-scale conductive networks using reel-to-reel flexographic printing. *Thin Solid Films*, 518(21):6113 – 6116, 2010.

[5] Research and Markets. Displays and lighting: Oled, e-paper, electroluminescent and beyond, October 2008.

[6] R. H. Leach and R. J. Pierce. *The Printing Manual.* 5th edition, 1993.

[7] E. H. Jewell. Inks and coatings. *MSc Course Booklet*, 2007.

[8] G. G. Barros, C. Fahlcrantz, and P. Johansson. Topographic distribution of uncovered areas (uca) in full tone flexographic prints. *Printing Industries of America*, page 13, 2004.

[9] H. A. Barnes. *The Handbook of Elementary Rheology.* 2000.

[10] R. G. Larson. *The Structure and Rheology of Complex Fluids.* Oxford University Press, Oxford, 1999.

[11] R. C. Weast. *Handbook of Chemistry and Physics.* CRC Press, 62 edition, 2006.

[12] W. Xiao-dong, P. Xiao-feng, and W. Bu-xuan. Effect of solid surface properties on dynamic contact angles. *Heat Transfer - Asian Research*, 35:12, 2005.

[13] R. Tadmor and K. G. Pepper. Interfacial tension and spreading coefficient for thin films. *Langmuir*, 24(2008):3185–3190, 10 November 2007.

[14] D. O. Njobuenwu. Complete wetting of acrylic solid substrate with silicone oil at the center of the substrate. *AU J.T*, 10(3):163–168, 2007.

[15] S. E. Orchard. On surface levelling in viscous liquids and gels. *Applied Scientific Research Section A*, 11:451–464, 1962.

[16] E. Tekin, B. de Gennes, P. Gans, and U. S. Schubert. Ink-jet printing of polymers- from single dots to thin film libraries. *Materials Chemistry*, 2004.

[17] A. D. Mujumdar. *Handbook of Industrial Drying.* 2006.

[18] C. M. Hansen. Polymer coatings, concepts of solvent evaporation phenomena. *Ind. Eng. Chem. Prod. Res. Develop*, Vol. 9(No. 3), 1970.

[19] P. Wedin, J. A. Lewis, and L. Bergstrm. Soluble organic additive effects on stress development during drying of calcium carbonate suspensions. *Colloid and Interface Science*, 3 April 2005.

[20] M. Gordon and J. S. Taylor. *Applied Chemistry*, 2(493), 1952.

[21] T. G. Fox. *Am. Phys. Soc.*, 1(123), 1956.

[22] P. R. Couchman and F. E. Karasz. *Macromolecules*, 11(117), 1978.

[23] C. M. Hansen. *The Three Dimensional Solubility Parameter and Solvent Diffusion Coefficient. Their Importance In Surface Coating Formulation.* Danish Technical Press, 1967.

[24] Z. W. Wicks Jr., F. N. Jones, and S. P. Pappas. *Organic Coatings. Science and Technology.*, volume Volume 1: Film Formation, Components, and Appearance. Wiley, 1992.

[25] C. Chen and C. Mao. Thermoreversible gelation of nitrocellulose solutions. *Applied Polymer Science*, 90:4000–4008, 10 May 2003.

[26] Siegwerk Technical Data Sheet. Evaporation rates of solvents, April 2008.

[27] D. Stoye and W. Freitag. *Resins for Coatings. Chemistry, Properties and Applications.* Hanser, 1996.

[28] D. B. van Dam. Layer thickness distribution of thin-film ink-jet printed structures. In *XXI International Conference of Theoretical and Applied Mechanics*, Warsaw, Poland, 2004.

[29] B. Zhmud. Dynamic aspects of ink-paper interaction in relation to inkjet printing. *Pisa International Printing Conference, Brussels*, 2003.

[30] H. S. Kheshgi. The fate of thin liquid films after coating. In P.M.Schweiser S.F.Kistler, editor, *Liquid Film Coatings*, pages 183 – 205. Chapman And Hall, London, 1 edition, 1997.

[31] E. L. Cussler. *Diffusion. Mass Transfer in Fluid Systems.* Cambridge University Press, 1997.

[32] G. P. Bierwagen. Film formation and mudcracking in latex coatings. *Journal of Coating Technology*, 51:117–126, 1979.

[33] P. K. Whitham and W. Perera. Prediction of coating thickness and drying rate for forced air dried slurry coatings. *AIChE*, 1992.

[34] S. J. Weinstein and H. J. Palmer. Capillary hydrodynamics and interfacial phenomena. In Peter M. Schweizer Stephan F. Kistler, editor, *Liquid Film Coating*, pages 19 – 62. Chapman and Hall, London, 1997.

[35] J. E. Glass and R. K. Prud'homme. Coating rheology:component influence on the rheological response and performance of water-borne coatings in roll applications. In Peter M. Schweizer stephan F. Kistler, editor, *Liquid Film Coating*, pages 137–182. Chapman and Hall, London, 1997.

[36] T. J. Rehg and B. G. Higgins. Spin coating of colloidal suspension. *AIChE*, 38(4):489–501, 1992.

[37] R. G. Larson and T. J. Rehg. Spin coating. In Peter M. Schweizer stephan F. Kistler, editor, *Liquid Film Coating*, pages 709–734. Chapman and Hall, London, 1997.

[38] A. Fick. Über diffusion. *Ann. Phys*, 94:59–86, 1855.

[39] T. M. Aminabhavi, U.S. Aithal, and S. S. Shukla. Molecular transport of organic liquids through polymer films. *Macromolecules Science, Rev Macromolecule Chemical Physics*, C29:319–363, 1989.

[40] J. S. Vrentas and C. M. Vrentas. Integral sorption in glassy polymers. *Chemical Engineering Science*, 53:629–638, 1998.

[41] T. M. Aminabhavi, U. S. Aithal, and S. S. Shukla. An overview of the theoretical models used to predict transport of small molecules through polymer membranes. *Macromolecules Science, Rev Macromolecule Chemical Physics*, c28:421–474, 1988.

[42] M. C. Ridge and J. L. Perkins. Permeation of solvent mixtures through protective clothing elastomers. *ASTM Spec. Tech. Publ.*, 1037:113–131, 1989.

[43] J. Crank. *The Mathematics of Diffusion.* Oxford University Press, Oxford, 1979.

[44] J. S. Vrentas, C. M. Vrentas, and W. J. Huang. Anticipation of anoalous effects in differential sorption experiments. *Applied Polymer Science*, 64:2007–2013, 1997.

[45] P. Neogi. Anomalous diffusion of vapors through solid polymers. part i: Irreversible thermodynamics of diffusion and solution processes. *AIChE*, 29:829–833, 1983.

[46] T. Alfrey, E. F. Gurnee, and W. G. Lloyd. Diffusion in glassy polymers. *Polymer Science, Part C: Polymer Symp.*, 12:249–261, 1966.

[47] T. Z. Fu and C. J. Durning. Numerical simulation of case ii transport. *AlChE*, 39:1030–1044, 1993.

[48] C. J. Wolf and H. Fu. Stress-enhanced transport of toluene in poly(aryl ether ether ketone) (peek). *Polymer Science Part B: Polymer Physics*, 34:75–82, 1996.

[49] S. V. Dixon-Garrett, K. Nagai, and B. D. Freeman. Sorption, diffusion, and permeation of ethylbenzene in poly(1-trimethylsilyl-1-propyne). *Polymer Science Part B: Polymer Physics*, 38:1078–1089, 2000.

[50] R. M. Ybarra, P. Neogi, and J. M. D. MacElroy. Osmotic stresses and wetting by polymer solutions. *Ind. Eng. Chem. Res.*, 37:427–434, 1998.

[51] D. S. Cohen and C. Goodhart. Sorption of a finite amount of swelling solvent in a glassy polymer. *Polymer Science Part B: Polymer Physics*, 25:611–617, 1987.

[52] C. P. A. Liu, D. C Nguyen, and P. Neogi. Effects of constrained chain conformations on polymer-solute interactions in semicrystalline polymers. *Macromolecule Science, Phys.*, B29:203–220, 1990.

[53] C. J. Durning and W. B. Russel. A mathematical model for diffusion with induced crystallization. 2. *Polymer*, 26:131–140, 1985.

[54] N. L. Thomas and A. H. Windle. A deformation model for case ii diffusion. *Polymer*, 21:613–619, 1980.

[55] N. L. Thomas and A. H. Windle. Diffusion mechanics of the system pmma-methanol. *Polymer*, 22:627–639, 1981.

[56] N. L. Thomas and A. H. Windle. A theory of case ii diffusion. *Polymer*, 23:529–542, 1982.

[57] J. C. Wu and N. A. Peppas. Modelling of penetrant diffusion in glass polymers with an integral sorption deborah number. *Polymer Science Part B: Polymer Physics*, 31:1503–1518, 1993.

[58] J. C. Wu and N. A. Peppas. Numerical simulation of anomalous penetrant diffusion in polymers. *Applied Polymer Science*, 49:1845–1856, 1993.

[59] M. Reiner. The deborah number. *Physics Today*, 17:62, 1964.

[60] C. F. Chan Man Fong, C. Moresoli, S. Xiao, Y. Li, J. Bovenkamp, and D. De Kee. Modelling diffusion through geomembranes. *Applied Polymer Science*, 67:1885–1889, 1998.

[61] R. W. Cox and D. S. Cohen. A mathematical model for stress- driven diffusion in polymers. *Polymer Science Part B: Polymer Physics*, 27:589–602, 1989.

[62] J. H. Petropoulos. Effect of a stress-dependent solubility coefficient on sorption kinetics in penetrant-polymer membrane systems. *Membrane Science*, 18:37–51, 1984.

[63] D. S. Cohen. Theoretical models for diffusion in glassy polymers. ii. *Polymer Science, Polymer Physics Ed.*, 22:1001–1009, 1984.

[64] D. A. Edwards and D. S. Cohen. A mathematical model for a dissolving polymer. *AIChE*, 41:2345–2355, 1995.

[65] R. B. Bird. Five decades of transport phenomena. *AIChE*, 50:273–287, 2004.

[66] A. El Afif and M. Grmela. Non-fickian mass transport in polymers. *Rheology*, 46:591–628, 2002.

[67] A. N. Beris and B. J. Edwards. Poisson bracket formulation of imncompressible flow equations in continuum mechanics. *Rheology*, 34:55–78, 1990.

[68] B. J. Edwards and A. N. Beris. Unified view of transport phenomena based on the generaliszed bracket formulation. *Ind. Eng. Chem.*, 30:873, 1991.

[69] A. El Afif, M. Grmela, and G. Lebon. Rheology and diffusion in simple and complex fluids. *Non-Newtonian Fluid Mechanics*, 86:253–275, 1999.

[70] A. El Afif and M. Grmela. Diffusion of one- and two- component fluids into polymeric membranes. *Cdn. J. Chem. Eng.*, 80:1197–1205, 2002.

[71] C. J. Guo, D. De. Kee, and B. Harrison. Effect of molecular structure on diffusion of organic solvents in rubbers. *Chemical Engineering Science*, 47:1525–1532, 1992.

[72] J. S. Vrentas and C. M. Vrentas. Solvent self-diffusion in glassy polymer-solvent systems. *Macromolecules*, 27:5570, 1994.

[73] M. Hedenqvist, A. Angelstok, L. Edsberg, P. T. Larsson, and U. W. Geddes. Diffusion of small-molecule penetrants in polyethylene: Free volume and morphology. *Polymer*, 37:2887–1902, 1996.

[74] J. Crank and G. S. Park. *Diffusion in Polymers.* Academic Press, London and NY, 1968.

[75] J. Stastna and D. De Kee. *Transport Properties in Polymers.* Technomic Publishing Co., Inc., Lancaster, 1995.

[76] I. E. Helmroth, M. Dekker, and T. Hankemeier. Influence of solvent absorption on the migration of irganox 1076 from ldpe. *Food Addit. Contam*, 19:176–183, 2002.

[77] G. Rossi. Macroscopic desciption of solvent diffusion in polymeric materials. *TRIP*, 40:337–342, 1996.

[78] H. Cornelis and R. G. Kander. Diffusion of methylene chloride and tetrahydrofuran in amorphous poly (ether ether ketone). *Polymer*, 37:5627–5637, 1996.

[79] R. P. Kambour, F. E. Karasz, and J. H. Daane. Kinetic and equilibrium phenomena in the system: Acetone vapor and polycarbonate film. *Polymer Science A-2*, 4:327–347, 1966.

[80] W. V. Titow, M. Braden, B. R. Currell, and R. J. Loneragan. Diffusion and some structural effects of two chlorinated hydrocarbon solvents in bisphenol a polycarbonate. *Applied Polymer Science*, 18:867–886, 1974.

[81] N. overbergh, H. Berghmans, and G. Smets. Crystallization of isotactic polystyrene induced by organic vapours. *Polymer*, 16:703–708, 1975.

[82] G. Unnikrishnan and S. Thomas. Molecular transport of benzene and methyl-substituted benzenes into filled natural rubber sheets. *Applied Polymer Science*, 60:963–970, 1996.

[83] C. Joubert, P. Cassagnau, L. Choplin, and A. Michel. Diffusion of plasticizer in elastomer probed by rheological analysis. *Journal of Rheology*, 46:629–650, February 2002.

[84] L. H. Sperling. *Introduction to Physical Polymer Science*. Wiley, 1992.

[85] P. C. Painter and M. M. Coleman. *Fundamentals of Polymer Science. An Introductory Text.* Technomic Publishing Co:, Inc., Lancaster, 1994.

[86] N.M.P.S. Ricardo, N.M.P.S. Ricardo, F. de M.L.L. Costa, C. Chaibundit, G. Portale, D. Hermida-Merino, S. Burattini, I.W. Hamley, C.A. Muryn, S.K. Nixon, and S.G. Yeates. The effect of n-, s- and t-butanol on the micellization and gelation of pluronic p123 in aqueous solution. *Colloid and Interface Science*, 353:482–489, 2011.

[87] C. Chaibundit, N.M.P.S. Ricardo, N.M.P.S. Ricardo, C.A. Muryn M. Madec, S.G. Yeates, and C. Booth. Effect of ethanol on the gelation of aqueous solutions of pluronic f127. *Colloid and Interface Science*, 351:190–196, 2010.

[88] W. O. Teeters and V. W. Ware. Evaluation of nitrocellulose lacquer solvents. comparison by means of a constant viscosity procedure. *Industrial and Engineering Chemistry*, 81(6), June 1939.

[89] J. E. Eldridge and J. D. Ferry. *Physical Chemistry*, 58:992–995, 1954.

[90] G. A. Viliegenthart, H. N. W. Lekkerkerker, and R. Tuinier. Depletion interaction between spheres immersed in a solution of ideal polymer chains. *Chemical Physics*, 113(23), 19 september 2000.

[91] W. C. K. Poon, P. N. Pusey, A. Stroobants, P. B. Warren, and H. N. W. Lekkerkerker. Phase behaivour of colloid + polymer mixtures. *Europhysics Letters*, 20(6):559–564, 10 september 1992.

[92] S. Asakura and F. Oosawa. *Chem. Phys*, 22:1255, 1954.

[93] A. Vrij. *Pure Appl. Chem*, 48:471, 1976.

[94] B. J. Vincent, J. Edwards, S. Emmett, and R. Groot. *Colloid Surf*, 31:267, 1988.

[95] P. R. Sperry, H. B. Hopfenberg, and N. L. Thomas. *Colloid Interface Sei*, 82:62, 1981.

[96] T. G. Mezger. *The rheology handbook: for users of rotational and oscillatory rheometers.* Vincentz, 2006.

[97] Bohlin Instruments. *User Manual for Bohlin Rheometers*, 3 edition, July 2004.

[98] G. G. Fuller. Rheology of mobile interfaces. *The British Society of Rheology: Rheology Reviews*, pages 77 – 123, 2003.

[99] L. Brunel. Horus. film formation analyser technical design report. Technical report, Formulaction, 20/12 2005.

[100] Thermo Nicolet Corporation. Introduction to fourier transform infrared spectrometry. 2001.

[101] B. Stuart. *Infrared Spectroscopy: Fundamentals and Applications*. John Wiley and Sons Ltd, 2004.

[102] M. J. Borda, M. V. Fey, D. L. Sparks, and C. E. Dowding. A new method for gaining insight into the chemistry of drying mineral surfaces using atr-ftir. *Colloid and Interface Science*, (292):148–151, 21 May 2005.

[103] C. P. S. Hsu. *Infrared Spectroscopy*, page chapter 15. NaN.

[104] http://www.autohotkey.com/, 1991.

[105] Cookham Spectroscopy Services. *Introduction to Infrared Spectroscopy Training Course Manual.* Perkin Elmer Ltd, 2002.

[106] P. D. Whyzmuzis and E. R. Hinden. Polyamide resin solubility. 14 March 1972.

[107] Dow wolff. Nitrocellulose. NaN.

[108] Kenji Kamide. *Cellulose and Cellulose Derivatives.* Elsevier Science, 31 Aug 2005.

[109] R. A. Cairncross, L. F. Francis, and L. E. Scriven. Predicting drying in coatings that react and gel: Drying regime maps. *AIChE*, 95, 1995.

[110] D. A. Edwards. An asymptotic analysis of polymer desorption and skinning. *Macromolecules Theory Simulation*, 8:10–14, 2 June 1998 1999.

[111] R.P. Woodward. Surface tension measurements using the drop shape method. Technical report, First Ten Angstroms.

[112] Y. Cohen, L. Avram, and L. Frish. Diffusion nmr spectroscopy in supramolecular and combinatorial chemistry: An old parameter-new insights. *Angew. Chem. Int. Ed.*, 44:520–554, 2005.

[113] M. J. Thrippleton, N. M. Loening, and J. Keeler. A fast method for the measurement of diffusion coefficients: one-dimensional dosy. *Magn. Reson. Chem.*, 41:441–447, 9 February 2003.

[114] D. B. van Dam and J. G. M. Kuerten. Modeling the drying of ink-jet-printed structures and experimental verification. *American Chemical Society*, 24:582–589, 2008.

[115] J. D. Ferry. *Viscoelastic Properties of Polymers.* Wiley, NY, 3 edition, 1980.

# Appendix A

# Further Result Plots

The bulk rheology results of the polyamide-based system are plotted.

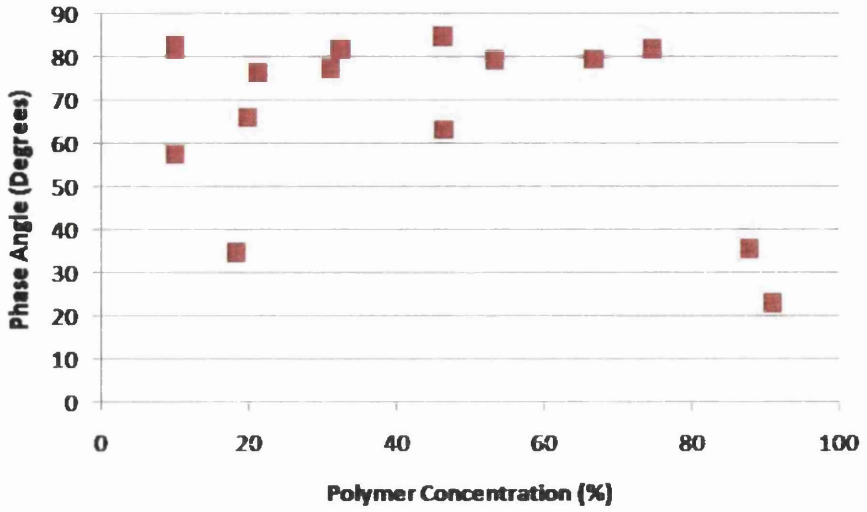


Figure A.1: Phase Angle of 10% Polyamide Resin Ink over Drying Period.

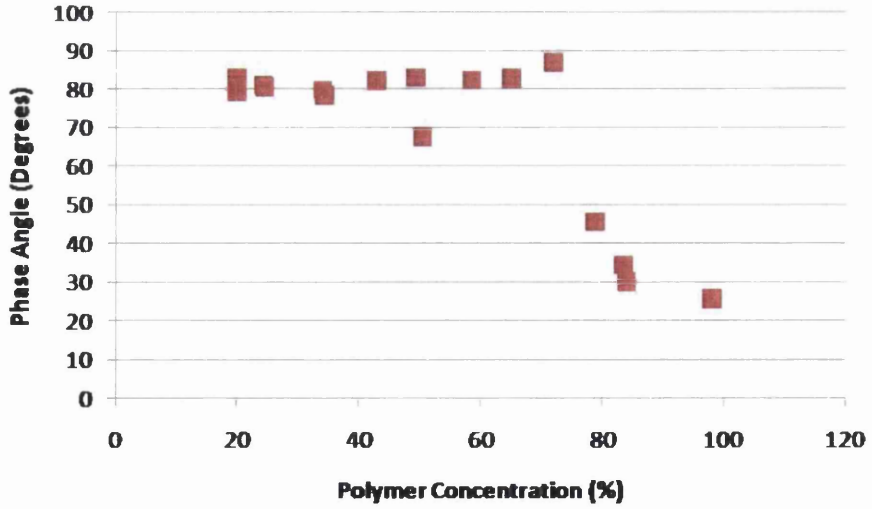


Figure A.2: Phase Angle of 20% Polyamide Resin Ink over Drying Period.

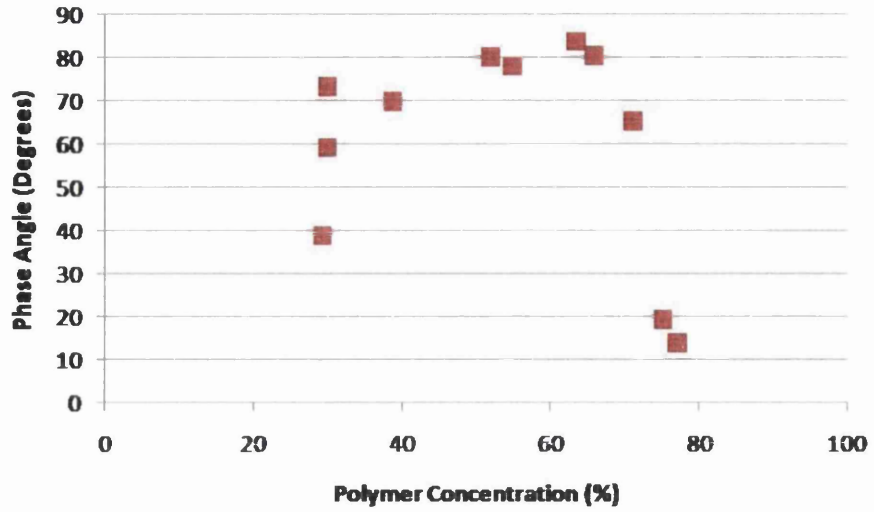


Figure A.3: Phase Angle of 30% Polyamide Resin Ink over Drying Period.

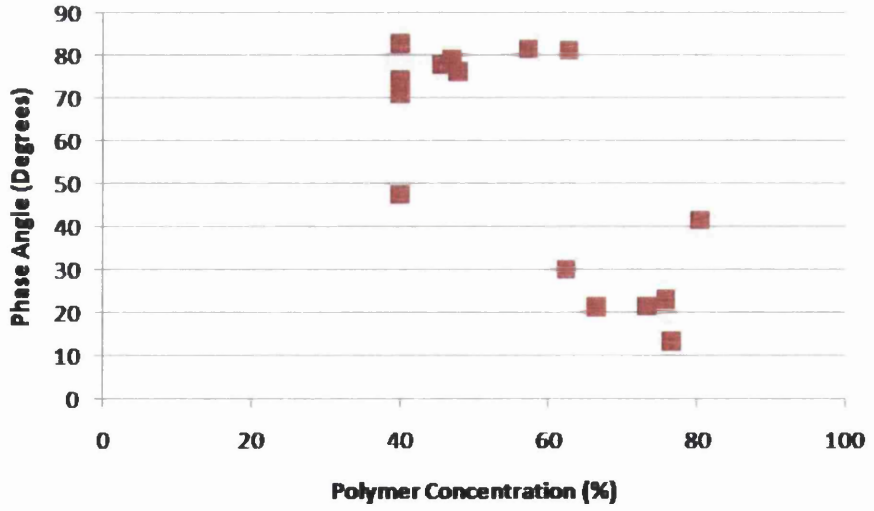


Figure A.4: Phase Angle of 40% Polyamide Resin Ink over Drying Period.

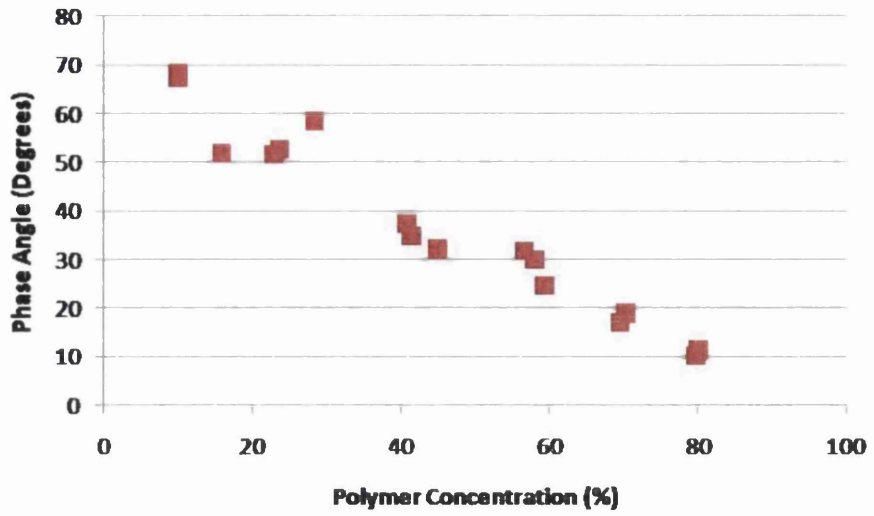


Figure A.5: Phase Angle of 10% Nitrocellulose Resin Ink over Drying Period.

The bulk rheology results of the polyamide-based system are plotted.

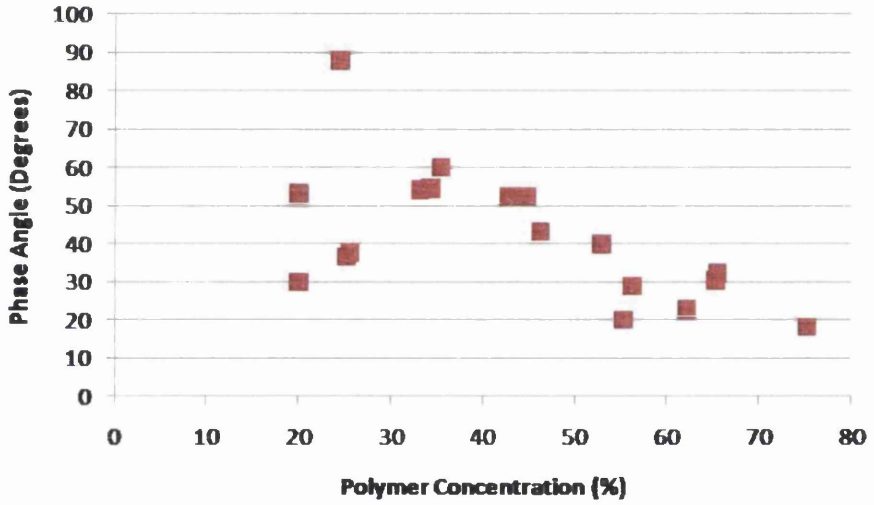


Figure A.6: Phase Angle of 20% Nitrocellulose Resin Ink over Drying Period.

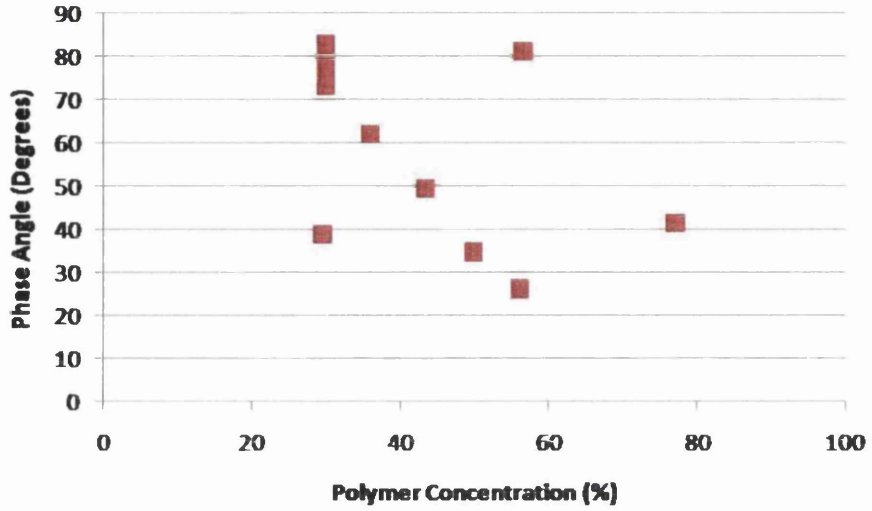


Figure A.7: Phase Angle of 30% Nitrocellulose Resin Ink over Drying Period.

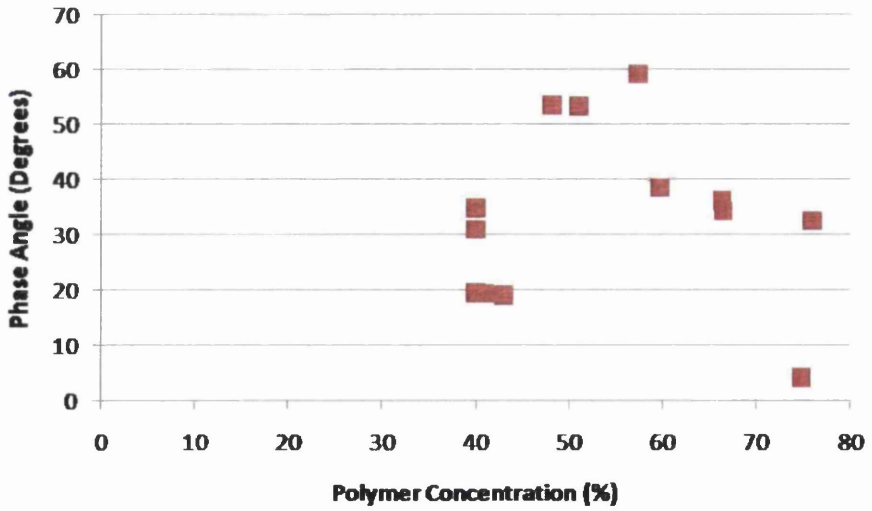


Figure A.8: Phase Angle of 40% Nitrocellulose Resin Ink over Drying Period.

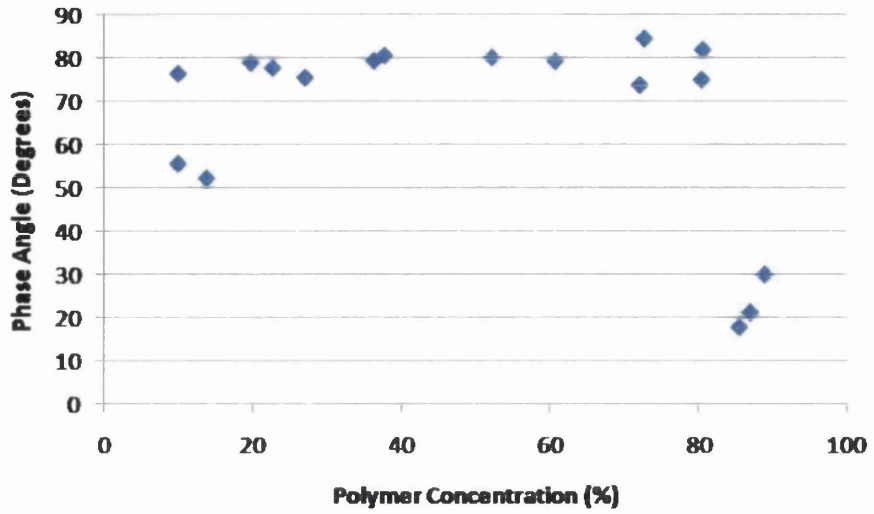


Figure A.9: Phase Angle of 10% Polyamide Resin Ink with Solid Content over Drying Period.

The bulk rheology results of the polyamide-based system with the addition of solid content are plotted.

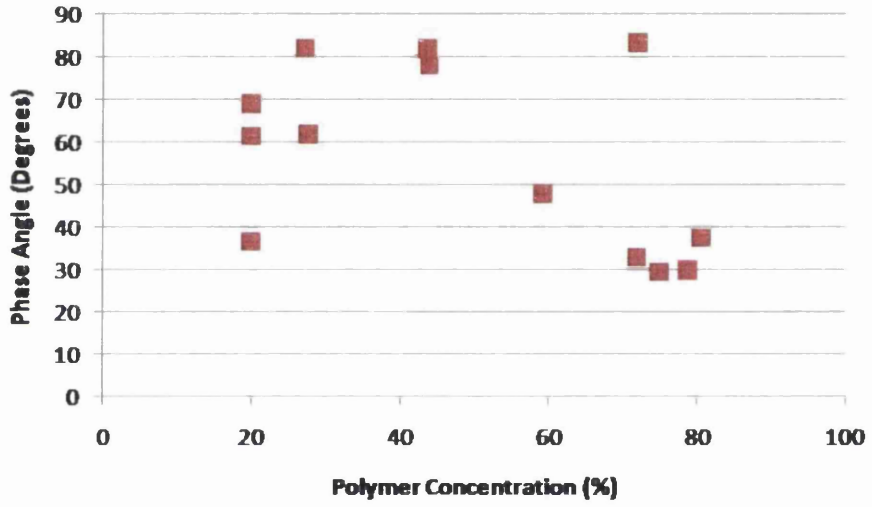


Figure A.10: Phase Angle of 20% Polyamide Resin Ink with Solid Content over Drying Period.

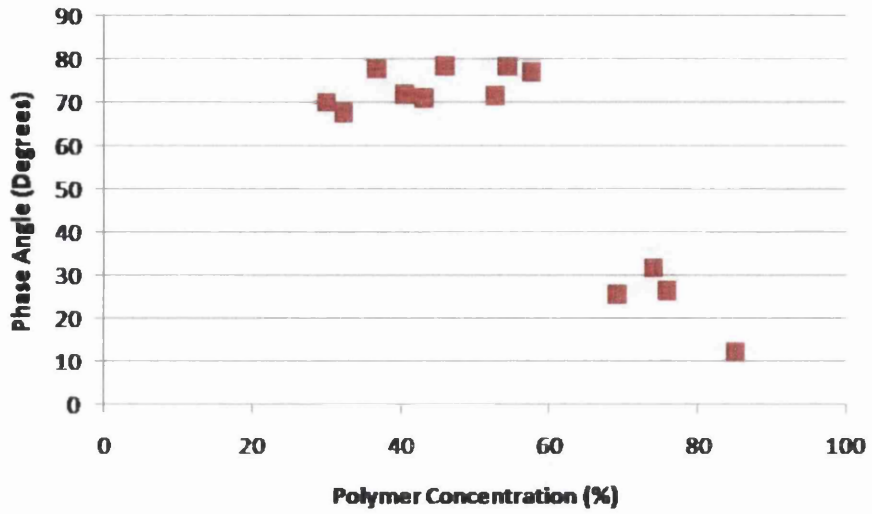


Figure A.11: Phase Angle of 30% Polyamide Resin Ink with Solid Content over Drying Period.

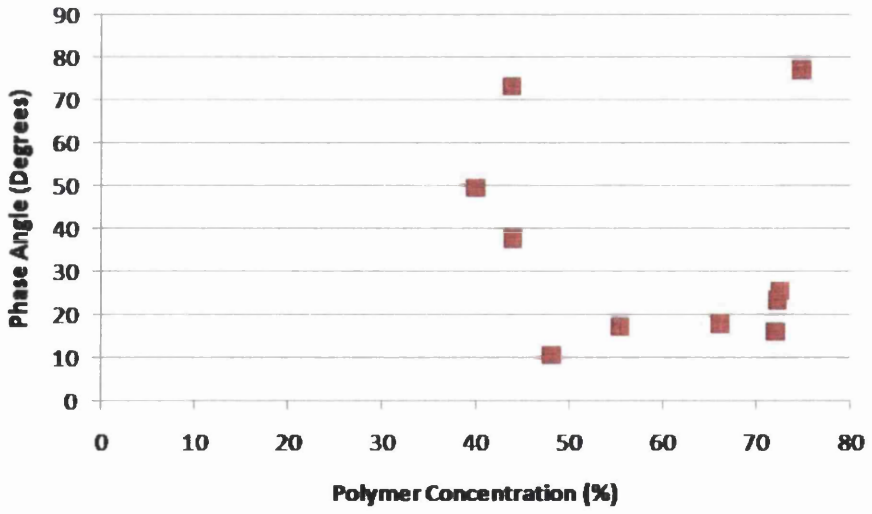


Figure A.12: Phase Angle of 40% Polyamide Resin Ink with Solid Content over Drying Period.

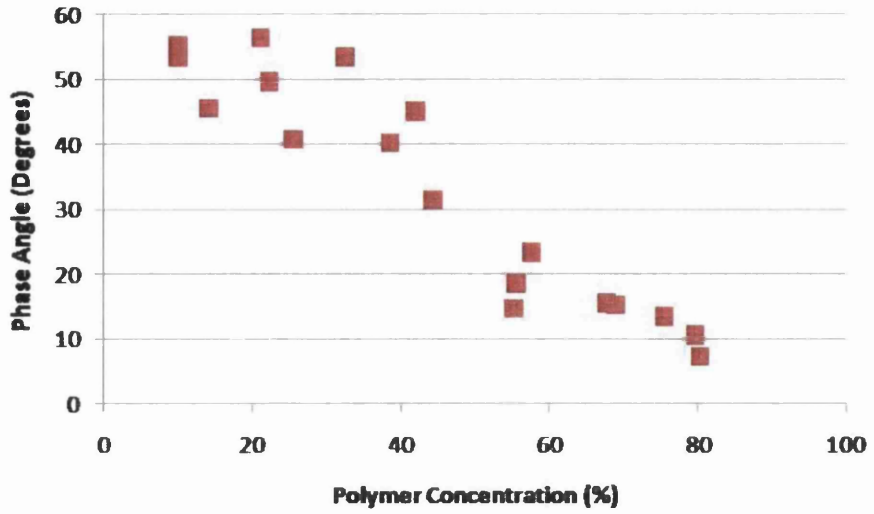


Figure A.13: Phase Angle of 10% Nitrocellulose Resin Ink with Solid Content over Drying Period.

The bulk rheology results of the nitrocellulose-based system with the addition of solid content are plotted.

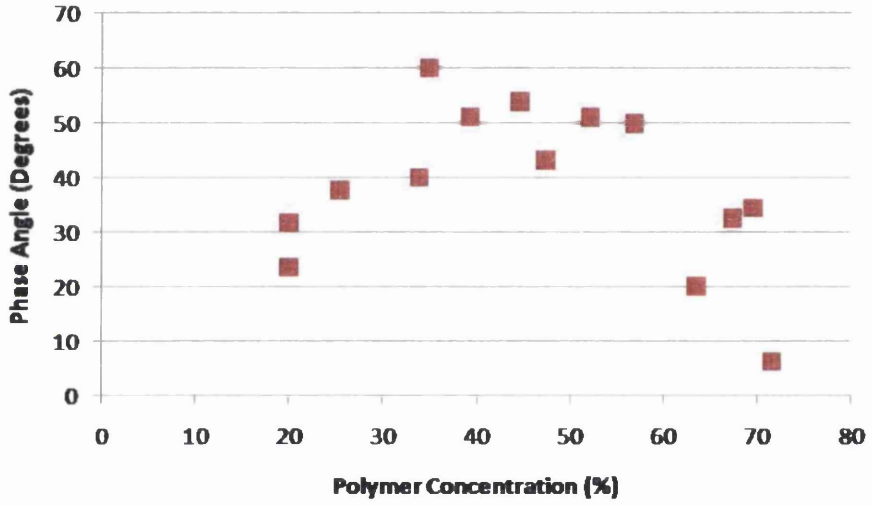


Figure A.14: Phase Angle of 20% Nitrocellulose Resin Ink with Solid Content over Drying Period.

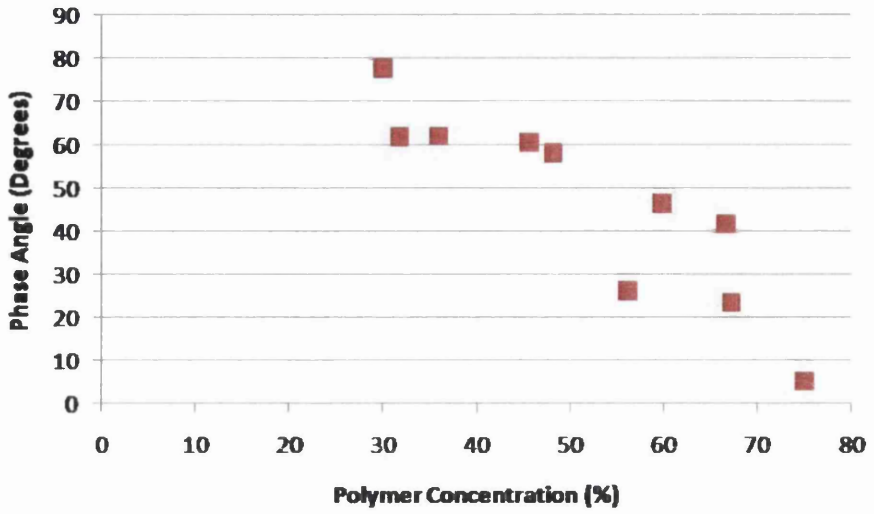


Figure A.15: Phase Angle of 30% Nitrocellulose Resin Ink with Solid Content over Drying Period.

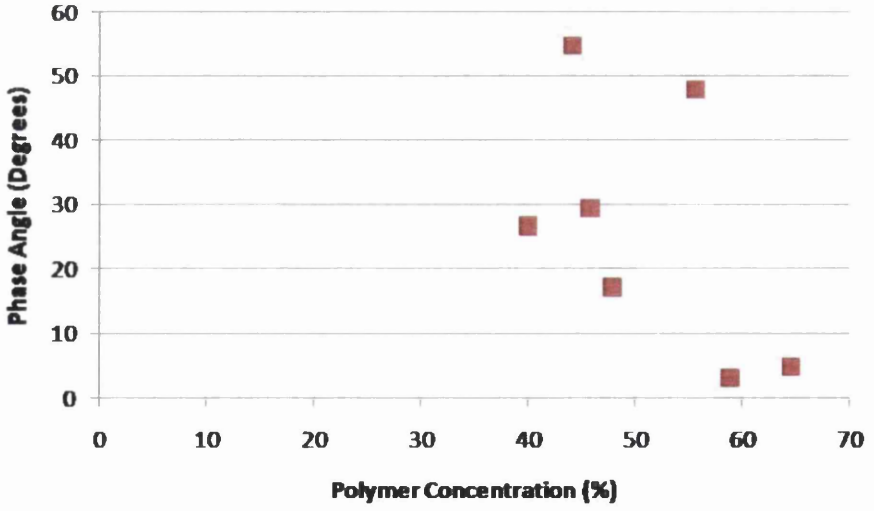


Figure A.16: Phase Angle of 40% Nitrocellulose Resin Ink with Solid Content over Drying Period.

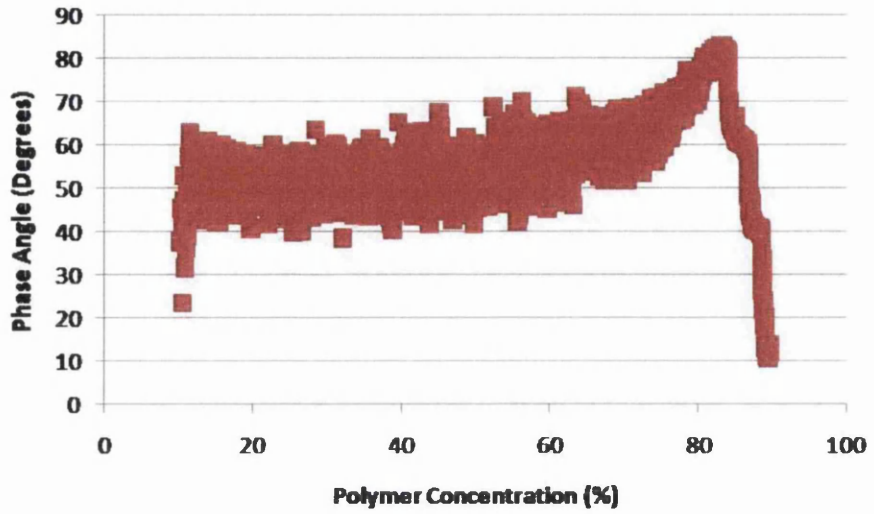


Figure A.17: Phase Angle of 10% Polyamide Resin Ink over Drying Period.

The surface rheology results using a bicone of the polyamide-based system are plotted.

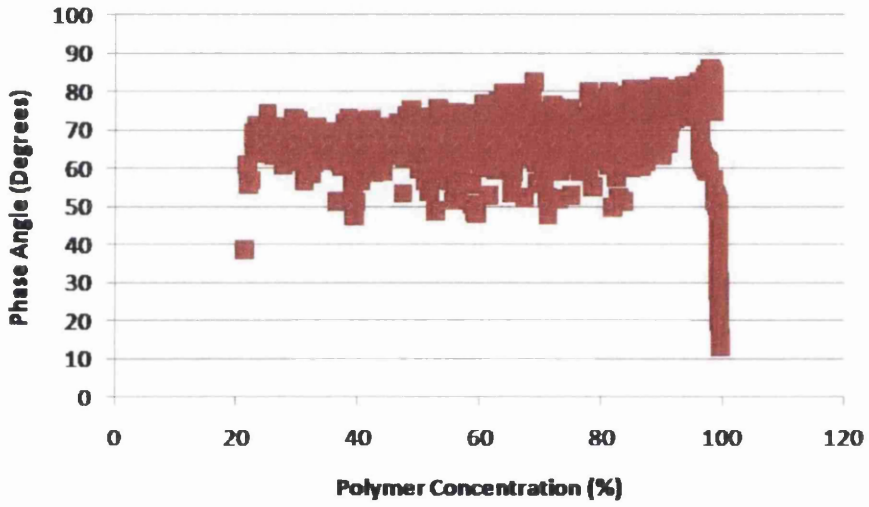


Figure A.18: Phase Angle of 20% Polyamide Resin Ink over Drying Period.

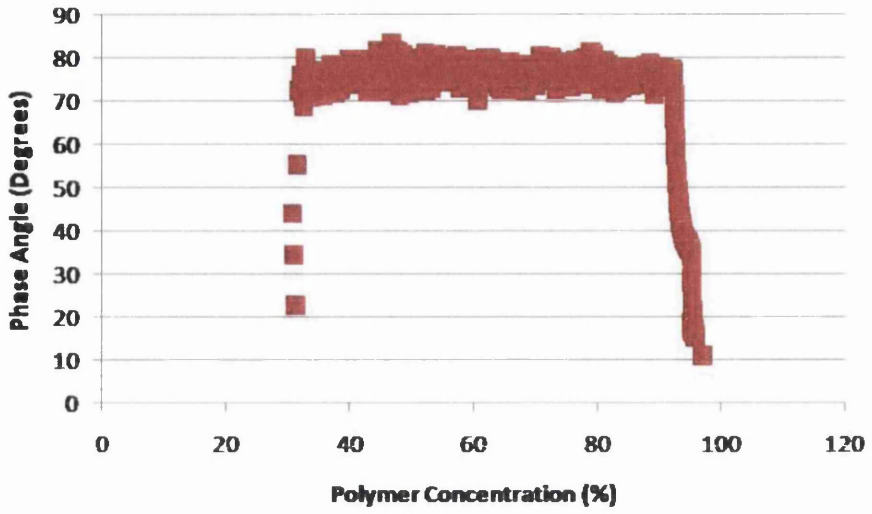


Figure A.19: Phase Angle of 30% Polyamide Resin Ink over Drying Period.

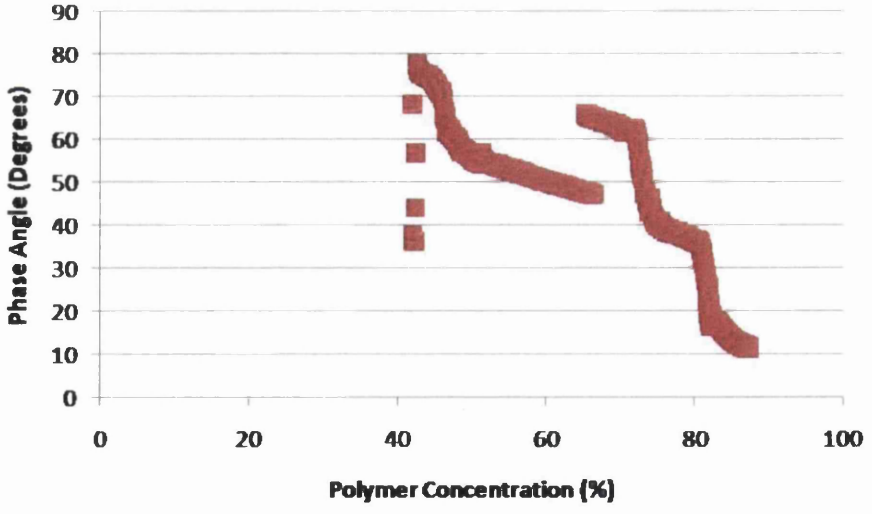


Figure A.20: Phase Angle of 40% Polyamide Resin Ink over Drying Period.

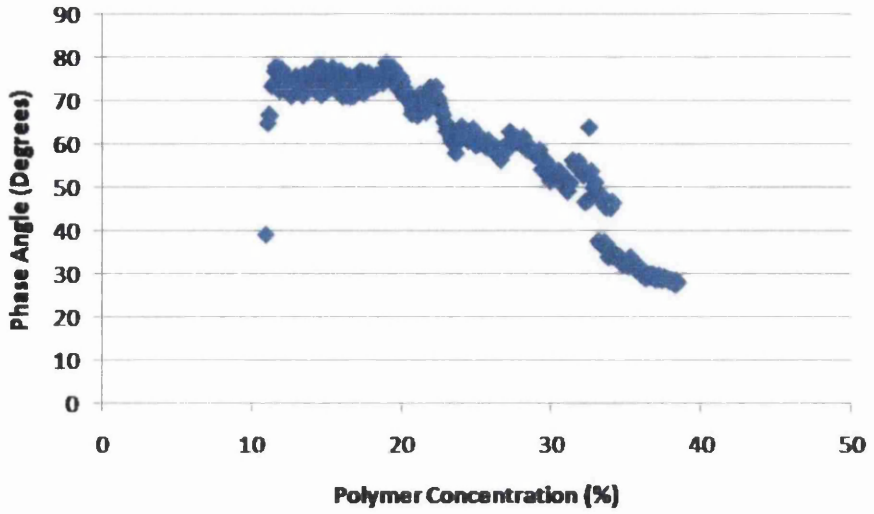


Figure A.21: Phase Angle of 10% Nitrocellulose Resin Ink over Drying Period.

The surface rheology results using a bicone of the nitrocellulose-based system are plotted.

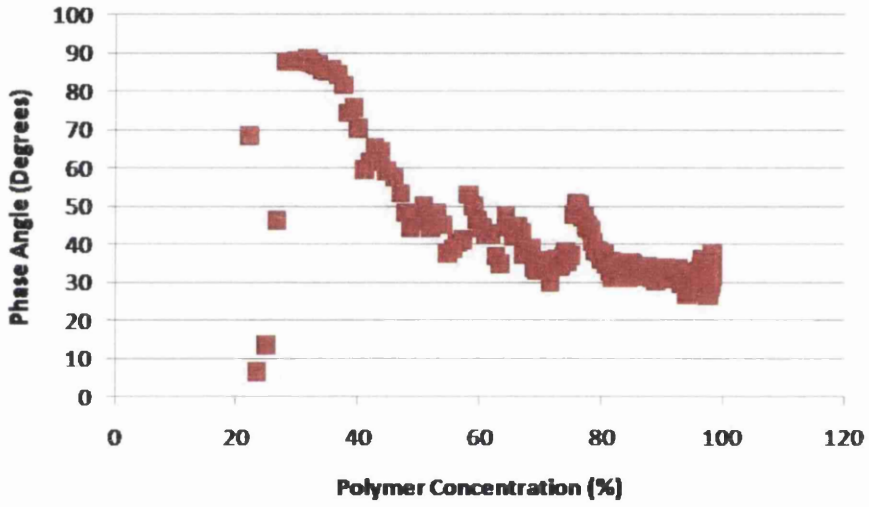


Figure A.22: Phase Angle of 20% Nitrocellulose Resin Ink over Drying Period.

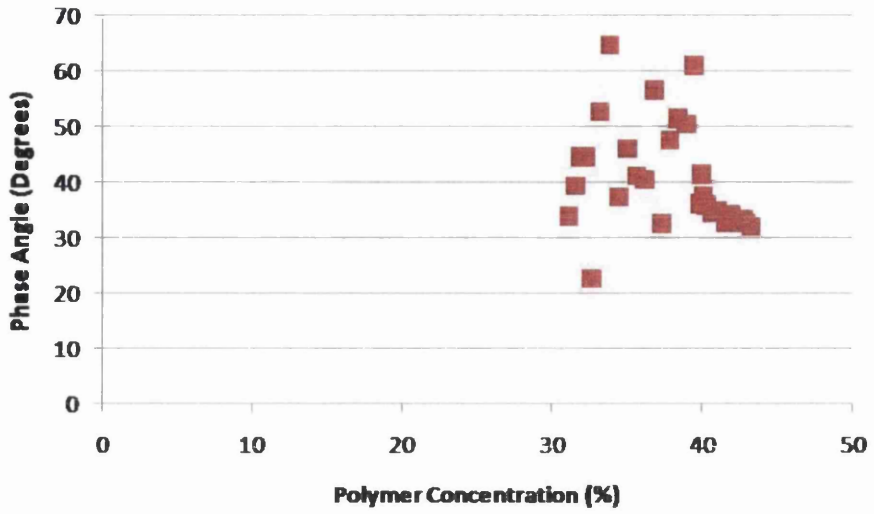


Figure A.23: Phase Angle of 30% Nitrocellulose Resin Ink over Drying Period.

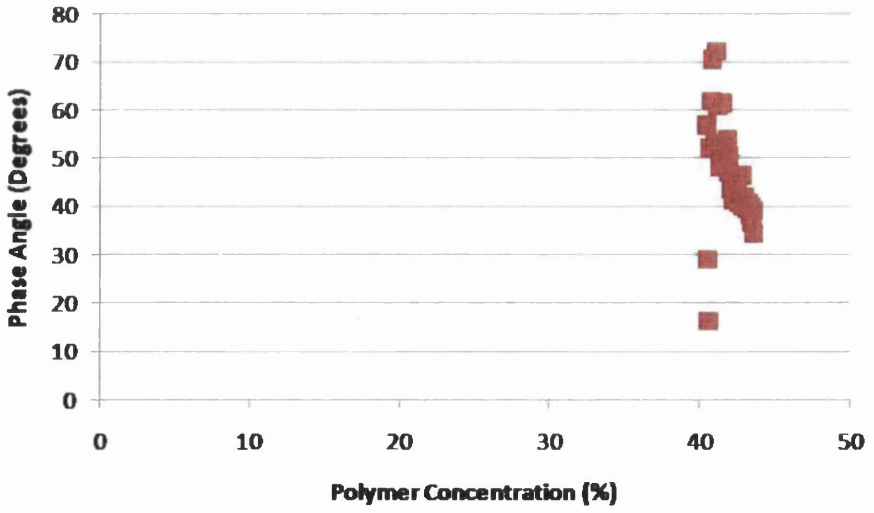


Figure A.24: Phase Angle of 40% Nitrocellulose Resin Ink over Drying Period.

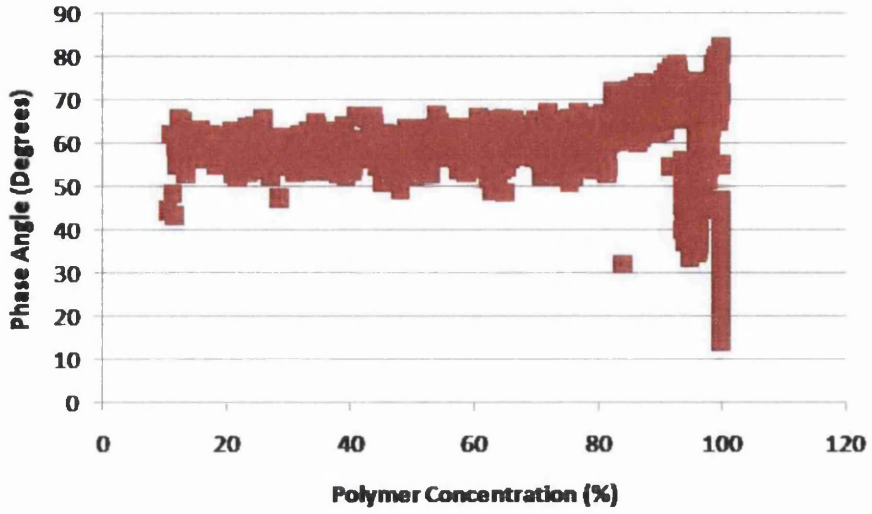


Figure A.25: Phase Angle of 10% Polyamide Resin Ink with Solid Content over Drying Period.

The surface rheology results using a bicone of the polyamide-based system with the addition of solid content are plotted.

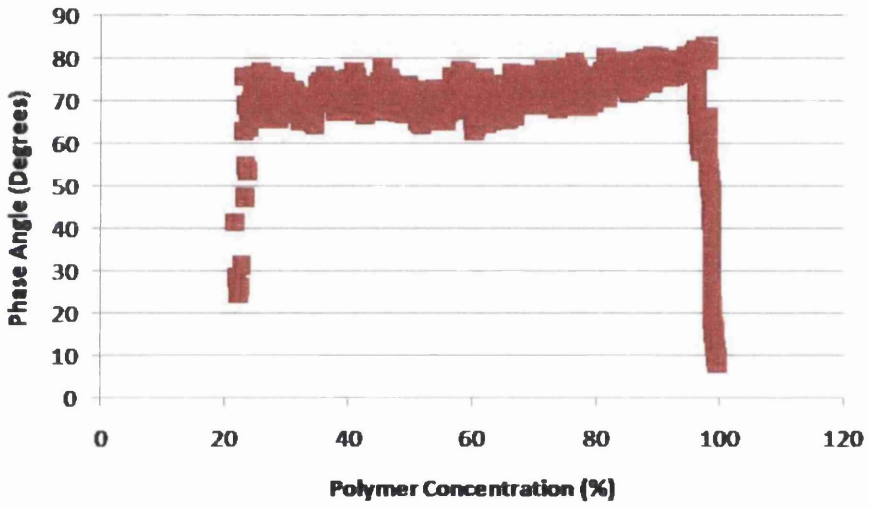


Figure A.26: Phase Angle of 20% Polyamide Resin Ink with Solid Content over Drying Period.

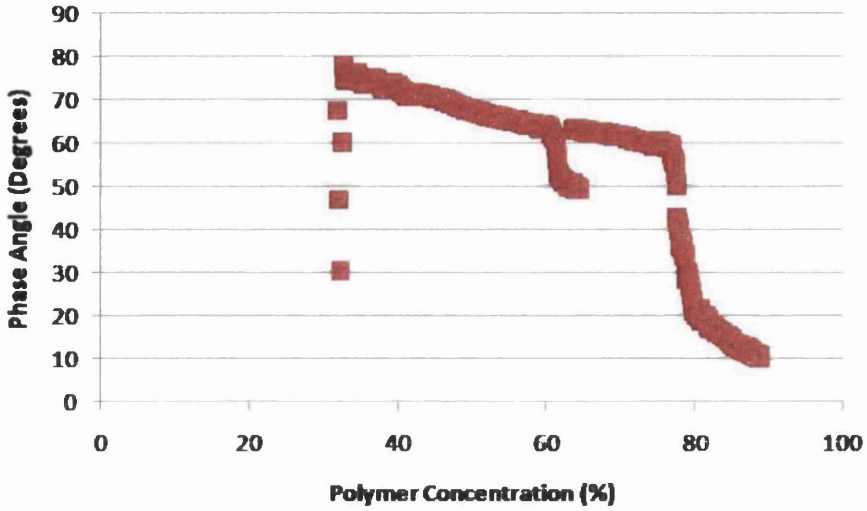


Figure A.27: Phase Angle of 30% Polyamide Resin Ink with Solid Content over Drying Period.

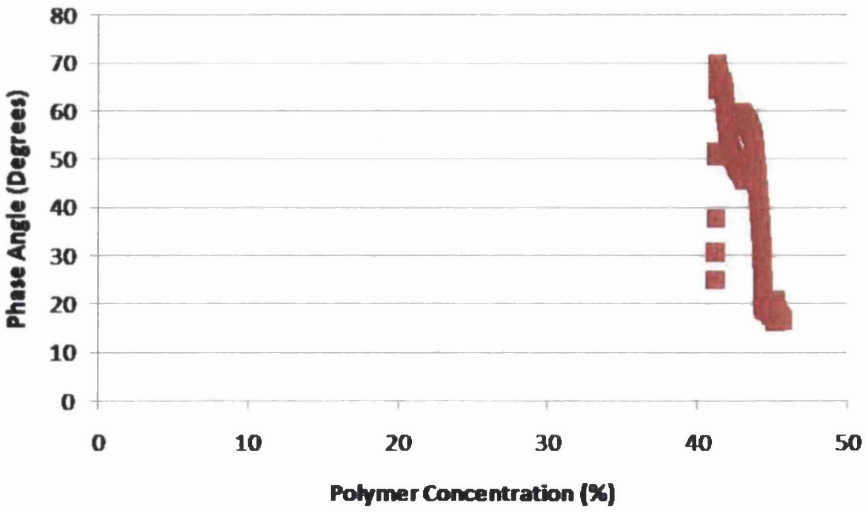


Figure A.28: Phase Angle of 40% Polyamide Resin Ink with Solid Content over Drying Period.

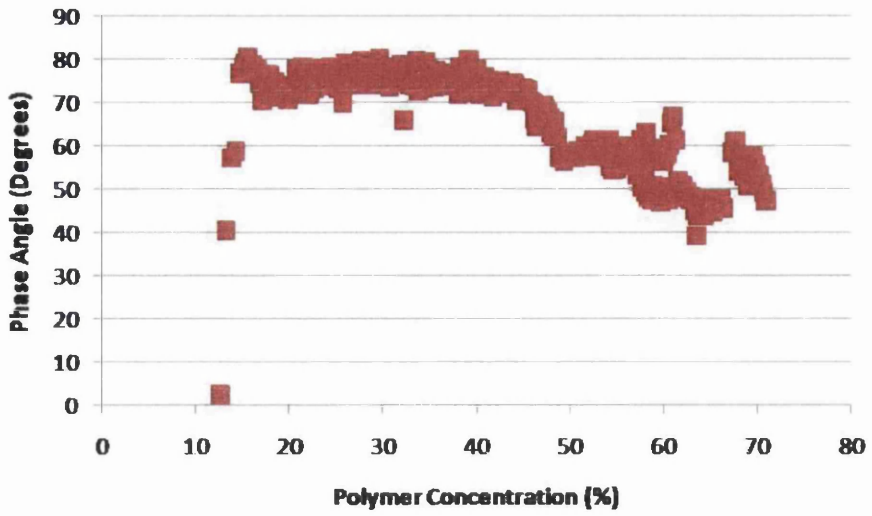


Figure A.29: Phase Angle of 10% Nitrocellulose Resin Ink with Solid Content over Drying Period.

The surface rheology results using a bicone of the nitrocellulose-based system with the addition of solid content are plotted.

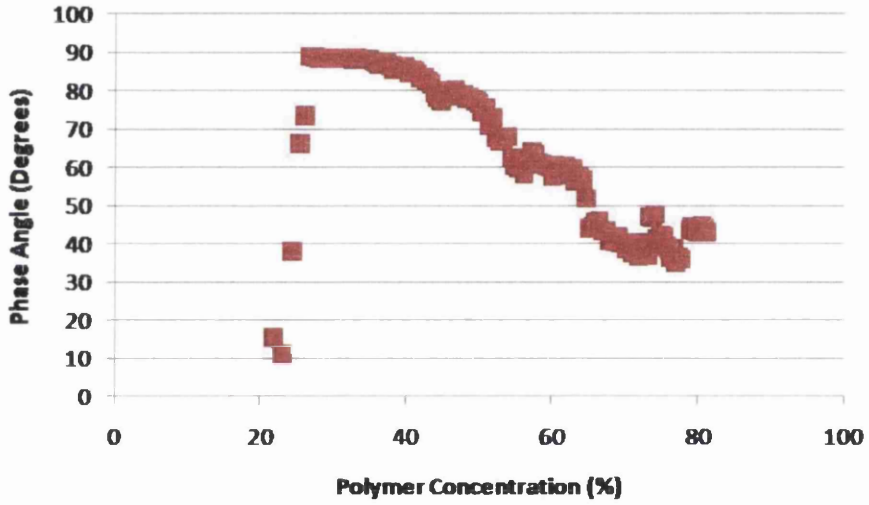


Figure A.30: Phase Angle of 20% Nitrocellulose Resin Ink with Solid Content over Drying Period.

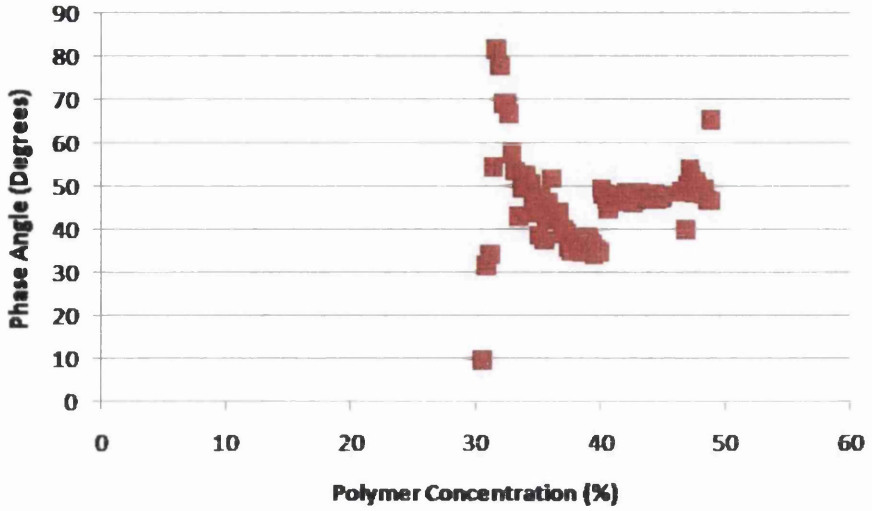


Figure A.31: Phase Angle of 30% Nitrocellulose Resin Ink with Solid Content over Drying Period.

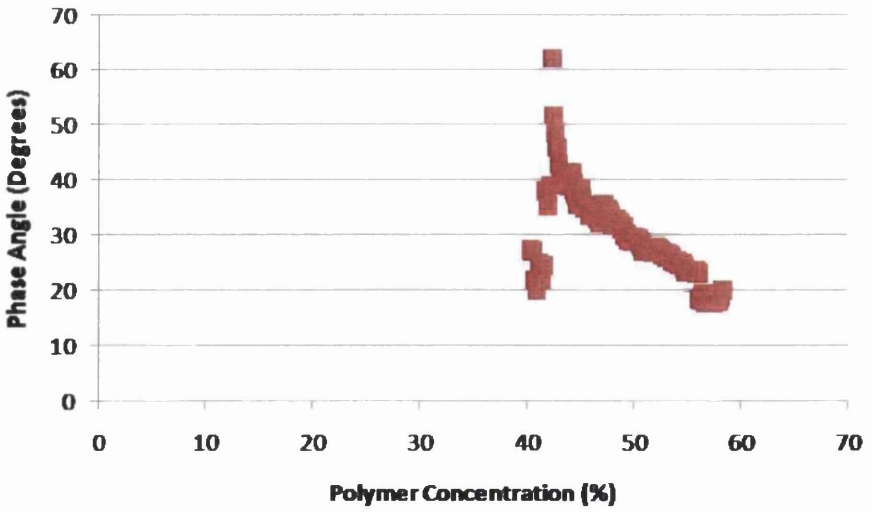


Figure A.32: Phase Angle of 40% Nitrocellulose Resin Ink with Solid Content over Drying Period.

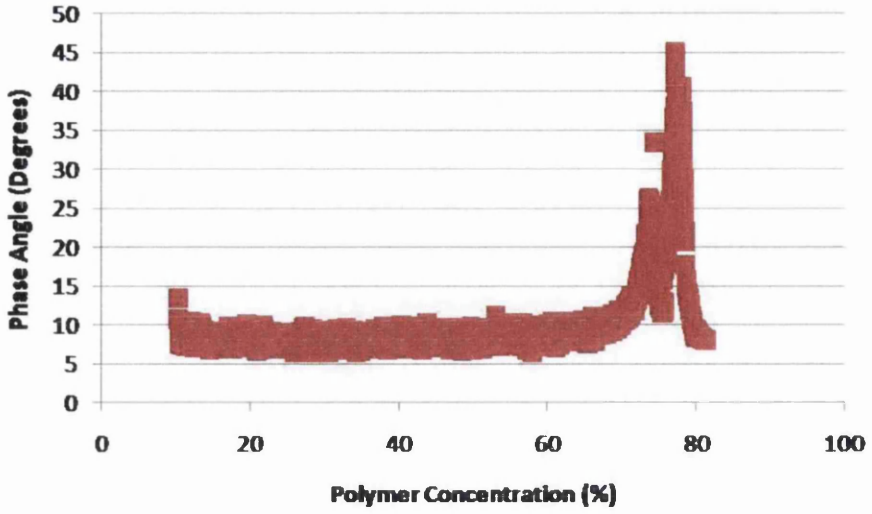


Figure A.33: Phase Angle of 10% Polyamide Resin Ink over Drying Period.

The surface rheology results using a Dunouy ring of the polyamide-based system are plotted.

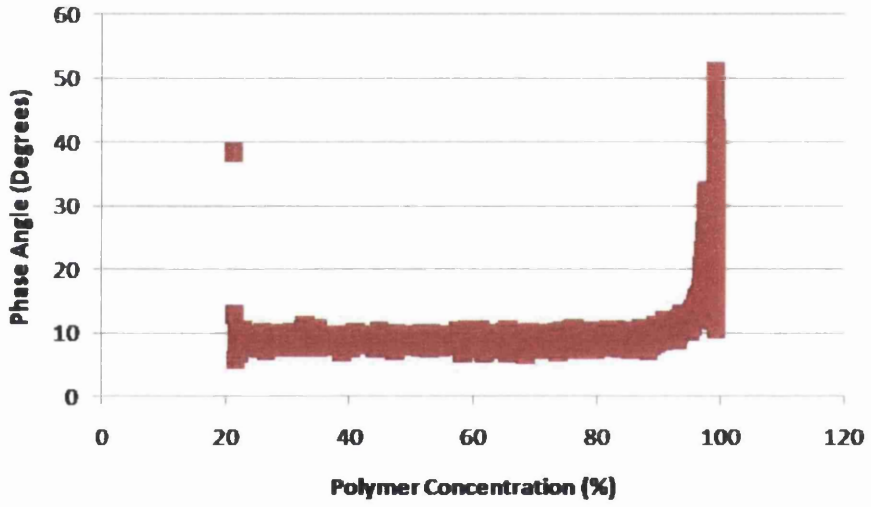


Figure A.34: Phase Angle of 20% Polyamide Resin Ink over Drying Period.

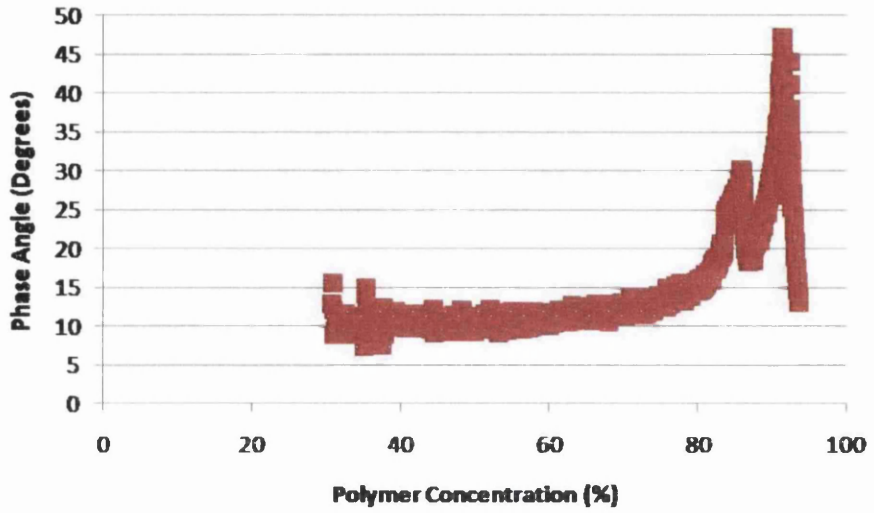


Figure A.35: Phase Angle of 30% Polyamide Resin Ink over Drying Period.

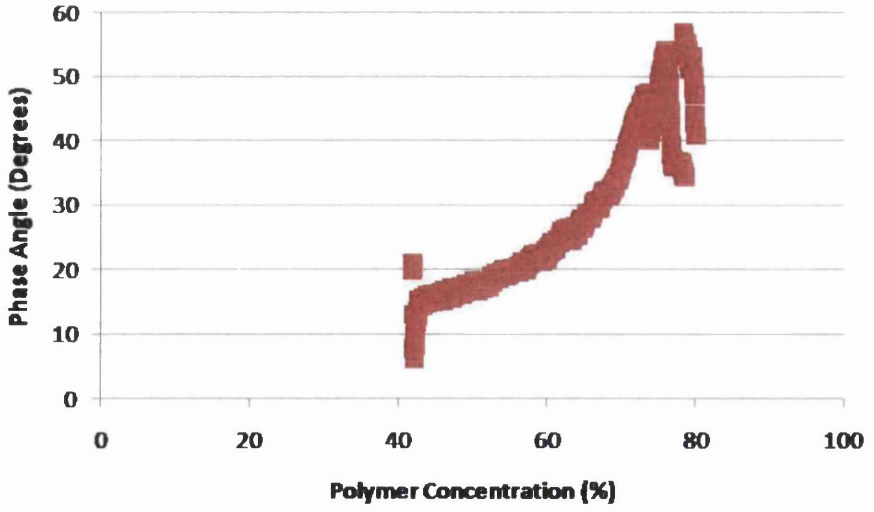


Figure A.36: Phase Angle of 40% Polyamide Resin Ink over Drying Period.

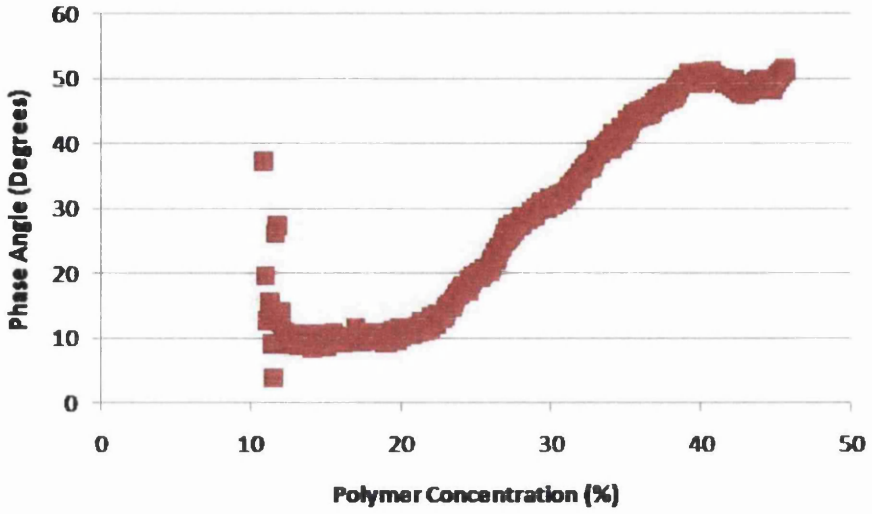


Figure A.37: Phase Angle of 10% Nitrocellulose Resin Ink over Drying Period.

The surface rheology results using a Dunouy ring of the nitrocellulose-based system are plotted.

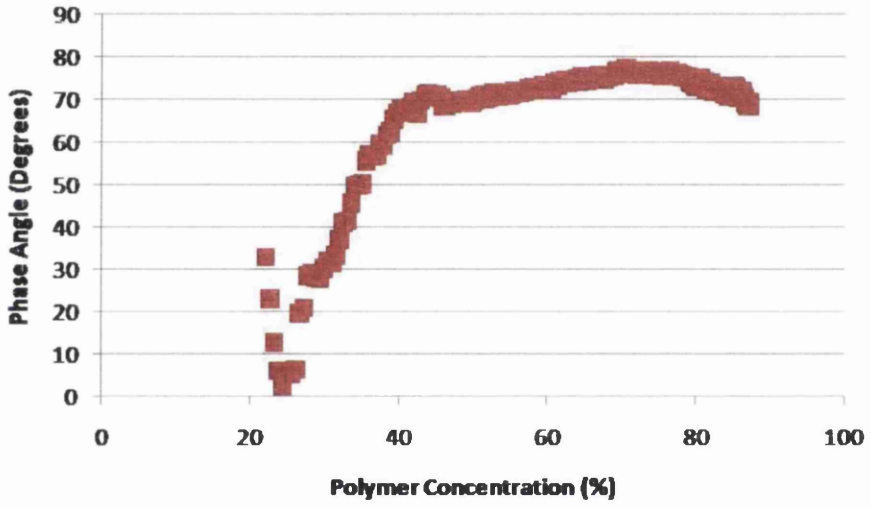


Figure A.38: Phase Angle of 20% Nitrocellulose Resin Ink over Drying Period.

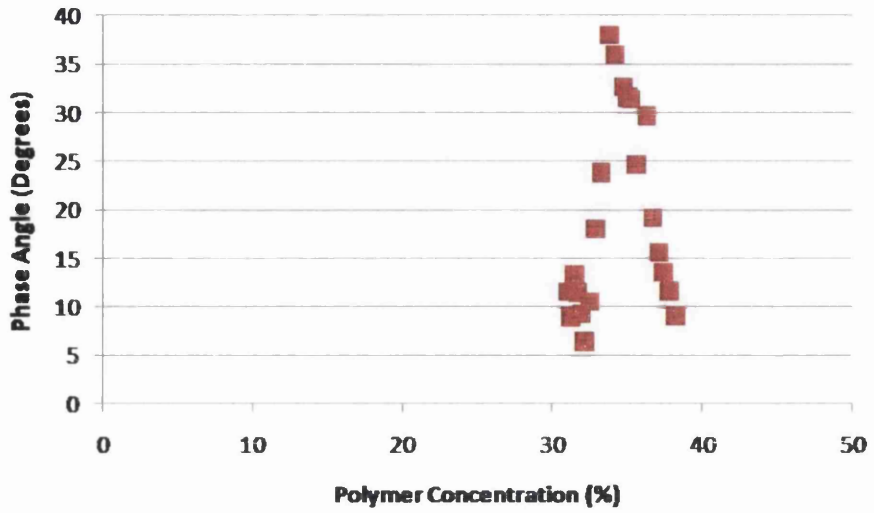


Figure A.39: Phase Angle of 30% Nitrocellulose Resin Ink over Drying Period.

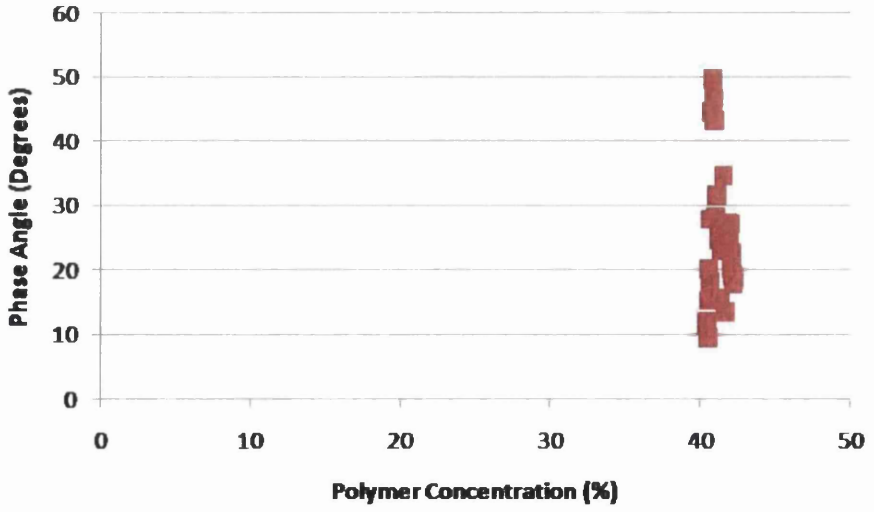


Figure A.40: Phase Angle of 40% Nitrocellulose Resin Ink over Drying Period.

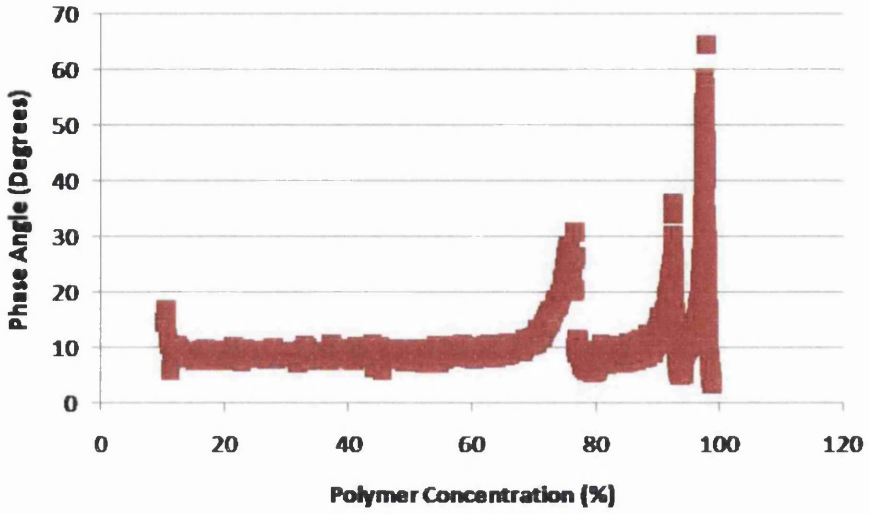


Figure A.41: Phase Angle of 10% Polyamide Resin Ink with Solid Content over Drying Period.

The surface rheology results using a Dunouy ring of the polyamide-based system with the addition of solid content are plotted.

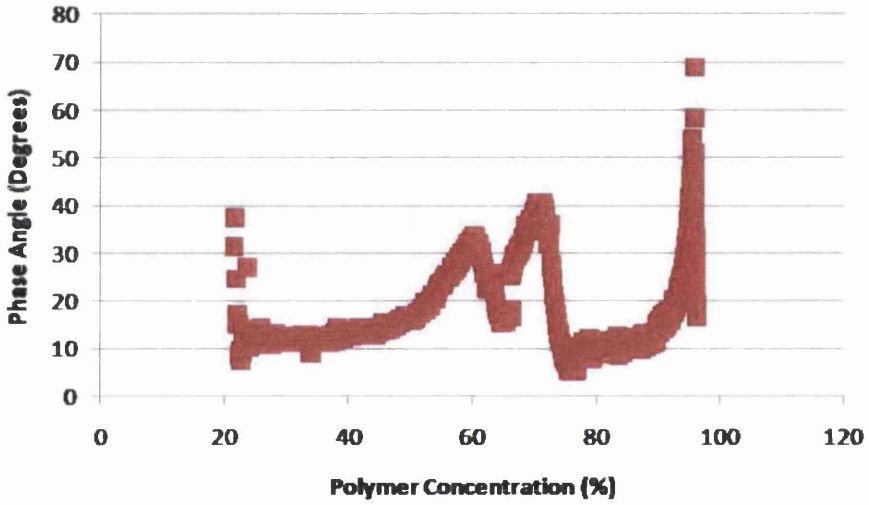


Figure A.42: Phase Angle of 20% Polyamide Resin Ink with Solid Content over Drying Period.

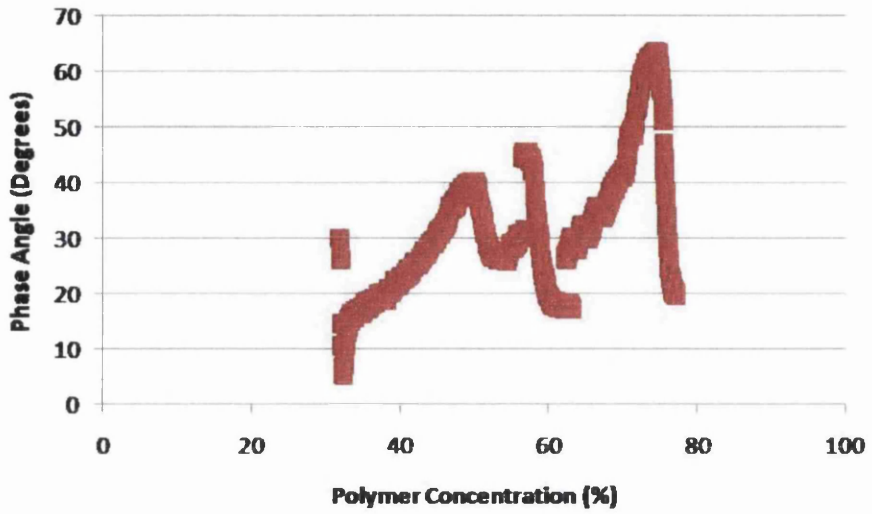


Figure A.43: Phase Angle of 30% Polyamide Resin Ink with Solid Content over Drying Period.

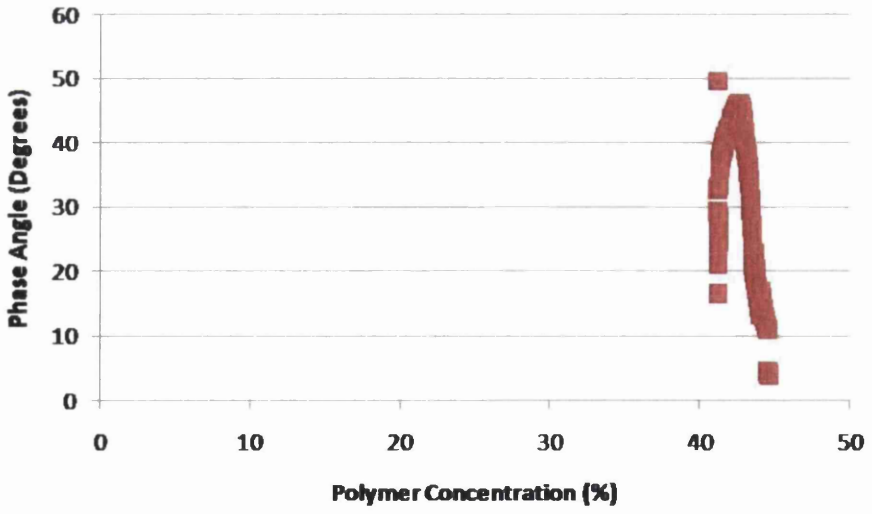


Figure A.44: Phase Angle of 40% Polyamide Resin Ink with Solid Content over Drying Period.

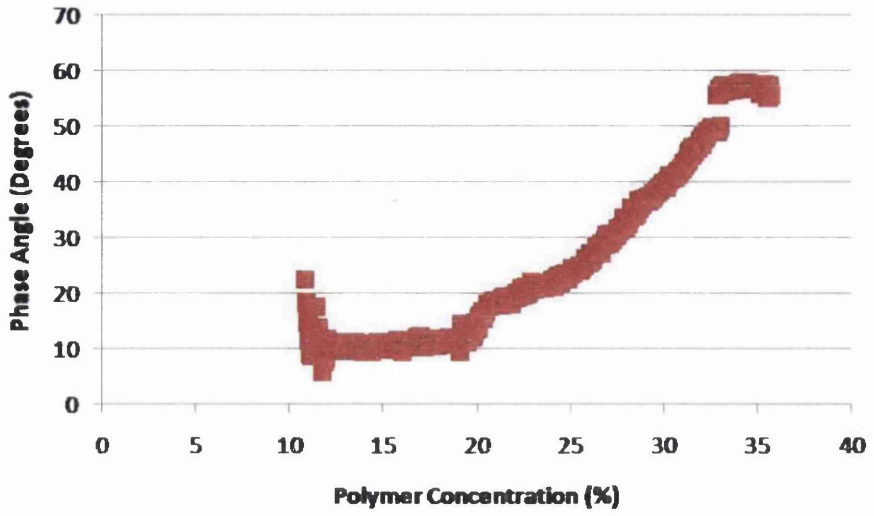


Figure A.45: Phase Angle of 10% Nitrocellulose Resin Ink with Solid Content over Drying Period.

The surface rheology results using a Dunouy ring of the nitrocellulose-based system with the addition of solid content are plotted.

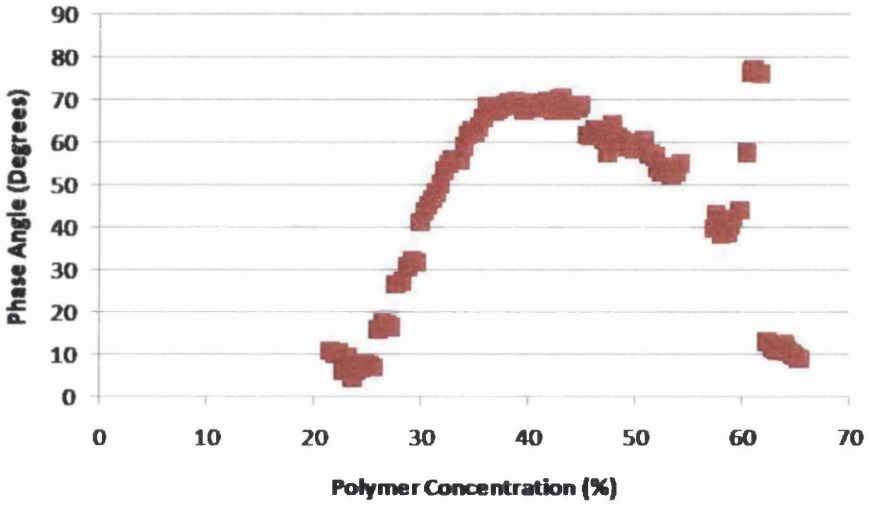


Figure A.46: Phase Angle of 20% Nitrocellulose Resin Ink with Solid Content over Drying Period.

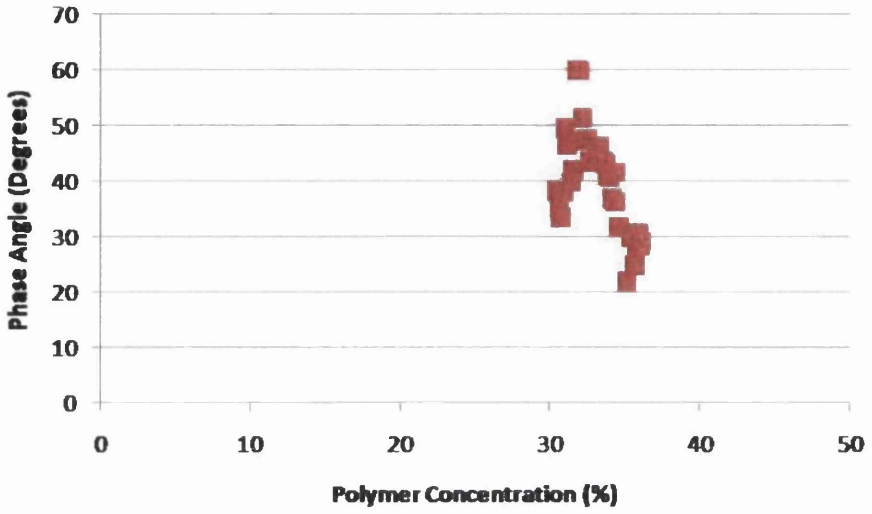


Figure A.47: Phase Angle of 30% Nitrocellulose Resin Ink with Solid Content over Drying Period.

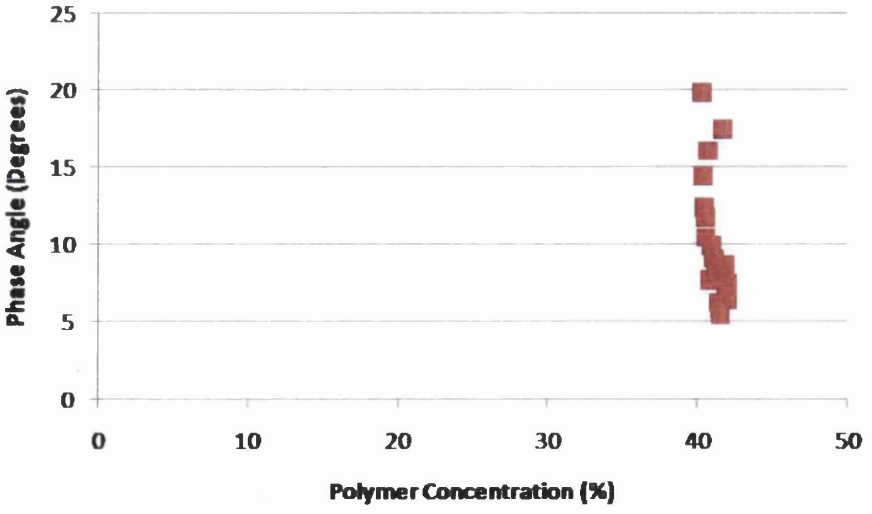


Figure A.48: Phase Angle of 40% Nitrocellulose Resin Ink with Solid Content over Drying Period.

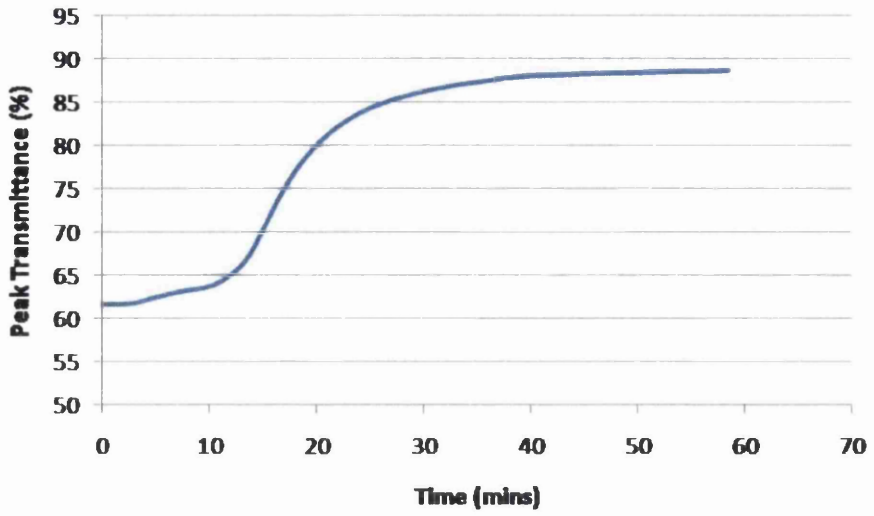


Figure A.49: Transmission Peak over Time for 10% Polyamide Resin Ink.

The FTIR results of the polyamide-based system are plotted.

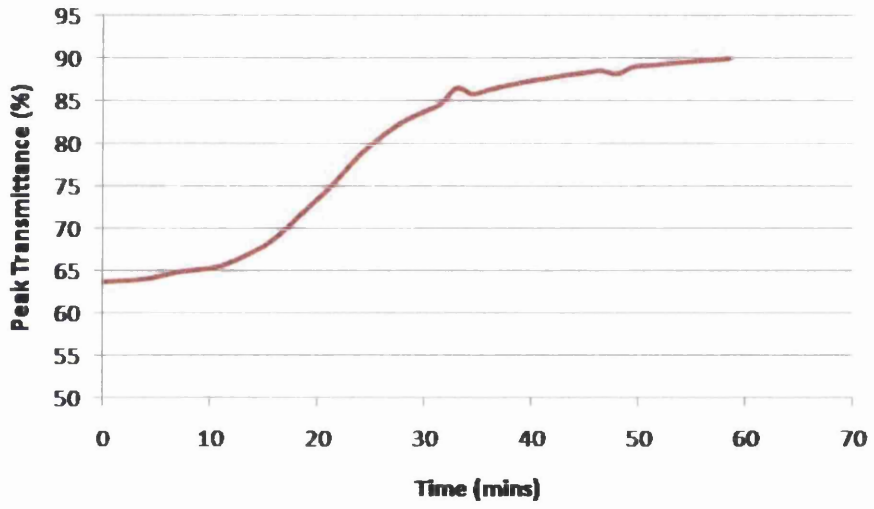


Figure A.50: Transmission Peak over Time for 20% Polyamide Resin Ink.

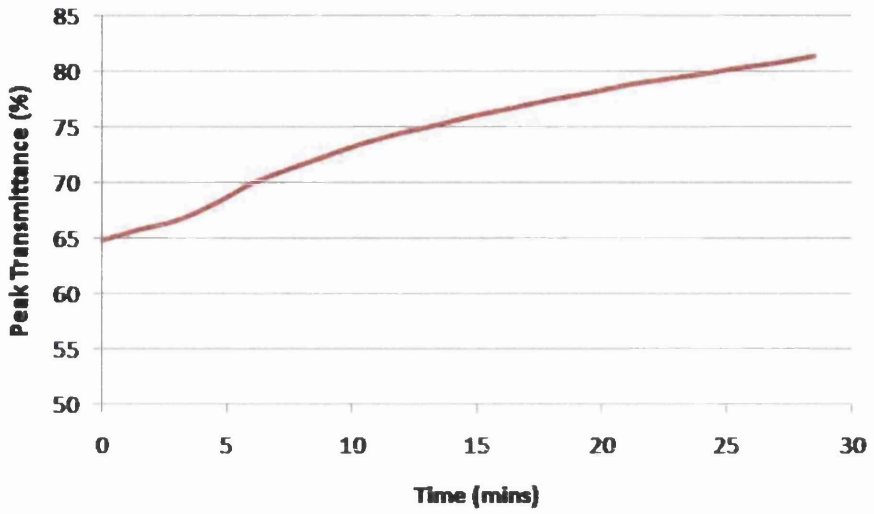


Figure A.51: Transmission Peak over Time for 30% Polyamide Resin Ink.

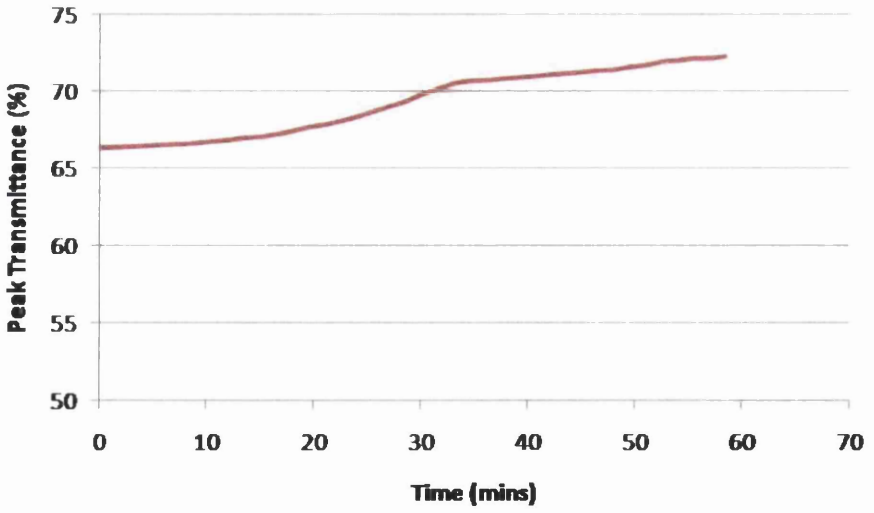


Figure A.52: Transmission Peak over Time for 40% Polyamide Resin Ink.

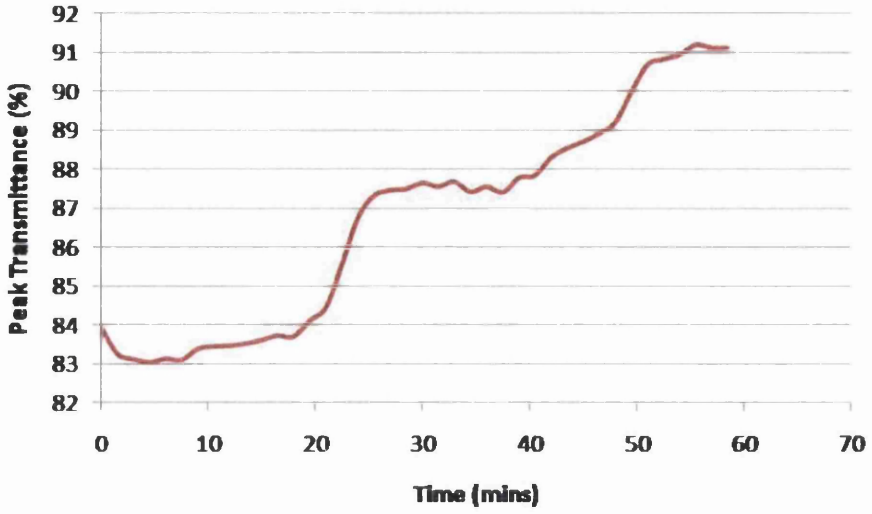


Figure A.53: Transmission Peak for IPA over Time for 10% Nitrocellulose Resin Ink.

The FTIR results of Isopropanol within the nitrocellulose-based system are plotted.

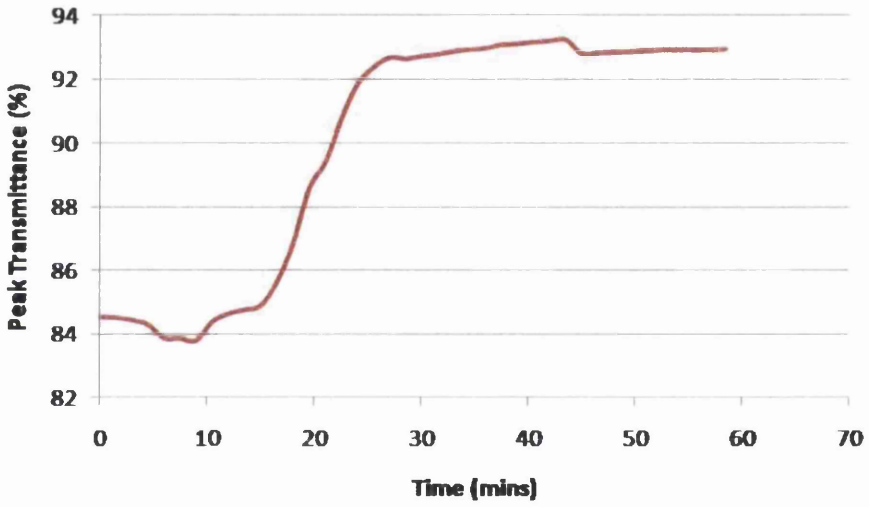


Figure A.54: Transmission Peak for IPA over Time for 20% Nitrocellulose Resin Ink.

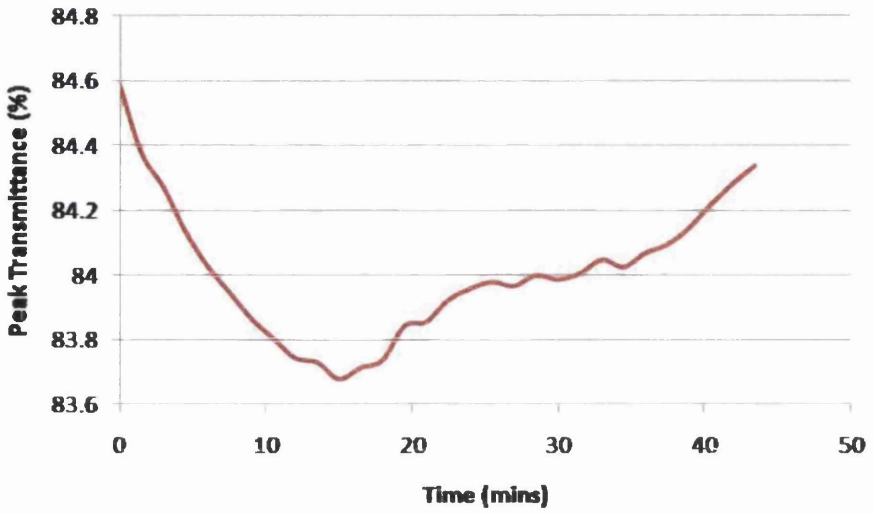


Figure A.55: Transmission Peak for IPA over Time for 30% Nitrocellulose Resin Ink.

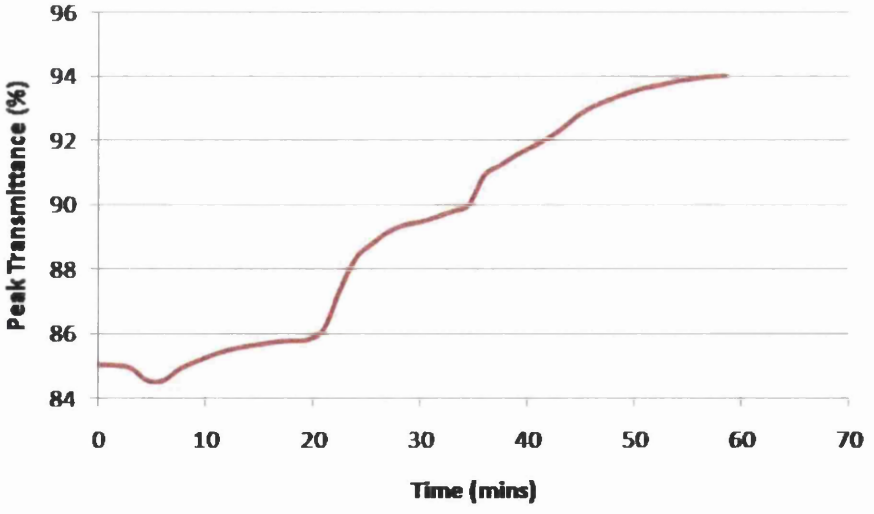


Figure A.56: Transmission Peak for IPA over Time for 40% Nitrocellulose Resin Ink.

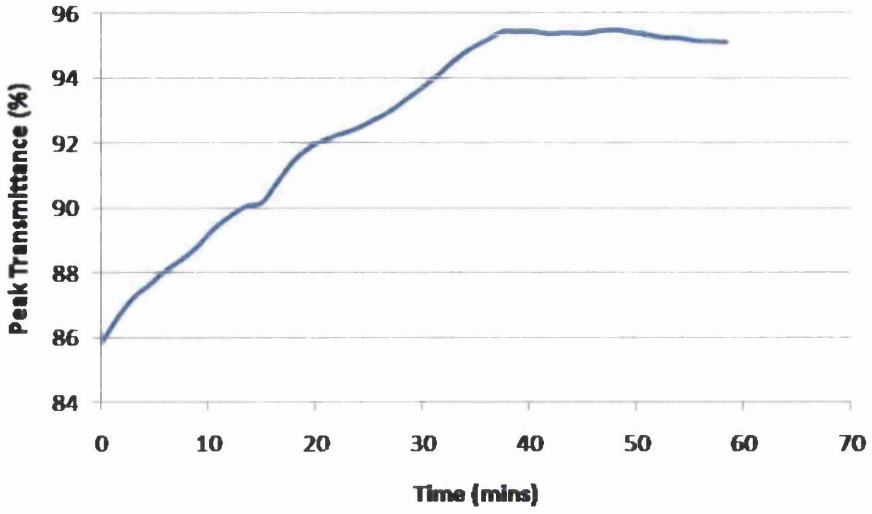


Figure A.57: Transmission Peak for EA over Time for 10% Nitrocellulose Resin Ink.

The FTIR results of Ethyl Acetate within the nitrocellulose-based system are plotted.

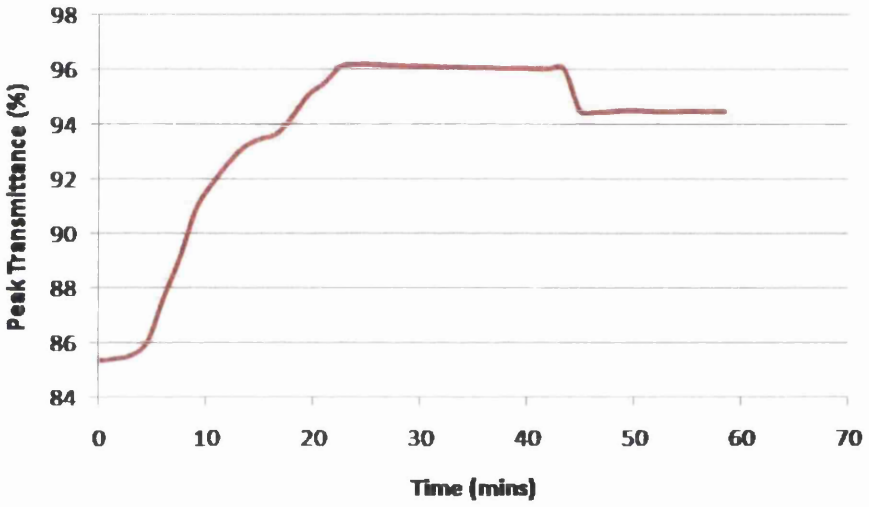


Figure A.58: Transmission Peak for EA over Time for 20% Nitrocellulose Resin Ink.

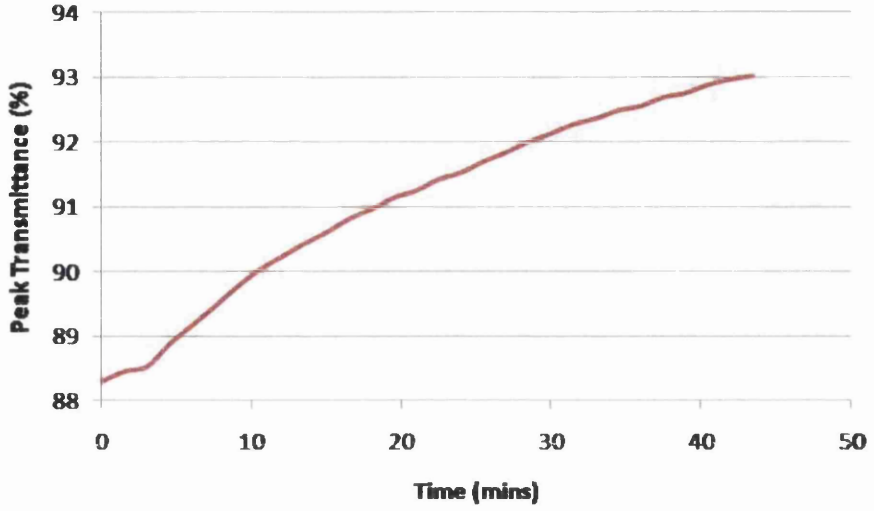


Figure A.59: Transmission Peak for EA over Time for 30% Nitrocellulose Resin Ink.

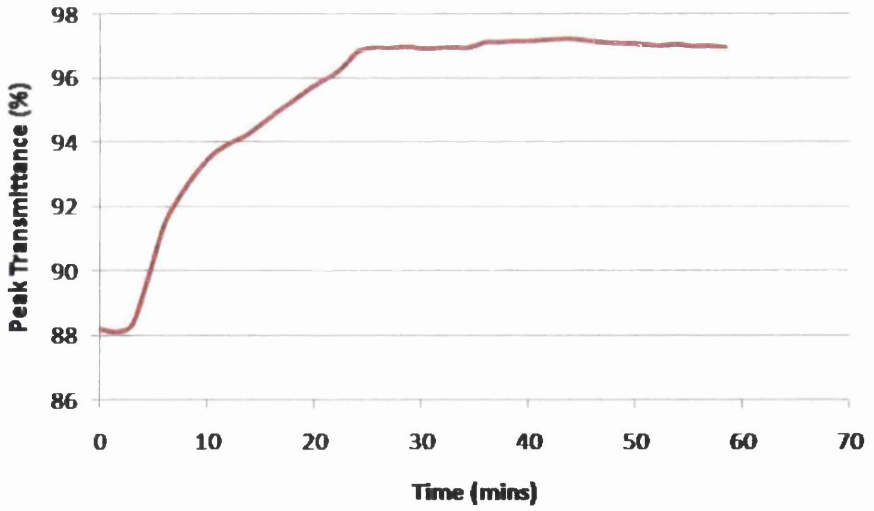


Figure A.60: Transmission Peak for EA over Time for 40% Nitrocellulose Resin Ink.

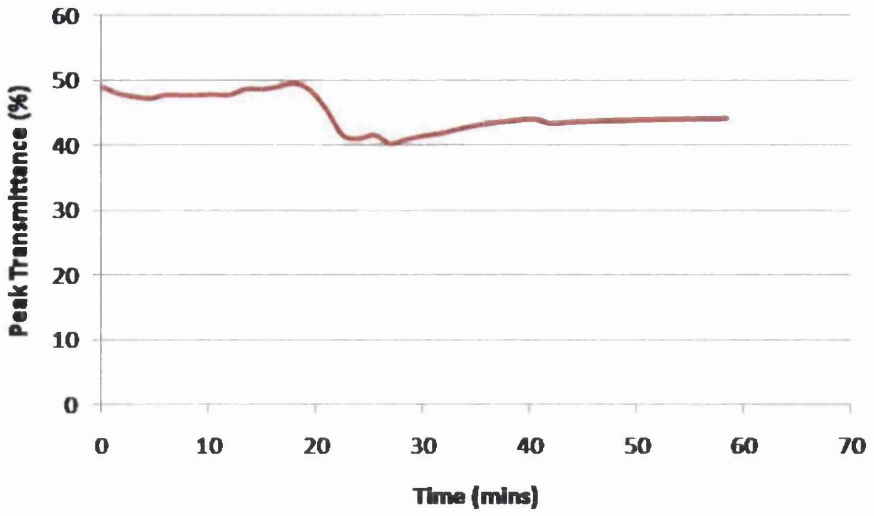


Figure A.61: Transmission Peak over Time for 10% Polyamide Resin Ink with Solid Content.

The FTIR results of the polyamide-based system with the addition of solid content are plotted.

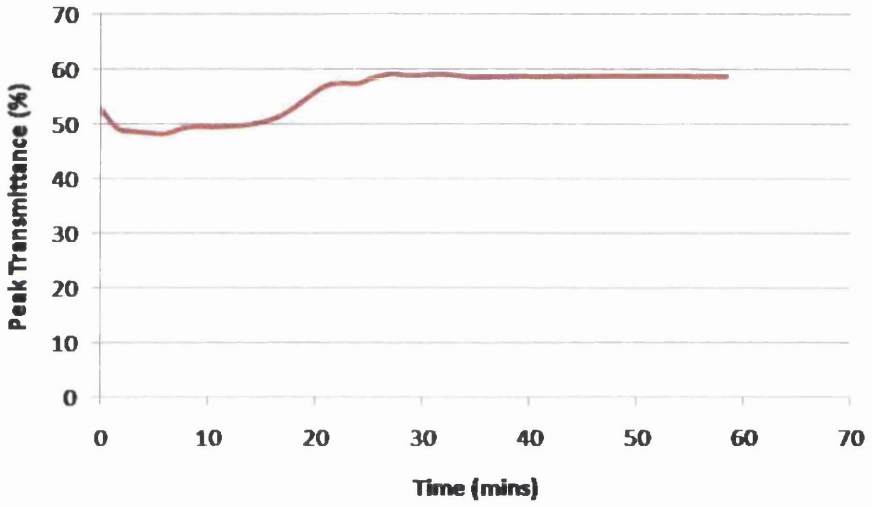


Figure A.62: Transmission Peak over Time for 20% Polyamide Resin Ink with Solid Content.

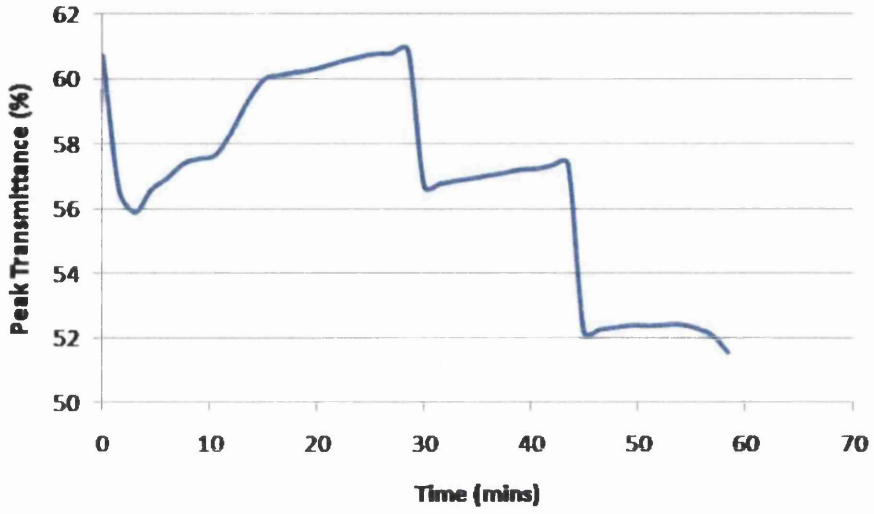


Figure A.63: Transmission Peak over Time for 30% Polyamide Resin Ink with Solid Content.

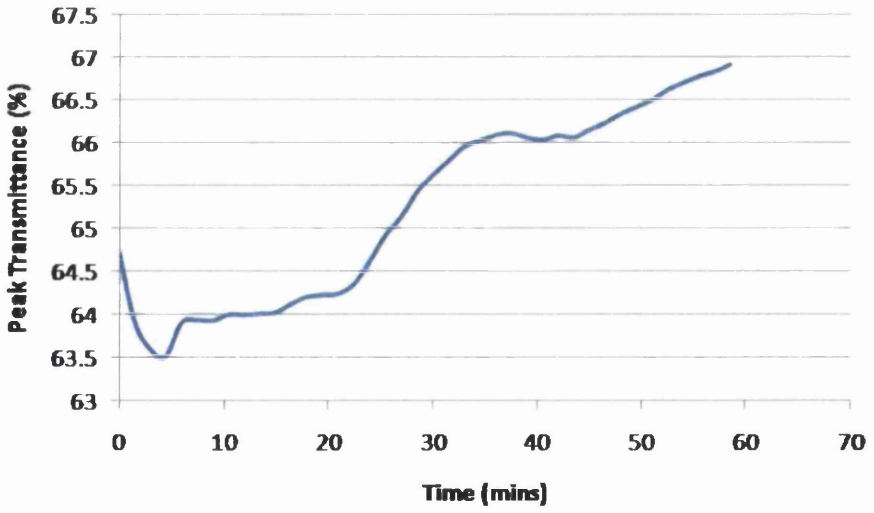


Figure A.64: Transmission Peak over Time for 40% Polyamide Resin Ink with Solid Content.

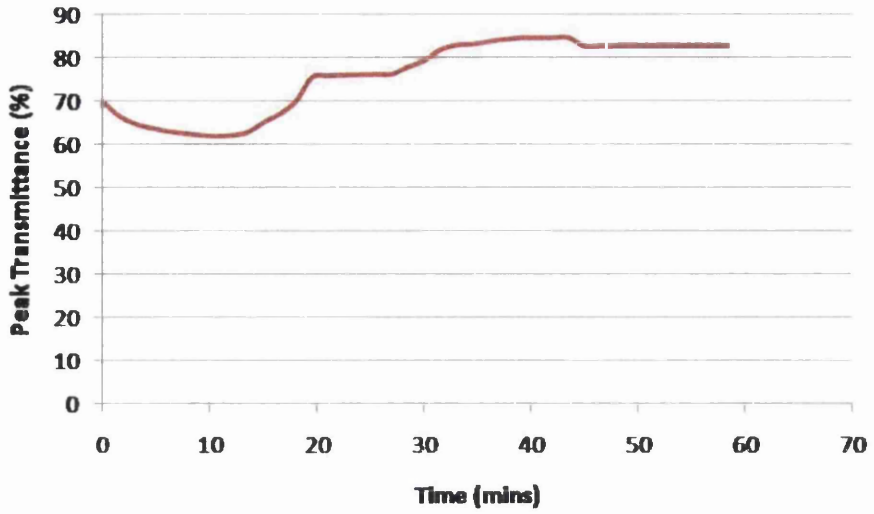


Figure A.65: Transmission Peak for IPA over Time for 10% Nitrocellulose Resin Ink with Solid Content.

The FTIR results of Isopropanol within the nitrocellulose-based system with the addition of solid content are plotted.

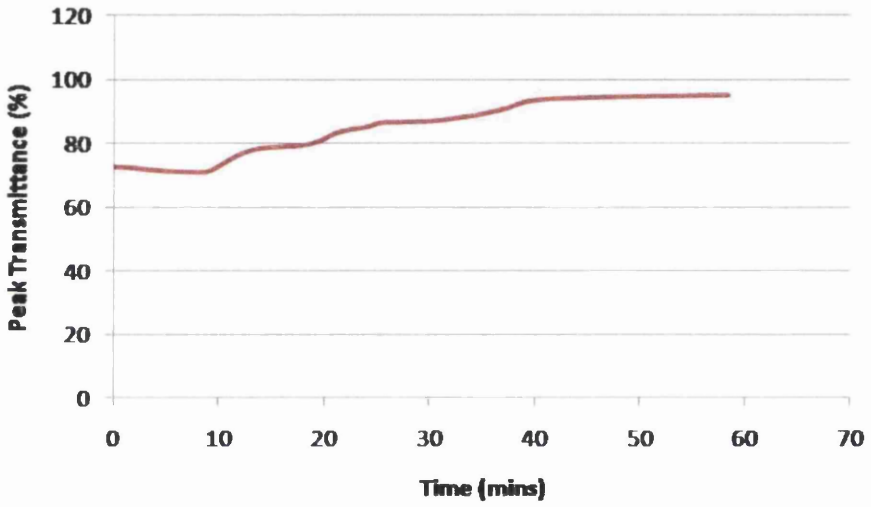


Figure A.66: Transmission Peak for IPA over Time for 20% Nitrocellulose Resin Ink with Solid Content.

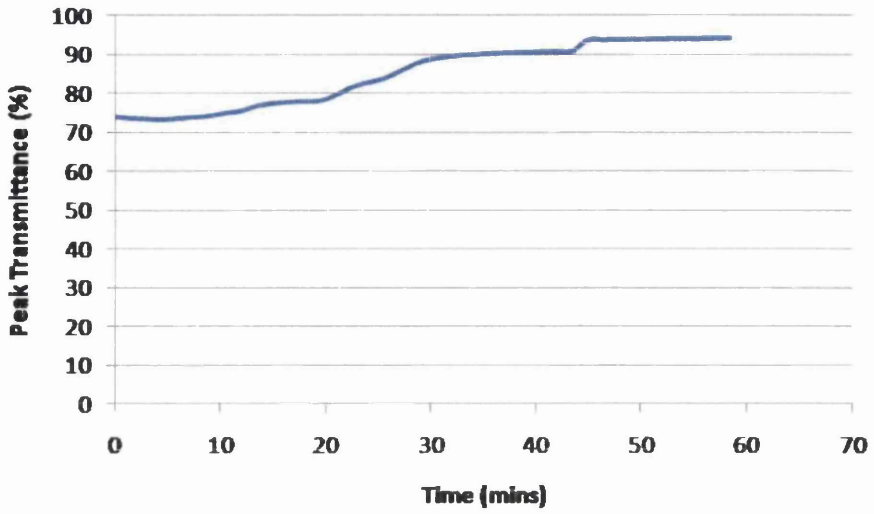


Figure A.67: Transmission Peak for IPA over Time for 30% Nitrocellulose Resin Ink with Solid Content.

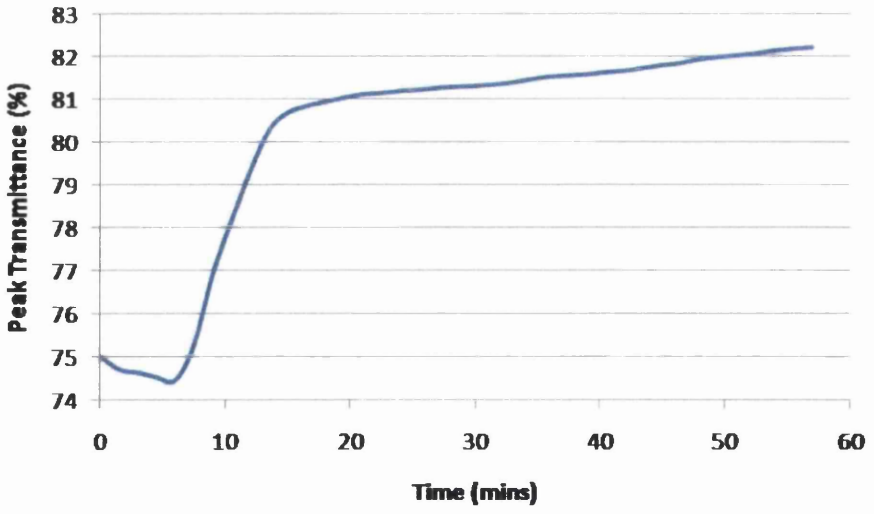


Figure A.68: Transmission Peak for IPA over Time for 40% Nitrocellulose Resin Ink with Solid Content.

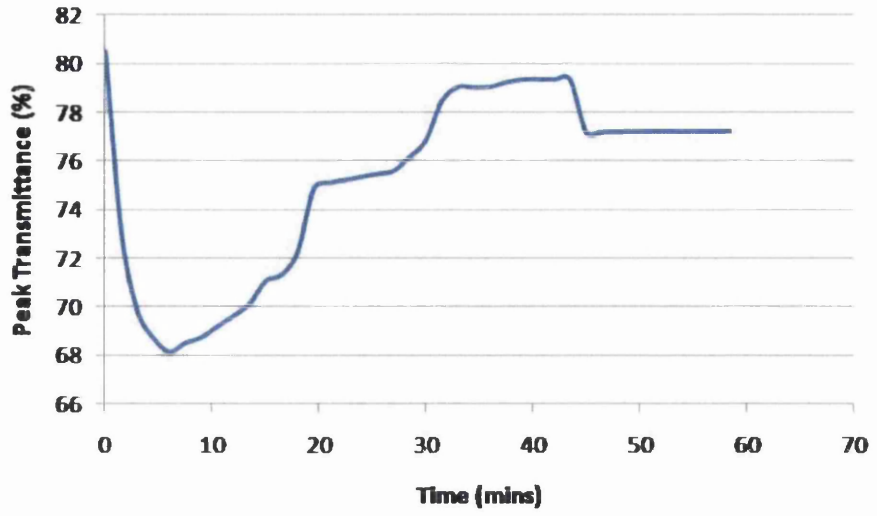


Figure A.69: Transmission Peak for EA over Time for 10% Nitrocellulose Resin Ink with Solid Content.

The FTIR results of Ethyl Acetate within the nitrocellulose-based system with the addition of solid content are plotted.

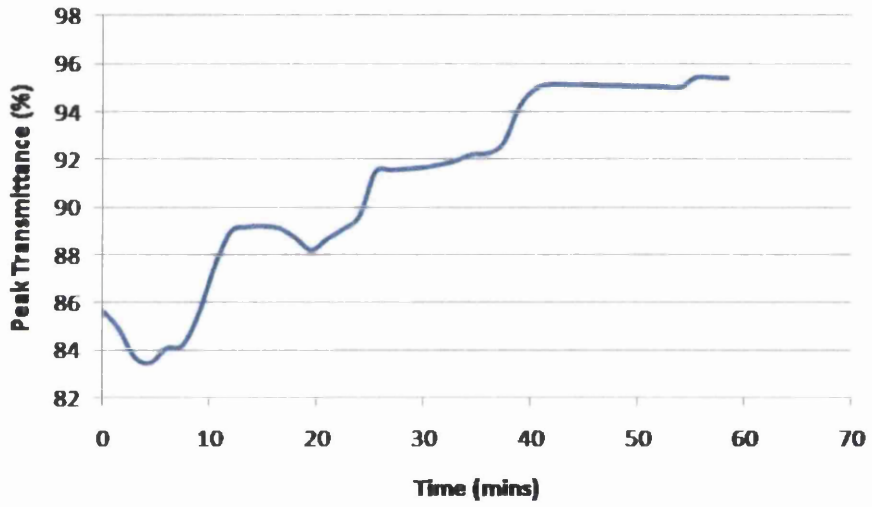


Figure A.70: Transmission Peak for EA over Time for 20% Nitrocellulose Resin Ink with Solid Content.

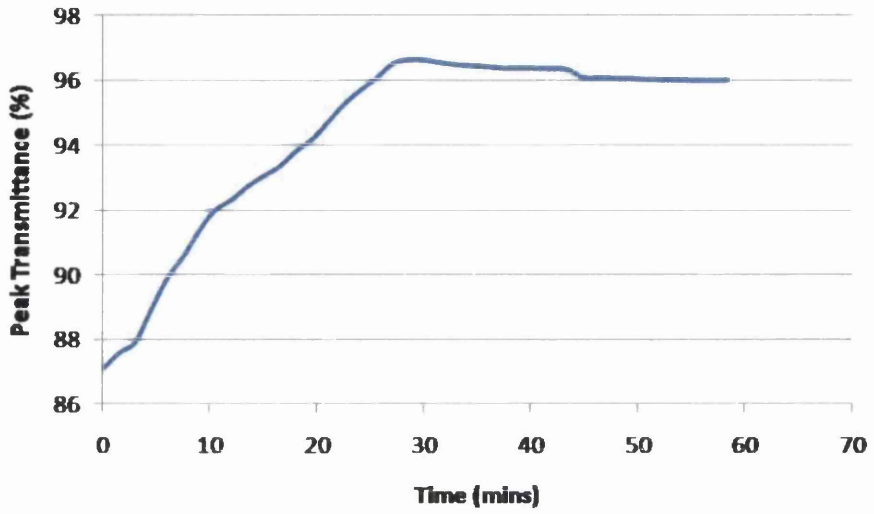


Figure A.71: Transmission Peak for EA over Time for 30% Nitrocellulose Resin Ink with Solid Content.

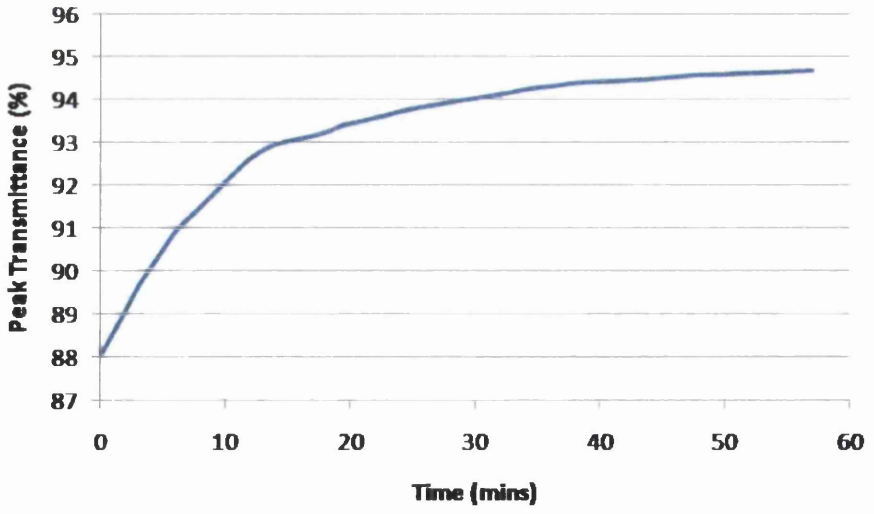


Figure A.72: Transmission Peak for EA over Time for 40% Nitrocellulose Resin Ink with Solid Content.

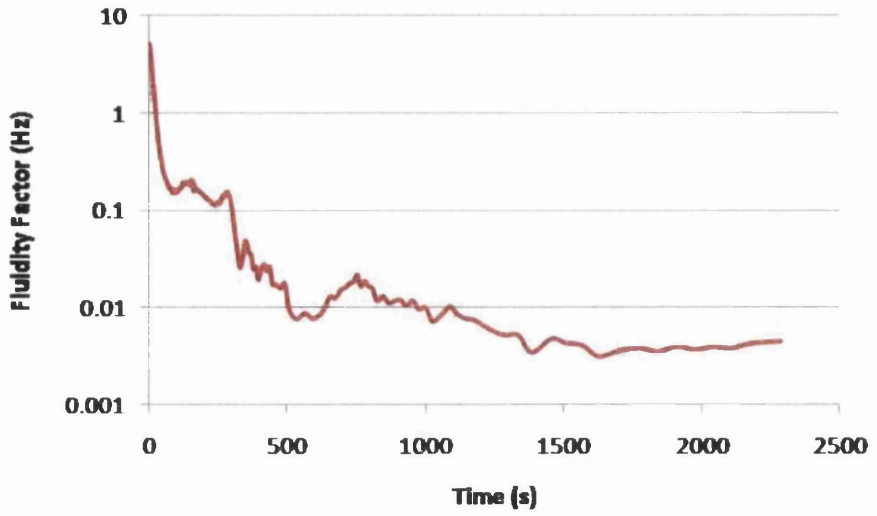


Figure A.73: Fluidity Factor with Time for 10% Polyamide Resin Ink.

The MS-DWS results of the polyamide-based system are plotted.

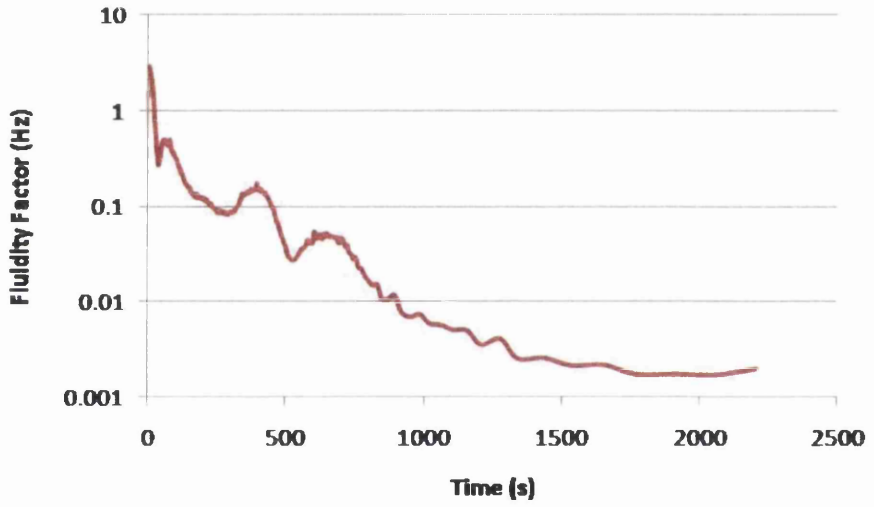


Figure A.74: Fluidity Factor with Time for 20% Polyamide Resin Ink.

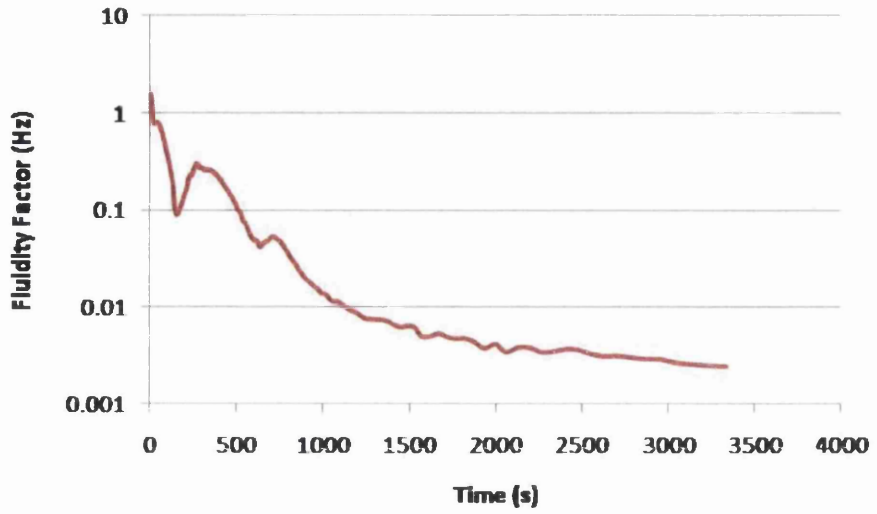


Figure A.75: Fluidity Factor with Time for 30% Polyamide Resin Ink.

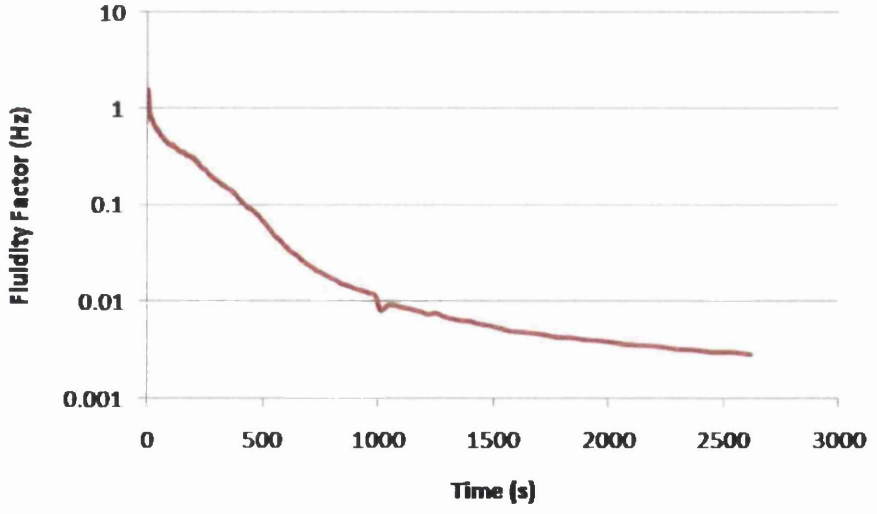


Figure A.76: Fluidity Factor with Time for 40% Polyamide Resin Ink.

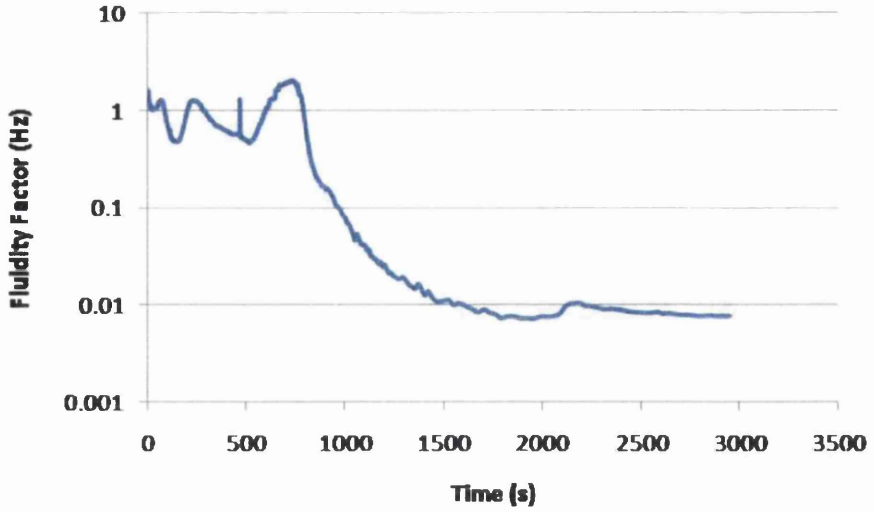


Figure A.77: Fluidity Factor with Time for 10% Nitrocellulose Resin Ink.

The MS-DWS results of the nitrocellulose-based system are plotted.

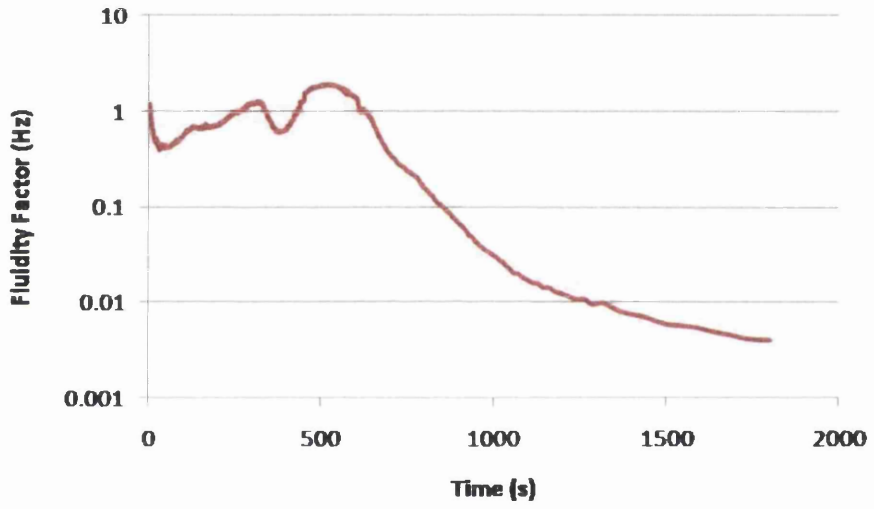


Figure A.78: Fluidity Factor with Time for 20% Nitrocellulose Resin Ink.

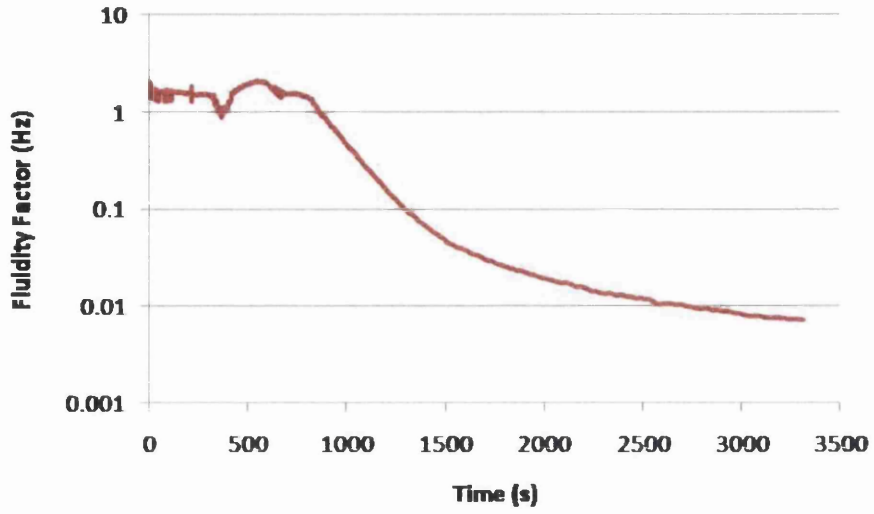


Figure A.79: Fluidity Factor with Time for 30% Nitrocellulose Resin Ink.

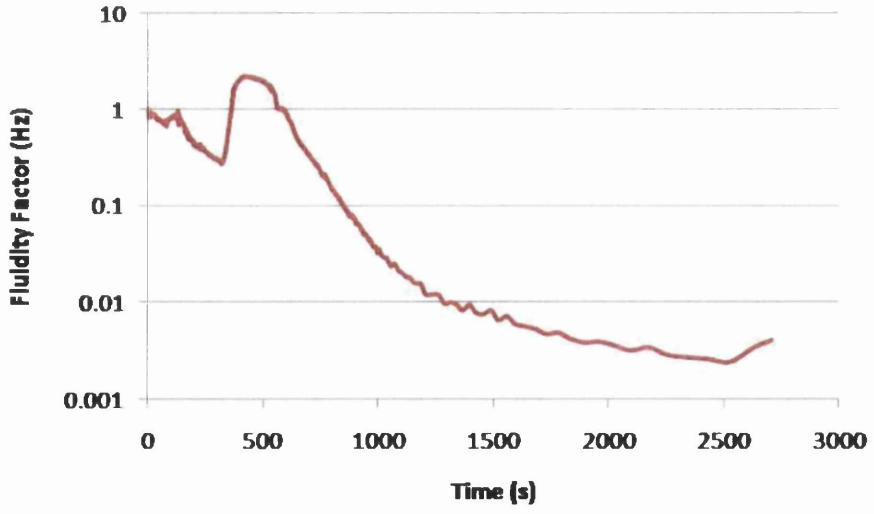


Figure A.80: Fluidity Factor with Time for 40% Nitrocellulose Resin Ink.

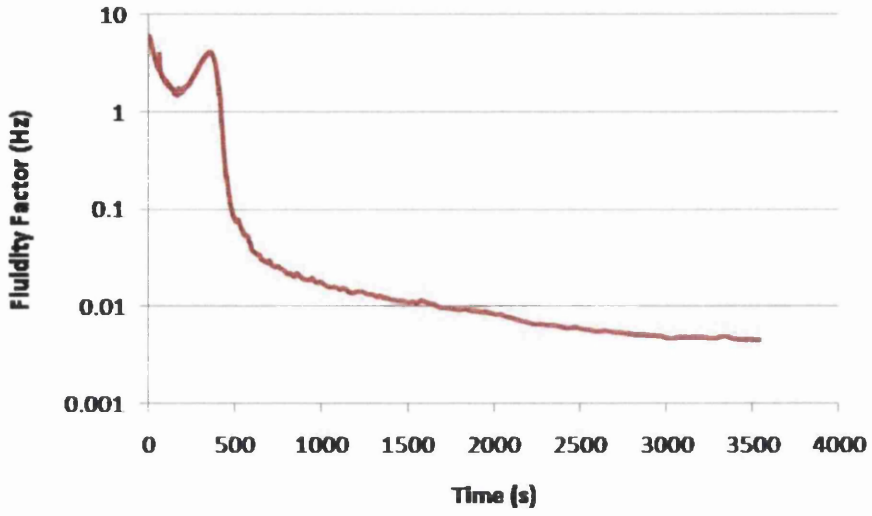


Figure A.81: Fluidity Factor with Time for 10% Polyamide Resin Ink with Solid Content.

The MS-DWS results of the polyamide-based system with the addition of solid content are plotted.

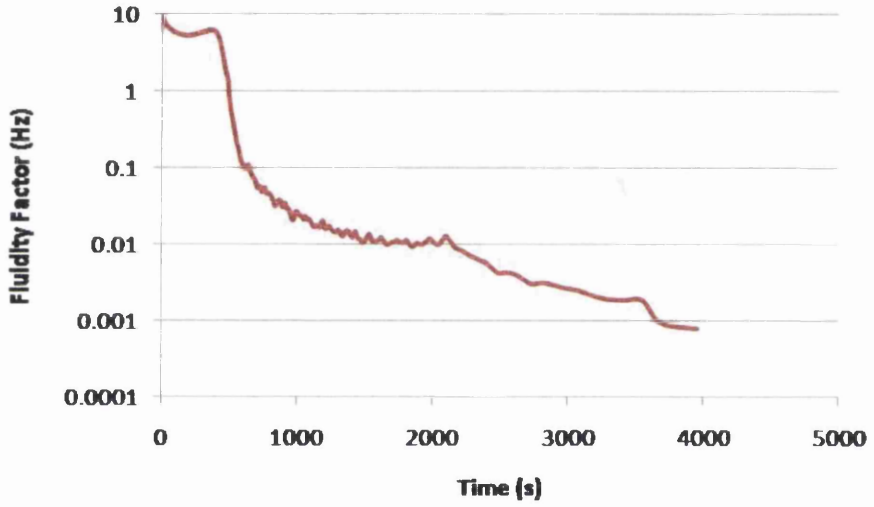


Figure A.82: Fluidity Factor with Time for 20% Polyamide Resin Ink with Solid Content.

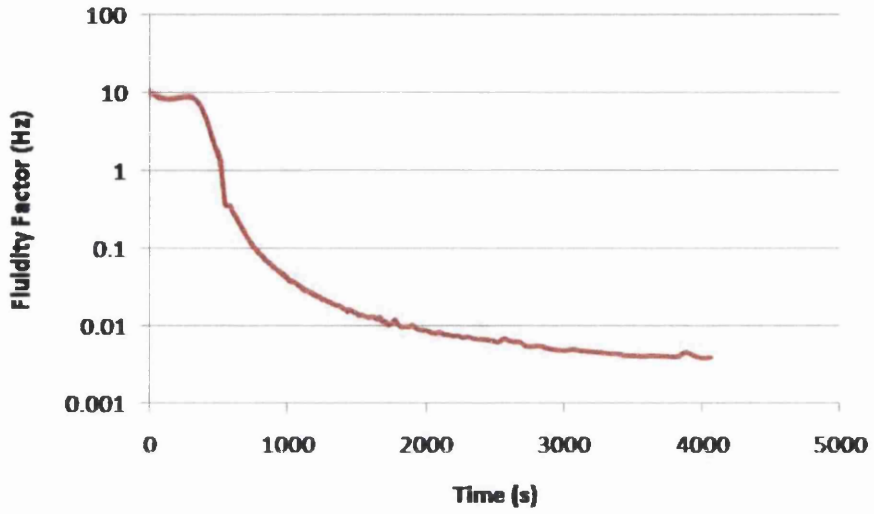


Figure A.83: Fluidity Factor with Time for 30% Polyamide Resin Ink with Solid Content.

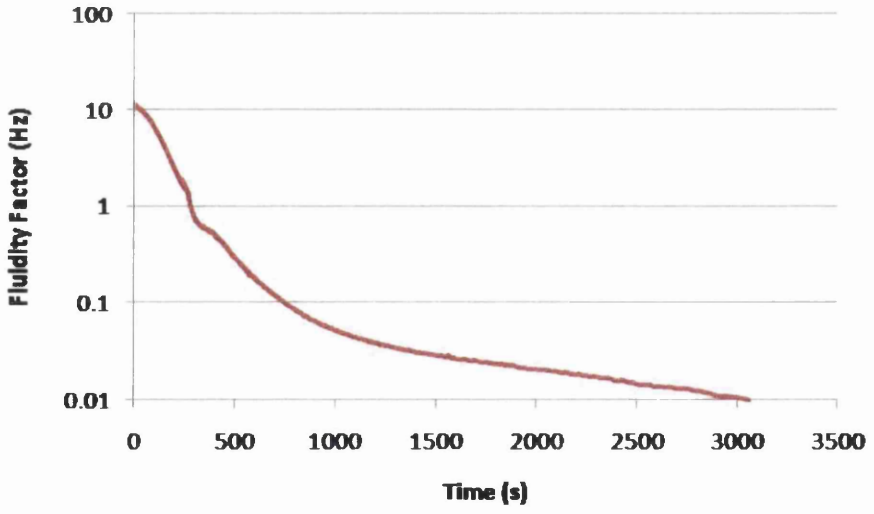


Figure A.84: Fluidity Factor with Time for 40% Polyamide Resin Ink with Solid Content.

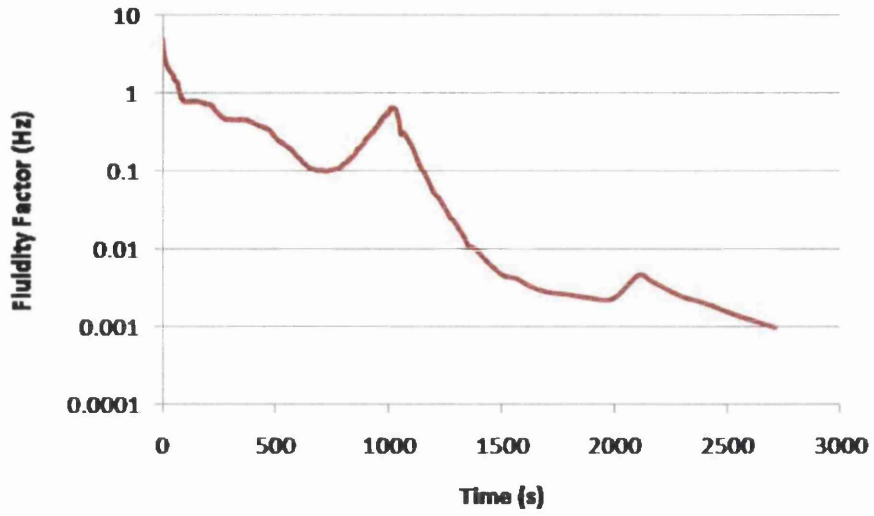


Figure A.85: Fluidity Factor with Time for 10% Nitrocellulose Resin Ink with Solid Content.

The MS-DWS results of the nitrocellulose-based system with the addition of solid content are plotted.

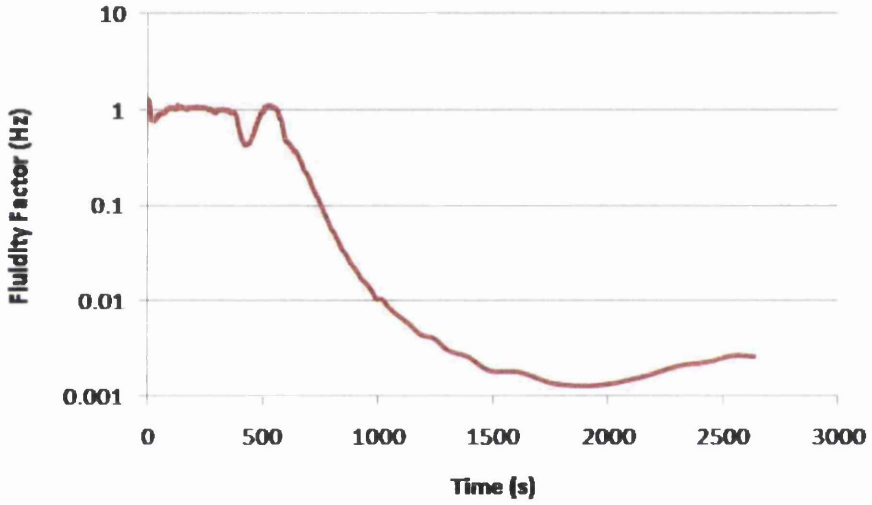


Figure A.86: Fluidity Factor with Time for 20% Nitrocellulose Resin Ink with Solid Content.

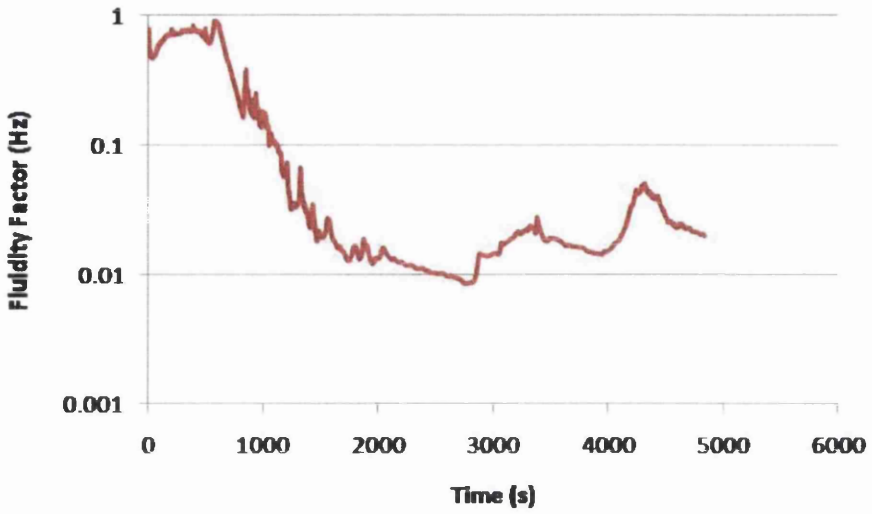


Figure A.87: Fluidity Factor with Time for 30% Nitrocellulose Resin Ink with Solid Content.

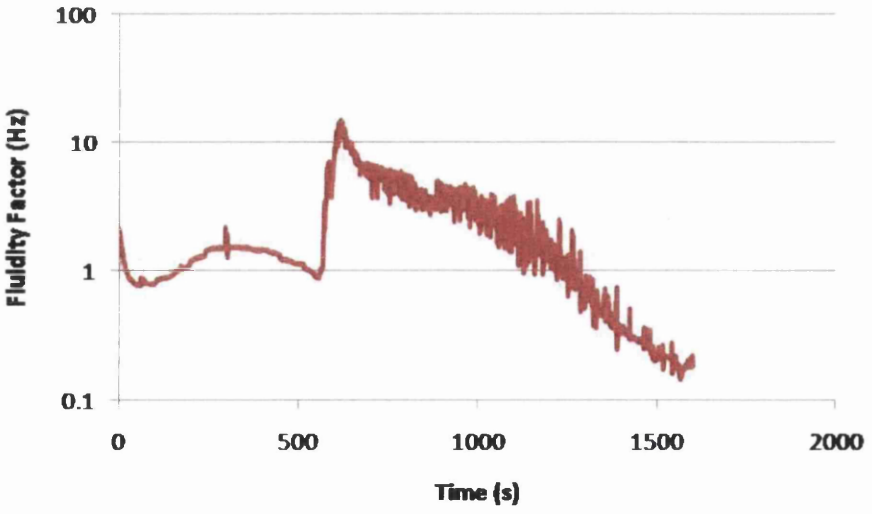


Figure A.88: Fluidity Factor with Time for 40% Nitrocellulose Resin Ink with Solid Content.

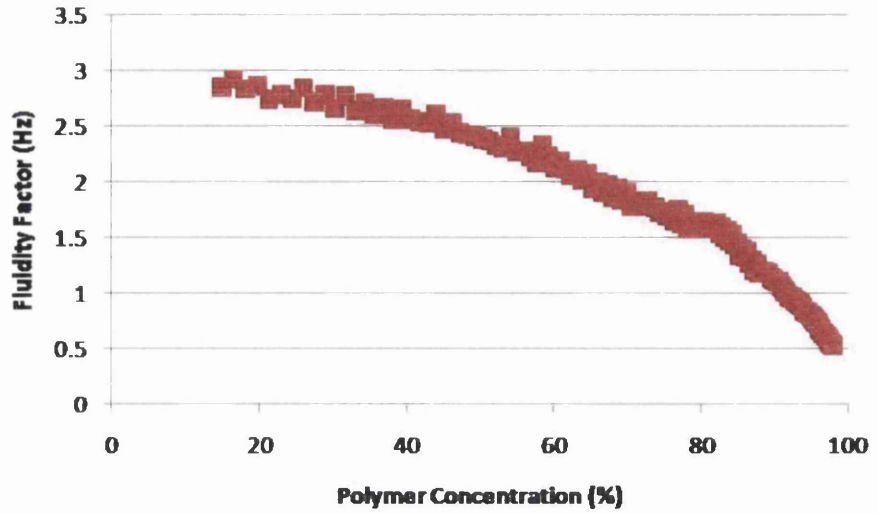


Figure A.89: Fluidity Factor with Polymer Concentration for 10% Polyamide Resin Ink.

The MS-DWS results of the polyamide-based system are plotted against polymer concentration.

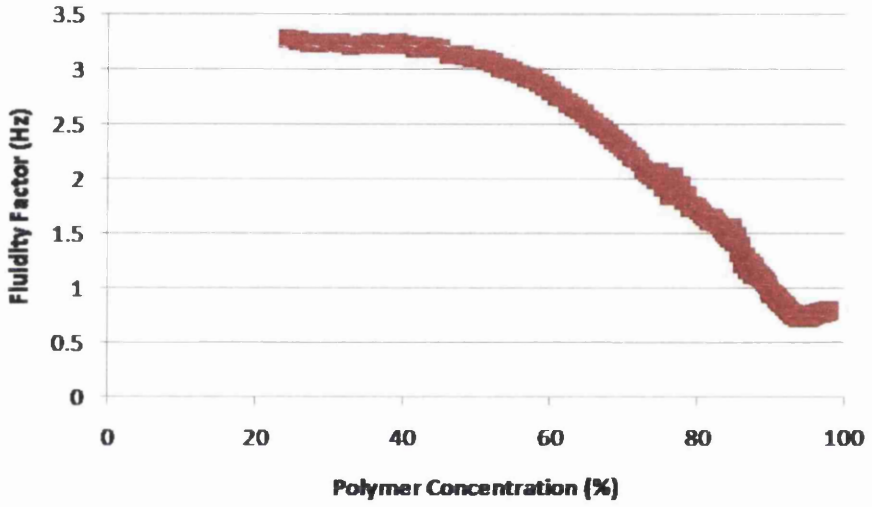


Figure A.90: Fluidity Factor with Polymer Concentration for 20% Polyamide Resin Ink.

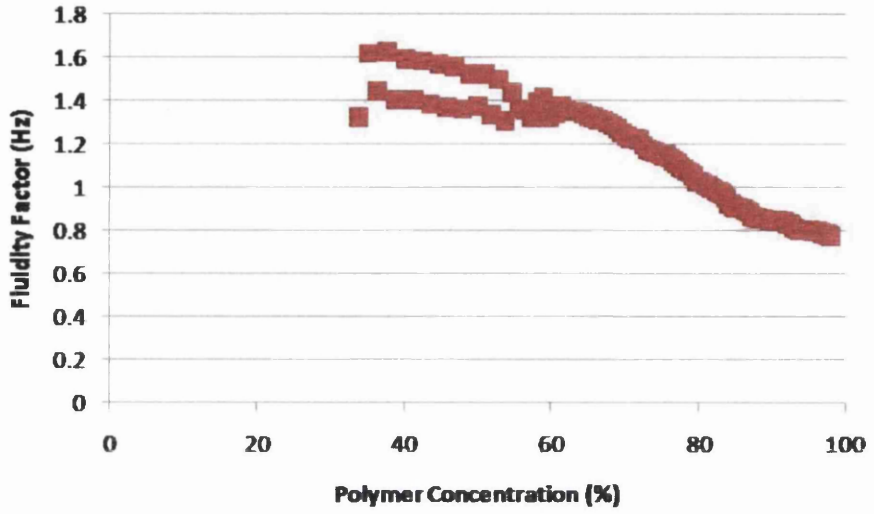


Figure A.91: Fluidity Factor with Polymer Concentration for 30% Polyamide Resin Ink.

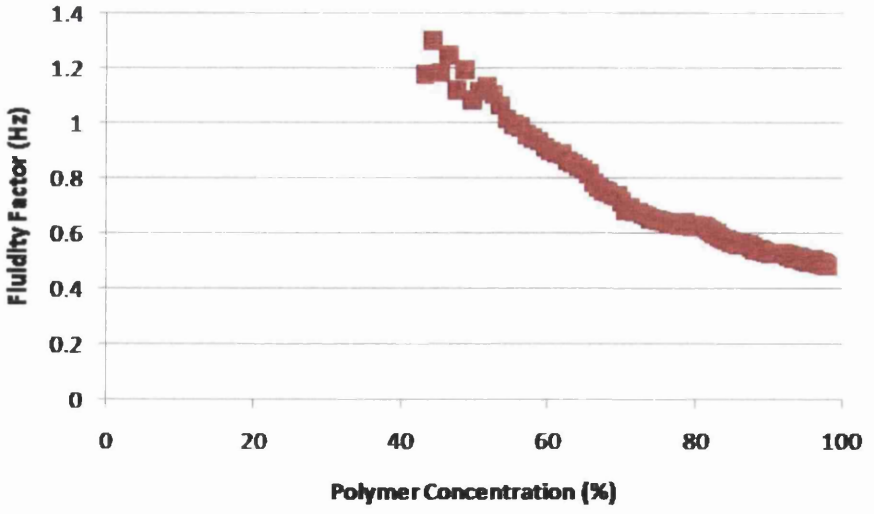


Figure A.92: Fluidity Factor with Polymer Concentration for 40% Polyamide Resin Ink.

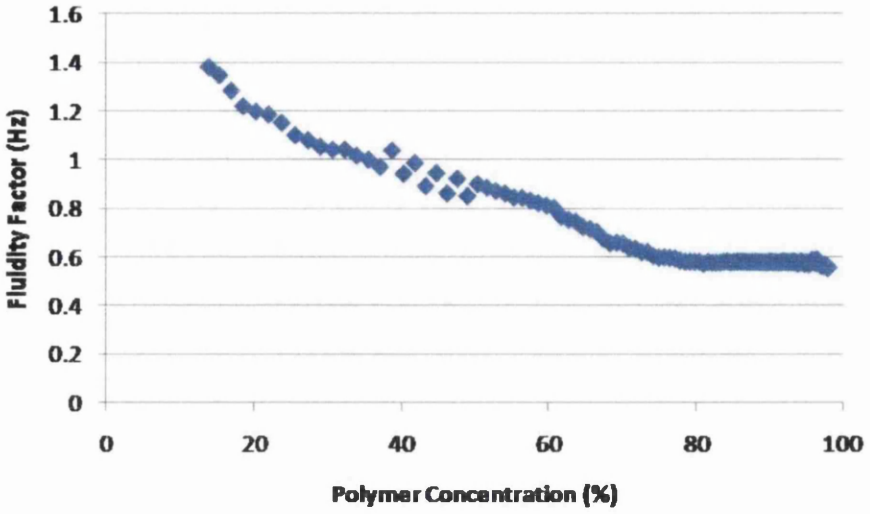


Figure A.93: Fluidity Factor with Polymer Concentration for 10% Nitrocellulose Resin Ink.

The MS-DWS results of the nitrocellulose-based system are plotted against polymer concentration.

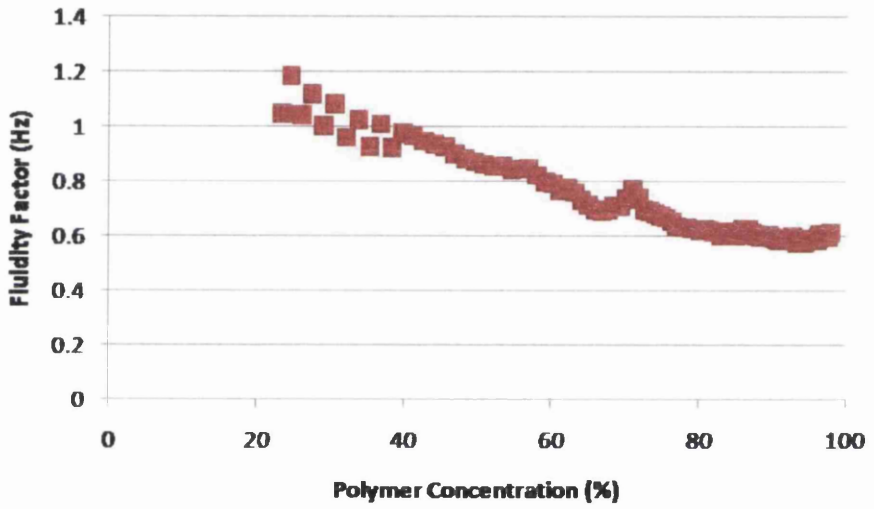


Figure A.94: Fluidity Factor with Polymer Concentration for 20% Nitrocellulose Resin Ink.

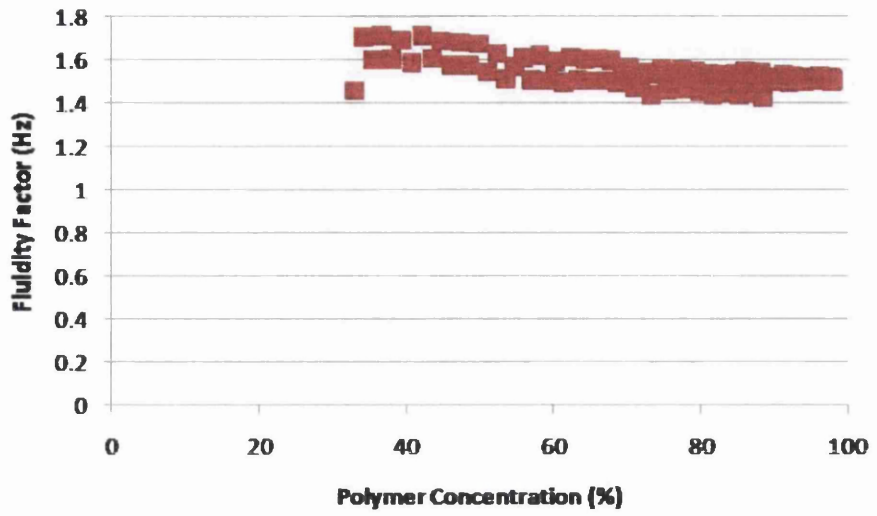


Figure A.95: Fluidity Factor with Polymer Concentration for 30% Nitrocellulose Resin Ink.

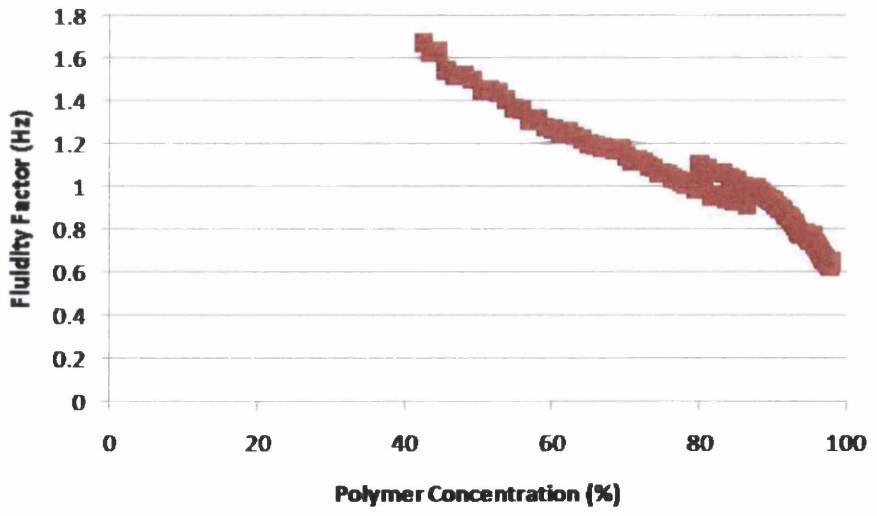


Figure A.96: Fluidity Factor with Polymer Concentration for 40% Nitrocellulose Resin Ink.

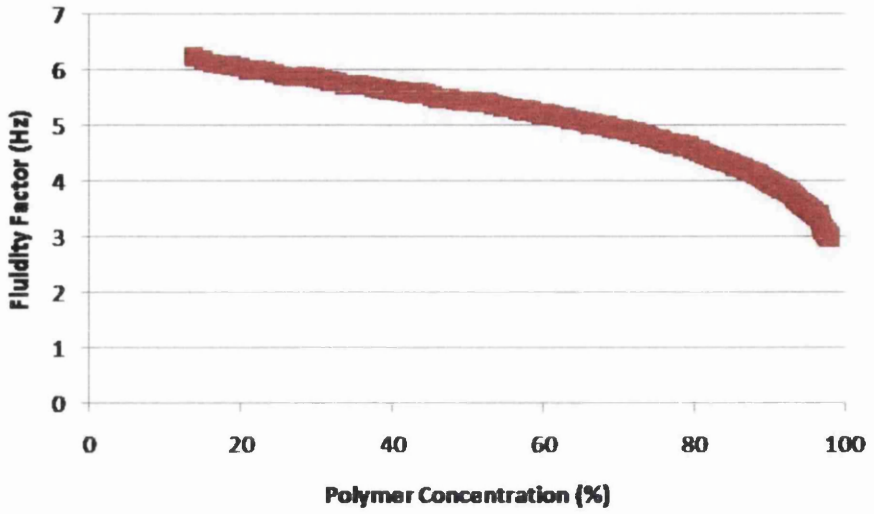


Figure A.97: Fluidity Factor with Polymer Concentration for 10% Polyamide Resin Ink with Solid Content.

The MS-DWS results of the polyamide-based system with the addition of solid content are plotted against polymer concentration.

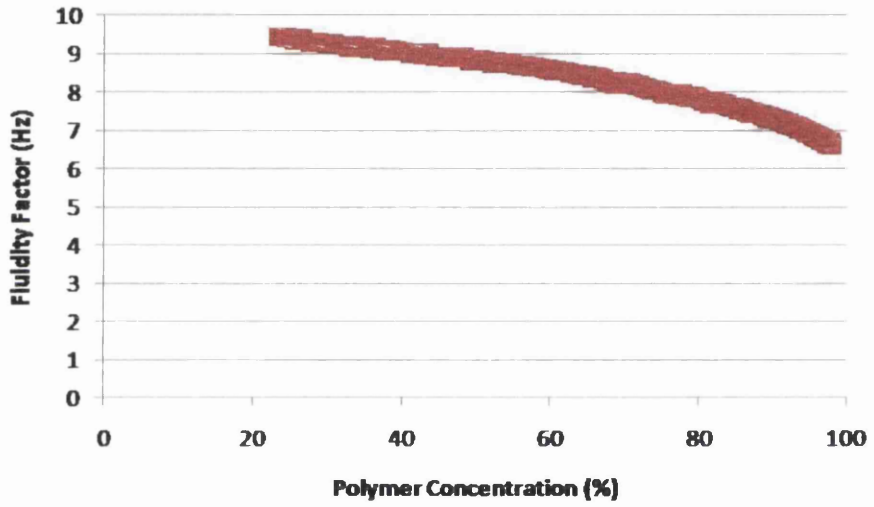


Figure A.98: Fluidity Factor with Polymer Concentration for 20% Polyamide Resin Ink with Solid Content.

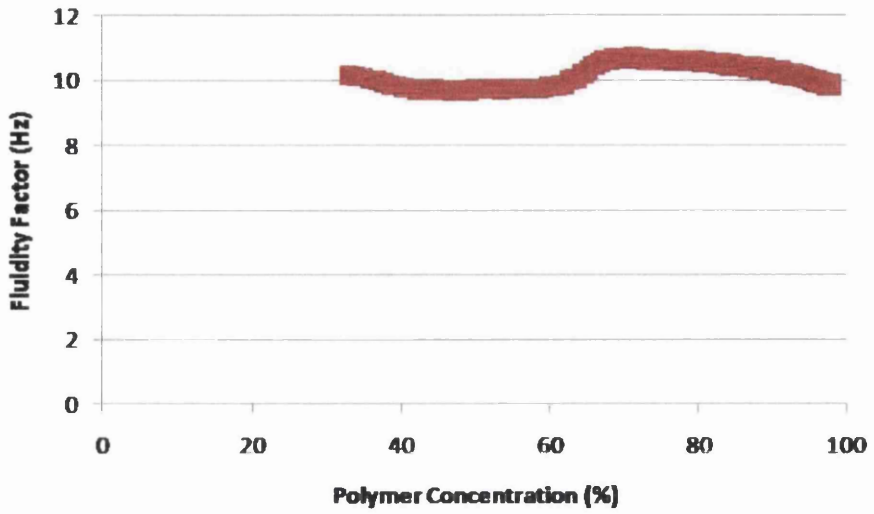


Figure A.99: Fluidity Factor with Polymer Concentration for 30% Polyamide Resin Ink with Solid Content.

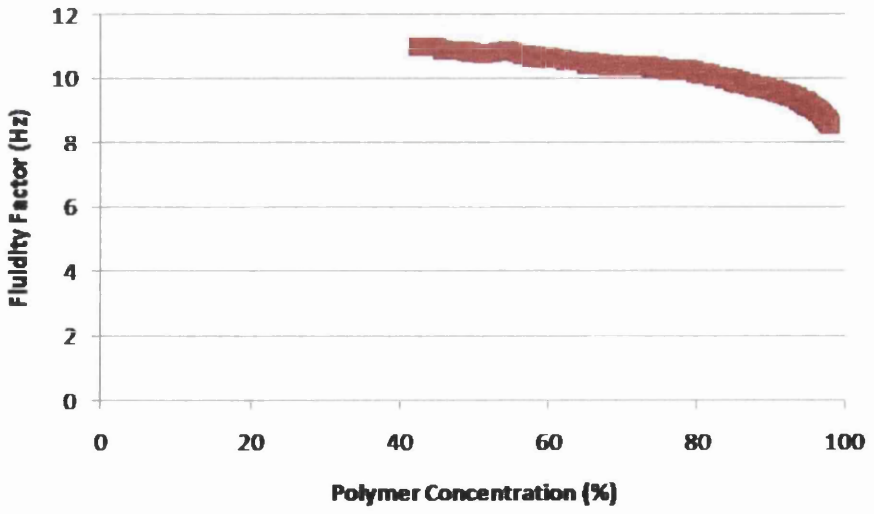


Figure A.100: Fluidity Factor with Polymer Concentration for 40% Polyamide Resin Ink with Solid Content.

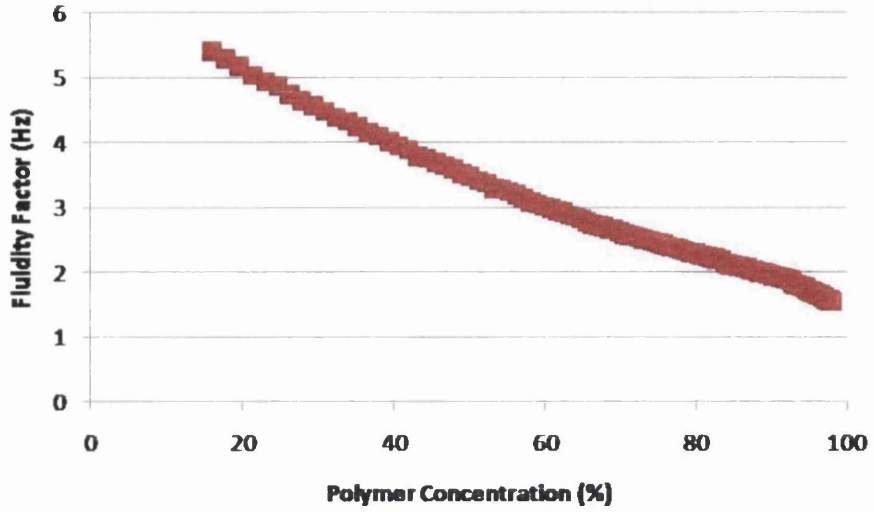


Figure A.101: Fluidity Factor with Polymer Concentration for 10% Nitrocellulose Resin Ink with Solid Content.

The MS-DWS results of the nitrocellulose-based system with the addition of solid content are plotted against polymer concentration.

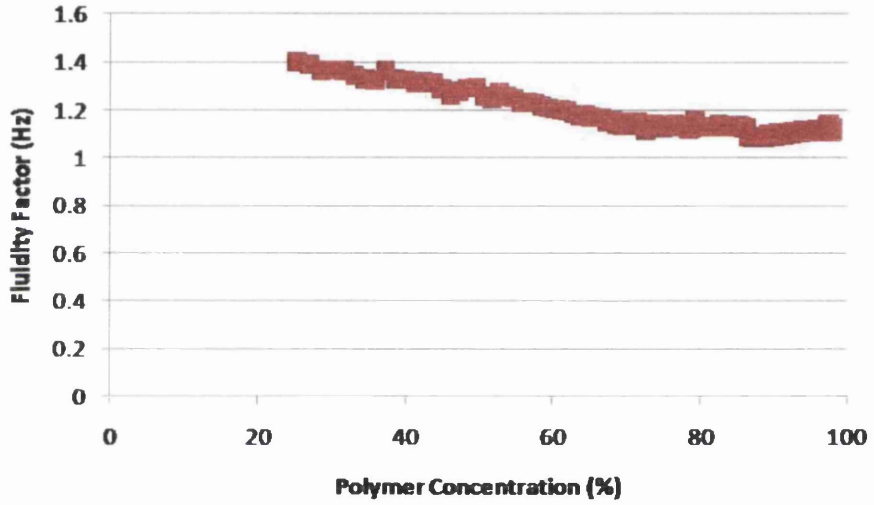


Figure A.102: Fluidity Factor with Polymer Concentration for 20% Nitrocellulose Resin Ink with Solid Content.

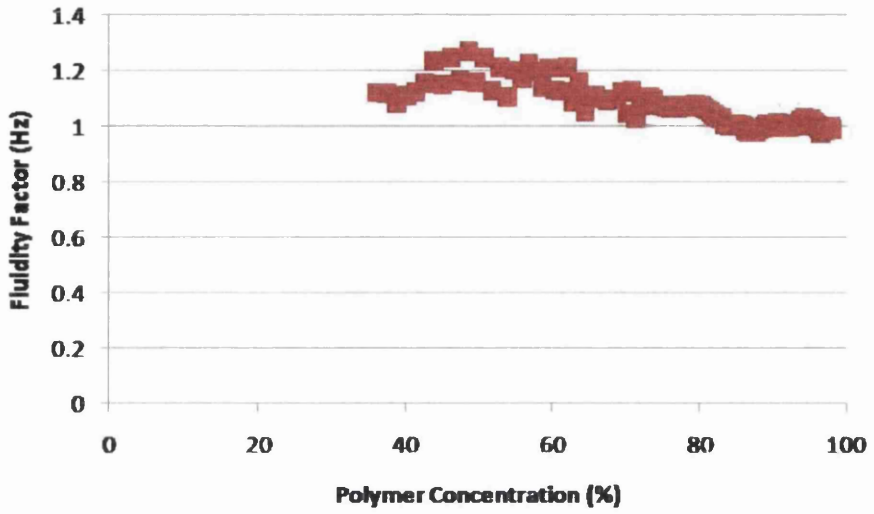


Figure A.103: Fluidity Factor with Polymer Concentration for 30% Nitrocellulose Resin Ink with Solid Content.

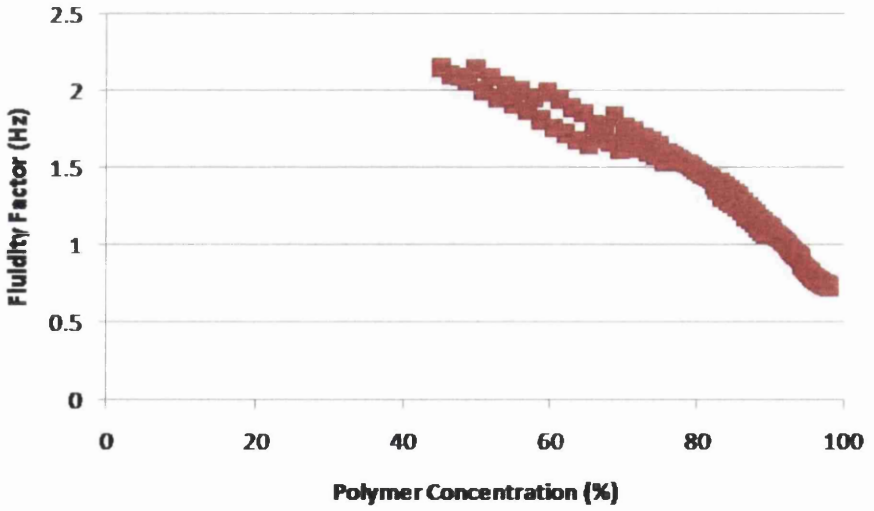


Figure A.104: Fluidity Factor with Polymer Concentration for 40% Nitrocellulose Resin Ink with Solid Content.

# Appendix B

# Error and Repeatability

The errors calculated upon the experimental techniques are shown in Figure B.1. Two standard deviations for each seperate test were taken. The minimum and maximum throughout all tests are shown as well as the absolute mean error for all tests.

| Equipment | Error upon | Minimum Error (%) | Maximum Error (%) | Absolute Error (%) |
|---|---|---|---|---|
| Bulk Rheology | Phase Angle | 8.89 | 15.56 | 12 |
| Bicone Rheology | Phase Angle | 2.22 | 30 | 12.78 |
| Dunouy Ring Rheology | Phase Angle | 1.11 | 28.89 | 9.25 |
| MS-DWS | Fluidity Factor | 1.2 | 15.7 | 4.08 |
| FTIR | Transmittance Peak | 0.44 | 4.87 | 2.52 |
| Bulk Rheology | Polymer Concentration | | | 0.1 |
| Bicone Rheology | Polymer Concentration | 2 | 20 | 8.85 |
| Dunouy Ring Rheology | Polymer Concentration | 0.04 | 25 | 6.93 |
| MS-DWS | Time | 0.48 | 30 | 9.44 |
| FTIR | Time | | | 1 |

Table B.1: The Calculated Errors for Experimental Tests

# Appendix C

# Derivations

## C.1 Physics of Oscillatory Shear Rheometry

The physics of oscillatory shear rheometry as applied to simple-shear deformation according to the theory of linear viscoelasticity [115]. Figure C.1 shows the principle of linear, simple-shear rheometry, where a small-amplitude, translational sinusoidal displacement $x$ is applied to a viscoelastic tissue or material specimen through a vibrating upper plate. The resulting shear force $F$ due to the viscoelastic response of the specimen is transmitted to the lower plate, and can then be detected by a transducer. Consider the illustration in Figure C.1 as a single degree-of-freedom system, with lumped elements of mass, stiffness, and damping, the displacement of the upper plate $x$ can be represented in complex notation as

$$x^* = x_0 e^{i\omega t} \tag{C.1}$$

where $x_0$ is the amplitude of displacement, $i$ is the imaginary number $\sqrt{-1}$, $\omega$ is the angular frequency, and $t$ is time. The equation of motion for the system is

$$m\frac{d^2x^*}{dt^2} + c\frac{dx^*}{dt} + kx^* = F^* \tag{C.2}$$

where $m$ is mass, $c$ is damping, $k$ is stiffness of the system, and $F^*$ is the resulting shear force in complex notation. For linear, small-amplitude shear, once steady state is reached, the applied sinusoidal displacement would result in a harmonic shear force at the same frequency, with a phase shift of $\delta$ according to the theory of linear viscoelasticity as follows:

$$F^* = F_0 e^{i(\omega t+\delta)} \tag{C.3}$$

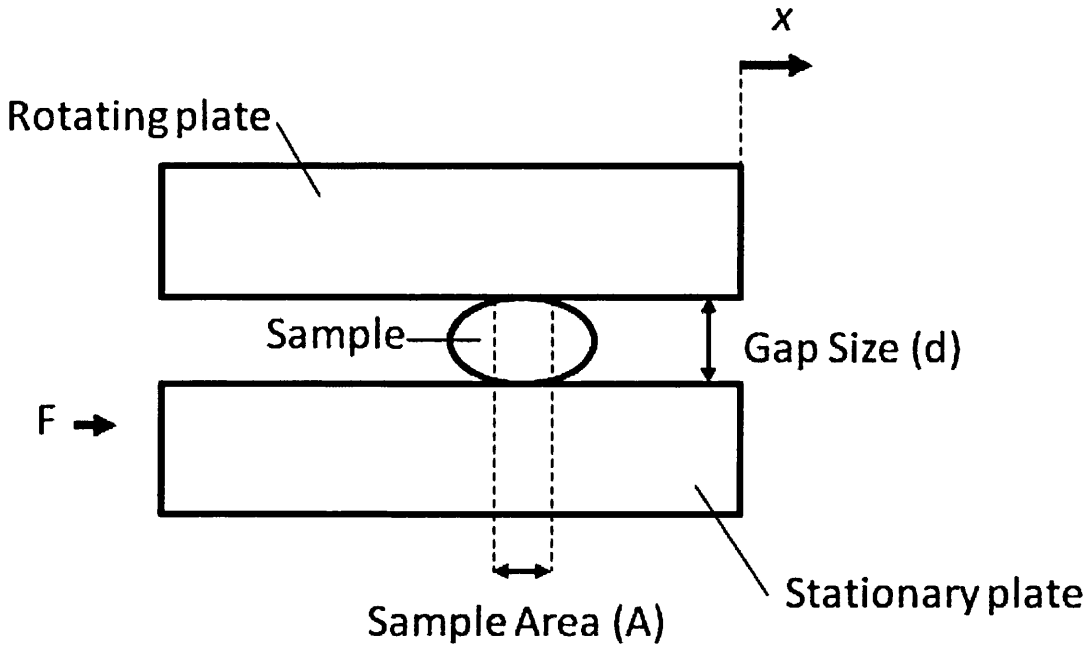


Figure C.1: Simple-shear Deformation by Oscillatory Shear Rheometry

where $F_0$ is the amplitude of $F^*$. For linear viscoelasticity, the phase shift $\delta$ will be independent of the displacement amplitude and the force amplitude ($x_0$ and $F_0$). Substituting $x^*$ and $F^*$ into the equation of motion yields

$$\left(k - m\omega^2\right) x_0 + ic\omega x_0 = F_0 e^{i\delta} \tag{C.4}$$

The complex frequency response of the system $H(\omega)$ can be defined as the displacement divided by the force as follows:

$$H(\omega) = \frac{x_0 e^{i\omega t}}{F_0 e^{i\omega t} e^{i\delta}} = \frac{x_0}{F_0 e^{i\delta}} \tag{C.5}$$

which results in the following expression from Equation C.4:

$$H(\omega) = \frac{1}{(k - m\omega^2) + ic\omega} \tag{C.6}$$

One could define the undamped resonant frequency $\omega_n = \sqrt{k/m}$and the damping ratio $\zeta = c/2\sqrt{km}$; the frequency response is then given by

$$H(\omega) = \frac{1/k}{1 - (\omega/\omega_n)^2 + i2\zeta\omega/\omega_n} \tag{C.7}$$

By considering the stiffness factor ($1/k$) together with the force term $F_0$, and by multiplying and dividing Equation C.7 by the complex conjugate of the denominator, a nondimensional expression can be derived for the complex system response $H(\omega)$ as follows:

$$H(\omega) = \frac{1 - (\omega/\omega_n)^2}{\left[1 - (\omega/\omega_n)^2\right]^2 + \left[2\zeta\omega/\omega_n\right]^2} - i\frac{2\zeta\omega/\omega_n}{\left[1 - (\omega/\omega_n)^2\right]^2 + \left[2\zeta\omega/\omega_n\right]^2} \tag{C.8}$$

where the magnitude response $|H(\omega)|$ and the phase response $\delta(\omega)$ are given by

$$|H(\omega)| = \frac{1}{\sqrt{\left[1 - (\omega/\omega_n)^2\right]^2 + \left[2\zeta\omega/\omega_n\right]^2}} \tag{C.9}$$

$$\delta(\omega) = -tan^{-1}\left(\frac{c\omega}{k - m\omega^2}\right) = -tan^{-1}\left(\frac{2\zeta\omega/\omega_n}{1 - (\omega/\omega_n)^2}\right) \tag{C.10}$$

By definition, the damped resonant frequency $\omega_0$ is the frequency at which the magnitude of the frequency response $|H(\omega)|$ is maximum. It can also be deduced from Equation C.9 that $\omega_0$ is related to the undamped resonant frequency $\omega_n$ by

$$\omega_0 = \omega_n\sqrt{1 - \zeta^2}\ for\ \zeta > 1/\sqrt{2} \tag{C.11}$$

$$\omega_0 = \omega_n\sqrt{1 - 2\zeta^2}\ for\ \zeta < 1/\sqrt{2} \tag{C.12}$$

In order to compute the viscoelastic shear properties of the specimen, shear strain and shear stress of the specimen can be defined based on the displacement and force given in Equations C.1,C.3. Shear strain can be defined as the displacement $x$ divided by the distance between the plates, or the gap size $d$ as follows:

$$\gamma^* = tan^{-1}\frac{x^*}{d} \approx \frac{x^*}{d}\ for\ x_0 \ll d \tag{C.13}$$

whereas shear stress is defined as

$$\tau^* = \frac{F^*}{A} \tag{C.14}$$

where $A$ is the area of the specimen experiencing the strain, as indicated by the area of contact between the specimen and the upper plate (Figure C.1). Hence,

$$\gamma^* = \gamma_0 e^{i\omega t} = \frac{x_0}{d}e^{i\omega t} \tag{C.15}$$

$$\tau^* = \tau_0 e^{i(\omega t+\delta)} = \frac{F_0}{A}e^{i(\omega t+\delta)} \tag{C.16}$$

where $\gamma_0$ is the amplitude of $\gamma^*$ and $\tau_0$ is the amplitude of $\tau^*$. The corresponding linear constitutive equation relating shear stress to shear strain is

$$\tau^* = G^* \gamma^* \tag{C.17}$$

where $G^*$ is the complex shear modulus. By definition, $G^*$ is composed of a real part and an imaginary part as follows:

$$G^* = G' + iG'' \tag{C.18}$$

The real part $G'$ is the elastic shear modulus, and the imaginary part $G''$ is the viscous shear modulus. Hence, for the linear theory of viscoelasticity [115], the constitutive equation can be expressed as

$$\tau^* = G' \gamma^* + \frac{G''}{\omega} \frac{d\gamma^*}{dt} \tag{C.19}$$

The elastic and viscous shear moduli $G'$ and $G''$ are related to the strain amplitude and the stress amplitude ($\gamma_0$ and $\tau_0$ ), and the phase shift ($\delta$). Based on Equations C.15,C.16, they are expressed in terms of the displacement amplitude and the force amplitude ($x_0$ and $F_0$) as follows:

$$G' = \frac{F_0 d \cos\delta}{A x_0} \tag{C.20}$$

$$G'' = \frac{F_0 d \sin\delta}{A x_0} \tag{C.21}$$

The dynamic viscosity $\eta'$ is related to the viscous shear modulus $G''$, and the damping ratio (also called loss factor or damping factor) $\zeta$ is the ratio of the viscous to the elastic moduli as follows:

$$\eta' = \frac{G''}{\omega} \tag{C.22}$$

$$\zeta = \frac{G''}{G'} \tag{C.23}$$

The amplitude of the displacement $x_0$ can be detected by a displacement transducer at the upper plate, and the amplitude of the shear force response $F_0$ of the specimen can be detected by a force transducer at the lower plate. The phase shift $\delta$ can be measured with a temporal analysis of the displacement and force signals, where it is shown as $\delta/\omega$ on the time axis. The area of contact between the specimen and the

plates ($A$ ) can be estimated by analysis of scaled images taken from directly above the upper plate. With $x_0$ , $F_0$ , $\delta$ , and $A$ determined, and given a known gap size $d$ , the viscoelastic functions can be calculated from Equations C.20,C.21,C.22,C.23.